Development and Synthesis of Nanomolar E-Selectin Antagonists

Using a Fragment-Based Approach

Inauguraldissertation

zur

Erlangung der Würde eines Doktors der Philosophie

vorgelegt der

Philosophisch-Naturwissenschaftlichen Fakultät

der Universtität Basel

von

Jonas Egger

aus St. Gallen-Tablat (SG) und Gossau (SG), Schweiz

Basel, Dezember 2012

Genehmigt von der Philosophisch-Naturwissenschaftlichen Fakultät

auf Antrag von

Prof. Dr. B. Ernst, Institut für Molekulare Pharmazie, Universität Basel,

Prof. Dr. K.-H. Altmann, Institut für Pharmazeutische Wissenschaften, ETH Zürich

Basel, den 14. Dezember 2010

<div style="text-align: right">Prof. Dr. Martin Spiess</div>

For instance, on the planet Earth, man had always assumed that he was more intelligent than dolphins because he had achieved so much – the wheel, New York, wars and so on – whilst all the dolphins had ever done was muck about in the water having a good time. But conversely, the dolphins had always believed that they were far more intelligent than man – for precisely the same reasons.

from *A Hitchhiker's Guide to the Galaxy* by Douglas Adams

Acknowledgements

Abstract

By mediating the extravasation of leukocytes from the blood stream, selectins are involved in a key step of the inflammatory cascade. The excessive recruitment of leukocytes into inflamed tissue is responsible for the onset and the progression of various inflammatory diseases (*e.g.* rheumatoid arthritis, reperfusion injuries or asthma). Furthermore, selectins contribute to the development and metastasis of cancer. Given the health impact of these diseases, selectins represent a valuable drug target.

Many research efforts for the development of small-molecule E-selectin antagonists have been based on sialyl Lewis^x (sLe^x), the minimal carbohydrate epitope recognized by the selectins. From this lead with affinities in the millimolar range, antagonists with more drug-like properties and affinities in the low micromolar range have been developed. However, the selectins have shaped up as difficult drug targets with only relatively few successful applications *in vivo* and no marketed anti-selectin drug. The comparably low affinities of E-selectin antagonists are an important reason for the lack of clinical success in this field.

In this work, the problem of modest affinity was approached from a new direction using a fragment-based approach (Figure I), as the possibility of forming high-affinity ligands from low-affinity fragments is one particular advantage of fragment-based drug discovery. Using a known sLe^x mimic ($\rightarrow$ first-site ligand) as starting point, an NMR-based screening was performed to identify small fragments ($\rightarrow$ second-site ligands) binding to a proximate second binding site. This led to the identification of 5-nitroindole as a second-site ligand. *In situ* click experiments based on the Huisgen 1,3-dipolar cycloaddition were performed to screen for a suitable linker to connect the two fragments. As this approach failed, a library of triazole–nitroindole antagonists was synthesized, and a ranking was performed using a specifically designed Biacore experiment.
The detailed investigation of the five most potent ligands identified in the screening revealed potent E-selectin antagonists with affinities ranging from 30 to 89 nM and improved binding kinetics, *i.e.* prolonged ligand–receptor half-life times in the range of minutes. Derivatives of the most potent antagonist were synthesized providing first insights into structure–activity relationships and a basis for the future development of these antagonists, also with respect to their physicochemical and pharmacokinetic properties.
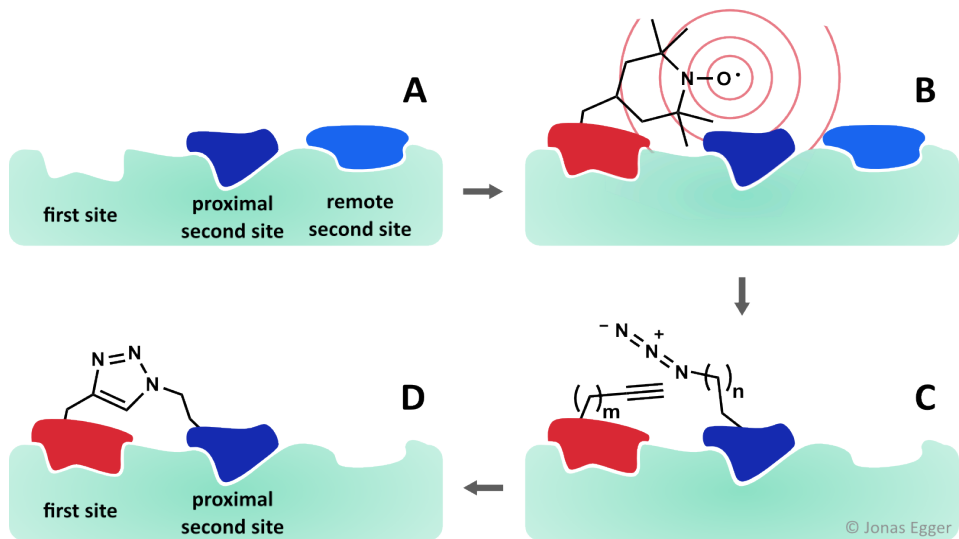
Figure I. Schematic representation of the "fragment-based *in situ* combinatorial approach" for the identification of high-affinity E-selectin antagonists. A) Identification of second-site ligands based on their transverse magnetization decay induced by the protein; B) identification of *proximal* second-site ligands using a spin-labeled first-site ligand; C) incubation of E-selectin with alkyne/azide libraries of first- and second site ligands (*in situ* click experiment) for the determination of a suitable linker pattern ; D) high-affinity ligand generated by receptor-mediated triazole formation. E-selectin is shown in green.

Abbreviations

Ac	Acetyl	HEPES	4-(2-Hydroxyethyl)-1-piperazineethanesulfonic acid
AcOH	Acetic acid		
AcOOH	Peracetic acid	HOBt	N-Hydroxybenzotriazol
AIBN	Azodiisobutyrodinitrile	IC_{50}	Inhibitory concentration 50%
aq.	Aqueous	ICAM-1	Intercellular cell adhesion molecule 1
Ar	Aryl		
ax	Axial	IL-1	Interleukine-1
Bn	Benzyl	IL-8	Interleukine-8
BnBr	Benzylbromide	Ind	Indole
BSA	Bovine serum albumine	IR	Infrared spectroscopy
Bz	Benzoyl	ISC	In situ click
cat.	catalyst/catalytic amount	kDa	Kilo Dalton
CD34	Cell differentiation antigen 34, sialomucin	Lac	Lactic acid
		LAD	Leukocyte adhesion deficiency
CDI	Carbonyl diimidazole	Le^a	Lewis^a
cHex	Cyclohexyl	Le^x	Lewis^x
CMC	Critical micelle concentration	LPS	Lipopolysaccharide
CR	Complement regulatory-like domains	mAb	Monoclonal antibody
CRD	Carbohydrate recognition domain	MadCAM-1	Mucosal vascular addressin cell adhesion molecule
Cy	Cyclohexyl		
d	Days	Man	Mannose
dba	1,5-Diphenyl-1,4-pentadien-3-one	MBP	Mannose binding protein
DBU	1,8-Diazabicyclo[5.4.0]undec-7-ene	MC	Monte-Carlo
DEAD	Diethyl azodicarboxylate	MD	Molecular dynamics
DMAP	4-Dimethylaminopyridine	Me	Methyl
DME	Dimethoxyethane	μW	Microwave (heating)
DMF	Dimethylformamide	min	Minute(s)
DMSO	Dimethylsulfoxide	MS	Molecular sieves
DMTST	Dimethyl(methylthio)sulfonium triflate	MTPA	α-Methoxy-α-(trifluoromethyl)-phenylacetyl
DTBMP	2,6-Di-tert-butyl-4-methylpyridine	MTPA-Cl	α-Methoxy-α-(trifluoromethyl)-phenylacetyl chloride
DTBP	2,6-Di-tert-butylpyridine		
e.g.	For example	NaOMe	Sodium methoxide
ee	Enantiomeric excess	Neu	Neuraminic acid
EGF	Epidermal growth factor	Neu5Ac	N-Acetyl neuraminic acid, sialic acid
eq	Equivalent	NHS	N-Hydroxysuccinimide
ESL-1	E-selectin ligand 1	NI	Nitroindole
FBDD	Fragment-based drug discovery	NMM	N-Methylmorpholine
Fuc	Fucose	NMO	4-Methylmorpholine N-oxide
Gal	Galactose	NMR	Nuclear magnetic resonance
GC	Gas chromatography	NOE	Nuclear Overhauser effect
GlcNAc	N-Acetylglucosamine	OH	Hydroxyl
Glc	Glucose	Ph	Phenyl
Gly-CAM-1	Glycosylated cell adhesion molecule-1	Pip	Piperazine
		PLE	Pig liver esterase
h	Hour(s)	PMB	p-Methoxybenzyl
H	Hydrogen	PSGL-1	P-selectin glycoprotein ligand 1
HBTU	O-Benzotriazole-N,N,N',N'-tetramethyluronium-hexafluoro-phosphate	PTFE	Polytetrafluoroethylene
		p-TsOH	p-Toluenesulfonic acid
		pyr	Pyridine
Hep	Heptose	QQQ-MS	Triple quadrupole mass spectrometry
		rac	Racemic

rIC_{50}	Relative IC_{50}
rot	Optical rotation
r.t.	Room temperature
s	seconds
SA	Surface activity
SAR	Structure-activity relationship
satd.	Saturated
SCR	Short consensus repeats
Sia	Sialic acid
sLe^a	Sialyl Lewis^a
sLe^x	Sialyl Lewis^x
SPR	Surface plasmon resonance
TBAB	Tetrabutylammonium bromide
TBAF	Tetrabutylammonium fluoride
TBS	tert-Butyldimethylsilyl
Temp	Temperature
TEG	Tetraethyleneglycol
TEMPO	2,2,6,6-Tetramethylpiperidine-1-oxyl
TES	Triethylsilane
Tf	Triflate, (triflouromethanesulfonate)
TFA	Trifluoroacetic acid
THF	Tetrahydrofuran
TIC	Total ion current/count
TIS	Triisopropylsilane
TLC	Thin-layer chromatography
TMS	Trimethylsilyl
TMSOTf	Trimethylsilyl triflate
TNF-α	Tissue necrosis factor α
Ts	Tosyl
TsCl	Tosyl chloride
VCAM-1	Endothelial vascular cell-adhesion molecule

Table of Contents

Chapter 2 is presented in the form of a paper manuscript forming a discrete part of the thesis. This includes compound numbering, which restarts at 1 in that section. In the other parts of the thesis, compounds appearing in this chapter are referred to as "**P1234**".

1. Introduction

Dolor, calor, rubor, tumor – the classical cardinal symptoms of inflammation have been known since before christ (1), indicating that the struggle with inflammation-associated problems has a long record in the history of mankind. Indeed, inflammatory processes play an important role in many diseases reaching far beyond their manifestation in the clinical symptoms mentioned above (for illustrative examples, see (2) or (3)), which themselves are troublesome enough. Examples for such "unhealthy" involvements of inflammation are cancer or reperfusion injuries. Rheumatoid arthritis and asthma are more direct manifestations of inflammation with a severe health impact.

The therapeutic relevance of anti-inflammatory and chemotherapeutic drugs is evident from the severity and prevalence of inflammatory and associated diseases. However, these drugs often cause severe side-effects or have limited efficacy, which explains the need for therapeutic alternatives. The specific role of the selectins at an early stage in the inflammatory cascade makes them an attractive target for the therapy of inflammation-related diseases. Here, a fragment-based approach towards the inhibition of the leukocyte–selectin interaction is presented.

1.1. Structure and function of the selectins

1.1.1. Structure of the selectins

The selectins are a family of Ca^{2+}-binding C-type lectins. Lectins are carbohydrate-binding proteins participating in cellular recognition (4). The selectin family comprises three members, E-, P-, and L-selectin[1], that have common structural features, as shown in Figure 1-1: The *N*-terminal carbohydrate recognition or lectin domain (CRD) is attached to an epidermal growth factor (EGF) domain, which is followed by a varying number (L-selectin: 2, E-selectin: 6, P-selectin: 9; in humans) of complement-like consensus repeats, a transmembrane region and a cytoplasmic tail at the *C* terminus (5).
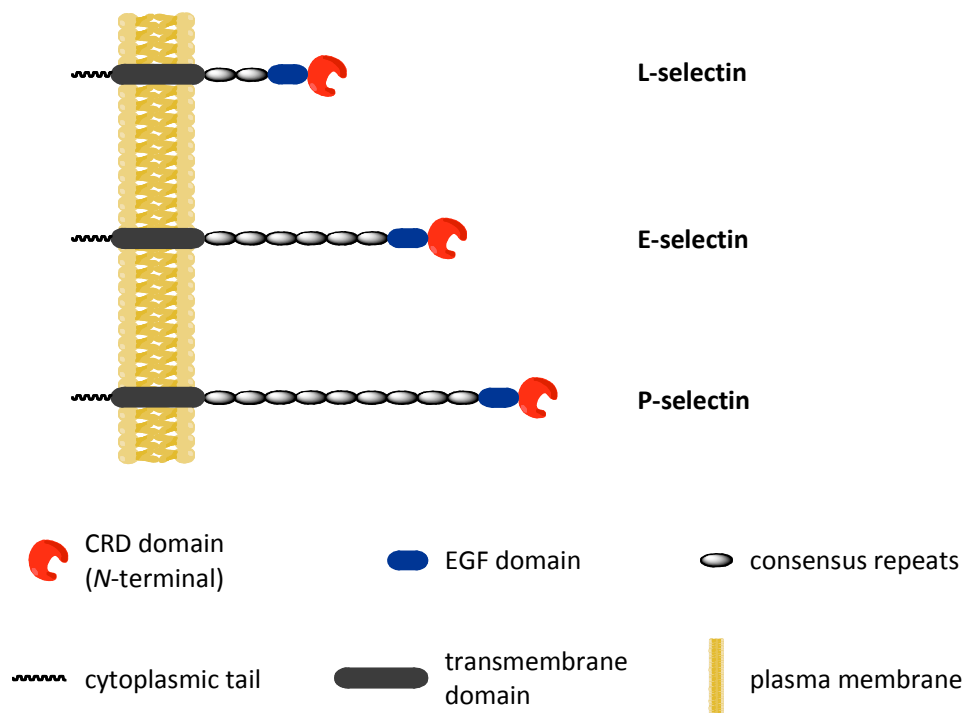
Figure 1-1. Structures of L-, E-, and P-selectin. After (6).

Among the 3 selectins, the lectin and the EGF domains show the highest degree of sequence homology (7). The lectin domain carries the carbohydrate binding site, which is conformationally stabilized by a Ca^{2+} ion (5), itself participating in ligand binding (8). With

---

[1] There exist alternative names: E-selectin: CD62E, ELAM-1, or LECAM-2; P-selectin: CD62P, GMP-140; L-selectin: CD62L, LAM-1, or LECAM-1).

5.8 and 10%, the content of tryptophan and tyrosine, respectively, is unusually high in the lectin domain (9). The EGF domain is required for binding, yet its function is not completely understood, and it may affect ligand binding either directly or via an allosteric effect (10, 11). Recently, a single residue in the EGF domain was suggested to be involved in the catch bond behavior of selectins (see Section 1.2.2) (9).

The consensus repeats are thought to act as spacers that allow an efficient presentation of the lectin domains on the cell surface (12). The extracellular part of the selectins is anchored in the cell membrane *via* the transmembrane domain. The cytoplasmic tail is thought to transduce outside-in signals triggered by ligand binding (13).

1.1.2. Natural selectin ligands

The natural selectin ligands are glycoproteins or glycolipids typically carrying terminal sialylated and fucosylated oligosaccharides or sulfopolysaccharides as their minimal binding epitopes (14-16). Four carbohydrates were found to represent common carbohydrate epitopes recognized by all three selectins: the trisaccharides Lewis^x (Le^x, **1**) and Lewis^a (Le^a, **2**) as well as the respective sialylated derivatives sialyl Lewis^x (sLe^x, **P1**) and sialyl Lewis^a (sLe^a, **3**; Figure 1-1) (14, 15, 17).
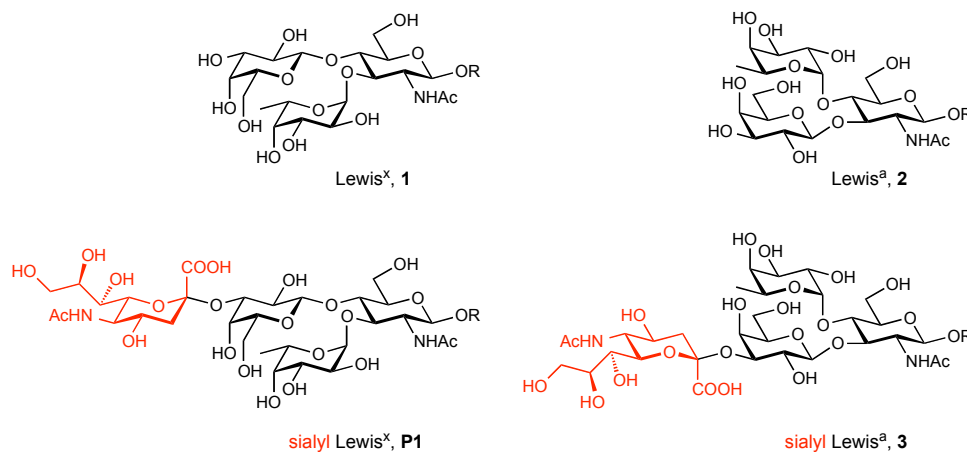
Figure 1-2. The minimal carbohydrate epitopes of E-selectin.

The following physiological selectin ligands have been identified so far (an overview of the ligands and their interactions is given in Figure 1-3):

▪ **L-selectin:**

Gly-CAM-1 (18), CD34 (19), MAdCAM-1 (20, 21), podocalyxin-like protein (22), endomucin (23), endoglycan (24), and PSGL-1 (24).

Gly-CAM-1 is the best-characterized L-selectin ligand. For its binding to L-selectin, sialic acid, fucose, and oligosaccharide sulfation were found to be critical (18, 25-29).

▪ **P-selectin:**

PSGL-1 (30).

P-selectin glycoprotein ligand 1 (PSGL-1) is the major natural ligand of P-selectin (30). For binding to P-selectin, two of the three *N*-terminal tyrosine residues (Tyr46, Tyr48, and Tyr51) need to be sulfated (31-33).

▪ **E-selectin:**

E-selectin ligand 1 (ESL-1), PSGL-1 (34-38), and L-selectin (39).

For functional binding *in vivo*, E-selectin has different requirements than L- and P-selectin, as it does not require ligand sulfation (14, 34, 35).
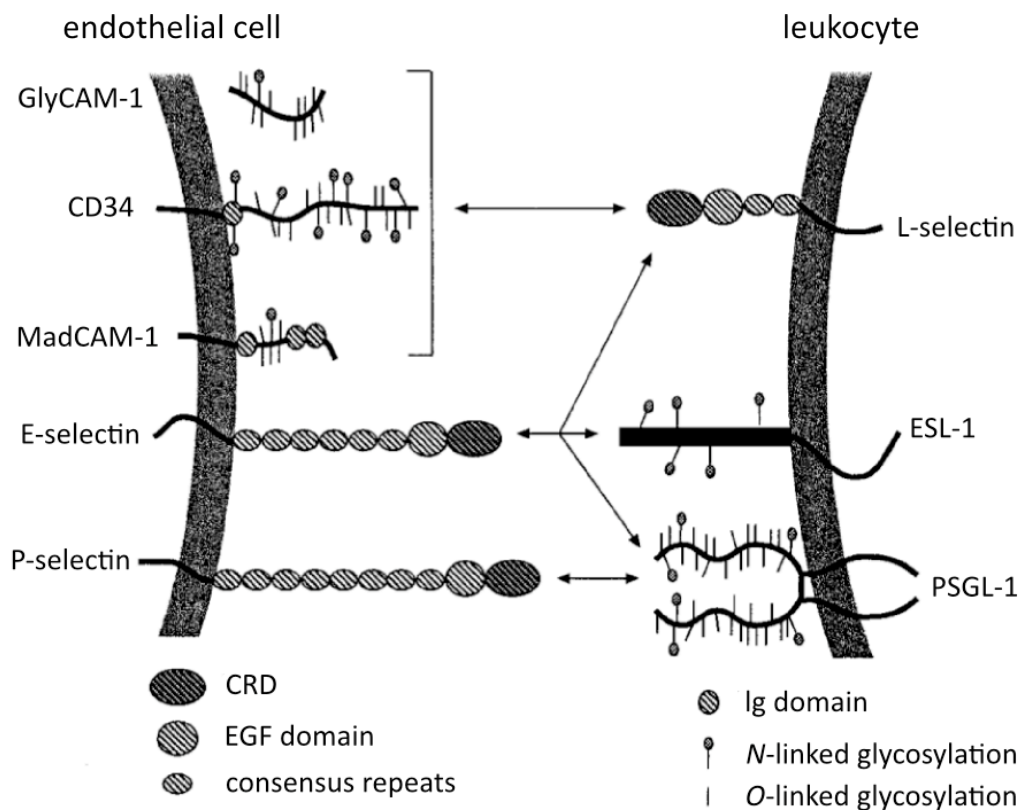
Figure 1-3. The selectins and their natural glycoprotein ligands. Adapted from (6).

1.1.3. Selectins in the inflammatory cascade

An inflammation is the body's reaction to a local damage, which can be of physical, chemical, infective, immunological or nutritive origin, and its progression can be acute, subacute or chronical. One of the processes triggered by an inflammatory stimulus is the

recruitement of leukocytes, on whose activities innate and adaptive immune responses depend, to the site of infection. The recruitement proceeds *via* 3 necessary key steps (40, 41): 1) Tethering and rolling of leukocytes on vessel walls, 2) release of chemoattractants inducing the expression of integrins on the leukocyte cell surface, which lead to 3) firm adhesion of the cell. Subsequently, the cell can penetrate the endothelium and migrate to the site of inflammation. The first process, *i.e.* the tethering and rolling of leukocytes, is mediated by the selectins, which are expressed on the cell surface upon the release of inflammatory mediators (Figure 1-4).
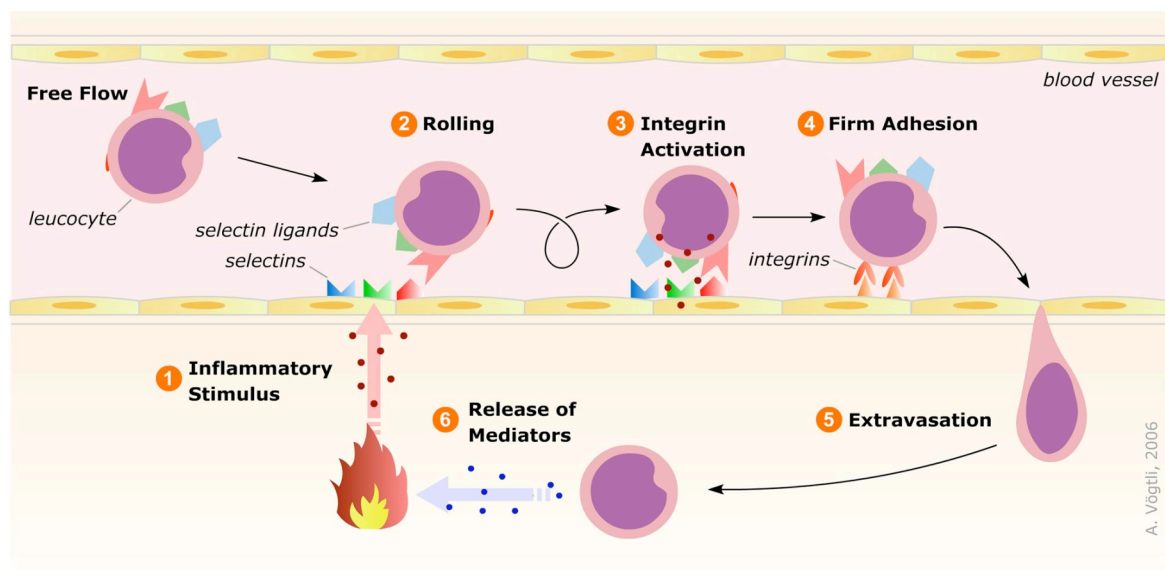
Figure 1-4. Schematic representation of the inflammatory cascade (42)

The selectins show overlapping, but temporally and spatially distinct expression patterns, which is exploited for a precise regulation of leukocyte recruitement (40, 41, 43).

E-selectin is expressed *de novo* upon the release of TNF-α, IL-1 or bacterial LPS exclusively on endothelia (44, 45). It peaks 3 to 4 h after stimulation to reach basal levels again within 16 to 24 h (46). A particular feature of E-selectin is its constitutional expression on skin and bone microvessels (47, 48).

P-selectin is special in that it is stored in α-granules of Waibel-Palade bodies cells, which allows it to be presented on the cell surface within minutes after stimulation by thrombin, histamine and other agonists (49, 50). As well as quick, this expression is transient, with the P-selectin being internalized rapidly (51). Additionally, TNF-α, IL-1 or LPS can induce the *de novo* synthesis of P-selectin, causing a later appereence on the cell surface after 2 to 4 h (52-54). While the latter process is restricted to endothelia, the quick expression occurs also on platelets, which is unique among the selectins.

L-selectin plays an important role in "secondary tethering". During this process, leukocytes adhere to already associated leukocytes on endothelia, thereby increasing the number of cells recruited to sites of inflammation (55, 56). Owing to its expression on different leukocytes, L-selectin is responsible for lymphocyte recirculation, and, like E- and P-selectin is involved in leukocyte recruitment during inflammation (43).

Firm adhesion is enabled by the cytokine-mediated activation of integrins, which bind to integrin ligands such as VCAM-1, ICAM-1, and MAdCAM-1 on endothelial cells (57, 58). Firmly attached cells can now penetrate the endothelial wall and migrate to the site of inflammation in the tissue (*cf.* Figure 1-5).
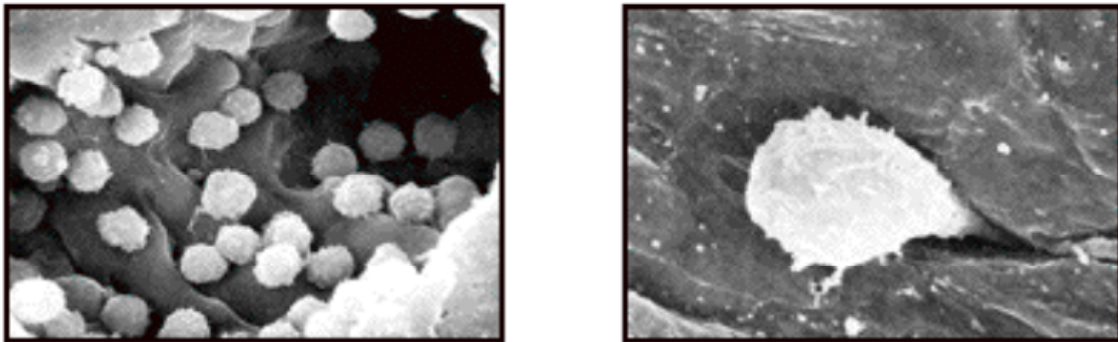
Figure 1-5. Left: leukocyte rolling on endothelial cells; right: migration into tissue (59).

1.1.4. Pathophysiological roles of E-selectin

Many acute or chronic inflammatory diseases are characterized by the excessive recruitment of leukocytes into inflamed tissues. Investigations with a number of mouse models showed that interfering with this process has a strong impact on the progression of these diseases (60-62). In humans, the importance of selectin–ligand interactions for appropriate immune responses was illustrated by cases of a rare genetic disorder, type 2 leukocyte adhesion deficiency (LAD-2). Patients affected by this disease exhibit reduced rolling of leukocytes, causing, among other severe symptoms, recurrent infections (63, 64).

In a number of diseases, selectins appear to play a detrimental role. Examples include reperfusion injury (65, 66), asthma (67-70), rheumatoid arthritis (71-74), and host-versus-graft disease (75, 76). Several model systems have demonstrated positive effects of blocking the selectin-mediated leukocyte recruitment, for example in the case of reperfusion injury (77, 78), asthma (79, 80), rheumatoid arthritis (81, 82), or host-versus-graft disease (75).

Inflammation is not only a direct cause of disease, but is also involved in the progression of tumors, as inflammatory cells contribute significantly to the tumor microenvironment (2). Specifically, the selectins are involved in cancer on three different levels: 1) Tumor cells form clusters with platelets and leukocytes, by means of which they circulate in the blood stream, 2) they use the same selectin-mediated pathway for extravasation as leukocytes, and 3) they exploit pro-malignancy signals delivered *via* the action of selectins (83). The potential usefulness of selectins in therapy of cancer was, for example, demonstrated by studies showing that the survival of colorectal cancer patients with high levels of sLe^x and sLe^a could be increased by suppressing the vascular expression of E-selectin (84).

For a more detailed account of the pathophysiological roles of selectins, one may consider the following recent reviews: (83, 85-89).

1.2. The ligand binding of selectins

1.2.1. Sialyl Lewis^x

In all three selectins, sialyl Lewis^x (sLe^x, **P1**) is the minimal carbohydrate epitope (14, 15, 17) showing a modest binding affinity in the millimolar range (90). It has served as a lead structure for the development of glycomimetic antagonists (91-93).

The pharmacophores of sLe^x were determined by systematic derivatization of functional groups. This revealed that the 3- and 4-hydroxyls of fucose (94, 95), the 4- and 6-hydroxyls of galactose (96, 97), and the carboxyl group of neuraminic acid contribute to binding (*cf.* Figure 1-7) (98, 99). In P-selectin, the neuraminic acid makes additional contributions to binding by the 4- hydroxyl and *via* hydrophobic interactions, as was revealed by the crystal structure of P-selectin co-crystallized with sLe^x (8). The Glc$N$Ac moiety is not directly involved in binding but rather serves as a spacer that orients fucose and galactose in an optimal position (94, 98, 99).

The crystal structure of the lectin/EGF domains of E- and P-selectin co-crystallized with sLe^x was solved in 2000 by Somers *et al.* (8). In contrast to the co-crystal structure of mannose binding protein (MBP-A) with its glycans (100), the Ca^{2+} ion was found to be complexed by the 3- and 4-hydroxyls of fucose, and not by the 2- and 3-hydroxyls (Figure 1-6 and Figure 1-7).
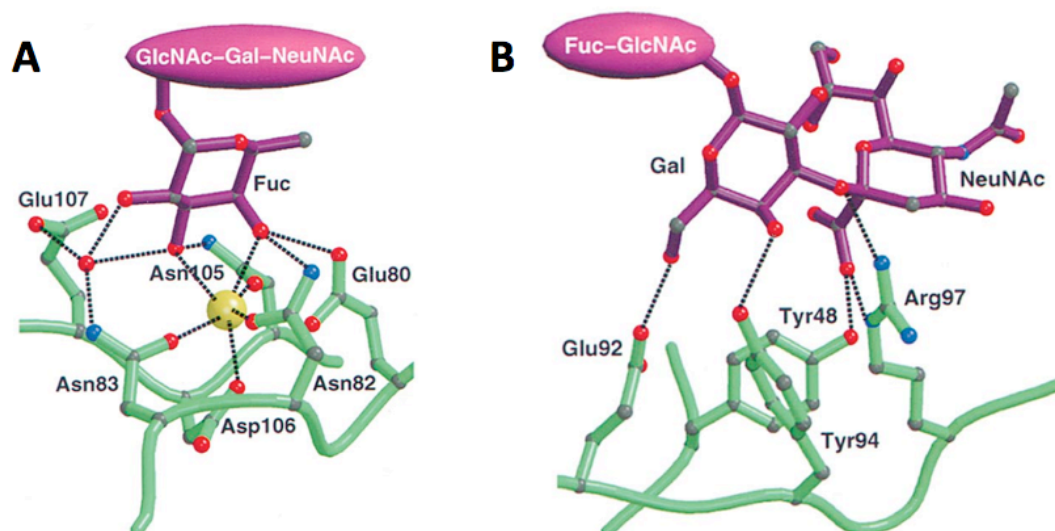
Figure 1-6. Interactions between sLe^x and E-selectin in the crystal structure by Somers *et al.*. A) Interactions of fucose; B) interactions of the galactose and the neuraminic acid. Adapted from (8).
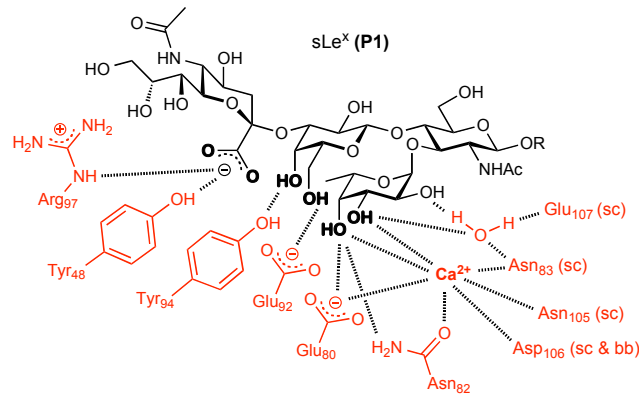
Figure 1-7. Schematic representation of sLe^x binding to E-selectin as identified in the crystal structure by Somers *et al.*.

1.2.2. The shear threshold requirement and catch bonds

Figure 1-8 illustrates a surprising phenomenon associated with selectin-mediated leukocyte rolling: a shear above a critical threshold is required to promote and maintain rolling. This effect was first described for L-selectin (101), but but also occurs with P- and E-selectin (102). The shear threshold requirement is a result of the selectins' ability to form catch bonds, which could be shown by single-molecule atomic force microscopy (103, 104). Such bonds, which are also found in FimH-mediated bacterial adhesion (105), show an increase of the mean bond lifetime with force below a critical value and a decrease when the force exceeds that value. This is in contrast to a "conventional" bond (slip bond), whose lifetime decreases with force (105, 106).
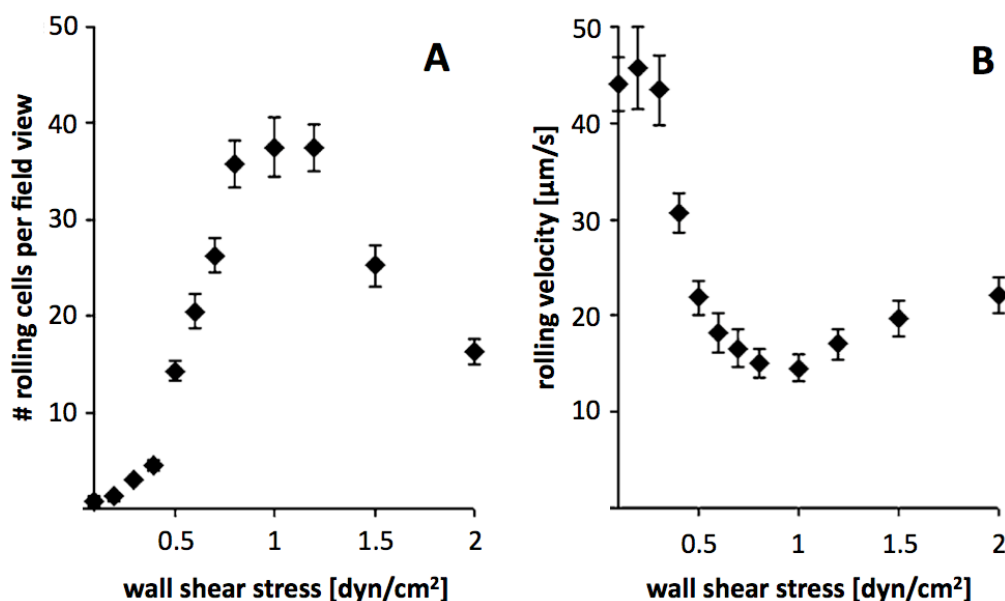
Figure 1-8. A) L-selectin mediated neutrophil tethering at different shear shear stresses; B) Neutrophil rolling velocity on PSGL-1. Adapted from (107).

The cause of the catch bond effect in selectins is not yet fully understood, but evidence suggests that the extension of the flexible region (interdomain region) between the selectin's lectin and EGF domains is crucial in this respect (108, 109):

The selectin crystal structures revealed two different selectin conformations, "bent" and "extended", differing by the angle between the EGF and the lectin domains (8, 110) (*cf.* Figure 1-9). In the absence of ligand (110) or after soaking the crystals with sLe^x, the bent conformation was obtained (8), but co-crystallization of P-selectin with a PSGL-1 fragment yielded the extended conformation, and thus it was hypothesized that P-selectin had a low- and a high-affinity state (8). This hypothesis was supported by investigations on selectin mutants (111). Phan *et al.* introduced a sterically demanding glycan in the hinge region of P-selectin (→ wedge mutant), which was predicted to induce the extended conformation of P-selectin. Indeed, compared to the wild-type protein, the wedge mutant's affinity to PSGL-1 was increased by a factor of 5, and cells expressing the mutant P-selectin exhibited stronger tethering. Likewise, an L-selectin–N138G mutant, which misses a hydrogen bond showed stronger tethering to PSGL-1–coated surfaces. This can be explained by the fact that, without the hydrogen bond, the extended conformation is favored (108). Lou *et al.* investigated the same modification using a single-molecule force probe. They found that the mutant needed less force to enter the catch-bond regime, *i.e.* bond lifetimes were prolongued. This finding is in accordance with the assumption that, *in vivo,* the pulling force applied by the rolling cell acts as an allosteric effector to induce the high-affinity bent conformation (Figure 1-9).
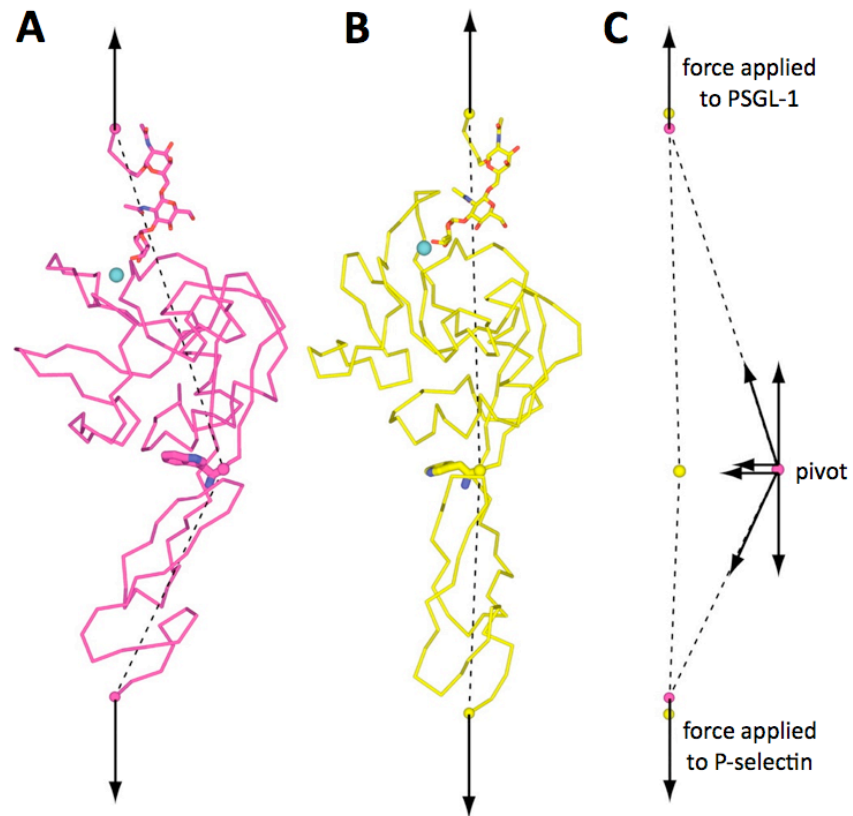
Figure 1-9. Bent (A) and extended (B) conformation of P-selectin and the application of force (B). Adapted from (9).

Two models were suggested to rationalize the different affinities of the two protein conformations, the "sliding–rebinding" (109, 112) and the "allostery" (9, 113) model.

According to the sliding–rebinding model, force-induced extension of the lectin/EGF domains leads to an alignment of the ligand–protein interface with the force vector. This allows the ligand to slide along the protein surface and to make new interactions on multiple overlapping binding sites, which then favors rebinding to the original site (Figure 1-10). Conformational changes of the binding site are not considered in this process.
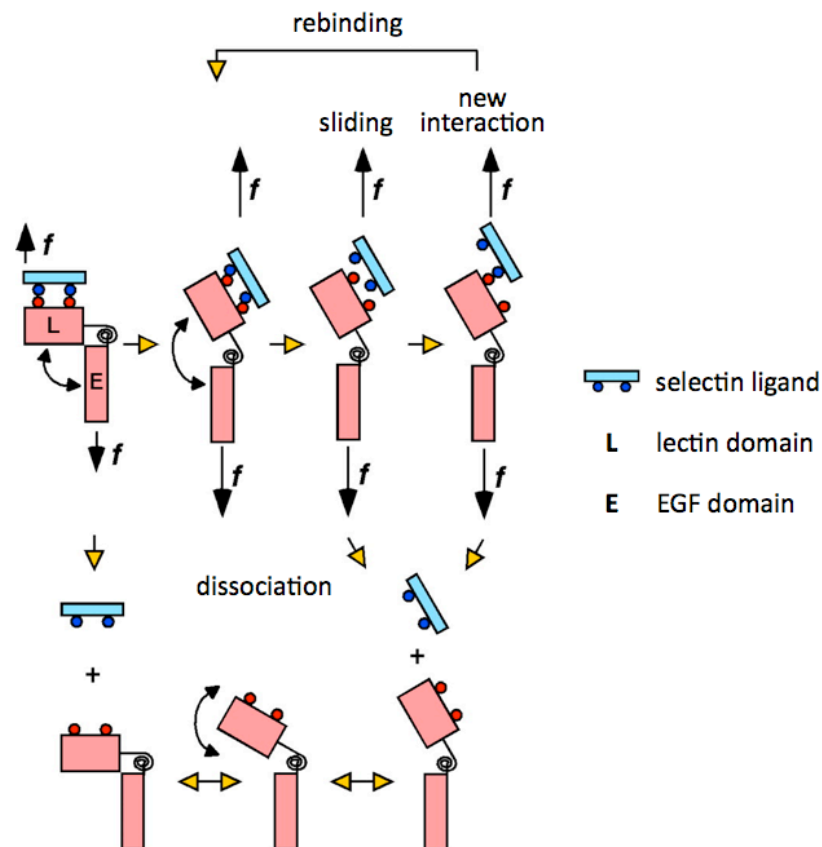
Figure 1-10. Sliding–rebinding model. Adapted from (109).

However, compared to the bent conformation, the crystal structure of extended P-selectin revealed pronounced structural changes throughout the lectin domain. These involve the movement of the Asn83–Asp89 loop towards the sLe^x binding site ("switch 3" in Figure 1-11), which establishes hydrogen bonds with the complexed Ca^{2+} and the sLe^x fucose (8). These observation are the basis of the allostery model, which proposes a single binding site that can adopt high- and low-affinity conformations. The bent and extended protein conformations are assumed to be in equilibrium, whereby the application of directional force (*cf.* Figure 1-11) favors the extended conformation (113). According to the allostery model, the movements of the lectin and EGF domains are allosterically transmitted via 3 switch regions to the Asn83–Asp89 loop. The movements of the switch regions are supported by a rigid part of the lectin domain, whereby the high Trp and Tyr content, two disulfide bridges, and two β-sheets act as "stiffeners" (Figure 1-11) (9). This explanation of allosteric transmission over the lectin domain is supported by a study in which a bulky substituent, *i.e.* the side chain of histidine, favoring the extended conformation was introduced into the lectin domain by a A28H mutation. The mutant had a 2.5-fold higher affinity and a 2-fold lower dissociation rate constant (k_{off}) than the wild type protein, suggesting that there indeed exists

an "allosteric pathway" for the transmission of allostery from the hinge region to the ligand binding site. The differential staining of the mutant provided some indirect evidence for a conformational change induced by the mutation (113).
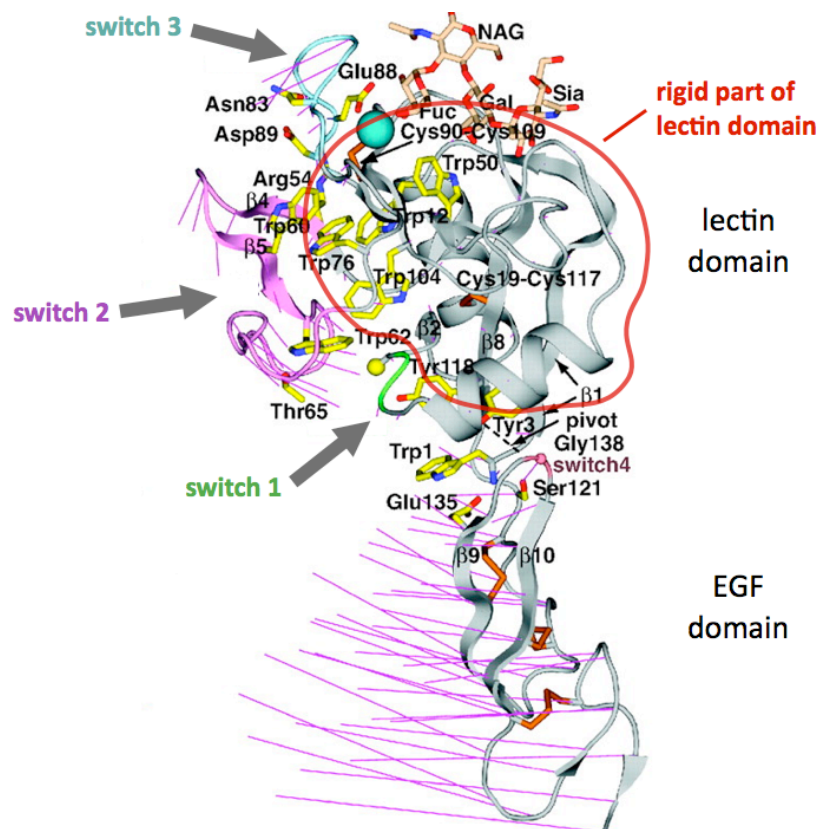
Figure 1-11. Allosteric transmission. The purple lines illustrate the movements of the switch regions. Adapted from (9).

It is noteworthy that the affinity increase described above cannot be explained by the sliding–rebinding model. In the SPR assays used for affinity determination, ligand dissociation is exclusively governed by Brownian motion and not by an external directional force as postulated by the sliding–rebinding model. Thus, unlike suggested by this model, the orientation of the binding site was irrelevant for ligand dissociation in these experiments (111).

The special characteristics of the selectins outlined above might be of considerable relevance for the development of selectin antagonists, especially for rational design approaches involving molecular modeling. On the one hand, the complexity of the system with the possibility of large structural arrangements aggravates predictions, *e.g.* by static docking experiments or even molecular dynamics simulations. On the other hand, these findings may open new possibilities for ligand design, for example by exploiting a potentially favorable

induced fit effect. Furthermore, given that the catch-bond behavior is a prerequisite for function *in vivo*, selectin inhibition could be achieved by allosterically preventing the protein from entering the catch-bond regime, *i.e.* by stabilizing the bent or low-affinity conformation. Allosteric antagonists might avoid some of the diffuculties typically encountered with carbohydrate mimetics (*cf.* Section 1.3.1).

However, structural data are needed to thoroughly validate the models suggested above. The current interpretations are solely based on *predicted* structural features of mutants. Only in the case of the P-selectin–A28H mutation, some indirect evidence was provided by differential antibody staining (113).

1.2.3. Ligand preorganization

Ligand preorganization is an important concept in medicinal chemistry. It was successfully used to rationalize the binding of sLe^x and of antagonists derived from it. According to this concept, the match of a ligand's preferred solution and bioactive conformations leads to an affinity improvement due to a smaller loss of conformational entropy upon binding (In practise, the prediction of the effect of ligand prieorganization on binding enthalpies and entropies is challenging, as demonstrated in a recent systematic study (114).).

Molecular dynamics simulation (MC(JBW)/SD) studies performed by Kolb and Ernst (90, 115) implied that the solution conformation of sLe^x is similar to its E-selectin–bound conformation as determined in transfer-NOE NMR experiments (116, 117) (see Figure 1-13A). For these simulations, two internal coordinates ("acid orientation" and "core conformation") defining the sLe^x conformation were introduced (Figure 1-12). This allows to compare the solution conformations of different ligands. Ligands showing a high probability for conformations in the bioactive window usually exhibited higher affinity to E-selectin, which is a result of the better preorganization in the bioactive conformation.
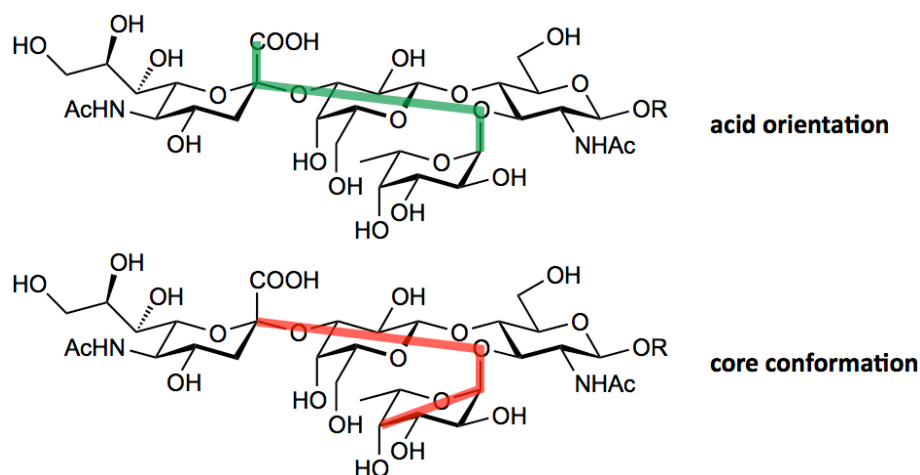
Figure 1-12. Graphical representation of the internal coordinates used for defining sLe^x conformations. After (90).
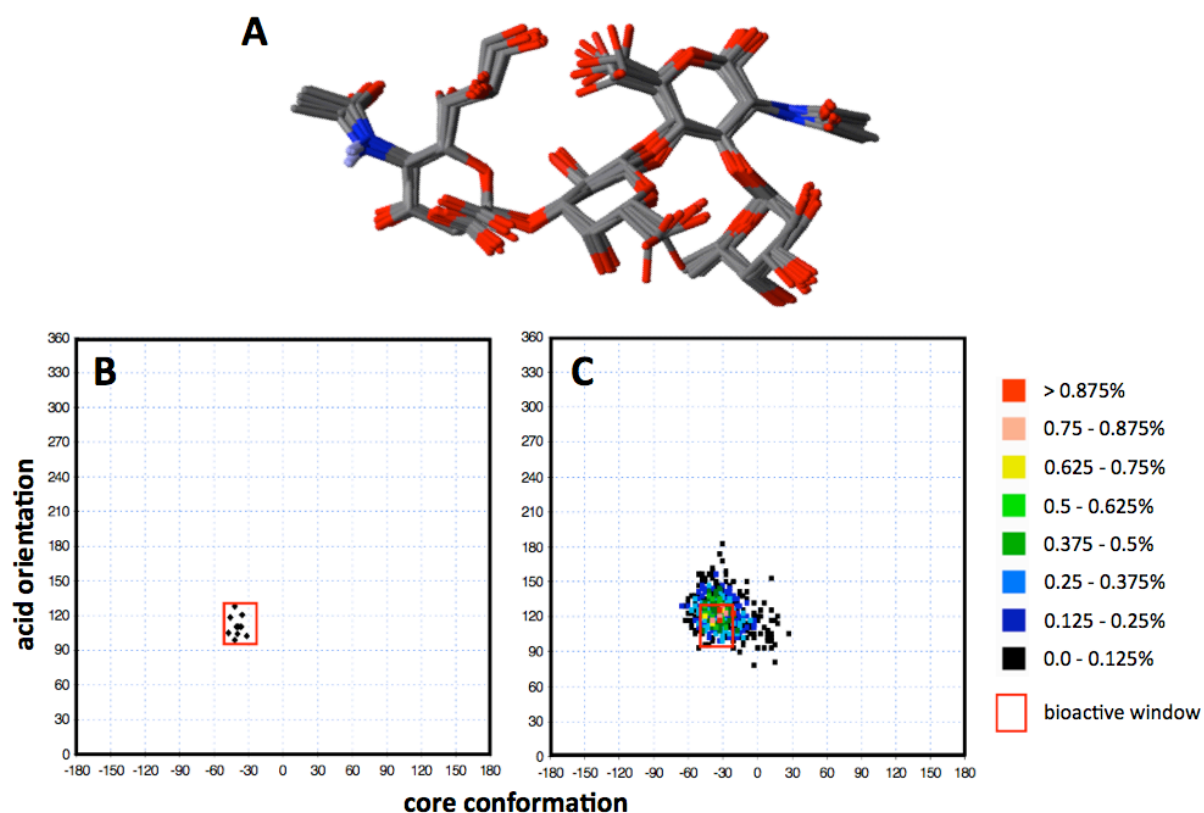
Figure 1-13. A) Bioactive conformation of sLe^x determined by Scheffler *et al.* (transfer-NOE NMR), adapted from (59); B) Representation of A) in an internal coordinate plot using the internal coordinates shown in Figure 1-12; C) solution conformation of sLe^x calculated by MC(JBW)/SD simulation, adapted from (90).

1.3. Selectin antagonists

The applicability of selectin inhibition to treat inflammatory disorders was demonstrated by Cylexin, an sLe^x pentasaccharide. Although not successful as a drug candidate, Cylexin can be seen as an initiator of the efforts directed towards identifying more drug-like selectin antagonists (59).

The use of conceptually different *in vitro* assays aggravates the comparison of standardized IC$_{50}$ values reported in literature (118). Relative IC$_{50}$s (rIC$_{50}$) are more suitable for such comparisons, whereby the IC$_{50}$ of sLe^x is measured along with the analytes. The IC$_{50}$ of the latter is given relative to the one of sLe^x, whereby the rIC$_{50}$ of sLe^x is set to 1. Furthermore, traces of polyanions released from ion exchange resins were found to be potent selectin antagonists (119). As these impurities are difficult to detect with the routine analytical tools, the existence of false-positive results originating from such contaminations cannot be exluded.

1.3.1. Challenges by glycomimetics

Typically, carbohydrate leads do not have drug-like properties (87), which is a result of

- **unfavorable pharmakokinetic properties** leading to low oral bioavailability (due to the high polarity and molecular weight) and a short plasma half-life time (due to fast renal excretion);

- **low hydrolytic and metabolic stability**;

- **low affinity**, especially in the case of lectins. It is a result of the typically shallow and unstructured binding site with a high solvent accessibility. *In vivo*, as functional affinity is often achieved *via* multivalency effects;

- **structural complexity** leading to difficult synthetic access.

These general drawbacks also apply to sLe^x, which has widely been used as a lead structure for the development of selectin antagonists. Furthermore, the dissociation half-life times (t$_{1/2}$) of ligand–selectin complexes are in the range of seconds only (120-122), while ranges of minutes to hours are expected for typical drugs (123, 124). The clinical relevance of a short t$_{1/2}$ (or a high dissociation rate constant, k$_{off}$) are further discussed in Section 1.5.3).

The efforts in the development of selectin antagonists have been targeted at solutions to overcome the typical drawbacks of carbohydrate leads. Two strategies were applied, namely (1) *de novo* design guided by the spatial orientation of sLe[x] in the bioactive conformation and (2) structural modification of sLe[x] using drug-like replacements for L-fucose, *N*-acetyl-D-glucosamine, D-galactose or *N*-acetyl-neuraminic acid (59).

The discussion below focuses on the development of the E-selectin antagonists that are relevant for this work. For a comprehensive overview of selectin antagonists, the reader is pointed at the following reviews: (59, 87, 91, 125-127).

1.3.2. Replacement of Glc*N*Ac and Neu5Ac

As previously mentioned, Glc*N*Ac does not directly interact with the selectins but rather serves as a spacer orienting the fucose and galactose moieties (94, 98, 99). Thus, it lends itself for a replacement by spacers with optimized properties. Among others, (1*R*,2*R*)-trans-cyclohexanediol (128) was a particularly interesting mimic, combining higher activity (threefold compared to sLe[x]), lower complexity and higher lipophilicity.

In the interaction with E-selectin (but not P-selectin), sialic acid is in direct contact to the protein only *via* the carboxyl group. As for Glc*N*Ac, replacements with less structural complexity and polarity were desirable. The modeling tool introduced by Ernst *et al.* (90, 115) (see Section 1.2.3) proved to be useful in the search of mimics, correctly predicting the suitability of (*S*)-cyclohexyl lactic acid. Albeit chemically simple, it is capable of correctly positioning the carboxyl in the bioactive conformation. Furthermore, it was found to be the best among a series of other replacments, *e.g.* (*S*)-phenyl or (*S*)-adamantanyl lactic acid (125, 129) .

The simultaneous replacement of Glc*N*Ac and Neu5Ac led to antagonist CGP69669 (**4**), which showed a tenfold improvement of affinity compared to sLe[x] (Figure 1-14) (90).
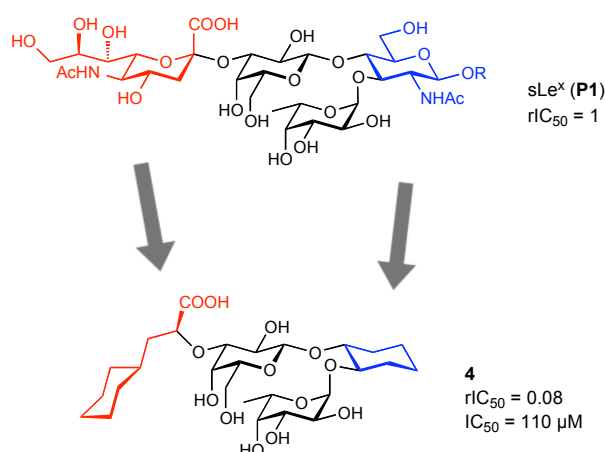
Figure 1-14. Replacement of GlcNAc and Neu5Ac by (1R,2R)-trans-cyclohexanediol and (S)-cyclohexyl lactic acid.

1.3.3. Modifications of the GlcNAc mimic to increase preorganization

The concept of preorganization outlined in Section 1.2.3 was further exploited by the introduction of modicifactions at the cyclohexanediol moiety. Such modifications include equatorial substituents at the former 2-position of GlcNAc, which exert their effect via beneficial steric constraints imposed on the fucose moiety, as was shown by the investigation of interglycosidic NOE effects. These were used to quantify the proximity of the fucose and galactose moieties. As shown in Figure 1-15, the NOEs correlated nicely with the affinity towards E-selectin. Antagonists **7** to **9** show that bulkier substituents do not lead to an additional increase in affinity. Furthermore, the lack of affinity of the flexible antagonist **5** clearly emphazises the importance of ligand preorganization (130).
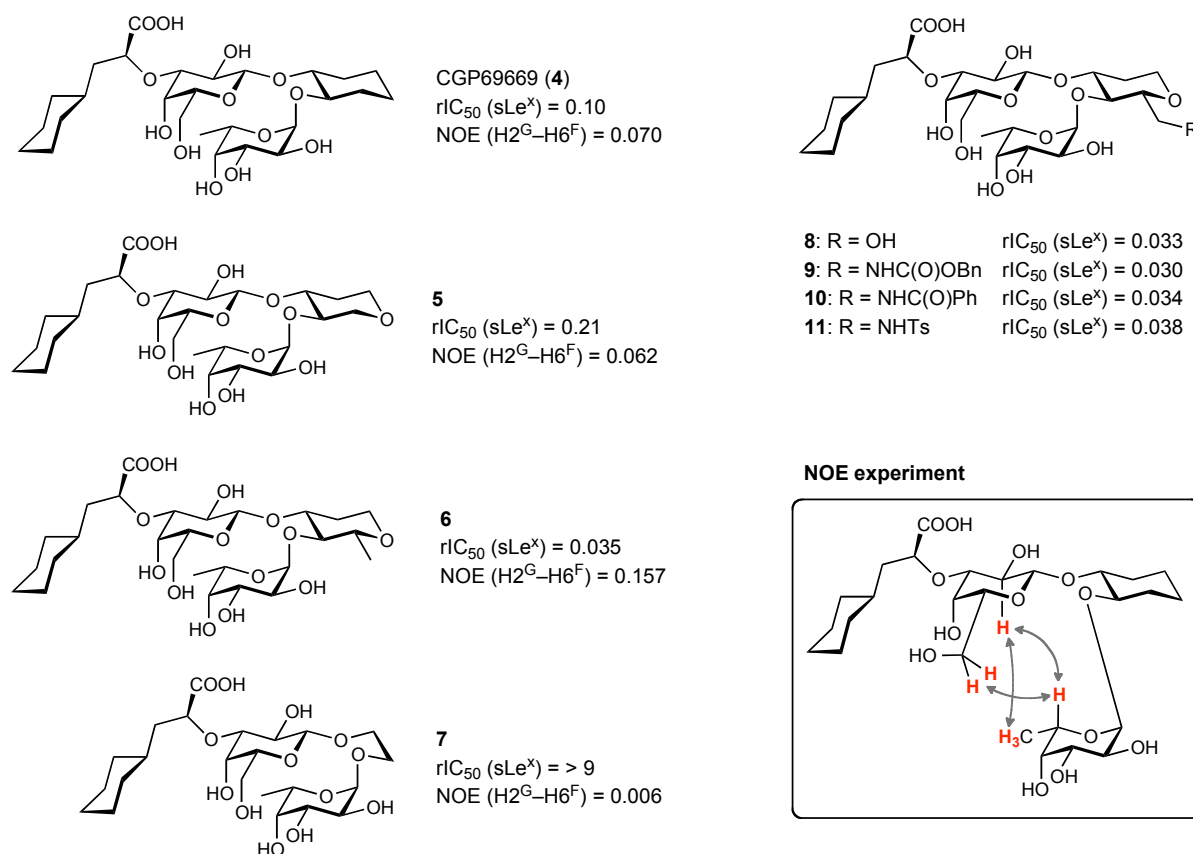
Figure 1-15. Ligand preorganization by substituents on the GlcNAc mimic. After (130).

An in-depth investigation of the substituent effects at the former 2-position of GlcNAc was performed by Schwizer (131, 132), Weckerle (133), Wagner, and Ernst (Table 1-1).

This newer class of antagonists has modified cyclohexanediols as GlcNAc replacements and may carry additional substituents (R^1) at the 2'-position of galactose (see Section 1.3.4) and at the former position of the ring oxygen of GlcNAc (R^3). The latter substitutions tend to increase the affinity, although, based on the crystal structure of sLe^x bound to E-selectin (8), no interaction with the protein is expected at the R^3 position. Instead, these substituents may stabilize the cyclohexanediol chair conformation, which was found to be distorted in antagonists with larger R^2 substituents such as cyclopropyl (131).

Table 1-1 shows that the introduction of a methyl group for R^2 ($\rightarrow$ **12**) causes a 5-fold, the introduction of a benzoate for R^1 ($\rightarrow$**14**) a 2-fold increase in affinity compared to the unsubstituted reference CGP69669 (**4**). The combination of these modifications is additive, *i.e.* derivative GMI-1077 (**15**) is 20 (rIC$_{50}$) to 30 (Biacore) times more potent than the reference. The rigid cyclopropyl substituent at R^2 is not tolerated well and shows a markedly reduced affinity compared to the methyl derivative GMI-1077 (**15**), while smaller and flexible residues such as ethyl (**13**), *n*-butyl (**17**), or methyl propionate (**19**) do not cause a

pronounced affinity change. Also the effect of the methyl ester at R^3 appears to be small. Due to its bulkiness, the *tert*-butyl residue at this position ($\rightarrow$ **21**) is expected to cause a strong preference for the all-equatorial chair conformation. However, **21** binds only weakly to E-selectin, which may result from poor solutility or from unfavorable interactions with the protein. Table 1-1 further illustrates that, generally, there is a good agreement of rIC$_{50}$s and K_D values determined by Biacore.
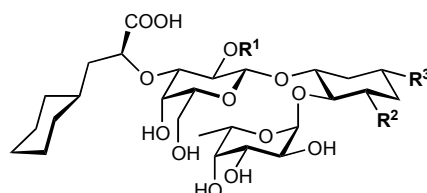
Figure 1-16. General structure of antagonists with modified cyclohexandioles as GlcNAc replacements.

Table 1-1. rIC$_{50}$ values (131) and K_Ds obtained by Biacore (133).

Compound	R^1	R^2	R^3	rIC$_{50}$[a]	K_D [μM][b]
CGP69669 (**4**)	H	H	H	0.080	45
12	H	Me	H	0.016	7.9
13	H	Et	H	0.009	–
14	Bz	H	H	0.040	19
GMI-1077 (**15**)	Bz	Me	H	0.004	1.5
16	Bz	Et	H	0.007	1.5
17	Bz	*n*Bu	H	0.009	–
18	Bz	*c*Pr	H	0.032	5.4
19	Bz	(CH$_2$)$_2$CO$_2$Me	H	0.008	1.6
20	Bz	Me	CO$_2$Me	0.002	1.9
21	Bz	H	*t*Bu	> 10	–

a) sLe^x (IC$_{50}$ = 1 mM; rIC$_{50}$ = 1) was used as reference; b) determined by Biacore from a steady state response fit to a 1:1 binding model.

1.3.4. Substituents at the 2'-position of galactose

Given the beneficial effects of benzoates at the 2'-position, a series of alternative substituents was investigated (Figure 1-17, Table 1-1) (133). Strikingly, a sub-micromolar K_D was measured for the *para*-methoxy–substituted antagonist **22**, which corresponds to a 20-fold increase in affinity compared to the unsubstituted reference **12**. Yet, this finding is not reflected in the rIC$_{50}$ values. Also the non-aromatic substitutions (**23** and **25**) have a pronounced positive effect on binding affinity, comparable to the benzoate.

15: R =   **22**: R =   **23**: R =

24: R =   **25**: R =
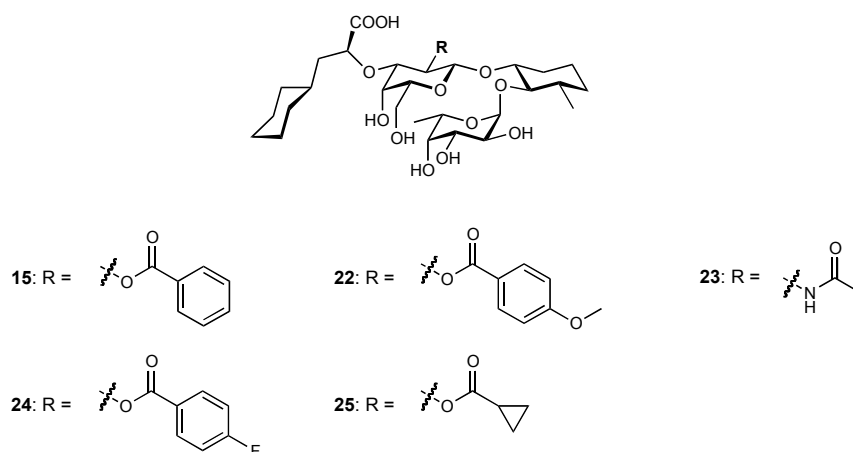
Figure 1-17. Antagonists with different 2'-substituents.

Table 1-2. 2'-modifications

Compound	rIC$_{50}$[a]	K_D [μM][b]
12	0.016	7.9
GMI-1077 (**15**)	0.004	1.5
22	0.006	0.4
23	–	1.2
24	0.005	1.3
25	0.006	2.0

a) sLe^x (IC$_{50}$ = 1 mM; rIC$_{50}$ = 1) was used as reference; b) determined by Biacore from a steady state response fit to a 1:1 binding model.

The affinity gain resulting from the substitutions at the 2'-position of galactose are difficult to rationalize, because crystallographic data for sLe^x (**8**) (see Figure 3-17) suggest that the 2-

hydroxyl group is exposed to bulk solvent, which is supported by docking experiments [unpublished results by Martin Smiesko, University of Basel]. In contrast to this, recent STD NMR studies (133) showed large STD values for the benzoate, indicating a direct interaction with E-selectin (Figure 1-18). Currently, these experiments lead to the conclusion that there is indeed an interaction of the benzoate with E-selectin. However, crystal structure data is needed to definitely elucidate the binding mode of benzoate-substituted antagonists.
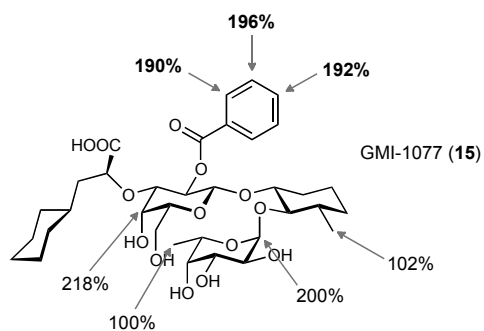
Figure 1-18. Epitope mapping of GMI-1077 (**15**) performed with monomeric E-selectin monomeric E-selectin (LecEGF_CR2).

1.4. Fragment-based drug discovery

In the past 15 years, the lack of productivity in pharmaceutical industry has been a concern. It was argued that short-sighted "strategical" considerations may have made some unhealthy contributions to the lack of innovation. However, the drug discovery process itself was also seen as one of the shortcomings (134, 135). Specifically, it became clear that high-throughput screening (HTS) cannot be reduced to a "game of numbers" (136) with rather blindfold screening of millions of compounds. There may well exist a positive correlation between the hit rate in a screening program and the size of the library being screened, but the screening is just one initial step in the development of a new chemical entity. The generally low hit rates of HTS, especially for challenging drug targets (137), may be further diminished by the high attrition rate of HTS hits in the development process. Often, this is attributed to inappropriate ADME properties of HTS hits (*e.g.* (138)), although this effect is probably overestimated (139). As a concequence, besides optimizing the HTS libraries with regard to drug- or lead-likeness, an alternative method, fragment-based drug discovery (FBDD), attracted the attention of pharmaceutical companies.

1.4.1. Characteristics

The underlying concept of FBDD, namely treating a ligand as a component of distinct parts was already raised in the 1980s (140), but the lack of suitable screening techniques for the detection of the inherently weak fragment affinities prevented the practical application of fragment-based approaches. Consequently, the publication by Fesik *et al.* (141), which describes the development of nanomolar ligands from low-affinity fragments using screening by NMR, is often seen as the first practical application of the concept (136). Since then, the methodologies have evolved, and FBDD has gained the status of a complementary strategy to HTS (142), which has led to a number of leads entering clinical trials (137).

What is responsible for the rapid and quite profound success of FBDD? Below, some of the main characteristics of fragment-based approaches are discussed based on several recent reviews (137, 138, 142-148) and a book (149) on the topic. Overall, FBDD is seen as a promising "new paradigm", which has been successfully applied to a variety of drug targets, including some where HTS failed to afford suitable hits. However, the experience with with FBDD is still quite limited, and the true value of this methodology may not yet be fully assessable (139).

Fragments

According to the Oxford Advanced Learner's Dictionary, a *fragment* is 1) *"a small part or piece broken off sth"*, or 2) *"a small part of sth, not complete in itself"*. In the language of chemistry, the following criteria are relevant for defining a good fragment (142): 1) physicochemical properties, 2) aqueous solubility, 3) molecular diversity, 4) chemical tractability, 5) absence of undesired chemical functionalities, 6) druglikeness (precedence of the structural moieties in oral drugs and natural products), and 7) sampling of priviledged medicinal chemistry scaffolds. In analogy to Lipinski's "rule of five", a "rule of three" was suggested for fragments, which resulted from an analysis of a diverse set of fragment hits (150):

- MW < 300

- number of hydrogen-bond donors ≤ 3

- number of hydrogen-bond acceptors ≤ 3

- ClogP ≤ 3

The chemical universe and complexity

Quite in contrast to HTS, FBDD has haystack-burning[2] properties because it reduces the number of compounds that have to be screened for covering a certain fraction of chemical space. Consequently, a typical fragment library is much smaller (thousands of compounds) than a HTS library (up to millions of compounds). This can be explained by the smaller number of drug-like molecules with 11 or less heavy atoms (approx. 10^9) compared to the total number of compounds (with heavy atom count < 36) that fulfill Lipinsky's rule-of-five (151), which was estimated to be 10^{20} to 10^{200}. A library of 1000 fragments therefore represent 1 millionth of the fragment universe, while 10^6 "large" molecules account for 10^{14} to 10^{194} times (!) less of their universe. Besides being advantageous to pharmaceutical companies the small fragment libraries make screening approaches more accessible to academic research.

The small size of fragments is furthermore advantageous in that less complex molecules are

---

[2] "If you want to find the needle, burn down the haystack". Quote of unknown origin.

more probable to match a receptor binding site without the occurrence of unfavorable interactions (138, 145). In fact, such "foul" parts in a larger molecule could even mask otherwise interesting structural features.

Entropy's soft spot for fragment linking

Fragments usually have K_Ds in the high micromolar to millimolar range (145), a factor of 10^3 to 10^6 lower than what is expected for a typical drug. Yet, linking two such fragments leads to a pronounced gain of free energy, which is much higher than the binding energy contribution from the individual fragments (140, 152, 153). Besides the additivity of the fragments' intrinsic binding engergy ("the Gibbs free energy change for the binding [of a fragment] in the absence of strain and losses in translational and rotational entropy") (140), the linking is highly advantageous by reducing the loss of rotational and translational rigid-body entropy: Upon binding to a target, a ligand has to overcome a significant entropic barrier as it loses 3 translational and 3 rotational degrees of freedom (153). Two individual fragments accordingly lose twice as many degress of freedom upon binding as if they were linked. In terms of energy, this can account for as much as 15 to 20 kJ/mol or 3 orders of magnitude in affinity (154).

These considerations apply to two of the FBDD strategies, fragment linking and fragment fusion (the third stategy, fragment growth, consists of expanding and optimizing a single fragment using rational design) (136). Some pitfalls are associated with fragment linking, which is relevant in the context of this work. In particular, it can be difficult to link two fragments without disrupting the quality of the fragments' individual interactions, and binding sites to which two fragments can bind simultaneously seem to be relatively rare, *e.g.* due to space restrictions (136, 138, 146). In the case of E-selectin or other proteins with a shallow and unstructured binding site (*cf.* Figure 3-17), spatial limitations are probably less of a concern. The fragment-linking is disscussed further in depth in Section 3.5.1.

Flexible linkers can be used to overcome the problem of inappropriate fragment orientation, particularly when no structural information is available. In such cases, the fragment-linking approach is additionally attractive because it allows to conduct target-guided screening procedures (see Section 2). However, the freezing of rotatable bonds in flexible linker is associated with entropic costs (5 kJ/mol per 2 bonds or a factor 10 in affinity). The linker itself may furthermore interact with the protein leading to positive or negative contributions to affinity.

Small but nice

Since the introduction of Lipinski's "Rule of five" (151), molecular weight has become an important criterion in drug development. According to these rules, compounds with a molecular weight < 500 Da have a higher probability of being orally available and thus increasing the size of lead molecules should be well justified, *i.e.* be accompanied by a reasonably high improvement of affinity. Ligand efficiency (LE) is a useful quantity for judging the quality of additions made to a molecule. It relates a ligand potency to size, for example by dividing ligand potency (pIC_{50}, pK_i or ΔG) by the size (*e.g.* number of heavy atoms) (155). Analyses of the evolution of LEs during the lead optimization process essentially showed that the development of fragments proceeds more efficiently, thereby increasing the probability of developing a drug-like compound.

1.4.2. Screening methods

Nuclear magnetic resonance ($\rightarrow$ "SAR by NMR" (141)) was the first analytical technique to overcome the detection problem that initially prevented the advancement of fragment-based discovery strategies. In the meantime, MS, X-ray crystallography, SPR, and ITC have been added to the fragment screening toolbox (156). Figure 1-19 gives an overview of these technologies in the "fragment-to-lead process" (147).

	Fragment hit identification			Fragment to hit
	Fragment library (number of samples which can generally be evaluated)	**Fragment screening** (throughput)	**Fragment hits prioritization** (type of information)	**Conversion of fragment hits to leads**
Crystallography	1K Small size	Low throughput	• 3D structure information regarding fragment-protein complex (this information is also utilized for fragment hits to leads conversion in structure-based drug)	
NMR	1K		• Information regarding location of fragment-protein interaction (for protein-based NMR screening)	
ITC	1 – 2K		• Thermodynamic properties of binding	
SPR	2 – 5K		• Kinetic properties of binding	
HCS	5 – 30K Large size	High throughput	• Enzyme inhibitory activity	

Figure 1-19. Crystallography, NMR, ITC, SPR and HCS in FBDD. HCS: high-concentration screening (functional and direct binding assays). From (147).

NMR-based screening

In general, NMR-based screening approaches have the advantage of producing fewer false positive hits and of providing some (but limited) information on the binding mode and/or location of fragments. Although NMR has a comparably low intrinsic sensitivity, its high dynamic range (*i.e.* the range of fragment affinities that can be detected) allows one to identify low-affinity fragments that are not be detectable with other screening methods (157). The often large amounts of protein needed represent a drawback, however (156). The methodologies can be divided into target- and ligand-based (144, 147), where signals of the protein and the ligands are observed, respectively.

Protein-based detection, of which "SAR by NMR" (141) is an example, relies on chemical shift perturbations induced by ligand binding and can detect interactions in the nano- to millimolar affinity range. It has the advantage of providing precise information about the location of the ligand binding site. On the other hand, it may require a relatively high concentration of labeled protein and of the ligands, which can be limited by low solubility of the protein or the ligands. Yet, there exist improvements of this technology, *e.g.* employing cryogenic NMR probes, ^{13}C labeling of methyl groups or protein deuteration, which allows the investigation of larger proteins at lower concentrations, accompanied by higher

throughput and by mor precise structural information (147, 157).

Ligand-based methods include WaterLOGSY, STD, and relaxation rate experiments (157). Generally, they require smaller amounts of protein and abolish the need for isotopic labeling, but deliver less structural information. Furthermore, the detection of high-affinity ligands ($K_D \leq 10^{-8}$ M) can be impaired by slow off rates, causing these ligands to be in the slow-exchange limit for chemical shifts and relaxation times (158). This limitation can be overcome by competition experiments or by the use of ^{19}F-labeled "spy" molecules (147). If one of the fragments or a binding site is already known, the introduction of a spin label allows the detection of ligands that bind simultaneously and in the vicinity of the existing ligand or the binding site (see Section 3.5.1) (159, 160). The spin-label also allows to derive the relative orientation of a fragment with respect to the spin label (161). The spin-label approach is further outlined in Section 2.

An overview of the use of NMR in FBDD is given in Figure 1-20.
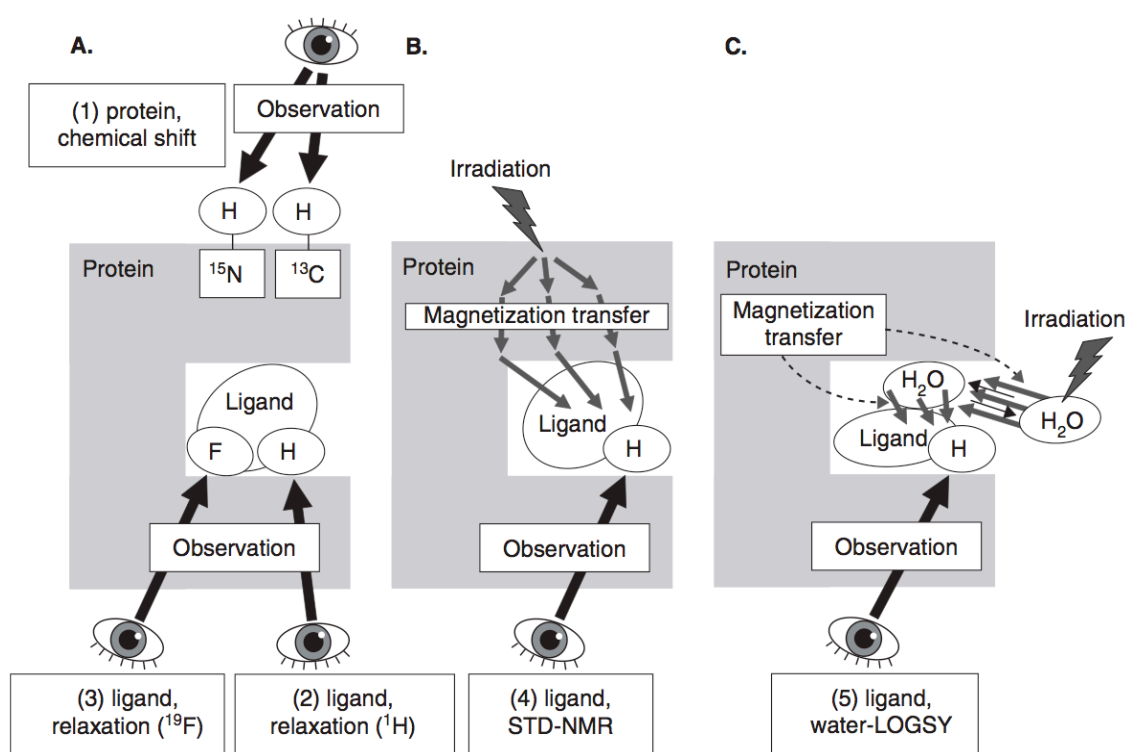
Figure 1-20. Frequently used NMR approaches for FBDD. From (147).

X-ray crystallography

The major advantage of X-ray crystallography is its inherent ability to provide very detailed structural information about fragment hits that are complexed with the target protein. The need for protein crystals has some inherent disadvantages, such as the relatively high protein

consumption, lower throughput or high technical hurdles. The application of robotics and analysis software as well as the advances in X-ray technology have helped increase the throughput, however. In addition, the information gained from the crystals can be vital for developing the fragments into leads and may thus compensate the initial slowness. One can discriminate between co-crystallization and soaking methods. The latter, where fragments are soaked into pre-formed crystals, is especially suited for high-throughput applications and requires lower protein amounts. In contrast, co-crystallization is tolerant to large induced-fit changes of protein conformation that may remain hidden in pre-formed crystals (147). Nevertheless, conformational changes of the target protein were also observed in ligand soaking screens (162).

Surface plasmon resonance

SPR screening is particularly beneficial in terms of protein consumption and the potentially high information content. In one measurement, k_{on}, k_{off} and K_D can be determined. Measurements at different temperatures could furthermore be used to obtain thermodynamic parameters. Such information is valuable in the decision-making for further development of the fragment hits (157). At the same time, throughput of SPR is reasonably high due to the existence of multiple biosensor channels or its use in microarry assay formats (156). A biosensor channel can additionally serve as reference cell, thus allowing the distinction of specific and nonspecific binding. One limitation of SPR is fragment solubility, which can prevent the detection of low-affinity fragments, especially for large proteins (157, 163).

Isothermal titration calorimetry

Owing to its low throughput, ITC is, at present, predominantly used for the thermodynamic evaluation of fragment-screening hits (There is a mention of the use of ITC as a "popular primary screening technique" in the review of Niimi *et al.* (147), referring to a conference report). The low affinity of fragments may necessitate competitive experiments for a full characterization (164). However, ΔH can also be measured for weakly-interacting fragments, thus allowing the incorporation of enthalpic efficiency measures into the decision making. For the selection of fragment hits, it can be advantageous to know whether the fragment's interaction is enthalpically or entropically driven, because it is generally more difficult to increase affinity via enthalpic interactions. Therefore, starting from a fragment with favorable enthalpic interactions may be preferrable (165).

Mass spectrometry

Despite the advantageous features of MS, *e.g.* the lack of analyte labeling, the high sensitivity and specificity and the possibility to perform qualitative or quantitative affinity analyses (166), examples of MS-driven fragment screening are rare. In 2005, an "SAR by MS" approach was described for small molecules binding to hepatitis C virus RNA (167). Here, a low-affinity hit (K_D > 100 µM) was identified and further improved ($\rightarrow$ K_Ds: 0.72-17 µM) with the assistance of MS.

1.5. Optical biosensors exploiting surface plasmon resonance

For simplicity, the *optical biosensors exploiting surface plamon resonance* are below referred to as *Biacore* (BIA: **b**iomolecular **i**nteraction **a**nalysis; Biacore is a trademark of GE healthcare. For the analysis of the antagonists presented in this work, a Biacore® 3000 system was used).

1.5.1. Technology

Surface plasmon resonance (SPR) is a phenomenon ultimately resulting from a light beam passing through two non-absorbing media of different refractive index. The occurrence of SPR leads to absorption of the incident light, while it is reflected when there is no SPR effect. In a Biacore instrument (*cf.* Figure 1-21), the first medium consists of a gold-coated glass chip (sensor chip), while the second medium is made up by the target structures (usually protein) immobilized on the sensor chip and floating in buffer. Given this setup, the occurrence of SPR, *i.e.* absorption, depends on the light's incident angle and on the refractive index of the second medium. The latter changes upon ligand binding to the target structures on the chip, whereby the strength of the effect is related on the ligands' mass. As a consequence, ligand binding induces a shift of the SPR angle, which can be detected and used for the real-time monitoring of ligand binding. The shift of SPR angle is expressed in resonance units (RU), 1 RU corresponding to approximately 10^{-4} °.
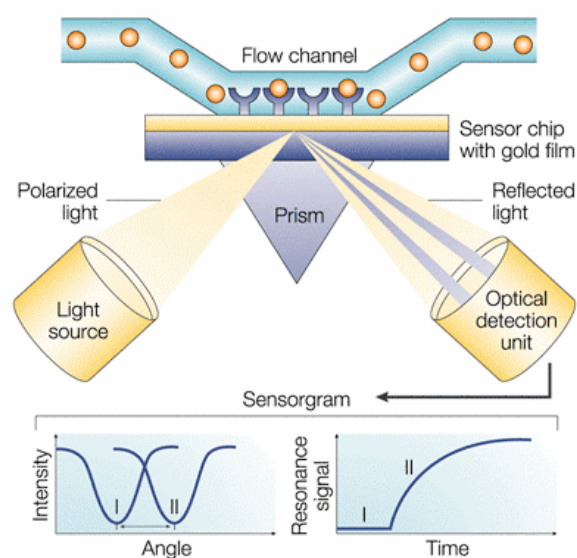
Figure 1-21. Setup of an optical biosensor. Adapted from (168).

Appropriate immobilization of the target is crucial to a Biacore experiment, as the target's binding properties must be retained. A summary of different immobilization techniques is given in (168). In the present context, the capture assay, as shown in Figure 1-22, is of particular relevance. The target is captured in a site-specific manner by a suitable capturing molecule (*e.g.* an antibody) linked to a dextrane matrix. Here, the antibody is chemically linked *via* amine coupling, the most frequently used immobilization technique (168).
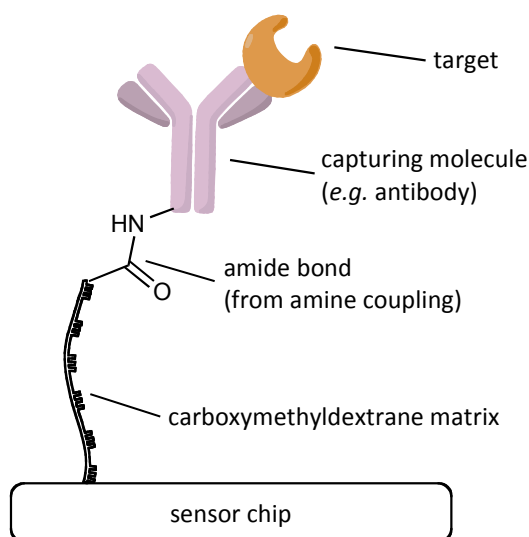
Figure 1-22. Schematic representation of the capture assay relevant in the present context.

1.5.2. Kinetic evaluation

In Figure 1-23, the course of the resonance signal during a typical Biacore experiment is illustrated (→ sensorgram). Four phases can be distinguished: 1) An association phase (ligand is floated over the sensor surface, resulting in its net association to the immobilized target), 2) a steady state (not shown; equilibrium of ligand binding and dissociation, 3) a dissociation phase (the ligand supply in the buffer is stopped, leading to net ligand dissociation, and 4) a regeneration phase (the original state of the surface is re-established). The maximum equilibrium response (R_{eq}) measured during an injection cycle depends on the concentration of the ligand that was injected.
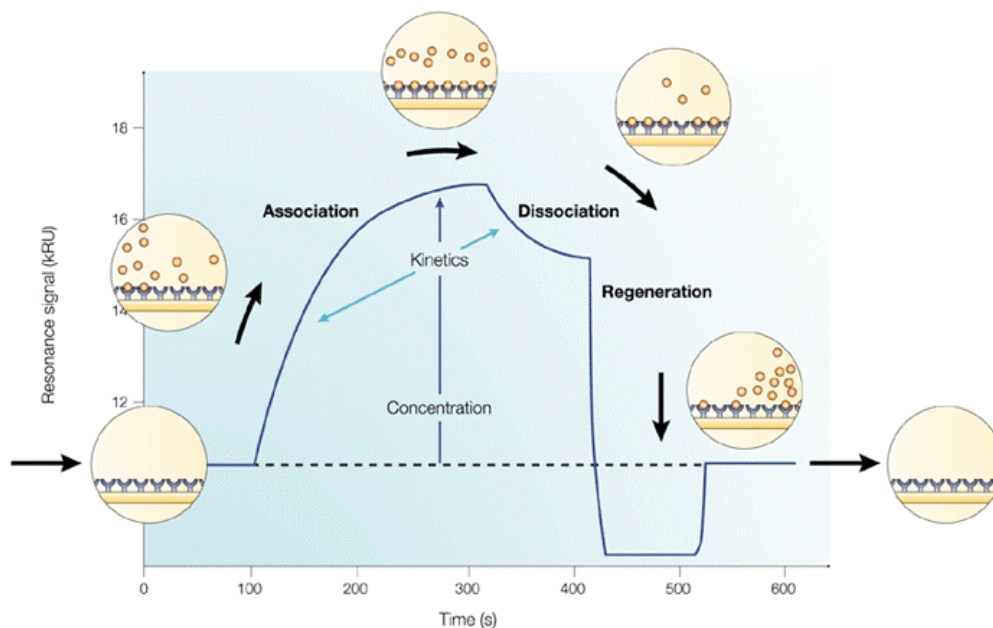
Figure 1-23. Biacore sensorgram. Adapted from (168).

The data points of the sensorgram can be fit to a 1:1 binding model, as represented by Equation 1 (k_{on}: association rate constant; k_{off}: dissociation rate constant):

$$A + B \xrightleftharpoons[k_{on}]{k_{off}} A{-}B$$

(1)

The K_D can be directly derived from k_{on} and k_{off} *via* Equation 2,

$$K_D = \frac{k_{off}}{k_{on}}$$

(2)

or from the steady state signals at different concentrations (saturation binding plot, equation not shown).

k_{on} and k_{off} further allow the determination of the ligand–receptor half-life time ($t_{1/2}$, Equation 3) or the target residence time (τ, Equation 4). Although they are not identical by definition, the terms half-life time and residence time are often used interchangeably.

$$t_{1/2} = \frac{\ln 2}{k_{off}}$$

(3)

$$\tau = \frac{1}{k_{off}}$$

(4)

33

With sensorgrams recorded at different temperatures, van't Hoff thermodynamic analyses can be performed, giving access to interaction enthalpies and entropies (169).

1.5.3. The relevance of binding kinetics in drug discovery

In vivo, the ligand concentration a protein is exposed to is not constant, *e.g.* due to ligand metabolism and excretion (ligand depletion). Therefore, the sole investigation of K_Ds during *in vitro* compound evaluation may be oversimplified because it does not reflect *in vivo* pharmacodynamics. For example, target residence time was found to impact efficacy, efficacy duration, target selectivity, and even *in vitro* cellular assays. Taken together, the relevance of target residence time for the *in vivo* situation makes Biacore a valuable tool for the early selection of lead candidates with properties that are beneficial for a drug (123, 124).

The relevance of binding kinetics for the development of E-selectin antagonists is further discussed in Section 2.

1.6.   In situ click chemistry

The fragment-screening with a TEMPO spin label allows to identify a second-site ligand with a minimum of structural information (160). However, the lack of structural information is a drawback for the design of a suitable linker connecting the fragments. This problem can be addressed by target-templated synthesis, where the structural information contained in the protein is used to guide a chemical reaction towards products having a structure complementary to the protein. In general, this selection process can be under thermodynamic or kinetic control, and the corresponding approaches are termed *in situ* dynamic combinatorial chemistry (DCC) or *in situ* click chemistry, respectively (170).

In DCC, dynamic combinatorial libraries (DCLs) are generated from the reversible but covalent reactions between fragments carrying suitable functional groups. The addition of target protein to such a library may remove complementary structures from the equilibrium and thus favor the formation of the most active products. Huc and Lehn (171) first demonstrated the applicability of the DCC approach by using it for the identification of carbonic anhydrase inhibitors formed from aldehyde and amine fragments. Since then, the approach has been applied successfully in a number of applications (172, 173). However, the DCC approach often employs strong nucleophilic and electrophilic functional groups, which may question its bioorthogonality in certain cases (170).

Also when using *in situ* click approaches, where the target protein (ideally (174)) selects complementary products by accelerating the reaction between the corresponding substrates (→ kinetic target-guided synthesis (175); *cf.* Figure 1-24), the degree of bioorthogonality depends on the reactants used. For example, Huc and Nguyen (176) generated carbonic anhydrase inhibitors from a thiol and an α-chloroketone in the presence of the target.
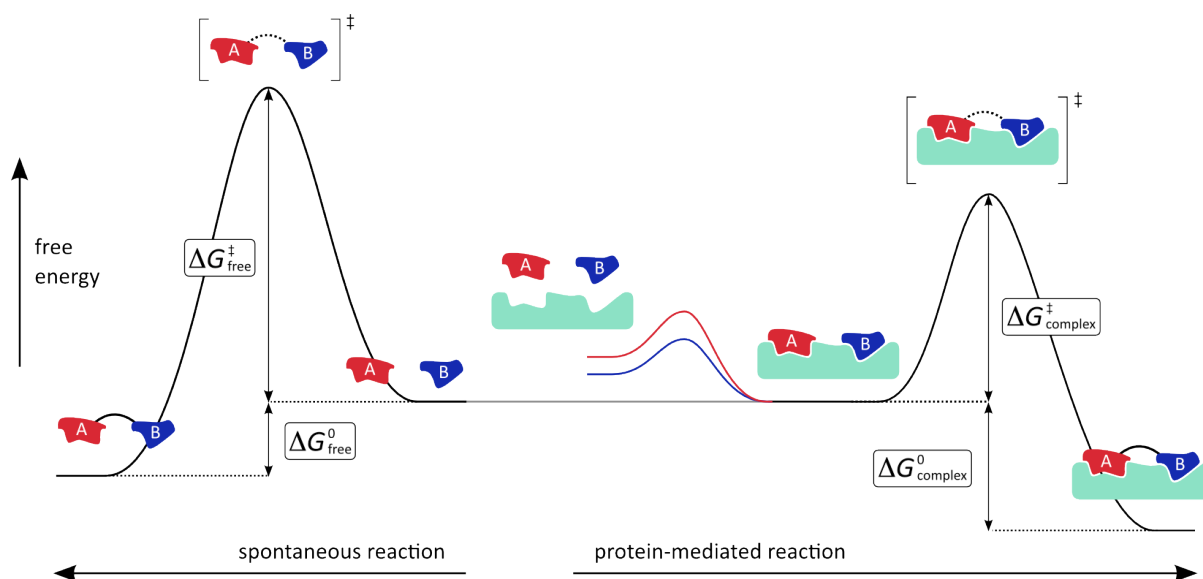
Figure 1-24. Free energy diagram of a spontaneous (left) and a target-guided (right) linking reaction. Simultaneous binding of ligands **A** and **B** to a template reduces the activation energy ($\Delta G^{\ddagger}_{complex} < \Delta G^{\ddagger}_{free}$) of a given coupling reaction and thus increases its rate. Ideally, but not necessarily, the product formed in the template-assisted reaction is tightly bound to the template, and thus ($\Delta G^{0}_{complex} > \Delta G^{0}_{free}$). After (174).

However, Sharpless and coworkers (177) introduced an *in situ* click approach devoid of these problems. It relies on the Huisgen 1,3-dipolar cycloaddition (178) between an alkyne and an azide, two functional groups unlikely to react with biomolecules under physiological conditions. The cycloaddition is very slow at room temperature, but can be accelerated by a suitable supramolecular template, *e.g.* a protein. The usability of the *in situ* click procedure has been demonstrated in several publications with different protein targets. In the case of acetylcholinesterase, inhibitors with low pico- to femtomolar K_{D}s were discovered (177, 179, 180), and in the case of bovine carbonic anhydrase II (181), Kolb, Tseng *et al.* (182) demonstrated the applicability of methodology in a microfluidic setup, and Heath *et al.* (183) discovered nanomolar-affinity peptide ligands of carbonic anhydrase *via* an iterative screening based on a one-bead–one-compound (OBOC) library. HIV-1 protease was targeted by Elder, Fokin *et al.* (184), who observed selective formation of a (previously known) nanomolar-affinity triazole antagonist. Further targets include DNA (185), chitinase (186), and, as a most recent example, myelin associated glycoprotein (MAG) (160). For a more detailed overview of these examples, the recent review by Finn *et al.* (187) is recommended.

In principle, the applicability of the Huisgen 1,3-dipolar cycloaddition for target-guided synthesis was demonstrated already in 1983 by Mock *et al.* (188). They found that catalytic amounts of cucurbit[6]uril strongly accelerate the alkyne–azide cycloaddition and render the

reaction regiospecific, leading to the exclusive formation of *anti* isomer **27** (Figure 1-25). The authors concluded that simultaneous binding and encapsulation of **26** and **27** preoriented the alkyne and azide moieties, thereby reducing entropic costs. Additionally, the investigation of binding constants suggested that the simultaneous binding of the substrates induces some strain into the substrates, which further contributed to the rate acceleration (188, 189).

A

B   **C**
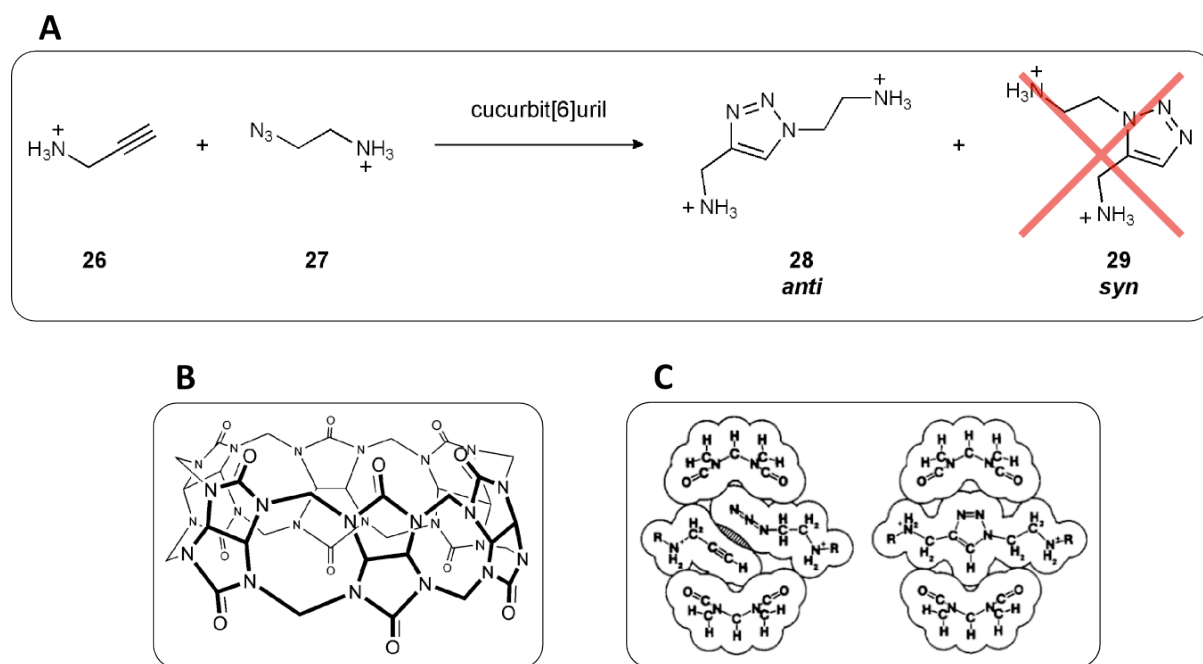
Figure 1-25. A) Kinetic study of triazole formation mediated by cucurbit[6]uril; K_D values: **26**: 0.65 mM, **27**: 2.5 mM (188, 189); B) Cucurbit[6]uril. An ammonium cation as in **26** and **27** can hydrogen bond to the urea carbonyl oxygens. Sufficiently small alkyl residues can be accomodated within the cavity mediated by the hydrophobic effect (190). Reproduced from (191) (modified); C) Conjectured cross-sectional representations of the cucurbituril–substrate and –product complexes (outlines: van der Waals radii) illustrating the strain-induced compression of the substrates (shaded region). Image taken from (189).

1.7. Triple quadrupole mass spectrometry (QQQ-MS)

For the analysis of the *in situ* click experiments (*c.f.* chapter 3.6), a triple quadrupole LC-MS equipped with an electrospry ionization (ESI) source was used. Quadrupole mass analyzers are particularly suitable for quantification (192) and offer the possibility to perform tandem mass spectrometry (MS/MS), which can be useful for the analysis of the products formed in an ISC experiment (→ Section 3.6.1.2). Figure 1-26 shows a schematic representation of the triple quadrupole MS available at the Institue of Molecular Pharmacy. In the present context, the three quadrupoles (the second "quadrupole" is actually a hexapole) are of particular interest.
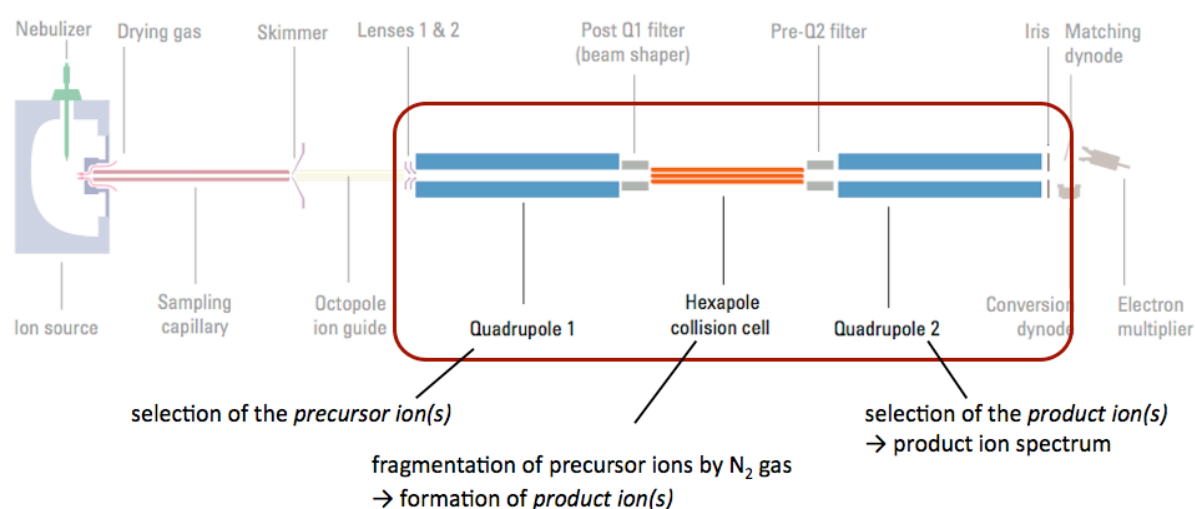
Figure 1-26. Schematic representation of the Agilent 6410 triple quadrupole MS.

A quadrupole is a parallell arrray of four circular or hyperbolic rods. Opposite pairs of rods are connected, and direct current (DC) negative potentials are applied to one, direct current positive potentials to the other pair. These potentials are superimosed by a radiofrequency (RF) potential, which is phase-shifted by 180° from one pair to the other. This setup allows to generate an oscillating electric field, which induces an oscillating movement in ions that are accelerated through the quadrupole. For a given m/z ratio, only a specific ratio of DC and RF voltages (→ Mathieu stability diagram) leads to a stable trajectory through the quadrupole. Thus, by setting the quadrupole to specific DC/RF voltage ratios, a quadrupole acts as a filter for ions with a specific m/z ratio. In the present case, quadrupoles 1 and 3 (Q1 and Q3) act as such mass filters.

Q2, on the other hand, serves as a collision cell where ions selected by Q1 are fragmented in a process called collision-induced dissociation (CID). The fragmentation is usually achieved

by introducing an inert gas such as N_2 into the collision cell. Upon collisions with the gas molecules, the kinetic energy of the ions is converted into internal energy, which may eventually lead to bond cleavage. Equation 5 shows this process, in which a product or daughter ion m_d^- is generated from the precursor or parent ion m_p^-. Neutral fragments (m_n) may also be formed.

$$m_p^- \rightarrow m_d^- + m_n \tag{5}$$
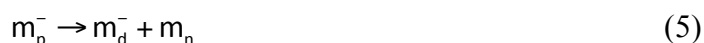
The charged product ion is passed on to Q3, where a second m/z filtering can be applied. The sequential arrangement of the three quadrupoles allows for different scan modes, which can extract different kinds of information from the analyzed sample. For the present work, product ion scan and selected reaction monitoring (Figure 1-27A and Figure 1-27D) were used to identify suitable fragments that could be used for the monitoring of the *in situ* click experiments based on these fragments ($\rightarrow$ product ion scan, *cf.* Section 3.6.1.2). Figure 1-27E shows the selected ion monitoring (SIM) mode. Here, neither Q1 or Q2 are operational, and only Q3 serves as a mass filter. This allows a detection with high sensitivity and selectivity.
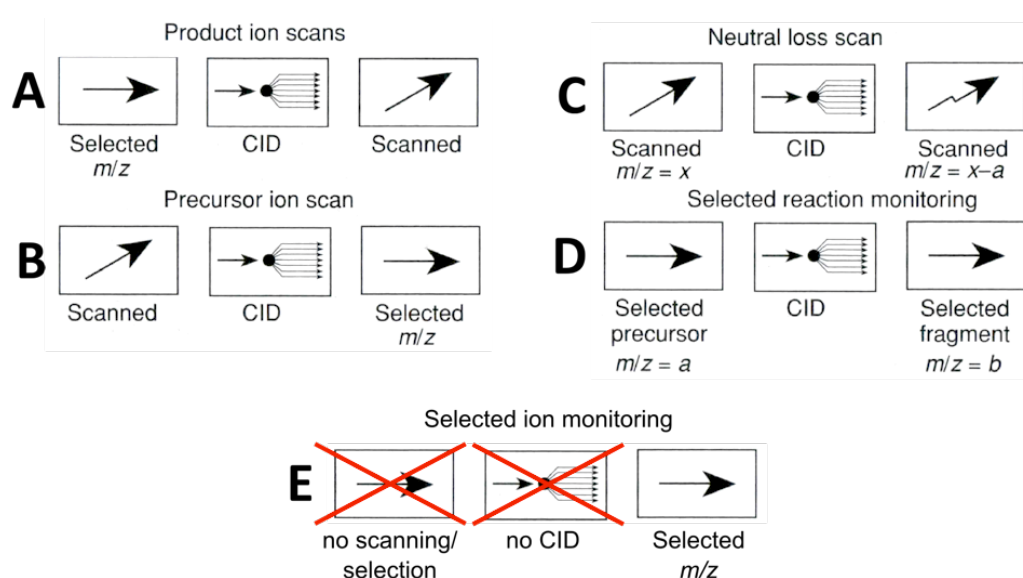
Figure 1-27. Main scan modes in (tandem) mass spectrometry. A) product ion scan, B) precursor/parent ion scan, C) neutral loss scan, D) selected reaction monitoring, E) selected/single ion monitoring. Reproduced from (193) (modified).

Clearly, QQQ-MS is not only defined by the nature of the mass analyzer, which was discussed here due its direct relevance for the different experiments that were performed. A more detailed discussion of other aspects, *e.g.* the ionization technique, is thus beyond the scope of this work.

2. Results and Discussion (paper manuscript)

This part of the thesis is presented in the form of a paper manuscript forming a discrete part of the thesis. This includes compound numbering, which restarts at 1 in this section. In the other parts of the thesis, compounds appearing in this chapter are referred to as **"P1234"**.

Nanomolar E-selectin Antagonists: A Fragment-based Approach

Jonas Egger, Céline Weckerle, Brian Cutting, Oliver Schwardt, Katrin Lemme, Beat Ernst[*]

Institute of Molecular Pharmacy, Pharmacenter, University of Basel, Klingelbergstrasse 50, CH-4056 Basel, Switzerland

[*] To whom correspondence should be addressed: Prof. Dr. Beat Ernst, Institute of Molecular Pharmacy, Pharmacenter, University of Basel, Klingelbergstrasse 50, CH-4056 Basel, Switzerland; Tel: +41 61 267 15 51, Fax: +41 61 267 15 52; E-mail: beat.ernst@unibas.ch.

Contributions:

Jonas Egger: Synthesis, writing of the manuscript; Céline Weckerle: NMR screening, SPR measurements, writing of the manuscript; Brian Cutting: NMR screening, writing of the manuscript; Oliver Schwardt: HRMS measurements, writing of the manuscript; Katrin Lemme: expression of E-selectin.

Keywords:

Fragment-based drug discovery, selectins (glycoproteins), NMR spectroscopy, Biacore, triazole formation

Abbreviations: CRD, carbohydrate recognition domain; DBU, 1,8-Diazabicyclo[5.4.0]undec-7-en; DCM, dichloromethane; DMF, dimethylformamide; DMSO, dimethylsulfoxide; DMTST, dimethyl(methylthio)sulfonium triflate; DPPA, diphenylphosphoryl azide; FBDD, fragment-based drug discovery; HBTU, 2-(1H-Benzotriazole-1-yl)-1,1,3,3-tetramethyluronium hexafluorophosphate; HOBt, 1-hydroxybenzotriazole; IgG, immunoglobulin; ITC, isothermal titration calorimetry; NMR, nuclear magnetic resonance; RU, resonance unit; Siglecs, sialic acid binding immunoglobulin-like lectins; sLeX , sialyl LewisX; SPR, surface plasmon resonace; TBAB, tetrabutylammonium bromide; TBAF, tetrabutylammonium fluoride; TEMPO, 2,2,6,6-tetramethylpiperidin-1-oxyl; TFA, trifluoroacetic acid; THF, tetrahydrofurane;

Abstract

Selectins, a family of C-type lectins, play a key role in inflammatory diseases (*e.g.* asthma or arthritis). However, the millimolar affinity of sialyl Lewis^x, which is the common tetrasaccharide epitope of all physiological selectin ligands, has been a major obstacle to the development of selectin antagonists for theraptic applications. In a fragment-based approach guided by NMR, ligands binding to a second binding site in close proximity to a sLe^x mimic were identified. A library of antagonists obtained by linking the sLe^x mimic with the best second-site ligand *via* triazole linkers of different length was evaluated by surface plasmon resonance. The detailed analysis of the five most promising candidates revealed antagonists with K_D values ranging from 30 to 89 nM. In contrast to carbohydrate-lectin complexes with half-lifes ($t_{1/2}$) generally in the second range or even below, these fragment-based selectin antagonists exhibit $t_{1/2}$ of several minutes. They exhibit a promising starting point for the development of novel anti-inflammatory drugs.

Introduction

Extravasation of leukocytes from the bloodstream into surrounding tissues is a crucial step in inflammation. Selectins, a family of calcium-dependent lectins (E-, L-, and P-selectin), mediate the first step in this process, the tethering and rolling of leukocytes on the endothelial surface.[1] This rolling is a prerequisite of the subsequent firm attachment mediated by the interaction of integrins with members of the IgG superfamily. In the final step, leukocytes extravasate and migrate to the site of inflammation. Excessive infiltration of leukocytes into the adjacent tissue leads, however, to its destruction as has been observed in many inflammatory diseases such as myocardial ischemia-reperfusion injury, asthma or rheumatoid arthritis. In these cases, E-selectin–mediated recruitment of leukocytes is associated with the etiology or progression of the disease.[4] Furthermore, tumor cells that extravasate out of the bloodstream use the selectin pathwayto metastazise.[3] Owing to their specific way of action, E-selectin antagonists have therefore untapped potential for the treatment of inflammatory and related diseases as well as cancer.[3,4] A recent example is the pan-selectin antagonist GMI-1070,[4a] which was shown to reverse acute vascular occlusions in sickle cell mice.[5] It has successfully completed clinical phase 1 studies, and its efficacy is currently investigated in humans with sickle cell disease.[6]

Sialyl Lewis^x (**1**, sLe^x, Figure 1) is the minimal carbohydrate epitope recognized by E-selectin.[7] Like carbohydrate–lectin interactions in general, the sLe^x/E-selectin interaction is characterized by a low binding affinity (IC$_{50} \approx 1$ mM[8]) and a short half-life (t$_{1/2}$) in the range of seconds,[4] a result of the shallow and solvent-accessible binding site of E-selectin. While this behavior is necessary for the selectin's physiological function,[14] it is a challenge for the development of selectin antagonists. Although numerous contributions presenting mimetic structures with considerably improved affinities have been published,[9] E-selectin antagonists with high affinities and slower dissociation rates[16] are still required.

The concept of fragment-based drug discovery (FBDD) has led to a paradigm shift in drug discovery.[17] One of the most striking features of FBDD is the fact that potent ligands can be obtained from low-affinity fragments, provided they are properly linked. The observed high affinity can be rationalized by the additivity of intrinsic binding energies of the fragments[22] and the loss of translational and rigid-body entropy costs upon fragment linking.[23] Fragment screens can be performed using analytical technologies that are broadly available, *e.g.* nuclear magnetic resonance (NMR), surface plasmon resonance (SPR), or isothermal titration calorimetry (ITC).[17d] Finally, suitable linkers can be identified by various procedures, *e.g.* (i) by rational design, (ii) by an *in situ* click chemistry approach as described by Sharpless and coworkers[28] or (iii) by the synthesis and biological screening of a classical ligand library.

Recently, we described the fragment-based discovery of high-affinity ligands for the myelin-associated glycoprotein (MAG), a member of the sialic acid binding immunoglobulin-like lectin familiy (Siglecs).[25] For this purpose, a suitable fragment (second-site ligand) was linked *via* triazole formation to a known carbohydrate-mimetic (first-site ligand, $K_D = 134$ μM) resulting in a new ligand with a more than 700-fold improved affinity ($K_D = 190$ nM). Because the challenges in the development of selectin antagonists are similar to those encountered with MAG (shallow, unstructured binding site),[4] a similar fragment-based approach was applied for the improvement of existing E-selectin antagonists.

Results and Discussion

Our starting point was the sLe^x mimic **2**, exhibiting low micromolar affinity for the carbohydrate recognition domain (CRD) of E-selectin (Figure 1).[10a] For the identification of second-site ligands binding in close proximity of the sLe^x mimic **2**, a low-molecular-weight

fragment library was screened by NMR. Binding was detected based on the accelerated transverse magnetization decay experienced by fragments bound to the target protein.[26] In a second step, these fragments were then subjected to spin-spin relaxation NMR experiments,[27] which allow to select those second-site hits that bind in the vicinity of the first-site ligand equipped with a spin label. Furthermore, the distance-dependence of the paramagnetic relaxation enhancement was exploited to obtain information about the relative orientation of the second-site ligands with respect to the first-site ligand.[BC1] In the last step, similar to our work on MAG,[25] the [3+2]-Huisgen cycloaddition[27a] of azides and alkynes was applied for linking first-site and second-site ligands.
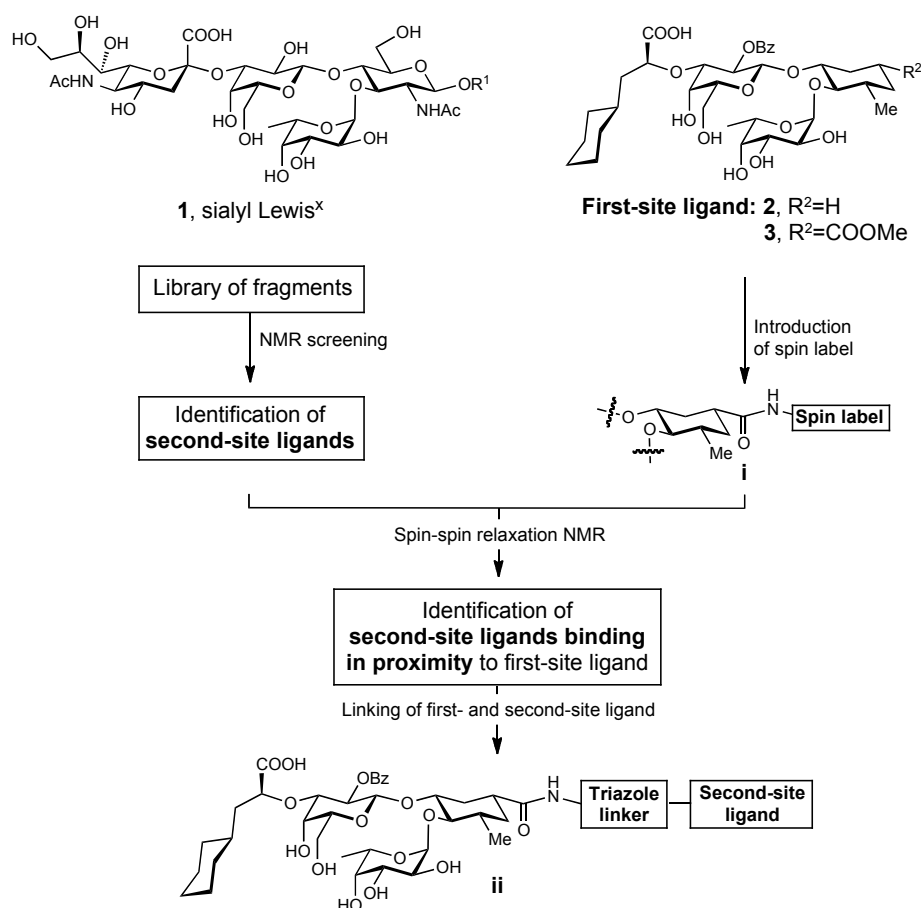
Figure 1. Sialyl Lewis^x (**1**) and the glycomimetic **2**[30b] which serves as first-site ligand. Via the modified cyclohexane moiety (→ **3**) a spin-label is introduced (→ **i**). From a fragment library, second-site ligands binding to E-selectin are identified. With a spin-spin relaxation NMR experiment those second-site ligands binding in proximity of the first-site ligand **i** are identified. In a final step, first- and second-site ligand are linked (→ **ii**).

Screening for second-site ligands. For the identification of fragments binding to E-selectin, NMR was used to screen a library composed of 80 water-soluble molecules obeying to the "Rule of Three"[44] for fragment libraries (MW $\leq$ 300, clogP $\leq$ 3, number of hydrogen-bond donors $\leq$ 3, number of hydrogen-bond acceptors $\leq$ 3). To perform the screens, the library was divided into sublibraries according to two criteria. First, 6 to 8 components that do not interact/react with each other were pooled. Second, each component can be identified by at least one isolated resonance in the ^{1}H NMR spectrum of the sublibrary.

The transverse magnetization decay of a nucleus is related to local fluctuations in its magnetic field and therefore, through molecular diffusion, to the molecular weight of the molecule. Nuclei in large molecules such as proteins exhibit a fast magnetization decay compared to those in small molecules. Likewise, when a small molecule binds to a large molecule such as a protein, it becomes a large molecule on his part. As a consequence, the magnetization decay of a small ligand's nuclei will be accelerated. This property can be exploited to identify ligand binding.[45] Accordingly, the rate of magnetization decay of the components of the sublibraries was determined by measuring the sxignal intensity of selected protons at different relaxation times in the absence and presence of E-selectin. With this approach, 5-nitroindole (**4**) (for an example of the experimental outcome see Figure 3a & 3b), benzimidazole derivative **5**, 3-phenylpyrazol (**6**), benzothiazoxle derivative **7**, and biphenyl-4-yl-methanol (**8**) were identified as fragments binding to E-selectin (Figure 2).
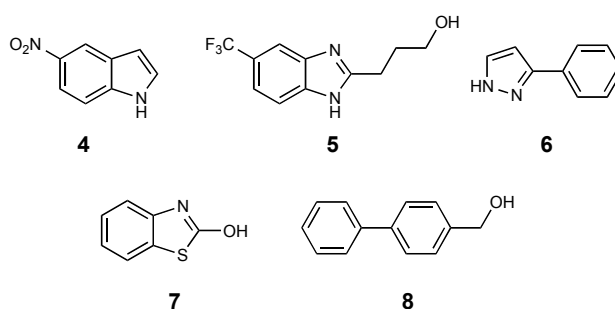
Figure 2. Second-site ligands **4** - **8** identified NMR screening of fragment libraries.

Synthesis of the spin-labeled first-site ligand. For the introduction of the spin label and later on for linking the first-site ligand with the second-site ligands, the sLe^x mimic **2**[30b] was equipped with a methyl ester ($\rightarrow$ **3**). Docking studies and the structural information from crystal structure of E-selectin soaked sLe$^{x[13]}$ suggested that the methyl ester in **3** is

positioned in a non-binding, sterically not restricted region, and therefore is suitable for the introduction of the 2,2,6,6-tetramethylpiperidin-1-oxyl (TEMPO) spin label (→ **18•**) as well as for the attachment of a second-site ligand (see below).

For the synthesis of Glc*N*Ac mimic **11**, we started from commercial *cis*-1,2,3,6-tetrahydrophthalic anhydride (**9**), which was transformed by literature procedures into (*R*)-cyclohex-3-ene carboxylic acid (**10**) with an enantiomeric excess of 96.3% ee, determined by chiral GC.[30b] Selective α-fucosylation[37] (→ **13**) followed by desilylation yielded the glycosylacceptor **14**. Its glycosylation with donor **15**[43] and dimethyl(methylthio)sulfonium triflate (DMTST) as promoter afforded β-selectively the tetrasaccharide mimic **16**. Hydrogenolysis of the benzyl groups with Pd(OH)$_2$/C and saponification under Zemplén conditions yielded the 2-monobenzoylated antagonist **3**.
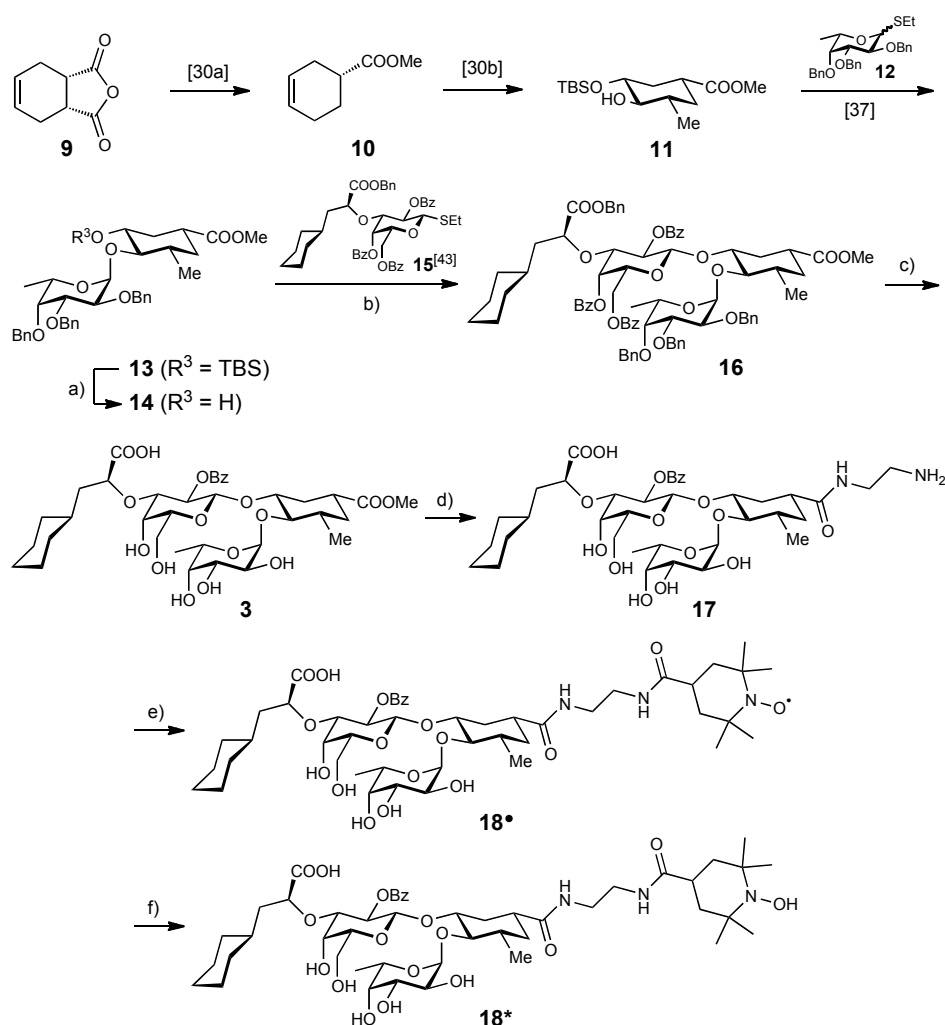

Scheme 1. a) TBAF, THF, rt, 13 h (76%) b) DMTST, MS 4 Å, DCM, rt (80%); c) i. Pd(OH)$_2$/C, H$_2$, dioxane/H$_2$O, ii. NaOMe, MeOH (71%); d) ethane-1,2-diamine, 65-70 °C, 2 h (93%); e) HBTU, HOBt, 4-carboxy-TEMPO, DIPEA, DMF, rt, 1 h (48%); f) Na-L-ascorbate, MeOH, rt, 1 h (68%).

As direct aminolysis of ester **3** with 4-amino-TEMPO gave only trace amounts of the amide, a diaminoethane spacer was introduced (→ **17**). The amide was then coupled to 4-carboxy-TEMPO using HBTU/HOBt for activation to afford the spin-labeled first-site ligand **18•**. For obtaining a high resolution NMR spectra, oxyl **18•** was reduced to hydroxide **18*** by adding Na-L-ascorbate.

Biological evaluation. The interactions between E-selectin and the antagonists **2**, **3** and **18•** towards E-selectin/IgG were analyzed by surface plasmon resonance (Biacore) at 25 °C.[43a] 6000-7000 RU of E-selectin/IgG - for preparation and purification see ref[61] - were immobilized on the chip surface *via* polyclonal goat anti-human Fc antibody as described in the experimental part. A reference cell providing only the antibody was used to compensate for unspecific binding to the matrix. Dilution series of the first-site ligands **2**, **3** and **18•** were prepared from stock solutions in DMSO using HBS-P buffer and passed over the flow cells. Neither the introduction of the ester (antagonist **3**) nor the TEMPO moiety (antagonist **18•**) had a substantial effect on the affinity and the kinetic profile of these first-site ligands (Table 1).

Identification of second-site fragments binding adjacent to the first-site ligand. In the next step, the spin-labeled antagonist **18•** was used to identify those fragments that bind simultaneously and in the vicinity of the sLe^x-binding site. The unpaired electron of the TEMPO spin label dramatically enhances the rate of transverse magnetization decay of surrounding protons within approximately 10 Å,[46] because the gyromagnetic ratio of an unpaired electron is 658 times larger than the one of a proton. This phenomenon, called paramagnetic relaxation enhancement, is distance dependent and thus allows the identification of second-site ligands binding in the vicinity of the first-site ligand. As illustrated in Figure 3c, the addition of **18•** further reduced the signal intensity (48% remaining) compared to the situation with only E-selectin (Figure 3b), suggesting simultaneous binding and proximity of 5-nitroindole (**4**) and **18•**. To ensure that the observed effect was truly a result of the spin label, we reduced the radical **18•** by adding Na-L-ascorbate to the NMR-sample (→ **18***). Indeed, this canceling of the paramagnetic effect led to an almost complete recovery of the signal (60% remaining, Figure 3d), indicating that 5-nitroindole (**4**) is a true second-site ligand. Corresponding experiments were performed with the other second-site ligands **5-8**. In this process, also **5** was confirmed as a second-site ligand

binding to E-selectin in vicinity of the first-site ligand. In contrast, for the derivatives **6-8** the presence of **18•** did not cause an enhancement of the paramagnetic relaxation, indicating that these fragments do not bind to E-selectin in the vicinity of the first-site ligand.
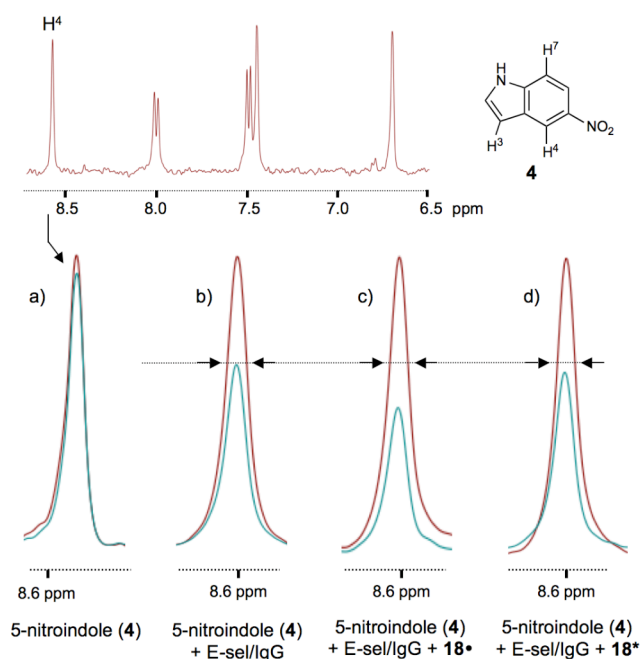
Figure 3. Principle of screening second-site ligands. ^{1}H NMR spectra of the H-4 of 5-nitroindole (**4**) recorded at spin lock times of 10 ms (red spectra) and 200 ms (green spectra) in different NMR samples: a) 5-nitroindole free in solution; b) decay of the transverse magnetization caused by the addition to E-selectin/IgG to the NMR sample; c) paramagnetic relaxation enhancement caused by the spin-labeled ligand **18•**; d) recovery of the signal by reduction of **18•** to **18*** by Na-L-ascorbate.

Orientation of the second-site ligand. The distance dependency of the relaxation enhancement of the radical[46] was further exploited to determine the orientation of the second-site ligand relative to the spin label, *i.e.* to the first-site ligand. In our case, the determination of the orientation was performed using the resonances of H-3, H-4 and H-7 of 5-nitroindole (**4**) because they show no (H-3 and H-4) or only minimal (H-7) overlap with resonances of **18•**. The differences in relaxation rates (indicated as Δ in Figure 4) obtained in the presence of **18•** or **18*** indicate that H-7 is located closer to the radical than H-3 and H-4. For the benzimidazole derivative **5**, the orientation cannot be determined unambigusously due to the inability to quantify a relaxation rate for H-7 and the conformational flexibility of the hydroxypropyl side-chain. Yet, the imidazole part of the molecule appears to point towards the spin label.
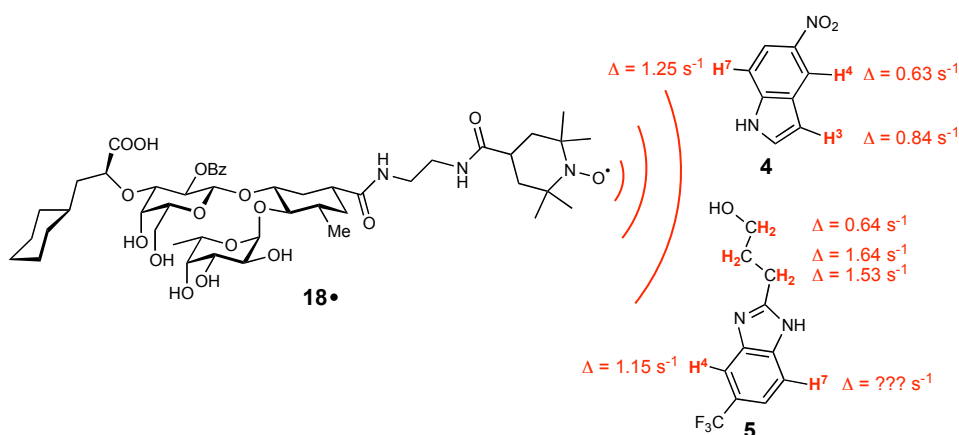
Figure 4. Relative orientation of the second-site ligands relative to the spin label. The changes in relaxation rates (Δ) experienced upon addition of **18•** to a mixture of nitroindole (**4**) and benzimidazole **5** with E-selectin/IgG reflect the distance of a nucleus to the unpaired electron.

Synthesis of the first-site library. The synthesis of the trimethylsilyl-protected amines started from the corresponding commercially available alcohols **20a-c** and by silylation of hex-5-yn-1-ol (**19d**) (Scheme 2). Mesylation ($\rightarrow$ **21a-d**) and substitution by azide ($\rightarrow$ **22a-d**) yielded, after reduction by a Staudinger reaction, the amines **23a-d**. In contrast to the treatment with diaminoethane (**3**→**12**, Scheme 1), direct aminolysis of **3** with alkyne amines **23a-d** afforded the amides **25a-d** only in moderate yields (2-18%). A possible reason is the low stability of the amines **23a-d** at elevated reaction temperatures (65-130 °C), leading to polymerization after cleavage of the trimethylsilyl group. In addition, the electron-withdrawing effect of the acetylene leads to a reduced nucleophilicity of the amines **23a-d**.
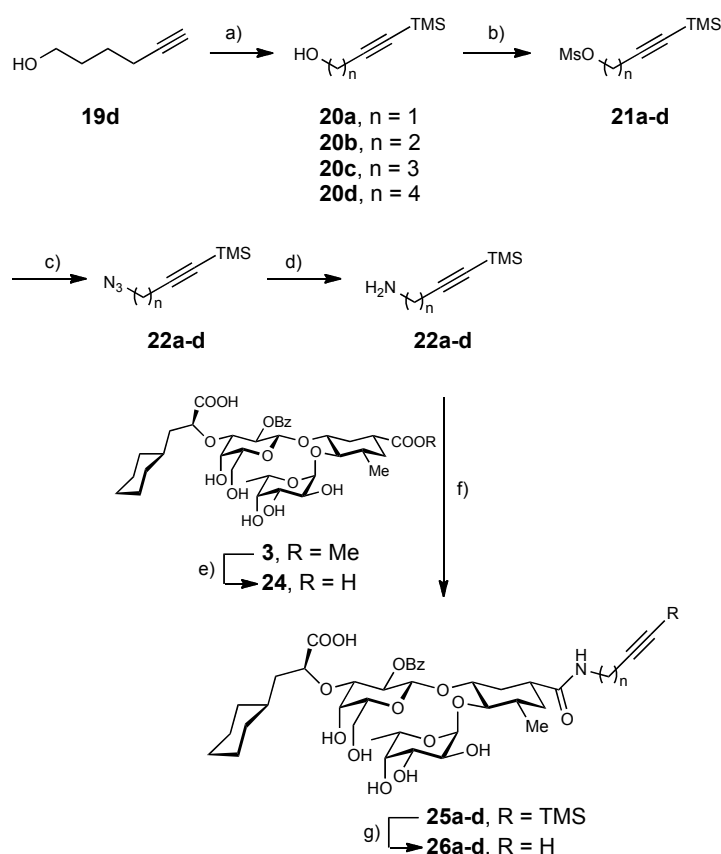
Scheme 2. a) ^{t}BuLi, Me$_3$SiCl, THF, -90 to -10°C; b) MeSO$_2$Cl, Et$_3$N, DCM, -78 °C to rt; c) NaN$_3$, DMF, 65 °C; d) PPh$_3$, THF/H$_2$O, 50 °C (**23a**: 83% over 3 steps; **23b**: 80% over 3 steps; **23c**: 43% over 3 steps; **23d**: 62% over 4 steps); e) NaOH, MeOH/H$_2$O, rt (79%); f) i. HBTU (1.2 eq), HOBt (3 eq), DMF, ii. alkyne amine, rt (**25a**: 35%; **25b**: 70%; **25c**: 40%; **25d**: 44%); g) TBAF, THF, rt (**26a**: 80%; **26b**: 93%; **26c**: 98%; **26d**: 87%).

In an alternative route, diacid **24** was selectively activated using standard peptide coupling reagents HBTU and HOBt. This gave the desired amides **25a-d** were obtained with excellent selectivity (93-99%) and fair to good yields (34-72%). Amides of the lactic acid (Lac) moiety are formed only in traces and could be removed by conventional HPLC-MS. The unexpected regioselectivity could result from different accessibilities of the two carboxylates in **24**, *e.g.* due to formation of intramolecular hydrogen bonds, other steric constraints or a reduced reactivity of the lactic acid moiety resulting from the electron-withdrawing oxygen in the α-position. Finally, the alkynes **26a-d** were obtained after cleavage of the trimethylsilyl groups with tetrabutylammonium fluoride (TBAF).

Synthesis of a second-site library. Of the two second-site fragments, 5-nitroindole (**4**) and the benzimidazole **5**, the former offers synthetic advantages and does not contain a highly

flexible side chain. In addition, its relative orientation could be determined more reliably, which made **4** the molecule of choice for the synthesis of a second-site library.

According to the orientation of 5-nitroindole (**4**) towards the first-site ligand (see Figure 4), the azidoalkyl linkers were introduced in **4** *via* *N*-alkylation (→ **28a-d**, Scheme 3) and, for proof of concept, in the 3-position as well (→ **32a-d**). *N*-alkylated 5-nitroindoles with 2-azidoethyl , 3-azidopropyl, and 4-azidobutyl linkers were obtained by *N*-alkylation of **4** with the corresponding dibromoalkanes followed by nucleophilic substitution with sodium azide (→ **28b-d**). For the introduction of the azidomethyl linker, hemiaminal **29** was synthesized from **4** and formaldehyde. Azide **28a** was obtained after *in situ* formation of the mesylate followed by nucleophilic substitution with sodium azide.

The *C*-alkylated 5-nitroindole **32a** was obtained *via* a Vilsmeier formylation of **4**[47] (→ **30**), followed by reduction to alcohol **31**, which was directly converted to azide **32a** using diphenylphosphoryl azide (DPPA).[48] The syntheses of the nitroindoles with 3-azidoethyl (→ **32b**), 3-azidopropyl (→ **32c**), and 3-azidobutyl (→ **32d**) linkers *via* a Larock indole synthesis[49,50] have been previously reported.[25]
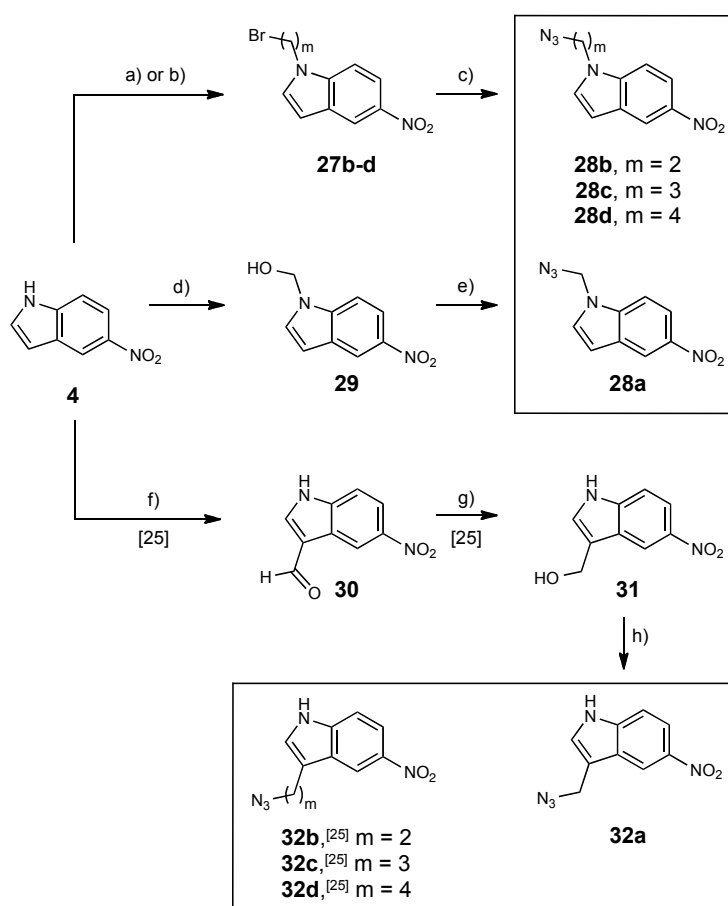
Scheme 3. a) Br(CH$_2$)$_2$Br or Br(CH$_2$)$_3$Br, KOH, DMF, rt (**27b:** 19%; **27c**: 46%); b) Br(CH$_2$)$_4$Br, K$_2$CO$_3$, TBAB, EtOAc, 50 °C (**27d**: 46%); c) NaN$_3$, DMF, 60 °C (**28b**: 52%; **28c**: 82%; **28d**: 79%); d) 30% aq. CH$_2$O, K$_2$CO$_3$, EtOH, 60 °C (66%); e) i. MeSO$_2$Cl, Et$_3$N, THF, -15 °C to rt; ii. NaN$_3$, rt (34%); f) POCl$_3$, DMF, -15 °C to rt (90%); g) NaBH$_4$, MeOH, rt (90%); h) DPPA, DBU, toluene/THF, -15 °C to rt, (78%).

***In situ* click experiments.** In a first attempt to identify a suitable linker to connect the first- and second-site ligands, a series of *in situ* click experiments[25,28] were performed. However, despite careful optimization of the experimental conditions with regard to ligand and protein concentrations, no evidence for the preferential formation of a specific linker combination was found. Obviously, the present example illustrates one limitation of the *in situ* click approach. With its distinctively flat binding site, E-selectin may not be an effective supramolecular catalyst for the alkyne–azide cycloaddition, since even upon simultaneous binding of first- and second-site ligand, their azide- and acetylene-substituted linkers may not be sufficiently pre-organized to accelerate the cycloaddition reaction. Furthermore, the ligands' low affinities in the micromolar (first-site ligand) and millimolar (second-site ligand) range leads to a small concentration of ternary complex, thus aggravating the detection of catalytically formed triazoles.

Synthesis and ranking of triazole antagonists. As the *in situ* click chemistry approach did not lead to the identification of a suitable linker pattern, a library of triazole antagonists with different linker lengths between first- and second-site fragment was synthesized using the copper-catalyzed alkyne-azide cycloaddition (CuAAC)[36] (Scheme 4).
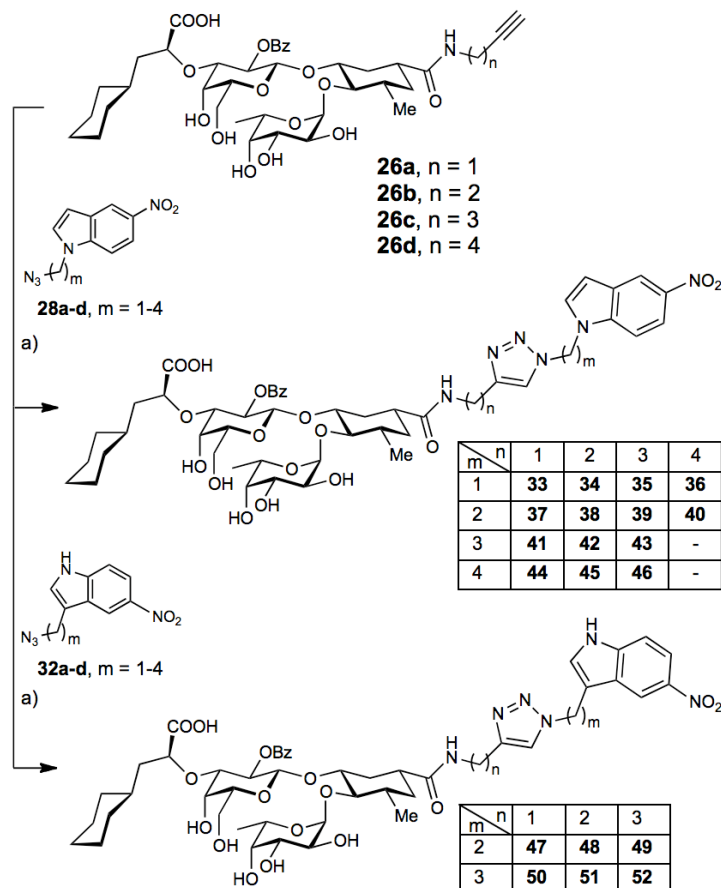
Scheme 4. a) Na-L-ascorbate, $CuSO_4 \cdot 5\ H_2O$, ^{t}BuOH/H_2O/THF, rt, 2 to 3 h (21-98%).

For the ranking, surface plasmon resonance (SPR) signals were recorded at a single antagonist concentration (0.05 μM). Since in SPR measurements of a biomolecular interaction the refractive index alters proportional to the mass of the bound ligand, the measured intensities (corresponding to resonance units [RU]) were adjusted according to the molecular weight of the ligand. To eliminate intensity differences resulting from the use of different chips and protein batches, **46** was used as internal standard. Five of the 21 tested antagonists showed a distinctively strong intensity/molecular weight ratio and were therefore subjected to a comprehensive SPR evaluation to obtain their K_D values and the on and off rates of binding. While the ester in **3** or the butynyl amide in **26b** did not affect the binding parameters, the triazole-nitroindole antagonists **35**, **41**, **43** and **45** bound E-selectin with a 16-

to 48-fold higher affinity (equilibrium K_Ds between 89 and 30 nM) compared to **2**. The order of affinities in the detailed analysis was the same as in the ranking procedure. In addition to the improved affinities, the triazole-nitroindole antagonists also exhibited substantially improved binding kinetics, with ligand-receptor half-lives of 4 to 5 minutes instead of the previsously observed half-lifes in the range of a second or even shorter (Figure 5).

Table 1. Kinetic and affinity evaluation of the best-ranked triazole-nitroindole antagonists and the precursors **2**, **3**, and **18•**. $K_{D,eq}$ is obtained from a steady-state fit to a single binding site model; $K_{D,kin}$ was obtained from k_{on} and k_{off} using $K_D = k_{off}/k_{on}$; $t_{1/2}$ is obtained from k_{off} using $t_{1/2} = \ln 2/k_{off}$.

Analyte	$K_{D,\,eq}$ [μM]	$K_{D,\,kin}$ [μM]	k_{on} [$10^5\,M^{-1}s^{-1}$]	k_{off} [s^{-1}]	$t_{1/2}$ [s]
2	1.45	1.0	8.5	0.9	0.77
3	1.90	1.7	11	1.9	0.37
18•	1.25	1.2	3	0.36	1.9
26b	1.12	1.12	35.4	3.98	0.174
35	0.089	0.036	0.635	0.0023	301
41	0.057	0.037	0.68	0.0025	280
43	0.030	0.018	1.42	0.0026	250
45	0.049	0.035	0.797	0.0028	240
51	0.050	-	-	-	-
57	0.544	-	-	-	-
58	0.186	0.189	0.3	0.0056	124

The five antagonists that were comprehensively evaluated by SPR had rather long linkers containing four (**35** and **41**), five (**51**) or six (**43** and **45**) methylene groups, and except for one case (**35**), the "nitroindole part" of the linker contained either three or four CH_2 groups. Four (**35**, **41**, **43** and **45**) of the five best antagonists contained an *N*-linked nitroindole, which supports the finding that the nitroindole preferentially binds with its indole nitrogen oriented towards the first-site ligand (see Figure 4). However, **51** represents a case where the linker configuration allows a favorable positioning of a *C*-linked nitroindole.

Tetrasaccharide mimics such as **3** interact with E-selectin mainly *via* a set of well-defined electrostatic interactions.[13] The high water accessibility of their binding site and the high degree of ligand pre-organization allows a fast exchange of ligand and solvent molecules, which may be the cause of the typical fast association and dissociation seen for these types of

ligands.[4] In contrast, the prolonged association and dissociation phases seen for the triazole–nitroindole antagonists indicate that the binding event might be accompanied by more pronounced structural rearrangements of the ligand and/or the protein.
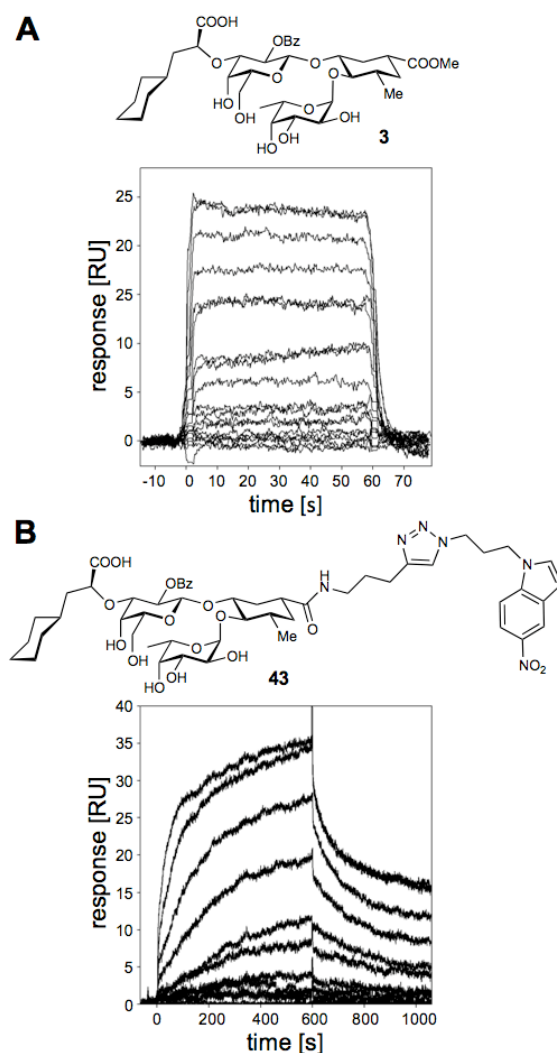
Figure 5. Sensorgrams of A) the tetrasaccharide mimic **3** with the characteristic block-like shape indicating fast on/off rates and B) sensorgram of the best triazole-nitroindole antagonist **43**.

Derivatization of the nitro group. The metabolic biotransformation of nitro arenes involves several reactive intermediates (*e.g.* nitroso derivatives or hydroxyl amines) with toxic or mutagenic potential.[51] Therefore, possible replacements for the nitro group were explored. Modifications leading to a decrease of the lipophilicity appeared particularly interesting. Accordingly, starting from **43** derivatives with a 5-aminoindole moiety (→ **58**) and the corresponding acetamide (→ **57**) were prepared (Scheme 5).
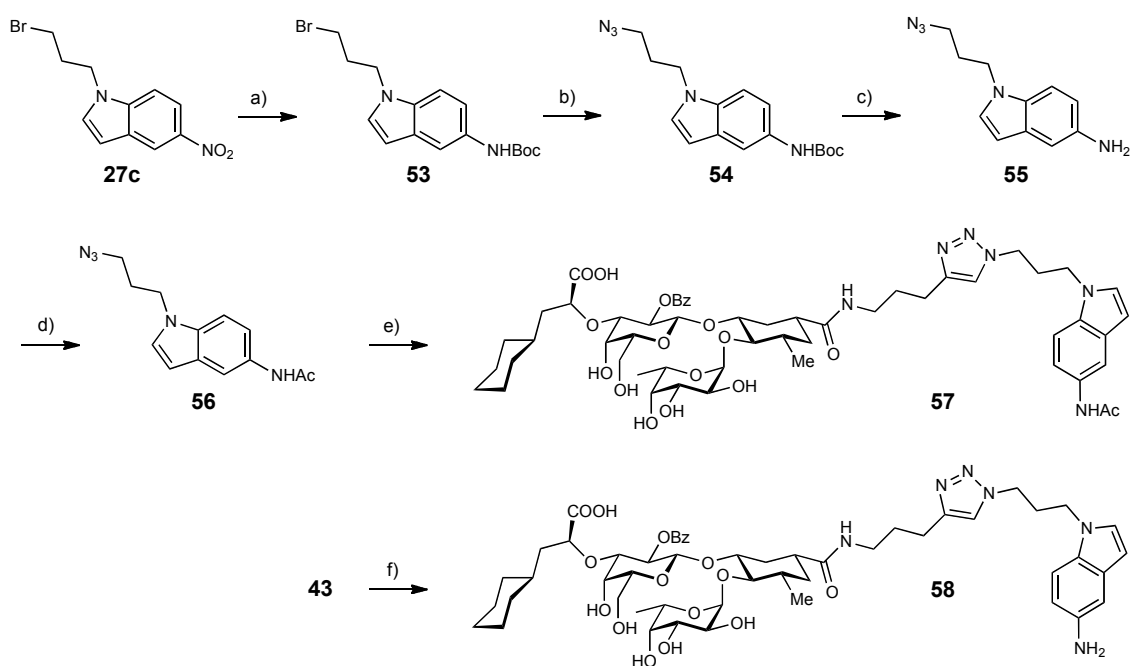
Scheme 5. a) Pt$_2$O, H$_2$, Boc$_2$O, EtOH, rt (72%); b) NaN$_3$, DMF, rt (90%); c) TFA, DCM, rt (86%); d) Ac$_2$O, Et$_3$N, DCM, rt (86%); e) **26c**, Na-L-ascorbate, CuSO$_4$·5H$_2$O, ^{t}BuOH/H$_2$O/THF, rt (95%); f) Pt$_2$O, H$_2$, morpholine, rt (54%).

The affinities of **57** and **58** are reported in Table 1. Surprisingly, the effect of the nitroindole modification on the affinity was quite strong. Compared to the parent compound **43**, the affinity of amine **58** (K_D = 186 nM) was reduced by a factor of 6, and for the acetamide **57** (K_D = 544 nM) even by a factor >16. The 5-position of the indole is apparently crucial for the binding of the second-site ligand. Although amines and amides are better hydrogen bond acceptors than the nitro group,[52c] the orientations of their acceptor lone pairs differ, making beneficial interaction impossible. In addition, nitro groups may electrostatically interact with carbonyl groups that are oriented orthogonal or antiparallel to the plane of the nitro group.[52] Additionally, unfavorable desolvation effects may explain the reduced affinity of amine **58** and acetamide derivative **57**.

Conclusions

With a previously published NMR approach, which we had successfully applied for the identification of Siglec-4 antagonists,[25] 5-nitroindole (**4**) and benzimidazole **5** were identified as small fragments binding in the vicinity of and simultaneously with a known selectin antagonist. For synthetic and structural reasons, the indole derivative **4** was selected for the further study. Since *in situ* click experiments[25, 28-34] failed, a library of 21 triazole–nitroindole antagonists was synthesized, and the antagonists were ranked according to their relative affinities using surface plasmon resonance experiments. The five most potent antagonists were characterized in detail using SPR, which revealed antagonists with K_D values between 30 and 89 nM and kinetic parameters characterized by extended ligand-protein half-lifes to the range of 4 to 5 minutes. This is a substantial improvement, since the half-lifes of carbohydrate-lectin interactions are generally in the range of seconds.

As shown for antagonist **43**, the nitro group of the indole moiety is substantial for binding and could not be replaced by an amino- (→ **58**) or acetamido group (→ **57**). In addition to the contribution of the second-site ligand to binding, the role of the linker is also of interest and may afford additional opportunities for ligand optimization. Thus, reduction of linker flexibility could be desirable in terms of reducing the entropy loss upon binding. Additionally, the present molecules have a pronounced amphiphilic nature, *i.e.* the introduction of polarity into the linker might be beneficial in terms of solubility.

The development of high-affinity ligands of lectins in general and E-selectin in particular has proven to be a notoriously difficult task. E-selectin antagonists with low nanomolar affinities therefore constitute a substantial step forward in the search for novel anti-inflammatory drugs and may foster a better understanding of binding processes at non-obstructed interfaces. These results further illustrate the usefulness of a fragment-based approach for the improvement of existing ligands with relatively low affinity which have proven to be difficult to optimize using "conventional" approaches.

Materials and Methods

NMR screening: All NMR experiments were performed on a Bruker AVANCE III 500 MHz (Bruker BioSpin AG, Fällanden, Switzerland) equipped with Z-gradient SEI probe at 298 K. Each NMR sample contained 0.5 mg/mL of E-selectin/IgG, equivalent to 15 μM of binding site (estimated by Bradford assay). The E-selectin/IgG was prepared in d_{11}-Tris buffer (50 mM d_{11}-Tris, 150 mM NaCl, 1 mM CaCl$_2$). Shigemi NMR tubes (Sigma Aldrich GmbH,

Buchs, Switzerland) were used for samples containing E-selectin/IgG (sample volume: 250 μL) and ordinary 5 mm NMR tubes were used for samples containing only ligands (sample volume: 500 μL). Bruker software XWINNMR 3.6 and TOPSPIN 2.1 were used as the interface with the spectrometer and to analyze the NMR data. MestReNova 5.2.3 was used for off-line analysis of the spectra. Prism 4 (GraphPad Software Inc., San Diego, USA) was used to fit the relaxation data.

Spin-spin relaxation experiments: The E-selectin/IgG was present at 20-30 μM in binding site concentration as determined by Bradford assay. A 50 mM stock solution of compound in d_6-DMSO was prepared and diluted with deutrated buffer (pH 7.4, 20 mM d_{11}-Tris, 150 mM NaCl, 1 mM $CaCl_2$ in D_2O, Armar Chemicals) to a final sample concentration of 1-5 mM. The pulse sequence used for T1ρ determination was adapted from Hajduk.[45] To determine the T1ρ relaxation rate, six experiments were performed with different durations of the continuous-wave spin-lock applied with a field strength of 2 kHz (10, 50, 100, 150, 200, 250 ms). Traces of non-deuterated D_2O resulted in significant water signals in samples containing the protein. Therefore, a DPFGSE water suppression sequence was added at the end of the pulse sequence.[56] For each experiment, eight scans were measured preceded by two dummy scans. The recovery delay between successive scans was set to 10 s and the fid was digitally sampled for 2 s.

Surface plasmon resonance (SPR) analysis: Biomolecular interaction analyses by surface plasmon resonance (SPR) were performed on a Biacore 3000 system (GE Healthcare, Uppsala, Sweden). CM5 research grade sensor chips, amine coupling immobilization kit, maintenance supply and HPS-P buffer were purchased from GE Healthcare (Freiburg, Germany). HBS-P buffer (10 mM HEPES, 150 mM NaCl, 0.005% P20, pH 7.5) supplemented with 5% (v/v) DMSO (D8418, Sigma-Aldrich Chemie, Steinheim, Germany) and 20 mM $CaCl_2$ (C3306, Sigma-Aldrich, Steinheim, Germany) was used as running buffer in all binding experiments. The capture assay for the immobilization of E-selectin/IgG was performed as follows. A polyclonal goat anti human Fc antibody (I2136, Sigma-Aldrich, Buchs, Switzerland) was first immobilized onto a CM5 sensor chip *via* the standard amine coupling method according to the manufacturers protocol. After the antibody immobilization, a solution of E-selectin/IgG (50 μg/mL, in acetate buffer 10 mM, pH 5.5) was injected at 5

µL/min for 20 min over a single-flow cell, designated as the active flow cell. A reference cell without immobilized E-selectin/IgG was prepared. Before injecting the antagonist, the reference and active flow cells were equilibrated for 2 h in running buffer, at 5 µL/min. For the evaluation of first-site ligands, serial dilutions were prepared in running buffer and injected using the KINJECT command with a 60 s association time and 60 s dissociation time at a flow rate of 20 µL/min over the reference and the active flow cell. Prior to each assay, a DMSO calibration was performed.[60] For the ranking of the triazole antagonists, the association and dissociation times were increased up to 600 s. SPR signals were recorded at a single concentration of ligand (50 nM, in running buffer) at a flow rate of 20 µL/min, a mean of the signal recorded 500 to 600 s after injection (plateau) was calculated and divided by the molecular weight of the analyte. To eliminate intensity differences resulting from the use of different chip batches and surfaces, the obtained results were normalized to the response of an internal standard (**46**) injected at a concentration of 50 nM. In addition, blank injections were performed between each injection of ligand to prevent the presence of residual traces of compound in the system. Similar conditions were applied for the K_D, k_{off}, and k_{on} determinations of the best antagonists, which were selected according to the data obtained by the ranking procedure. For each antagonist ten dilutions were measured. The data were processed with Scrubber 2.0a (BioLogic Software, Campbell, Australia) for equilibrium binding constants (K_D) measurements and determination of kinetik parameters (k_{on}, k_{off}). K_{DS} were determined using a simple steady-state affinity 1:1 binding model. Double referencing (subtraction of reference surface and blank injection) was applied to correct bulk effects and other systematic artifacts.[57]

Acknowledgement

References

[1]   a) D. Neil Granger and G. Schmid-Schönbein, *Physiology and Pathophysiology of Leukocyte Adhesion*, Oxford University Press, New York **1995**; b) G. S. Kansas, *Blood* **1996**, *88*, 3259-3287.

[3]   S. Gout, P.-L. Tremblay, J. Huot, *Clin. Exp. Methastasis* **2008**, *25*, 335-344.

[4]   B. Ernst and J.L. Magnani, *Nat. Rev. Drug Discovery* **2009**, *8*, 661-677.

[4a]   J. L. Magnani, J. T. Patton, A. K. Sarkar, S. A. Svarovsky and B. Ernst, Preparation of hetero-bifunctional pseudooligosaccharides as pan-selectin inhibitors and inflammatory agents, J. L. Magnani, J. T. Patton, A. K. Sarkar, S. A. Svarovsky, B. Ernst, PTC/WO2007/028050 A1, priority date: September 2, 2005.

[5]   J. Chang, J. T. Patton, A. Sarkar, B. Ernst, J. L. Magnani and P. S. Frenette, *Blood* **2010**, *116*, 1779-1786.

[6]   http://clinicaltrials.gov/ct2/results?term=pan-selectin

[7]   a) M. L. Phillips, E. Nudelman, F. C. A. Gaeta, M. Perez, A. K. Singhal, S. I. Hakomori, J. C. Paulson, *Science* **1990**, *250*, 1130-1132; b) G. Walz, A. Aruffo, W. Kolanus, M. Bevilacqua, B. Seed, *Science* **1990**, *250*, 1132-1135.

[8a]   a) R. M. Cooke, R. S. Hale, S. G. Lister, G. Shah, M. P. Weir, *Biochemistry* **1994**, *33*, 10591-10596; b) L. Poppe, G. S. Brown, J. S. Philo, P. V. Nikrad, B. H. Shah, *J. Am. Chem. Soc.* **1997**, *119*, 1727-1736.

[9]   a) B. Ernst, H. C. Kolb, O. Schwardt in *Carbohydrate Mimetics in Drug Discovery* (Eds.: D. E. Levy, P. Fügedi), CRC Press/Taylor & Francis, Boca Raton, **2006**, pp. 803-845; b) N. Kaila, B. E. Thomas, *Med. Res. Rev.* **2002**, *22*, 566-601; c) E. E. Simanek, G. J. McGarvey, J. A. Jablonowski, C. H. Wong, *Chem. Rev.* **1998**, *98*, 833-862; d) H. C. Kolb, B. Ernst, *Chem. Eur. J.* **1997**, *3*, 1571-1578.

[13]   W. S. Somers, J. Tang, G. D. Shaw, R. T. Camphausen, *Cell* **2000**, *103*, 467-479.

[14]   a) K. Baumann, D. Kowalczyk, T. Gutjahr, M. Pieczyk, C. Jones, M. K. Wild, D. Vestweber, H. Kunz, *Angew. Chem. Int. Ed.* **2009**, *48*, 3174-3178; b) M. K. Wild, M. C. Huang, U. Schulze-Horsel, P. A. van der Merwe, D. Vestweber, *J. Biol. Chem.* **2001**, *276*, 31602-31612.

[16] R. A. Copeland, D. L. Pompliano, T. D. Meek, *Nat. Rev. Drug Discovery* **2006**, *5*, 730-739.

[17] a) A. G. Coyne, D. E. Scott and C. Abell, *Curr. Opin. Chem. Biol.* **2010**, *14*, 299-307; b) C. Murray and D. Rees, *Nature Chemistry* **2009**, *1*, 187-192; c) G. Chessari ,A. J. Woodhead, *Drug Discovery Today* **2009**, *14*, 668-675; d) M. Congreve, G. Chessari, D. Tisi, A. J. Woodhead, *J. Med. Chem.* **2008**, *51*, 3661-3680; e) P. J. Hajduk and J. Greer, *Nat. Rev. Drug Discovery* **2007**, *6*, 211-219.

[22] W. Jencks, *Proc. Nat. Acad. Sci. U.S.A.* **1981**, *78*, 4046-4050.

[23] a) A. V. Finkelstein and J. Janin, *Protein Eng.* **1989**, *3*, 1-3; b) C. W. Murray and M. L. Verdonk, *J. Comput.-Aided Mol. Des.* **2002**, *16*, 741-753.

[25] S. Shelke, B. Cutting, X. Jiang, H. Koliwer-Brandl, D. Strasser, O. Schwardt, S. Kelm and B. Ernst, *Angew. Chem. Int. Ed.* **2010**, *49*, 5721-5725.

[26] G. Otting, *Curr. Opin. Struct. Biol.* **1993**, *3*, 760-768.

[27] W. Jahnke, L. B. Perez, C. G. Paris, A. Strauss, G. Fendrich and C. M. Nalin, *J. Am. Chem. Soc.* **2000**, *122*, 7394-7395.

[27a] a) R. Huisgen, G. Szeimies and L. Moebius, *Chem. Ber.* **1967**, *100*, 2494-2507; b) R. Huisgen in *1,3-Dipolar Cycloaddition Chemistry*, Vol. 1 (Ed.: A. Padwa), Wiley, New York, 1984, pp. 1-176.

[30a] a) G. Cerichelli, C. Grande, L. Luchetti and G. Mancini, *J. Org. Chem.* **1991**, *56*, 3025-3030; b) H. J. Gais and K. L. Lukas, *Angew. Chem. Int. Ed. Engl.* **1984**, *23*, 142-143; c) S. M. Roberts, *Biocatalysts or Fine Chemicals Synthesis*, John wiley and Sons, Chichester, **1999**; d) D. H. R. Barton, D. Crich, W. B. Motherwell, *J. Chem. Soc., Chem. Commun.* **1983**, 939-941; e) D. H. R. Barton, D. Crich, W. B. Motherwell, *Tetrahedron Lett.* **1983**, *24*, 4979-4982.

[10a] D. Schwizer, J. T. Patton, B. Cutting, M. Smieško, B. Wagner, A. Kato, C. Weckerle, F. P. C. Binder, S. Rabbani, O. Schwardt, J. L. Magnani, B. Ernst, *Chem. Eur. J.* **2012**, *18*, 1342-1351.

[28] a) H. D. Agnew, R. D. Rohde, S. W. Millward, A. Nag, W. Yeo, J. E. Hein, S. M. Pitram, A. A. Tariq, V. M. Burns, R. J. Krom, V. V. Fokin, K. B. Sharpless and J. R. Heath, *Angew. Chem. Int. Ed.* **2009**, *48*, 4944-4948; b) T. Hirose, T. Sunazuka, A.

Sugawara, A. Endo, K. Iguchi, T. Yamamoto, H. Ui, K. Shiomi, T. Watanabe, K. B. Sharpless and S. Omura, *J. Antibiot.* **2009**, *62*, 277-282; c) M. Whiting, J. Muldoon, Y. C. Lin, S. M. Silverman, W. Lindstrom, A. J. Olson, H. C. Kolb, M. G. Finn, K. B. Sharpless, J. H. Elder and V. V. Fokin, *Angew. Chem. Int. Ed.* **2006**, *45*, 1435-1439; d) A. Krasiński, Z. Radić, R. Manetsch, J. Raushel, P. Taylor, K. B. Sharpless and H. C. Kolb, *J. Am. Chem. Soc.* **2005**, *127*, 6686-6692, e) V. P. Mocharla, B. Colasson, L. V. Lee, S. Roper, K. B. Sharpless, C.-H. Wong and H. C. Kolb, *Angew. Chem. Int. Ed.* **2005**, *44*, 116-120; f) R. Manetsch, A. Krasiński, Z. Radić, J. Raushel, P. Taylor, K. B. Sharpless and H. C. Kolb, *J. Am. Chem. Soc.* **2004**, *126*, 12809-12818; g) W. G. Lewis, L. G. Green, F. Grynszpan, Z. Radic, P. R. Carlier, P. Taylor, M. G. Finn and K. B. Sharpless, *Angew. Chem. Int. Ed.* **2002**, *41*, 1053-1057.

[35] C. W. Tornoe, C. Christensen and M. Meldal, *J. Org. Chem.* **2002**, *67*, 3057-3064.

[36] V. V. Rostovtsev, L. G. Green, V. V. Fokin and K. B. Sharpless, *Angew. Chem. Int. Ed.* **2002**, *41*, 2596-2599.

[37] S. Sato, M. Mori, Y. Ito and T. Ogawa, *Carbohydr. Res.* **1986**, *155*, C6-C10.

[43] B. Ernst, B. Wagner, G. Baisch, A. Katopodis, T. Winkler and R. Öhrlein, *Can. J. Chem.* **2000**, *78*, 892-904.

[43a] a) R. L. Rich and D. G. Myszka, *Current Opinion in Biotechnology* **2000**, *11*, 54-61; b) T. A. Morton and D. G. Myszka, *Methods Enzymol.* **1998**, *295*, 268-294; c) K. Nagata and H. Handa, *Real-Time Analysis of Biomolecular Interactions: Applications of Biacore*, Springer-Verlag, Berlin, **2000**.

[44] M. Congreve, R. Carr, C. Murray and H. Jhoti, *Drug Discovery Today* **2003**, *8*, 876-877.

[45] P. J. Hajduk, E. T. Olejniczak and S. W. Fesik, *J. Am. Chem. Soc.* **1997**, *119*, 12257-12261.

[46] I. Bertini, C. Luchinat, G. Parigi and R. Pierattelli, *ChemBioChem* **2005**, *6*, 1536-1549.

[47] S. F. Safe in *Indole-3-carbinol, diindolylmethane and substituted analogs as antiestrogens*, Vol. *WO9850357* USA, **1998**, p. WO9850357.

[48] R. J. W. Cremlyn, *Aust. J. Chem.* **1973**, *26*, 1591-1593.

[49] R. C. Larock, E. K. Yum and M. D. Refvik, *J. Org. Chem.* **1998**, *63*, 7652-7662.

[50] J. A. Gylys, E. H. Ruediger, D. W. Smith, C. Solomon and J. P. Yevich in *Antimigraine cyclobutenedione derivatives of tryptamines*, *Vol.* USA, **1995**.

[51] A.-C. Macherey and P. M. Dansette in *Chemical mechanisms of toxicity: Basic knowledge for designing safer drugs*, *Vol.* (Ed. W. C. G.), Elsevier Academic Press, Amsterdam, **2003**, pp. 545-560.

[52] R. Paulini, K. Müller and F. Diederich, *Angew. Chem. Int. Ed.* **2005**, *44*, 1788-1805; b) J. M. A. Robinson, D. Philp, K. D. M. Harris and B. M. Kariuki, *New J. Chem.* **2000**, *24*, 799-806; c) M. H. Abraham, P. P. Duce, D. V. Prior, D. G. Barratt, J. J. Morris and P. J. Taylor, *J. Chem. Soc., Perkin Trans. 2* **1989**, 1355-1375; d) T. W. Panunto, Z. Urbanczyk-Lipkowska, R. Johnson and M. C. Etter, *J. Am. Chem. Soc.* **1987**, *109*, 7786-7797.

[56] T.-L. Hwang and A.J. Shaka, *J. Magn. Reson. A*, **1995**, *112*, 275-279.

[57] A. Frostell-Karlsson, A. Remaeus, H. Roos, K. Andersson, P. Borg, M. Hamalainen and R. Karlsson, *J. Med. Chem.* **2000**, *43*, 1986-1992.

[60] S. Mesch, K. Lemme, H. Koliwer-Brandl, D. S. Strasser, O. Schwardt, S. Kelm and B. Ernst, *Carbohydr. Res.* **2010**, *345*, 1348-1359.

[BC1] I. Bertini, M. Fragai, Y.-M. Lee, C. Luchinat and B. Terni, *Angew. Chem. Int. Ed.* **2004**, *43*, 2254-2256.

[61] a) L. Scheffler, B. Ernst, A. Katopodis, J. L. Magnani, W. T. Wang, R. Weisemann and T. Peters, *Angew. Chem., Int. Ed.* **1995,** *34*, 1841-1844; b) F. P. C. Binder, K. Lemme, R. C. Preston and B. Ernst, *Angew. Chem., Int. Ed.* **2012**, in press.

Supporting Information

Nanomolar E-selectin Antagonists: A Fragment-based Approach

Jonas Egger, Céline Weckerle, Brian Cutting, Oliver Schwardt, Katrin Lemme, Beat Ernst[*]

Institute of Molecular Pharmacy, Pharmacenter, University of Basel, Klingelbergstrasse 50, CH-4056 Basel, Switzerland.

Contents

Synthesis:

General methods: NMR spectra were recorded on a Bruker Avance DMX-500 (500 MHz) spectrometer. Assignment of ^{1}H and ^{13}C NMR spectra was achieved using 2D methods (COSY, HSQC, TOCSY and HMBC). Chemical shifts are expressed in ppm using residual $CHCl_3$, $CHDCl_2$, CHD_2OD, $CHD_2S(=O)CD_3$ and HDO as references. For complex molecules, the following prefixes for substructures are used: Cy (cyclohexyl), Fuc (fucose), Gal (galactose), Ind (indole), and Lac (lactate). Optical rotations were measured on a Perkin-Elmer Polarimeter 341. IR spectra were recorded on a Perkin Elmer Spectrum One FT-IR spectrometer as KBr pellets or films on NaCl plates. Electron spray ionization mass spectra (ESI-MS) were obtained on a Waters micromass ZQ. The LC/HRMS analysis were carried out using a Agilent 1100 LC equipped with a photodiode array detector and a Micromass QTOF I equipped with a 4 GHz digital-time converter. Gas chromatography was carried out on a VARIAN 3600 or CE Intruments 8000Top using a chiral betacyclodextrine DEtTBuSil (SE54) column (Brechbühler). Microanalyses were performed at the Department of Chemistry, University of Basel, Switzerland. Reactions were monitored by TLC using glass plates coated with silica gel 60 F_{254} (Merck) and visualized by using UV light and/or by heating to 140°C for 5 min with aq. $KMnO_4$ solution or a molybdate solution (a 0.02 M solution of ammonium cerium sulfate dihydrate and ammonium molybdate tetrahydrate in aq. 10% H_2SO_4). Column chromatography was performed on a CombiFlash Companion (Teledyne-ISCO, Inc.) using RediSep® normal phase disposable flash columns (silica gel). Reversed phase chromatography was performed on LiChroprep®RP-18 (Merck, 40-63 μm). LC-MS separations were carried out using Sunfire C_{18} columns (analytical: 2.1 × 50 mm, 3.5 μm; preparative: 19 × 150 mm, 5.0 μm) on a Waters 2525 LC, equipped with a Waters 2996 photodiode array and a Waters micromass ZQ for detection. Hydrogenation reactions were performed in a shaking apparatus (Parr Instruments Company, Moline, Illinois, USA) in 250 mL or 500 mL bottles with 4 bar H_2 pressure. Solvents and phosphate buffer solutions were purchased from Fluka or Acros. Solvents were dried prior to use where indicated. Methanol (MeOH) was dried by refluxing with sodium methoxide and distilled immediately before use. Dichloromethane (DCM) was dried by filtration through Al_2O_3 (Fluka, type 5016 A basic). Tetrahydrofurane (THF) was dried by distillation from sodium/benzophenone. *N,N*-Dimethylformamide (DMF) was dried by stirring over activated MS 4 Å overnight, followed by microfiltration.

Methyl (1*R*,3*R*,4*R*,5*S*)-4-*O*-(2,3,4-tris-*O*-benzyl-6-deoxy-α-L-galactopyranosyl)-3,4-dihydroxy-5-methyl-cyclohexane-1-carboxylate (14). To a solution of **13** (677 mg, 0.942 mmol) in THF (7 mL), TBAF (1 M, in THF, 3.77 mL, 3.77 mmol) was added. The reaction was stirred for 9 h and concentrated *in vacuo*. The crude product was purified by silica gel chromatography (petroleum ether/EtOAc) to afford **14** (533 mg, 76%) as a white solid. $[\alpha]_D^{20}$ -43.0 (*c* 1.09, CHCl$_3$); ^{1}H NMR (CDCl$_3$, 500 MHz): δ = 1.11 (d, *J* = 6.4 Hz, 3H, Fuc-H6), 1.15 (d, *J* = 6.5 Hz, 3H, Me), 1.23 (m, 1H, H-6a), 1.48 (m, 1H, H-2a), 1.59 (m, 1H, H-5), 1.92 (m, 1H, H-6b), 2.24 (m, 1H, H-2b), 2.39 (m, 1H, H-1), 2.89 (dd, *J* = 8.6, 10.0 Hz, 1H, H-4), 3.43 (ddd, *J* = 4.7, 8.4, 11.5 Hz, 1H, H-3), 3.67 (s, 3H, Me), 3.70 (m, 1H, Fuc-H4), 3.96 (dd, *J* = 2.7, 10.2 Hz, 1H, Fuc-H3), 4.08-4.12 (m, 2H, Fuc-H2, -H5), 4.65, 4.69, 4.67, 4.78, 4.85, 4.99 (6 m, 6H, 3 C*H*$_2$Ph), 4.97 (d, *J* = 3.8 Hz, 1H, Fuc-H1), 7.26-7.39 (m, 15H, 3 C$_6$H$_5$); ^{13}C NMR (CDCl$_3$, 125 MHz): δ = 16.61 (Fuc-C6), 18.35 (Me), 34.77 (C-2), 35.44 (C-5), 35.84 (C-6), 40.33 (C-1), 51.77 (Me), 67.63 (Fuc-C5), 71.99 (C-3), 72.97, 73.52, 74.86 (3 C*H*$_2$Ph), 76.32 (Fuc-C2), 77.38 (Fuc-C4), 78.87 (Fuc-C3), 92.12 (C-4), 98.74 (Fuc-C1), 127.36, 127.49, 127.63, 127.66, 127.91, 128.23, 128.27, 128.35, 128.38, 138.23, 138.35, 138.70 (18C, 3 C$_6$H$_5$), 174.89 (CO); IR (KBr): ν = 3424 (s, OH), 3031 (vw), 2998 (w), 2952 (s), 2904 (s), 1737 (vs, C=O), 1497 (w), 1454 (m), 1384 (w), 1344 (s), 1305 (m), 1273 (w), 1248 (w), 1191 (s), 1138 (s), 1157 (s), 1102 (vs), 1037 (vs), 973 (w), 957 (w), 909 (w), 823 (vw), 802 (vw), 743 (s), 720 (w), 697 (m) cm^{-1}; elemental analysis: calcd (%) for C$_{36}$H$_{44}$O$_8$ (604.73): C 71.50, H 7.33; found: C 71.51, H 7.36.

{(1*R*,3*R*,4*R*,5*S*)-4-[(2,3,4-tris-*O*-benzyl-6-deoxy-α-L-galactopyranosyl)oxy]-1-methoxycarbonyl-5-methyl-cyclohex-3-yl} 2,4,6-tri-*O*-benzoyl-3-*O*-[(1*S*)-1-benzyloxycarbonyl-2-cyclohexyl-ethyl]-β-D-galactopyranoside (16). A mixture of thioglycoside **15**[S1] (433 mg, 0.554 mmol), **14** (258 mg, 0.427 mmol), and activated molecular sieves (4 Å, 2.5 g) was dissolved in anhydrous DCM (8.5 mL) under argon. A suspension of DMTST (331 mg, 1.28 mmol) and activated molecular sieves (4 Å, 1.3 g) in DCM (5 mL) was prepared in a second flask. Both suspensions were stirred at rt for 4 h, then the DMTST suspension was added *via* syringe to the other suspension with some additional DCM (3.5 mL). After 6 d of stirring at rt, the reaction mixture was filtered through celite. The filtrate was successively washed with satd aq. NaHCO$_3$ (40 mL) and water (100 mL). The aqueous layers were extracted with DCM (3 × 60 mL). The combined organic layers were dried with Na$_2$SO$_4$, filtered and concentrated *in vacuo*. The crude product was purified by

silica gel chromatography (petroleum ether/Et$_2$O) to afford **16** (450 mg, 80%) as white foam. [α]$_D^{20}$ -52.8 (*c* 1.05, CHCl$_3$); ^{1}H NMR (CDCl$_3$, 500 MHz): δ = 0.45-2.23 (m, 18H, CyCH$_2$, Cy), 1.07 (d, *J* = 6.4 Hz, 3H, Me), 1.43 (d, *J* = 6.4 Hz, 3H, Fuc-H6), 1.51 (m, 1H, H-5), 3.21 (t, *J* = 9.5 Hz, 1H, H-4), 3.53-3.56 (m, 5H, H-3, Fuc-H4, Me), 3.81 (dd, *J* = 3.2, 9.9 Hz, 1H, Gal-H3), 3.91 (m, 1H, Gal-H5), 4.00-4.05 (m, 2H, Fuc-H2, Fuc-H3), 4.12 (dd, *J* = 4.5, 7.9 Hz, 1H, Lac-H2), 4.24-4.28 (m, 2H, Gal-H6a, C*H*$_2$Ph), 4.36 (dd, *J* = 5.6, 11.4 Hz, 1H, Gal-H6b), 4.51, 4.62, 4.67, 4.74, 4.79 (5 m, 5H, 3 C*H*$_2$Ph), 4.56 (d, *J* = 8.2 Hz, 1H, Gal-H1), 4.89 (m, 1H, Fuc-H5), 5.04 (m, 1H, C*H*$_2$Ph), 5.04 (m, 1H, Fuc-H1), 5.12 (m, 1H, C*H*$_2$Ph), 5.61 (m, 1H, Gal-H2), 5.85 (m, 1H, Gal-H4), 7.19-7.33, 7.42-7.48, 7.53-7.58, 8.04-8.12 (4 m, 35H, 7 C$_6$H$_5$); ^{13}C NMR (CDCl$_3$, 125 MHz): δ = 16.77 (Fuc-C6), 18.51 (Me), 25.46, 25.71, 26.07, 32.60, 33.19, 33.40, 35.37, 38.04, 40.21, 40.46 (11C, Cy, CH$_2$Cy), 51.68 (Me), 62.50 (Gal-C6), 66.38 (Fuc-C5), 66.65 (*C*H$_2$Ph), 70.20 (Gal-C4), 71.60 (Gal-C5), 71.99 (Gal-C2), 72.05, 74.39, 74.90 (3 *C*H$_2$Ph), 76.18 (Fuc-C2), 78.02 (Gal-C3), 78.41 (Lac-C2), 79.23 (Fuc-C4), 79.84 (Fuc-C3), 80.08 (C-3), 80.64 (C-4), 98.11 (Fuc-C1), 100.13 (Gal-C1), 126.91, 127.05, 127.20, 127.45, 127.71, 128.04, 128.09, 128.12, 128,42, 128.45, 128.52, 128.56,129.56, 129.65, 129.75, 129.93, 133.09, 133.21, 133.30, 135.40, 138.49, 138.95, 139.15 (42C, 7 C$_6$H$_5$), 164.60, 166.08, 166.15, 172.43, 174.09 (5 CO); IR (KBr): ν = 2925 (s), 1731 (vs, C=O), 1602 (w), 1497 (w), 1452 (m), 1267 (vs), 1176 (m), 1097 (vs), 712 (s) cm^{-1}; elemental analysis: calcd (%) for C$_{79}$H$_{86}$O$_{18}$ (1323.53): C 71.69, H 6.55; found: C 71.73, H 6.65.

{(1*R*,3*R*,4*R*,5*S*)-4-[(α-L-fucopyranosyl)oxy]-1-methoxycarbonyl-5-methyl-cyclohex-3-yl} 2-*O*-benzoyl-3-*O*-[(1*S*)-1-carboxy-2-cyclohexyl-ethyl]-β-D-galactopyranoside (3). A mixture of **16** (310 mg, 0.234 mmol), Pd(OH)$_2$/C (115 mg), dioxane (4.8 mL) and water (1.4 mL) was hydrogenated (70 psi H$_2$) at rt. After 5 h, the mixture was filtered through a PTFE membrane filter and evaporated to dryness. The residue was redissolved in anhydrous MeOH (5.5 mL) and 0.1 M NaOMe/MeOH (370 μL) was added. After stirring at rt for 16 h the reaction was quenched by addition of acetic acid (35 μL). The mixture was concentrated *in vacuo* and purified by preparative HPLC to afford compound **3** (125 mg, 71%) as a white solid. [α]$_D^{20}$ -85.0 (*c* 0.57, MeOH);^{1}H NMR (CD$_3$OD, 500 MHz): δ = 0.55-0.75 (m, 4H, Cy), 0.92 (m, 1H, Cy), 1.04-1.15 (m, 2H, H-6a, H-2a), 1.10 (d, *J* = 6.5 Hz, 3H, CH$_3$), 1.21-1.36 (m, 5H, Cy), 1.33 (d, *J* = 6.5 Hz, 3H, Fuc-H6), 1.43 (ddd, *J* = 3.0, 9.6, 13.9 Hz, 1H, Lac-H3a), 1.52 (ddd, *J* = 4.0, 10.0, 14.0 Hz, 1H, Lac-H3b), 1.60 (m, 1H, Cy), 1.64 (m, 1H, H-5),

1.76 (m, 1H, H-6b), 2.28 (m, 1H, H-2b), 2.40 (m, 1H, H-1), 3.10 (t, J = 9.6 Hz, 1H, H-4), 3.56-3.58 (m, 4H, Gal-H5, Me), 3.63-3.68 (m, 2H, Gal-H3, H-3), 3.71-3.79 (m, 4H, Gal-H6, Fuc-H2, -H4), 3.85 (dd, J = 3.3, 10.3 Hz, 1H, Fuc-H3), 3.97 (m, 1H, Gal-H4), 4.07 (dd, J = 3.0, 9.9 Hz, 1H, Lac-H2), 4.69 (d, J = 8.1 Hz, 1H, Gal-H1), 4.94 (d, J = 4.0 Hz, 1H, Fuc-H1), 4.99 (m, 1H, Fuc-H5), 5.43 (dd, J = 8.2, 9.7 Hz, 1H, Gal-H2), 7.49-7.52, 7.62-7.65, 8.07-8.09 (3 m, 5H, C_6H_5); ^{13}C NMR (CD$_3$OD, 125 MHz): δ = 16.72 (Fuc-C6), 19.18 (Me), 26.59, 26.78, 27.32, 33.13, 34.23 (5C, Cy), 34.95 (C-2), 35.12 (Cy), 36.98 (C-6), 39.17 (C-5), 41.40 (C-1), 42.80 (Lac-C3), 52.27 (Me), 62.68 (Gal-C6), 67.72 (Fuc-C5), 67.78 (Gal-C4), 70.35 (Fuc-C2), 71.47 (Fuc-C3), 73.11 (Gal-C2), 74.00 (Fuc-C4), 75.92 (Gal-C5), 77.91 (Lac-C2), 79.97 (C-3), 83.06 (C-4), 83.60 (Gal-C3), 100.53 (Fuc-C1), 100.76 (Gal-C1), 129.71, 130.96, 131.60, 134.40 (6C, C_6H_5), 166.88 (COPh), 176.18 (COOMe), 178.81 (COOH); elemental analysis: calcd (%) for $C_{37}H_{54}O_{16} \cdot H_2O$ (754.82): C 57.50, H 7.30; found: C 57.53, H 7.16; HR-MS: m/z: calcd for $C_{37}H_{53}O_{16}$ [M-H]⁻: 753.3339; found: 753.3331.

(1R,3R,4R,5S)-N-(2-Aminoethyl)-3-[2-O-benzoyl-3-O-((1S)-1-carboxy-2-cyclohexyl-ethyl)-(β-D-galactopyranosyl)oxy]-4-[(α-L-fucopyranosyl)oxy]-5-methyl-cyclohexanecarboxamide (17). Ester **3** (31 mg, 41.1 µmol) was dissolved in ethane-1,2-diamine (2.5 mL) in a bomb tube and stirred at 65 to 70°C for 2 h. The diamine was removed under reduced pressure, and the residue was purified by preparative HPLC-MS (H$_2$O/MeCN + 0.2% HCO$_2$H). To increase solubility, **17** was dissolved in MeOH, 1 equivalent of aq. NaOH (101.75 mM, 148 µL) was added, and the solvent was removed *in vacuo* to yield the sodium salt **17B** (30 mg, 93%). $[\alpha]_D^{20}$ (**17B**) -77.2 (*c* 1.13, MeOH); ^{1}H NMR (500 MHz, CD$_3$OD): δ = 0.42-0.72 (m, 4H, Cy), 0.88 (m, 1H, Cy), 1.05-1.20 (m, 6H, Me, H-2a, Cy, H-6a), 1.20-1.34 (m, 7H, 4 Cy, Fuc-H6), 1.39 (m, 1H, Lac H-3a), 1.43-1.58 (m, 2H, Lac H-3b, Cy), 1.62-1.73 (m, 2H, H-6, H-5), 2.17 (m, 1H, H-2b), 2.35 (m, 1H, H-1), 3.04 (t, J = 6.2 Hz, 2H, H-2'), 3.15 (t, J = 9.5 Hz, 1H, H-4), 3.34-3.45 (m, 2H, H-1'), 3.63-3.71 (m, 2H, Gal-H5, Gal-H3), 3.71-3.84 (m, 5H, Gal-H6, H-3, Fuc-H, -H4), 3.89 (dd, J = 3.3, 10.4 Hz, 1H, Fuc-H3), 3.93 (dd, J = 2.7, 10.2 Hz, 1H, Lac-H1), 3.99 (d, J = 2.6 Hz, 1H, Gal-H4), 4.75 (d, J = 8.1 Hz, 1H, Gal-H1), 4.97 (q, J = 6.5 Hz, 1H, Fuc-H5), 5.02 (d, J = 4.0 Hz, 1H, Fuc-H1), 5.35 (dd, J = 8.5, 9.3 Hz, 1H, Gal-H2), 7.51-7.58, 7.66-7.73, 8.03-8.10 (m, 5H, C_6H_5); ^{13}C NMR (**17B**) (125 MHz, CD$_3$OD/D$_2$O 1:1): δ = 16.54 (Fuc-C6), 18.96 (Me), 26.22, 26.45, 26.92, 32.53, 34.14, 34.88 (6C, Cy), 35.25 (C-2), 36.66 (C-6), 38.52 (C-5), 40.82 (2C, C-1', C-2'), 42.57 (C-1), 43.02 (Lac-C3), 62.85 (Gal-C6), 67.44, 67.69 (Fuc-C5, Gal-C4), 69.54

68

(Fuc-C2), 70.68 (Lac-C2), 73.04 (Gal-C2), 73.32 (Fuc-C3), 75.61 (Gal-C3), 79.57 (C-3), 80.11 (Fuc-C4), 82.78 (Gal-C5), 83.21 (C-4), 99.97 (Fuc-C1), 100.12 (Gal-C1), 129.75, 130.57, 130.73, 134.86 (6C, C_6H_5), 168.06 (COPh), 178.13 (CONH), 183.36 (COOH); IR (KBr): ν = 3430 (vs, OH), 2926 (s), 2852 (w), 1725 (m, C=O), 1651 (m, C=O), 1586 (m), 1451 (w), 1383 (w), 1272 (s), 1097 (vs), 1075 (vs), 1026 (s), 963 (vw), 801 (vw), 765 (vw), 711 (w), 678 (vw) cm^{-1}; HR-MS: m/z: calcd for $C_{38}H_{58}N_2O_{15}$ [M+H]$^+$: 783.3910; found: 783.3922.

(1R,3R,4R,5S)-3-[2-O-Benzoyl-3-O-((1S)-1-carboxy-2-cyclohexyl-ethyl)-(β-D-galactopyranosyl)oxy]-4-[(α-L-fucopyranosyl)oxy]-5-methyl-N-{2-[2,2,6,6-tetramethyl-1-oxyl-piperidine-4-carboxamido]ethyl}cyclohexanecarboxamide (18•). HBTU (11.3 mg, 29.8 µmol), HOBt (9.0 mg, 58.8 µmol) and 4-carboxy-TEMPO (5.8 mg, 29.1 µmol) were dissolved in anhydrous DMF (1 mL) in an Eppendorf tube. After shaking for 10 min, the solution was transferred to a flask containing amine **17** (11 mg, 0.0137 mmol), and DIPEA (10 µL, 58.8 µmol) was added. The solvent was removed under reduced pressure after 1 h, and the residue was purified by preparative HPLC-MS (H$_2$O/MeCN + 0.2% HCO$_2$H) giving the product **18•** as a reddish solid (6.3 mg, 48%). [α]$_D^{20}$ -63.5 (c 0.56, MeOH); HR-MS: m/z: calcd for $C_{48}H_{74}N_3O_{17}^\bullet$ [M+Na]$^+$: 987.4910; found: 987.4920.

For obtaining the NMR data, oxyl **18•** (6.3 mg, 6.53 µmol) was reduced to hydroxide **18*** by treatment with a solution of Na-L-ascorbate (5.8 mg, 29.3 µmol) in MeOH (1 mL) at rt for 1 h. The solvent was removed under reduced pressure, and the residue was purified by preparative HPLC-MS (H$_2$O/MeCN + 0.2% HCO$_2$H) to yield **18*** (4.3 mg, 68%) as a colorless powder. ^{1}H NMR (500 MHz, CD$_3$OD): δ = 0.43-0.68 (m, 4H, Cy), 0.87 (m, 1H, Cy), 1.08 (s, 3H, Me), 1.12-1.22 (m, 3H, H-2a, H-6a, Cy), 1.22-1.39 (m, 20H, Cy, TEMPO-CH$_3$, Fuc-H6, Lac-H3a), 1.45 (m, 1H, Lac-H3b), 1.51-1.68 (m, 3H, Cy, H-6b, H-5), 1.78-1.88 (m, 4H, TEMPO-H3), 2.10-2.25 (m, 2H, H-2, H-1), 2.72 (dt, J = 7.7, 15.1 Hz, 1H, TEMPO-H4), 3.07-3.22 (m, 5H, H-4, H-1', H-2'), 3.49-3.59 (m, 2H, Gal-H3, -H5), 3.62-3.78 (m, 5H, H-3, Gal-H6, Fuc-H2, -H4), 3.80-3.91 (m, 3H, Fuc-H3, Gal-H4, Lac H-2), 4.66 (d, J = 7.8 Hz, 1H, Gal-H1), 4.91-4.97 (m, 2H, Fuc-H1, -H5), 5.41 (t, J = 8.3 Hz, 1H, Gal-H2), 7.42-7.50, 7.54-7.61, 7.76-7.83 (m, 5H, C_6H_5); ^{13}C NMR (125 MHz, CD$_3$OD): δ = 16.77 (Fuc-C6), 19.38 (Me), 20.33 (2C, TEMPO-Me), 26.59, 26.78, 27.34 (3C, Cy), 29.66 (2C,

TEMPO-Me), 33.19, 34.36 (2C, Cy), 35.16, 35.23 (2C, Cy, C-2), 36.15 (TEMPO-C4), 37.59 (C-6), 39.36 (C-5), 40.14, 40.22 (C-1', C-2'), 41.57 (2C, TEMPO-C3), 43.05 (2C, C-1, Lac-C3), 43.20 (Gal-C6), 65.05 (2C, TEMPO-C2), 67.76 (2C, Gal-C4, Fuc-C5), 70.36 (Fuc-C2), 71.41 (Fuc-C3), 72.99 (Gal-C2), 73.92 (Fuc-C4), 76.07 (Gal-C5), 79.60 (Lac-C3), 79.70 (C-3), 83.09 (C-4), 83.65 (Gal-C3), 100.49 (Gal-C1), 100.58 (Fuc-C1), 129.71, 130.97, 131.66, 134.31 (6C, C_6H_5), 166.83 (COPh), 176.38, 177.32 (2 CONH).

6-(Trimethylsilyl)-hex-5-yn-1-ol (20d). Under argon, hex-5-yn-1-ol (**19d**, 1.03 g, 10.5 mmol) was dissolved in anhydrous THF (10 mL) and cooled to -90°C. ^{t}BuLi (1.6 M in pentane; 14.4 mL, 23.1 mmol) was added over a period of 10 min, which lead to refreezing of the reaction mixture. Gradual warming to -10 °C over 15 min led to liquefaction, and after 2 h of stirring, Me_3SiCl (3.0 mL, 23.1 mmol) was added. After 2 h, 1 M aq. HCl (3 mL) was added and stirring was continued for another hour. The reaction mixture was extracted with Et_2O (3 × 40 mL), the combined organic layers were washed with satd aq. $NaHCO_3$ (20 mL) and brine (20 mL). The dried (Na_2SO_4) organic phases were concentrated *in vacuo* to give **20d** (2.10 g) as colorless oil, which was used without further purification.

3-(Trimethylsilyl)prop-2-ynyl methanesulfonate (21a). 3-(Trimethylsilyl)prop-2-yn-1-ol (**20a**, 1.56 g, 12.2 mmol) was dissolved in anhydrous DCM (37 mL) under argon. The solution was cooled to -78 °C, followed by addition of Et_3N (3.37 mL, 24.3 mmol). $MeSO_2Cl$ (0.948 mL, 12.2 mmol) was added over a period of 10 min, leading to the formation of a white precipitate. After stirring at -78 °C for 30 min, the reaction mixture was washed with 0.5 M aq. HCl (15 mL), satd aq. $NaHCO_3$ (20 mL), and brine (20 mL). After extraction of the aqueous layers with DCM (2 × 30 mL), the combined organic layers were dried over Na_2SO_4, and the solvent was removed *in vacuo* to give **21a** (2.46 g) as a pale yellow liquid, which was used without further purification.

4-(Trimethylsilyl)but-3-ynyl methanesulfonate (21b). Following the procedure for **21a**, 4-(trimethylsilyl)but-3-yn-1-ol (**20b**, 3.12 g, 21.9 mmol) was treated with Et_3N (6.07 mL, 43.8 mmol) and $MeSO_2Cl$ (2.05 mL, 26.3 mmol) in DCM (65 mL) for 1.5 h at -15 °C. After workup **21b** (4.88 g) was obtained as pale yellow oil, which was used without further purification.

5-(Trimethylsilyl)pent-4-ynyl methanesulfonate (21c). Following the procedure for **21a**, 5-(trimethylsilyl)pent-4-yn-1-ol (**20c**, 2.29 g, 14.7 mmol) was treated with Et$_3$N (4.07 mL, 29.4 mmol) and MeSO$_2$Cl (1.37 mL, 17.6 mmol) in DCM (50 mL) for 2 h at -15 °C. After workup **21c** (3.56 g) was obtained as pale yellow oil, which was used without further purification.

6-(Trimethylsilyl)hex-5-ynyl methanesulfonate (21d). MeSO$_2$Cl (0.98 mL, 12.6 mmol) was added to a solution of **20d** (2.10 g) and Et$_3$N (2.9 mL, 21.0 mmol) in anhydrous DCM (35 mL) at -15 °C. The reaction mixture was allowed to warm to rt, and after 1.5 h it was washed with 0.5 M aq. HCl (10 mL), satd aq. NaHCO$_3$ (15 mL), and brine (15 mL). After extraction of the aqueous layers with DCM (2 × 30 mL), the combined organic layers were dried over Na$_2$SO$_4$, and the solvent was removed *in vacuo*. The residue was purified by silica gel chromatography (petroleum ether/DCM) to afford **21d** (2.26 g) as a colorless liquid.

(3-Azidoprop-1-ynyl)trimethylsilane (22a). To a solution of **21a** (2.46 g, 11.9 mmol) in anhydrous DMF (50 mL) was added NaN$_3$ (870 mg, 13.4 mmol), and the suspension was heated to 65 °C with vigorous stirring for 35 min under argon. Then water (30 mL) was added, the suspension was filtered through a plug of celite, and the celite was washed with Et$_2$O (80 mL). The water-DMF mixture was extracted with Et$_2$O (3 × 60 mL), and the organic layers were thoroughly washed with water (2 × 40 mL) and brine (40 mL). The combined organic layers were dried over Na$_2$SO$_4$ and the solvent was removed *in vacuo* to give **22a** (1.82 g) as a yellow liquid, which was used without further purification.

(4-Azidobut-1-ynyl)trimethylsilane (22b). Following the procedure for **22a**, mesylate **21b** (4.88 g, 22.1 mmol) was reacted with NaN$_3$ (1.57 g, 24.1 mmol) in DMF (55 mL) for 3 h. After workup **22b** (3.35 g) was obtained as a yellow liquid, which was used without further purification.

(5-Azidopent-1-ynyl)trimethylsilane (22c). Following the procedure for **22a**, mesylate **21c** (3.56 g, 15.2 mmol) was reacted with NaN$_3$ (1.10 g, 16.9 mmol) in DMF (35 mL) for 2.5 h.

After workup **22c** (2.62 g) was obtained as a yellow liquid, which was used without further purification.

(5-Azidohex-1-ynyl)trimethylsilane (22d). Following the procedure for **22a**, mesylate **21d** (2.26 g, 9.10 mmol) was reacted with NaN_3 (716 mg, 11.0 mmol) in DMF (20 mL) for 1 h. After workup **22d** (1.41 g) was obtained as a yellow liquid, which was used without further purification. ^{1}H NMR (500 MHz, $CDCl_3$): δ = 0.12 (s, 9H, $Si(CH_3)_3$), 1.57-1.66 (m, 2H, H-3), 1.81-1.89 (m, 2H, H-2), 2.99 (s, 3H, CH_3SO_2), 4.24 (t, J = 6.4 Hz, 2H, H-1); ^{13}C NMR (125 MHz, $CDCl_3$): δ = 0.18 ($Si(CH_3)_3$), 19.32 (C-4), 24.49 (C-3), 28.22 (C-2), 37.49 (CH_3SO_2), 69.59 (C-1), 85.52 (C-6), 106.19 (C-5).

3-(Trimethylsilyl)-prop-2-yn-1-amine (23a). To a solution of **22a** (1.82 g, 11.9 mmol) in THF (50 mL) and water (1 mL) was added PPh_3 (3.18 g, 12.2 mmol). The solution was stirred at 50 °C for 2 h. After careful removal of the solvents *in vacuo* ($\geq$ 200 mbar), the reaction mixture was subjected to vacuum distillation (oil bath temperature: 100 °C; approx. 5 mbar; additional cooling trap with liquid nitrogen) to give **23a** (1.29 g, 83% over 3 steps from **20a**) as a colorless liquid. ^{1}H NMR (500 MHz, $CDCl_3$): δ = 0.11 (s, 9H, $Si(CH_3)_3$), 1.37 (s, 2H, NH_2), 3.38 (s, 2H, H-1); ^{13}C NMR (125 MHz, $CDCl_3$): δ = 0.09 (3C, $Si(CH_3)_3$), 32.51 (C-1), 86.72 (C-2), 107.41 (C-3); IR (film): v = 3375 (s, NH_2), 3295 (s, NH_2), 3181 (m, NH_2), 2960 (vs), 2900 (s), 2850 (m), 2167 (vs, C≡C), 1599 (w, NH_2), 1409 (w), 1379 (w), 1332 (s), 1251 (s, $Si(CH_3)_3$), 1074 (m), 998 (s), 955 (m), 908 (m), 842 (m, $Si(CH_3)_3$), 760 (m, $Si(CH_3)_3$), 734 (m), 699 (m), 642 (m), 584 (m) cm^{-1}.

The NMR data were in accordance with previously published values.[S2]

4-(Trimethylsilyl)-but-3-yn-1-amine (23b). To a solution of **22b** (3.35 g, 20.0 mmol) in THF (90 mL) and water (1.8 mL) was added PPh_3 (5.76 g, 21.9 mmol). The solution was stirred at 50 °C for 1.5 h. After removal of the solvents *in vacuo*, the reaction mixture was subjected to vacuum distillation (oil bath temperature: 120 °C; approx. 0.1 mbar; additional cooling trap with liquid nitrogen) to give **23b** (2.49 g, 80% over 3 steps from **20b**) as a colorless liquid. ^{1}H NMR (500 MHz, $CDCl_3$): δ = 0.12 (s, 9H, $Si(CH_3)_3$), 1.40 (s, 2H, NH_2), 2.34 (t, 2H, H-1), 2.80 (t, 2H, H-2); ^{13}C NMR (125 MHz, $CDCl_3$): δ = 0.23 ($Si(CH_3)_3$), 25.08

(C-2), 41.09 (C-1), 86.29 (C-3), 105.09 (C-4); IR (film): v = 3373 (m, NH$_2$), 3297 (m, NH$_2$), 2959 (vs), 2896 (s,), 2868 (s, C-H), 2174 (vs, C≡C), 1678 (m, NH$_2$), 1621 (w), 1455 (m), 1425 (m), 1409 (m), 1383 (m), 1355 (m), 1250 (vs, Si(CH$_3$)$_3$), 1179 (vw), 1157 (vw), 1119 (vw), 1085 (w), 1034 (s), 979 (m), 908 (s), 844 (vs, Si(CH$_3$)$_3$), 760 (vs, Si(CH$_3$)$_3$), 734 (vs), 699 (m), 639 (s), 574 (m) cm^{-1}.

The ^{1}H NMR data were in accordance with previously published values.[S3]

5-(Trimethylsilyl)-pent-4-yn-1-amine (23c). To a solution of **22c** (1.30 g, 7.17 mmol) in THF (100 mL) and water (1 mL) was added PPh$_3$ (2.24 g, 8.5 mmol). The solution was stirred at 50 °C for 4.5 h. After removal of the solvents *in vacuo*, the reaction mixture was subjected to vacuum distillation (oil bath temperature: 120 °C; approx. 0.1 mbar) to give **23c** (973 mg, 43% over 3 steps from **20c**) as colorless oil. ^{1}H NMR (500 MHz, CDCl$_3$): δ = 0.12 (s, 9H, Si(CH$_3$)$_3$), 1.18 (s, 2H, NH$_2$), 1.62 (m, 2H, H-2), 2.27 (t, J = 7.0 Hz, 2H, H-3), 2.77 (t, J = 6.9 Hz, 2H, H-1); ^{13}C NMR (125 MHz, CDCl$_3$): δ = 0.23 (Si(CH$_3$)$_3$), 17.42 (C-3), 32.42 (C-2), 41.34 (C-1), 84.95 (C-4), 106.92 (C-5); IR (film): v = 3376 (m, NH$_2$), 3297 (w, NH$_2$), 3181 (w, NH$_2$), 2955 (vs), 2861 (vs), 2173 (vs, C≡C), 1682 (w), 1602 (w, NH$_2$), 1431 (s), 1408 (m), 1324 (m), 1250 (vs, Si(CH$_3$)$_3$), 1087 (s), 1000 (m), 914 (s), 843 (vs, Si(CH$_3$)$_3$), 760 (vs, Si(CH$_3$)$_3$), 734 (vs), 698 (s), 640 (s), 579 (w) cm^{-1}.

The spectral data were in accordance with previously published values.[S4]

6-(Trimethylsilyl)-hex-5-yn-1-amine (23d). To a solution of **22d** (1.41 g, 7.22 mmol) in THF (100 mL) and water (1 mL) was added PPh$_3$ (2.27 g, 8.65 mmol). The solution was stirred at 50-60 °C for 4.5 h. After removal of the solvents *in vacuo*, the reaction mixture was subjected to vacuum distillation (oil bath temperature: 120 °C; approx. 0.1 mbar) to give **23d** (1.10 g, 62% over 4 steps from **19d**) as colorless oil. ^{1}H NMR (500 MHz, CDCl$_3$): δ = 0.43 (s, 9H, Si(CH$_3$)$_3$), 1.39 (s, 2H, NH$_2$), 1.82-1.87 (m, 4H, H-2, H-3), 2.53 (t, J = 6.6 Hz, 2H, H-4), 2.98-3.03 (m, 2H, H-1); ^{13}C NMR (125 MHz, CDCl$_3$): δ = 0.06 (Si(CH$_3$)$_3$), 19.62 (C-4), 25.89 (C-3), 32.87 (C-2), 41.65 (C-1), 84.89 (C-6), 107.12 (C-5); IR (film): v = 3371 (s, NH$_2$), 3296 (s, NH$_2$), 3181 (m, NH$_2$), 2957 (vs), 2929 (vs), 2901 (vs), 2860 (vs), 2173 (vs, C≡C), 1596 (m, NH$_2$), 1455 (m), 1431 (m), 1408 (m), 1364 (w), 1326 (m), 1249 (vs, Si(CH$_3$)$_3$), 1051 (m), 1027 (m), 998 (w), 937 (m), 842 (vs, Si(CH$_3$)$_3$), 760 (vs, Si(CH$_3$)$_3$), 698 (s), 639 (s), 619 (vw), 461 (s) cm^{-1}.

(1*R*,3*R*,4*R*,5*S*)-3-[2-*O*-Benzoyl-3-*O*-((1*S*)-1-carboxy-2-cyclohexyl-ethyl)-(β-ᴅ-galactopyranosyl)oxy]-4-[(α-ʟ-fucopyranosyl)oxy]-5-methyl-cyclohexanecarboxylic acid (24). Ester **3** (268 mg, 0.355 mmol) was dissolved in a 1 M solution of NaOH in H_2O/MeOH (1:1, 8 mL) and stirred at rt for 3 h. The reaction was quenched by addition of 0.5 M aq. HCl (1.6 mL), and the solvents were removed *in vacuo*. The residue was purified by preparative HPLC-MS (H_2O/MeCN + 0.2% HCO_2H) yielding **24** (207 mg, 79%) as a white powder. The starting material was partially recovered (25 mg, 9%). $[\alpha]_D^{20}$ -67.2 (*c* 0.40, MeOH); ^{1}H NMR (500 MHz, CD_3OD): δ = 0.50-0.75 (m, 4H, Cy), 0.92 (m, 1H, Cy), 1.11 (d, *J* = 6.4 Hz, 3H, Me), 1.06-1.16 (m, 2H, H-6a, H-2a), 1.33 (d, *J* = 6.5 Hz, 3H, Fuc-H6), 1.19-1.38 (m, 5H, 5Cy), 1.43 (m, 1H, Lac-H3a), 1.52 (m, 1H, Lac-H3b), 1.56-1.72 (m, 2H, Cy, H-5), 1.78 (d, *J* = 12.8 Hz, 1H, H-6), 2.29-2.40 (m, 2H, H-2, H-1), 3.11 (t, *J* = 9.5 Hz, 1H, H-4), 3.58 (t, *J* = 5.6 Hz, 1H, Gal-H5), 3.64-3.80 (m, 6H, Gal-H3, -H6, H-3, Fuc-H2, -H4), 3.85 (dd, *J* = 3.0, 10.3 Hz, 1H, Fuc-H3), 3.96 (s, 1H, Gal-H4), 4.03-4.08 (m, 1H, Lac-H2), 4.71 (d, *J* = 8.1 Hz, 1H, Gal-H1), 4.95 (m, 1H, Fuc-H1), 4.99 (dd, *J* = 6.1, 12.6 Hz, 1H, Fuc-H5), 5.44 (t, *J* = 8.8 Hz, 1H, Gal-H2), 7.46-7.52, 7.58-7.64, 8.04-8.11 (m, 5H, C_6H_5); ^{13}C NMR (125 MHz, CD_3OD): δ = 16.70 (Fuc-C6), 19.20 (Me), 26.53, 26.72, 27.28, 33.08, 34.17 (5 Cy), 35.05, 35.08 (Cy, C-2), 37.10 (C-6), 39.20 (C-5), 41.38 (C-1), 42.78 (Lac-C3), 62.68 (Gal-C6), 67.70, 67.75 (Gal-C4, Fuc-C5), 70.32 (Fuc-C2), 71.44 (Fuc-C3), 73.01 (Gal-C2), 73.97 (Fuc-C4), 75.89 (Gal-C5), 77.91 (Lac-C2), 79.95 (C-3), 83.16 (C-4), 83.67 (Gal-C3), 100.49 (Fuc-C1), 100.61 (Gal-C1), 129.68, 130.92, 131.53, 134.35 (6C, C_6H_5), 166.94 (*C*OPh), 177.88 (Cy-COOH), 178.89 (Lac-COOH); IR (KBr): v = 3433 (vs, OH), 2927 (s), 2854 (m) 1720 (vs, C=O), 1638 (w), 1450 (m), 1339 (m), 1316 (m), 1272 (vs), 1207 (m), 1167 (m), 1111 (vs), 1079 (vs), 999 (m), 967 (w), 846 (w), 806 (vw), 771 (vw) 712 (s), 677 (w), 628 (w), 559 (w) cm^{-1}; elemental analysis: calcd (%) for $C_{36}H_{52}O_{16}\cdot H_2O$ (758.80): C 56.98, H 7.14; found: C 57.08, H 6.97.

General procedure A for the synthesis of 25a-d. Dicarboxylic acid **24** (1 eq.) and HOBt (3 eq.) were dissolved in anhydrous DMF (approx. 0.025 M) under argon. HBTU (1.1-1.2 eq.) was added and the solution was stirred at rt for 5 min. An excess of alkyne amine (approx. 10% v/v) was added, and stirring was continued until no further consumption of starting material was observed in MS (after 1.5 to 3 h). The solvent was removed *in vacuo*, and the residue was purified by preparative HPLC-MS (H_2O/MeCN + 0.2 % HCO_2H), and the

desired monoamide was isolated based on its retention time ($t_{R(Cy\ amide)} > t_{R(Lac\ amide)}$). The identity of the amide was verified by 2D HMBC NMR (coupling of linker and cyclohexyl protons to the amide C=O).

General procedure B for the synthesis of 26a-d. To an approx. 0.03 mM solution of TMS-protected alkyne amide **25a-d** (1 eq.) in anhydrous THF, TBAF (2 eq.; 1 M solution in THF) was added at rt under argon. The solution was stirred for 1-2 h, and the solvent was removed *in vacuo*. The residue was purified by RP-18 chromatography (water/MeOH) or preparative HPLC-MS (H_2O/MeCN + 0.2 % HCO_2H).

(1R,3R,4R,5S)-3-[2-O-Benzoyl-3-O-((1S)-1-carboxy-2-cyclohexyl-ethyl)-(β-ᴅ-galactopyranosyl)oxy]-4-[(α-ʟ-fucopyranosyl)oxy]-5-methyl-N-[3-(trimethylsilyl)prop-2-yn-1-yl]cyclohexanecarboxamide (25a). Following general procedure A, **24** (100 mg, 0.135 mmol), HOBt (55.2 mg, 0.408 mmol), HBTU (53.6 mg, 0.141 mmol) and **23a** (500 μL) were stirred at rt for 3 h to afford **25a** (41 mg, 35%) as a white solid. The starting material **24** (28 mg, 28%) was partially recovered. ^{1}H NMR (500 MHz, CD$_3$OD): δ = 0.15 (s, 9H, Si(CH$_3$)$_3$), 0.52-0.75 (m, 4H, Cy), 0.91 (d, J = 12.6 Hz, 1H, Cy), 1.10 (d, J = 6.3 Hz, 3H, Me), 1.14-1.39 (m, 10H, H-2a, H-6a, 5Cy, Fuc-H6), 1.43 (m, 1H, Lac-H3a), 1.51 (m, 1H, Lac-H3b), 1.55-1.71 (m, 3H, Cy, H-6b, H-5), 2.15 (m, 1H, H-2b), 2.27 (s, 1H, H-1), 3.14 (t, J = 9.5 Hz, 1H, H-4), 3.57 (t, J = 5.7 Hz, 1H, Gal-H5), 3.62-3.81 (m, 6H, Gal-H3, -H6, H-3, Fuc-H2, -H4), 3.83-3.90 (m, 2H, Fuc-H3, H-1'a), 3.92-3.99 (m, 2H, Gal-H4, H-1'b), 4.04 (dd, J = 2.7, 9.5 Hz, 1H, Lac-H2), 4.69 (d, J = 8.0 Hz, 1H, Gal-H1), 4.94-5.00 (m, 2H, Fuc-H1, -H5), 5.43 (t, J = 8.8 Hz, 1H, Gal-H2), 7.48-7.54, 7.59-7.64, 8.03-8.08 (m, 5H, C$_6$H$_5$); ^{13}C NMR (125 MHz, CD$_3$OD): δ = -0.07 (Si(CH$_3$)$_3$), 16.69 (Fuc-C6), 19.22 (Me), 26.55, 26.68, 27.24 (3 Cy), 30.37 (C-1'), 33.12, 34.17, 35.02 (3 Cy), 35.31 (C-2), 37.25 (C-6), 39.25 (C-5), 42.73 (Lac-C3), 42.87 (C-1), 62.71 (Gal-C6), 67.68, 67.77 (Fuc-C5, Gal-C4), 70.30 (Fuc-C2), 71.43 (Fuc-C3), 72.99 (Gal-C2), 73.94 (Fuc-C4), 75.94 (Gal-C5), 77.99 (Lac-C2), 79.89 (C-3), 83.02 (C-4), 83.68 (Gal-C3), 87.81 (C-3'), 100.41 (Fuc-C1), 100.54 (Gal-C1), 103.04 (C-2'), 129.74, 130.87, 131.53, 134.34 (6C, C$_6$H$_5$), 166.84 (COPh), 176.41 (CONH), 178.81 (COOH); ESI-MS: m/z: calcd for C$_{42}$H$_{63}$NO$_{15}$Si [M-H]$^-$: 848.39; found: 848.54.

(1*R*,3*R*,4*R*,5*S*)-3-[2-*O*-Benzoyl-3-*O*-((1*S*)-1-carboxy-2-cyclohexyl-ethyl)-(β-D-galactopyranosyl)oxy]-4-[(α-L-fucopyranosyl)oxy]-5-methyl-*N*-[4-(trimethylsilyl)but-3-yn-1-yl]cyclohexanecarboxamide (25b). Following general procedure A, **24** (31.7 mg, 42.8 µmol), HOBt (17.7 mg, 135 µmol), HBTU (19.1 mg, 50.4 µmol) and **23b** (200 µL) were stirred at rt for 1.5 h to afford **25b** (30 mg, 70%) as a white solid. The starting material **24** (6.5 mg, 18%) was partially recovered. ^{1}H NMR (500 MHz, CD$_3$OD): δ = 0.15 (s, 9H, Si(CH$_3$)$_3$), 0.52-0.73 (m, 4H, Cy), 0.91 (d, J = 12.1 Hz, 1H, Cy), 1.11 (d, J = 6.4 Hz, 3H, Me), 1.14-1.38 (m, 10H, H-2a, H-6a, 5Cy, Fuc-H6), 1.42 (m, 1H, Lac-H3a), 1.47-1.71 (m, 4H, Lac-H3b, Cy, H-6b, H-5), 2.13 (m, 1H, H-2b), 2.27 (m, 1H, H-1), 2.32-2.38 (m, 2H, H-2'), 3.11-3.20 (m, 2H, H-4, H-1'a), 3.24 (m, 1H, H-1'b), 3.55 (t, J = 5.8 Hz, 1H, Gal-H5), 3.63 (dd, J = 2.8, 9.7 Hz, 1H, Gal-H3), 3.66-3.81 (m, 5H, H-3, Fuc-H2, -H4, Gal-H6), 3.86 (dd, J = 3.2, 10.3 Hz, 1H, Fuc-H3), 3.97 (d, J = 2.1 Hz, 1H, Gal-H4), 4.05 (dd, J = 2.6, 9.7 Hz, 1H, Lac-H2), 4.67 (d, J = 8.1 Hz, 1H, Gal-H1), 4.97-5.02 (m, 2H, Fuc-H1, -H5), 5.44 (dd, J = 8.5, 9.3 Hz, 1H, Gal-H2), 7.48-7.53, 7.60-7.65 (m 3H, C$_6$H$_5$), 7.94 (t, J = 5.8 Hz, 1H, NH), 8.04-8.09 (m, 2H, C$_6$H$_5$); ^{13}C NMR (125 MHz, CD$_3$OD): δ = 0.30 (Si(CH$_3$)$_3$), 16.70 (Fuc-C6), 19.26 (Me), 21.02 (C-2'), 26.53, 26.68, 27.23, 33.07, 34.14, 35.02 (6 Cy), 35.51 (C-2), 37.33 (C-6), 39.24 (C-5), 39.29 (C-1'), 42.72 (Lac-C3), 43.11 (C-1), 62.69 (Gal-C6), 67.66, 67.73 (Gal-C4, Fuc-C5), 70.26 (Fuc-C2), 71.38 (Fuc-C3), 72.94 (Gal-C2), 73.93 (Fuc-C4), 75.94 (Gal-C5), 77.93 (Lac-C2), 79.86 (C-3), 82.96 (C-4), 83.62 (Gal-C3), 86.23 (C-4'), 100.41 (Fuc-C1), 100.56 (Gal-C1), 105.35 (C-3'), 129.73, 130.87, 131.48, 134.37 (6C, C$_6$H$_5$), 166.78 (*C*OPh), 177.06 (CONH), 178.71 (COOH); ESI-MS: *m/z*: calcd for C$_{43}$H$_{65}$NO$_{15}$Si [M-H]$^-$: 862.41; found: 862.38.

(1*R*,3*R*,4*R*,5*S*)-3-[2-*O*-Benzoyl-3-*O*-((1*S*)-1-carboxy-2-cyclohexyl-ethyl)-(β-D-galactopyranosyl)oxy]-4-[(α-L-fucopyranosyl)oxy]-5-methyl-*N*-[5-(trimethylsilyl)pent-4-yn-1-yl]cyclohexanecarboxamide (25c). Following general procedure A, **24** (120 mg, 0.159 mmol), HOBt (67 mg, 0.496 mmol), HBTU (74 mg, 0.195 mmol) and **23c** (520 µL) were stirred at rt for 2 h to afford **25c** (57 mg, 40%) as a white solid. The starting material **24** (23 mg, 19%) was partially recovered. [α]$_D^{20}$ -61.5 (*c* 0.79, MeOH); ^{1}H NMR (500 MHz, CD$_3$OD): δ = 0.13 (s, 9H, Si(CH$_3$)$_3$), 0.57 (m, 1H, Cy), 0.62-0.73 (m, 3H, Cy), 0.91 (m, 1H, Cy), 1.11 (d, J = 6.5 Hz, 3H, Me), 1.15-1.38 (m, 10H, H-2a, H-6a, 5 Cy, Fuc-H6), 1.41 (m, 1H, Lac-H3a), 1.51 (m, 1H, Lac-H3b), 1.55-1.69 (m, 6H, Cy, H-6b, H-5, H-2'), 2.12 (d, J = 11.1 Hz, 1H, H-2), 2.19-2.25 (m, 3H, H-3', H-1), 3.10-3.24 (m, 3H, H-1', H-4), 3.56 (t, J =

5.7 Hz, 1H, Gal-H5), 3.62 (dd, J = 2.9, 9.7 Hz, 1H, Gal-H3), 3.65-3.81 (m, 5H, H-3, Fuc-H2, -H4, Gal-H6), 3.87 (dd, J = 3.3, 10.3 Hz, 1H, Fuc-H3), 3.93-3.98 (m, 2H, Lac-H2, Gal-H4), 4.68 (d, J = 8.1 Hz, 1H, Gal-H1), 4.95-5.02 (m, 2H, Fuc-H1, -H5), 5.43 (dd, J = 8.3, 9.4 Hz, 1H, Gal-H2), 7.48-7.53, 7.59-7.64 (m, 3H, C_6H_5), 7.77 (t, J = 5.6 Hz, 1H, NH), 8.04-8.08 (m, 2H, C_6H_5); ^{13}C NMR (125 MHz, CD_3OD): δ = 0.23 ($Si(CH_3)_3$), 16.72 (Fuc-C6), 18.03 (C-2'), 19.22 (Me), 26.56, 26.70, 27.26 (3 Cy), 29.64 (C-3'), 33.09, 34.15, 35.06 (4C, 3 Cy, C-2), 37.35 (C-6), 39.33 (C-5), 39.43 (C-1'), 42.76 (Lac-C3), 43.34 (C-1), 62.70 (Gal-C6), 67.69, 67.72 (Gal-H4, Fuc-H5), 70.28 (Fuc-C2), 71.40 (Fuc-C3), 72.96 (Gal-C2), 73.97 (Fuc-C4), 75.93 (Gal-C5), 77.77 (Lac-C2), 79.90 (C-3), 83.01 (C-4), 83.67 (Gal-C3), 85.42 (C-5'), 100.49 (Fuc-C1), 100.56 (Gal-C1), 107.62 (C-4'), 129.79, 130.87, 131.56, 134.41 (6C, C_6H_5), 166.77 (COPh), 177.12 (CONH), 178.75 (COOH); IR (KBr): ν = 3430 (vs, OH), 2927 (s), 2854 (m), 2175 (vw), 1726 (s, C=O), 1650 (m, C=O), 1542 (vw), 1535 (vw), 1450 (w), 1369 (w), 1338 (w), 1315 (w), 1271 (s), 1250 (m), 1166 (w), 1140 (vs), 1079 (vs) 1036 (s), 1001 (w), 969 (vw), 844 (m, $Si(CH_3)_3$), 760 (vw), 709 (w) cm^{-1}; ESI-MS: calcd for $C_{44}H_{67}NO_{15}Si$ [M-H]$^-$: 876.42; found: 862.63.

(1R,3R,4R,5S)-3-[2-O-Benzoyl-3-O-((1S)-1-carboxy-2-cyclohexyl-ethyl)-(β-D-galactopyranosyl)oxy]-4-[(α-L-fucopyranosyl)oxy]-5-methyl-N-[6-(trimethylsilyl)hex-5-yn-1-yl]cyclohexanecarboxamide (25d). Following general procedure A, **24** (47 mg, 63.4 µmol), HOBt (26 mg, 192 µmol), HBTU (29 mg, 76.5 µmol) and **23d** (200 µL) were stirred at rt for 2 h to afford **25d** (25 mg, 44%) as a white solid. The starting material **24** (5.5 mg, 12%) was partially recovered. ^{1}H NMR (500 MHz, CD_3OD): δ = 0.12 (s, 9H, $Si(CH_3)_3$), 0.51-0.75 (m, 4H, Cy), 0.91 (m, 1H, Cy), 1.11 (d, J = 6.4 Hz, 3H, Me), 1.15-1.28 (m, 3H, H-6a, H-2a, Cy), 1.27-1.38 (m, 7H, Fuc-H6, 4 Cy), 1.42 (m, 1H, Lac-H3a), 1.45-1.62 (m, 7H, Lac-H3b, H-3', H-2', H-6b, 3 Cy), 1.67 (m, 1H, H-5), 2.11 (m, 1H, H-2b), 2.21-2.28 (m, 3H, H-4', H-1), 3.08-3.12 (m, 2H, H-1'), 3.15 (t, J = 9.6 Hz, 1H, H-4), 3.56 (t, J = 5.9 Hz, 1H, Gal-H5), 3.65 (dd, J = 2.7, 9.8 Hz, 1H, Gal-H3), 3.67-3.81 (m, 5H, H-3, Fuc-H2, Gal-H6), 3.86 (dd, J = 3.2, 10.3 Hz, 1H, Fuc-H3), 3.96 (d, J = 2.3 Hz, 1H, Gal-H4), 4.06 (dd, J = 2.7, 9.7 Hz, 1H, Lac-H2), 4.69 (d, J = 8.0 Hz, 1H, Gal-H1), 4.95-5.01 (m, 2H, Fuc-H1, -H5), 5.43 (t, J = 8.9 Hz, 1H, Gal-H2), 7.48-7.53, 7.60-7.65 (m, 3H, C_6H_5), 7.77 (t, J = 5.6 Hz, 1H, NH), 8.05-8.08 (m, 2H, C_6H_5); ^{13}C NMR (125 MHz, CD_3OD): δ = 0.28 ($Si(CH_3)_3$), 16.71 (Fuc-C6), 19.25 (Me), 20.07 (C-4'), 26.53, 26.68 (2 Cy), 26.96 (C-3'), 27.24 (Cy), 29.54 (C-2'), 33.11, 34.15, 35.02 (3 Cy), 35.36 (C-2), 37.51 (C-6), 39.33 (C-5), 39.70 (C-1'), 42.72 (Lac-

C3), 43.31 (C-1), 62.71 (Gal-C6), 67.69 (Gal-C4), 67.74 (Fuc-C5), 70.27 (Fuc-C2), 71.39 (Fuc-C3), 72.99 (Gal-C2), 73.95 (Fuc-C4), 75.92 (Gal-C5), 77.85 (Lac-C2), 79.84 (C-3), 83.00 (C-4), 83.63 (Gal-C3), 85.22 (C-6'), 100.44 (Fuc-C1), 100.52 (Gal-C1), 108.17 (C-5'), 129.76, 130.85, 131.53, 134.40 (6C, C_6H_5), 166.78 (COPh), 176.96 (CONH), 178.72 (COOH).

(1R,3R,4R,5S)-3-[2-O-Benzoyl-3-O-((1S)-1-carboxy-2-cyclohexyl-ethyl)-(β-D-galactopyranosyl)oxy]-4-[(α-L-fucopyranosyl)oxy]-5-methyl-N-(prop-2-yn-1-yl)cyclohexanecarboxamide (26a). Following general procedure B, **25a** (49 mg, 57.6 μmol) was reacted with TBAF (115 μL, 115 μmol) in THF (2 mL) to give **26a** (36 mg, 80%) as a white solid. [α]$_D^{20}$ -67.5 (c 1.60, MeOH); ^{1}H NMR (500 MHz, CD$_3$OD): δ = 0.52-0.75 (m, 4H, Cy), 0.91 (m, 1H, Cy), 1.11 (d, J = 6.4 Hz, 3H, Me), 1.14-1.27 (m, 6H, 4 Cy, H-6a, H-2a), 1.27-1.38 (m, 4H, 4 Cy), 1.34 (d, J = 6.5 Hz, 3H, Fuc-H6a), 1.42 (m, 1H, Lac-H3a), 1.51 (m, 1H, Lac-H3b), 1.54-1.71 (m, 3H, H-6b, Cy, H-5), 2.15 (m, 1H, H-2b), 2.27 (m, 1H, H-1), 2.59 (t, J = 2.3 Hz, 1H, H-3'), 3.14 (t, J = 9.5 Hz, 1H, H-4), 3.57 (t, J = 5.9 Hz, Gal-H5), 3.65 (dd, J = 2.9, 9.8 Hz, 1H, Gal-H3), 3.67-3.92 (m, 8H, H-3, Fuc-H3, -H4, Gal-H6, H-1'), 3.96 (d, J = 2.2 Hz, 1H, Gal-H4), 4.05 (dd, J = 2.7, 9.6 Hz, 1H, Lac-H2), 4.69 (d, J = 8.0 Hz, 1H, Gal-H1), 4.96-5.00 (m, 2H, Fuc-H1, -H5), 5.42-5.45 (m, 1H, Gal-H2), 7.50 (t, J = 7.7 Hz, 2H, C_6H_5), 7.62 (t, J = 7.4 Hz, 1H, C_6H_5), 8.06 (d, J = 7.4 Hz, 2H, C_6H_5); ^{13}C NMR (125 MHz, CD$_3$OD): δ = 16.70 (Fuc-C6), 19.22 (Me), 26.51, 26.68, 27.25 (3 Cy), 29.39 (C-1'), 33.12, 34.17, 35.02 (3 Cy), 35.25 (C-2), 37.25 (C-6), 39.26 (C-5), 42.72 (Lac-C3), 42.93 (C-1), 62.72 (Gal-C6), 67.69, 67.78 (Fuc-C5, Gal-C4), 70.31 (Fuc-C2), 71.42 (Fuc-C3), 72.17 (C-3'), 72.98 (Gal-C2), 73.95 (Fuc-C4), 75.94 (Gal-C5), 77.96 (Lac-C2), 79.86 (C-3), 80.67 (C-2'), 83.00 (C-4), 83.65 (Gal-C3), 100.42 (Fuc-C1), 100.55 (Gal-C1), 129.74, 130.86, 131.51, 134.38 (6C, C_6H_5), 166.85 (COPh), 176.52 (CONH), 178.75 (COOH); IR (KBr): v = 3436 (vs, OH), 3308 (s, C≡C), 2927 (s), 2851 (m), 1727 (s, C=O), 1651 (m, C=O), 1534 (w), 1450 (m), 1341 (m), 1314 (m), 1270 (s), 1160 (m), 1111 (vs), 1079 (vs), 1030 (s), 966 (w), 773 (w), 712 (m), 674 (w), 631 (w) cm^{-1}; HR-MS: m/z: calcd for $C_{39}H_{55}NO_{15}$ [M+Na]$^+$: 800.3464; found: 800.3465.

(1R,3R,4R,5S)-3-[2-O-Benzoyl-3-O-((1S)-1-carboxy-2-cyclohexyl-ethyl)-(β-D-galactopyranosyl)oxy]-N-(but-3-yn-1-yl)-4-[(α-L-fucopyranosyl)oxy]-5-methyl-

cyclohexanecarboxamide (26b). Following general procedure B, **25b** (80 mg, 92.5 μmol) was reacted with TBAF (185 μL, 185 μmol) in THF (3.5 mL) to give **26b** (68 mg, 93%) as a white solid. $[\alpha]_D^{20}$ -72.8 (*c* 1.15, MeOH); ^{1}H NMR (500 MHz, CD$_3$OD): δ = 0.53-0.76 (m, 4H, 4 Cy), 0.91 (m, 1H, Cy), 1.11 (d, *J* = 6.3 Hz, 3H, Me), 1.14-1.27 (m, 3 H, Cy, H-6a, H-2a), 1.27-1.38 (m, 4H, 4 Cy), 1.34 (d, *J* = 6.5 Hz, 3H, Fuc-H6), 1.42 (m, 1H, Lac-H3a), 1.50 (m, 1H, Lac-H3b), 1.54-1.73 (m, 3H, H-6b, Cy, H-5), 2.13 (d, *J* = 11.8 Hz, 1H, H-2b), 2.21-2.32 (m, 4H, H-1, H-2', H-4'), 3.15 (t, *J* = 9.5 Hz, 1H, H-4), 3.18-3.27 (m, 2H, H-1'), 3.57 (m, 1H, Gal-H5), 3.63-3.82 (m, 6H, Gal-H3, -H6, H-3, Fuc-H2, -H4), 3.87 (dd, *J* = 3.1, 10.3 Hz, 1H, Fuc-H3), 3.96 (d, *J* = 1.8 Hz, 1H, Gal-H4), 4.05 (dd, *J* = 2.7, 9.6 Hz, 1H, Lac-H1), 4.68 (d, *J* = 8.0 Hz, 1H, Gal-H1), 4.94-5.92 (m, 2H, Fuc-H1, -H5), 5.41-5.45 (m, 1H, Gal-H2), 7.48-7.51, 7.61-7.64, 8.06-8.07 (m, 5H, C$_6$H$_5$); ^{13}C NMR (125 MHz, CD$_3$OD): δ = 16.69 (Fuc-C6), 19.25 (Me), 19.77 (C2'), 26.50, 26.67, 27.24, 33.13, 34.16, 35.00 (6 Cy), 35.44 (C-2), 37.36 (C-6), 39.27 (C-5), 39.33 (C-1'), 42.71 (Lac-C3), 43.18 (C-1), 62.72 (Gal-C6), 67.68, 67.77 (Fuc-C5, Gal-C4), 70.31 (Fuc-C2), 70.78 (C-4'), 71.41 (Fuc-C3), 72.99 (Gal-C2), 73.94 (Fuc-C4), 75.93 (Gal-C5), 77.96 (Lac-C2), 79.87 (C-3), 82.22 (C-3'), 82.98 (C-4), 83.61 (Gal-C3), 100.40 (Fuc-C1), 100.56 (Gal-C1), 129.71, 130.86, 131.52, 134.36 (6C, C$_6$H$_5$), 166.79 (*C*OPh), 177.12 (CONH), 178.74 (COOH); IR (KBr): v = 3435 (s), 3311(s, C≡C), 2927 (s), 2853 (m), 2115 (vw), 1727 (s, C=O), 1648 (m, C=O), 1544 (w), 1450 (m), 1364 (m), 1340 (m), 1315 (m), 1270 (s), 1221 (m), 1166 (m), 1111 (vs), 1073 (vs), 1031 (s), 999 (m), 966 (m), 901 (vw), 867 (vw), 806 (vw), 770 (w), 712 (m), 675 (w), 632 (w) cm^{-1}; HR-MS: *m/z*: calcd for C$_{40}$H$_{57}$NO$_{15}$ [M+Na]$^+$: 814.3620; found: 814.3620.

(1*R*,3*R*,4*R*,5*S*)-3-[2-*O*-Benzoyl-3-*O*-((1*S*)-1-carboxy-2-cyclohexyl-ethyl)-(β-D-galactopyranosyl)oxy]-4-[(α-L-fucopyranosyl)oxy]-5-methyl-*N*-(pent-4-yn-1-yl)cyclohexanecarboxamide (26c). Following general procedure B, **25c** (77 mg, 87.7 μmol) was reacted with TBAF (175 μL, 175 μmol) in THF (3.5 mL) to give **26c** (69 mg, 98%) as a white solid. $[\alpha]_D^{20}$ -66.4 (*c* 2.07, MeOH); ^{1}H NMR (500 MHz, CD$_3$OD): δ = 0.56 (m, 1H, Cy), 0.61-0.75 (m, 3H, 3 Cy), 0.92 (m, 1H, Cy), 1.11 (d, *J* = 6.5 Hz, 3H, Me), 1.15-1.26 (m, 3H, Cy, H-6a, H-2a), 1.27-1.38 (m, 4H, 4 Cy), 1.34 (d, *J* = 6.5 Hz, 3H, Fuc-H6), 1.44 (m, 1H, Lac-H3a), 1.51 (m, 1H, Lac-H3b), 1.55-1.61 (m, 2H, Cy, H-6b), 1.61-1.71 (m, 3H, H-2', H-5), 2.12 (m, 1H, H-2b), 2.18 (td, *J* = 2.6, 7.2 Hz, 2H, H-3'), 2.24 (m, 1H, H-1), 2.29 (t, *J* = 2.6 Hz, 1H, H-5'), 3.14 (t, *J* = 7.6 Hz, 1H, H-4), 3.14-3.24 (m, 2H, H-1'), 3.57 (m, 1H, Gal-H5), 3.64-3.80 (m, 6H, Gal-H3, -H6, H-3, Fuc-H2, -H4), 3.86 (dd, *J* = 3.2, 10.3 Hz, 1H, Fuc-

H3), 3.96 (d, J = 2.3 Hz, 1H, Gal-H4), 4.04 (dd, J = 2.6, 9.8 Hz, 1H, Lac-H2), 4.69 (d, J = 8.0 Hz, 1H, Gal-H1), 4.96 (d, J = 4.0 Hz, 1H, Fuc-H1), 5.00 (m, 1H, Fuc-H5), 5.43 (dd, J = 8.6, 9.2 Hz, 1H, Gal-H2), 7.50 (t, J = 7.7 Hz, 2H, C$_6$H$_5$), 7.62 (t, J = 7.4 Hz, 1H, C$_6$H$_5$) 7.80 (t, J = 5.6 Hz, 1H, NH), 8.05-8.07 (m, 2H, C$_6$H$_5$); ^{13}C NMR (125 MHz, CD$_3$OD): δ = 16.66, 16.71 (C-3', Fuc-C6), 19.23 (Me), 26.53, 26.70, 27.27 (3 Cy), 29.48 (C-2'), 33.11, 34.17 (2 Cy), 35.06, 35.47 (Cy, C-2), 37.39 (C-6), 39.31, 39.39 (C-1', C-5), 42.79 (Lac-C3), 43.31 (C-1), 62.75 (Gal-C6), 67.70, 67.74 (Gal-C4, Fuc-C5), 70.10, 70.29 (Fuc-C2, C-5'), 71.40 (Fuc-C3), 72.99 (Gal-C2), 73.96 (Fuc-C4), 75.95 (Gal-C5), 78.01 (Lac-C2), 79.89 (C-3), 83.00 (C-4), 83.65 (Gal-C3), 84.23 (C-4'), 100.46 (Fuc-C1), 100.57 (Gal-C1), 129.76, 130.85, 131.54, 134.42 (6C, C$_6$H$_5$), 166.8 (COPh), 177.10 (CONH), 179.01 (COOH); IR (KBr): v = 3443 (vs, OH), 2928 (s, C≡C), 2115 (vw), 1726 (s, C=O), 1648 (m, C=O), 1544 (w), 1450 (m), 1270 (s), 1166 (m), 1111 (s), 1078 (vs), 1031 (s), 966 (s), 712 (m) cm^{-1}; HR-MS: m/z: calcd for C$_{41}$H$_{59}$NO$_{15}$ [M+Na]$^+$: 828.3777; found: 828.3776.

(1R,3R,4R,5S)-3-[2-O-Benzoyl-3-O-((1S)-1-carboxy-2-cyclohexyl-ethyl)-(β-D-galactopyranosyl)oxy]-4-[(α-L-fucopyranosyl)oxy]-N-(hex-5-yn-1-yl)-5-methyl-cyclohexanecarboxamide (26d). Following general procedure B, **25d** (25 mg, 28.0 μmol) was reacted with TBAF (84 μL, 84 μmol) in THF (1 mL) to give **26d** (20 mg, 87%) as a white solid. ^{1}H NMR (500 MHz, CD$_3$OD): δ = 0.51-0.75 (m, 4H, 4 Cy), 0.92 (m, 1H, Cy), 1.11 (d, J = 6.4 Hz, 3H, Me), 1.16-1.27 (m, 3H, H-6a, H-2a, Cy), 1.27-1.38 (m, 7H, Fuc-H6, 4 Cy), 1.42 (m, 1H, Lac-H3a), 1.46-1.62 (m, 7H, Lac-H3b, H-3', H-2', H-6b, Cy), 1.67 (m, 1H, H-5), 2.12 (m, 1H, H-2b), 2.16-2.30 (m, 4H, H-4', H-6', H-1), 3.05-3.13 (m, 2H, H-1'), 3.15 (t, J = 9.5 Hz, 1H, H-4), 3.57 (t, J = 5.8 Hz, 1H, Gal-H5), 3.63-3.82 (m, 6H, H-3, Gal-H3, -H6, Fuc-H2, -H4), 3.87 (dd, J = 2.9, 10.3 Hz, 1H, Fuc-H3), 3.96 (m, 1H, Gal-H4), 4.05 (m, 1H, Lac-H2), 4.69 (d, J = 8.0 Hz, 1H, Gal-H1), 4.95-5.03 (m, 2H, Fuc-H1, -H5), 5.44 (t, J = 8.9 Hz, 1H, Gal-H2), 7.47-7.53, 7.60-7.65, 8.04-8.09 (m, 5H, C$_6$H$_5$); ^{13}C NMR (125 MHz, CD$_3$OD): δ = 16.71 (Fuc-C6), 18.70 (C-4'), 19.25 (Me), 26.52, 26.68 (2 Cy), 26.90 (C3'), 27.25 (Cy), 29.46 (C-2'), 33.12, 34.16, 35.04 (3 Cy), 35.36 (C-2), 37.50 (C-6), 39.33 (C-5), 39.68 (C-1'), 42.77 (Lac-C3), 43.32 (C-1), 62.74 (Gal-C6), 67.69 (Gal-C4), 67.75 (Fuc-C5), 69.85 (C-6'), 70.29 (Fuc-C2), 71.40 (Fuc-C3), 72.98 (Gal-C2), 73.94 (Fuc-C4), 75.94 (Gal-C5), 78.02 (Lac-C2), 79.83 (C-3), 83.00 (C-4), 83.64 (Gal-C3), 84.70 (C-5'), 100.42 (Fuc-C1), 100.51 (Gal-C1), 129.73, 130.85, 131.54, 134.38 (6C, C$_6$H$_5$), 166.79 (COPh), 176.96 (CONH), 178.99 (COOH); IR (KBr): v = 3436 (s, OH), 2928 (s, C≡C), 2868

(m), 1731 (s, C=O), 1653 (m), 1550 (w), 1451 (m), 1350 (w), 1298 (m), 1270 (s), 1114 (vs), 1078 (vs), 1034 (s), 996 (w), 966 (w), 712 (m) cm^{-1}; HR-MS: m/z: calcd for $C_{42}H_{61}NO_{15}$ [M+Na]$^+$: 842.3933; found: 842.3919.

1-(2-Bromoethyl)-5-nitro-1*H*-indole (27b). 5-Nitro-1*H*-indole (**4**, 1.00 g, 6.17 mmol) was added to powdered KOH (431 mg, 7.68 mmol) dissolved in DMF (40 mL) at rt. Then, 1,2-dibromoethane (1.55 mL, 18.5 mmol) was added, and the solution was stirred for 25 h. Water (100 mL) was added and the reaction mixture was extracted with Et$_2$O (3 × 100 mL). The organic phases were washed with 0.5 M aq. HCl, satd aq. NaHCO$_3$ and brine (60 mL). The organic layer was dried over Na$_2$SO$_4$, and the solvent was removed under reduced pressure. Silica gel chromatography (petroleum ether/EtOAc) afforded **27b** (198 mg, 19%) as a yellow solid. Approximately 600 mg of the starting material **4** was recovered. ^{1}H NMR (500 MHz, CDCl$_3$): δ = 3.68 (t, J = 6.6 Hz, 2H, H-1'), 4.59 (t, J = 6.6 Hz, 2H, H-2'), 6.73 (m, 1H, H-3), 7.31 (m, 1H, H-2), 7.38 (m, 1H, H-7), 8.15 (m, 1H, H-6), 8.62 (m, 1H, H-4).

1-(3-Bromopropyl)-5-nitro-1*H*-indole (27c). 5-Nitro-1*H*-indole (**4**, 2.01 g, 12.3 mmol) was added to powdered KOH (0.692 g, 12.3 mmol) dissolved in DMF (100 mL) at rt, leading to a read solution. Then, 1,3-dibromopropane (3.77 mL, 37.0 mmol) was added, accompanied by a color change to yellow. After 40 min, additional dibromopropane (0.5 mL, 4.90 mmol) was added, whereupon some precipitation occurred. The reaction mixture was stirred for 17 h at rt, then water (200 mL) was added and the suspension was extracted with Et$_2$O (3 × 200 mL). The organic phases were washed with 0.5 M aq. HCl, satd aq. NaHCO$_3$ and brine (100 mL). The organic layers were dried over Na$_2$SO$_4$, and the solvent was removed under reduced pressure. Silica gel chromatography (petroleum ether/EtOAc) afforded **27c** (1.59 g, 46%) as yellow crystals. The starting material **4** (565 mg, 28%) was partially recovered. ^{1}H NMR (500 MHz, CDCl$_3$): δ = 2.33-2.44 (m, 2H, H-2'), 3.28-3.35 (m, 2H, H-3'), 4.40 (t, J = 6.5 Hz, 2H, H-1'), 6.78 (d, J = 3.1 Hz, 1H, H-3), 7.67 (d, J = 3.2 Hz, 1H, H-2), 7.71 (d, J = 9.1 Hz, 1H, H-7), 8.04 (dd, J = 2.3, 9.1 Hz, 1H, H-6), 8.58 (d, J = 2.2 Hz, 1H, H-4); ^{13}C NMR (125 MHz, CDCl$_3$): δ = 30.05 (C-3'), 32.70 (C-2'), 44.53 (C-1'), 104.54 (C-3), 109.33 (C-7), 117.52 (C-6), 118.42 (C-4), 127.92 (C-9), 131.22 (C-2), 138.84 (C-8), 141.79 (C-5); IR (KBr): ν = 1606 (vw), 1577 (vw), 1511 (s, NO$_2$), 1480 (m), 1459 (m), 1431 (vw), 1404 (w), 1331 (vs, NO$_2$), 1296 (s), 1253 (m), 1226 (m), 1183 (w), 1157 (w), 1068 (m), 975 (vw), 934

(vw), 902 (w), 816 (w), 768 (w), 749 (s) cm^{-1}.

1-(4-Bromobutyl)-5-nitro-1*H*-indole (27d). To a solution of 5-nitro-1*H*-indole (**4**, 2.00 g, 12.3 mmol) in anhydrous EtOAc (20 mL) were added K$_2$CO$_3$ (3.39 g, 24.5 mmol) and TBAB (4.76 g, 14.8 mmol). The suspension was stirred at 50 °C for 30 min followed by the addition of 1,4-dibromobutane (1.74 mL, 14.8 mmol). Stirring was continued under reflux for 21 h. Then, water (20 mL) was added to the reaction mixture, the phases were separated, and the aqueous phase was extracted with EtOAc (2 × 40 mL). The organic layers were washed with 0.5 M aq. HCl, satd aq. NaHCO$_3$ and brine (20 mL), dried over Na$_2$SO$_4$ and concentrated. The residue was purified by silica gel chromatography (petroleum ether/EtOAc) to yield **27d** (1.67 g, 46%) as a yellow solid. ^{1}H NMR (500 MHz, CDCl$_3$): δ = 1.83-1.90 (m, 2H, H-2'), 2.02-2.09 (m, 2H, H-3'), 3.40 (t, J = 6.4 Hz, 2H, H-4'), 4.22 (t, J = 7.0 Hz, 2H, H-1'), 6.70 (m, 1H, H-3), 7.25 (m, 1H, H-2), 7.36 (m, 1H, H-7), 8.13 (m, 1H, H-6), 8.60 (m, 1H, H-4).

1-(2-Azidoethyl)-5-nitro-1*H*-indole (28b). NaN$_3$ (69.6 mg, 1.07 mmol) was added to a solution of **27b** (198 mg, 0.736 mmol) in DMF (2 mL), and the resulting suspension was stirred at 60 °C. After 12 h water (10 mL) was added and the reaction mixture was extracted with EtOAc (3 × 20 mL). The organic layers were washed with water and brine (10 mL) and dried over Na$_2$SO$_4$. Silica gel chromatography (petroleum ether/EtOAc) gave **28b** (90 mg, 52%) as a yellow solid. ^{1}H NMR (500 MHz, DMSO-*d$_6$*): δ = 3.76 (t, J = 5.6 Hz, 2H, H-2'), 4.48 (t, J = 5.6 Hz, 2H, H-1'), 6.80 (d, J = 3.2 Hz, 1H, H-3), 7.68 (d, J = 3.2 Hz, 1H, H-2), 7.77 (d, J = 9.1 Hz, 1H, H-7), 8.05 (dd, J = 2.2, 9.1 Hz, 1H, H-6), 8.58 (d, J = 2.2 Hz, H-4); ^{13}C NMR (125 MHz, DMSO-*d$_6$*): δ = 45.32 (C-1'), 50.66 (C-2'), 104.18 (C-3), 110.51 (C-7), 116.53 (C-6), 117.59 (C-4), 127.50 (C-9), 132.56 (C-2), 138.95 (C-8), 140.86 (C-5); IR (KBr): ν = 2122 (m, N$_3$), 2102 (m, N$_3$), 1611 (w), 1515 (s, NO$_2$), 1478 (w), 1453 (w), 1494 (w), 1338 (vs, NO$_2$), 1292 (s), 1227 (w), 1068 (m), 745 (s) cm^{-1}.

1-(3-Azidopropyl)-5-nitro-1*H*-indole (28c). NaN$_3$ (434 mg, 6.68 mmol) was added to a solution of **27c** (1.34 g, 4.73 mmol) in DMF (10 mL), and the resulting suspension was stirred at 55 °C. After 12 h water (20 mL) was added and the reaction mixture was extracted with EtOAc (3 × 30 mL). The organic layers were washed with water and brine (20 mL) and dried over Na$_2$SO$_4$. Silica gel chromatography (petroleum ether/EtOAc) gave **28c** (950 mg,

82%) as a yellow solid. ^{1}H NMR (500 MHz, DMSO-d_6): δ = 2.03 (p, J = 6.8 Hz, 2H, H-2'), 3.32 (t, J = 6.7 Hz, 2H, H-3'), 4.34 (t, J = 7.0 Hz, 2H, H-1'), 6.78 (d, J = 3.1 Hz, 1H, H-3), 7.67 (d, J = 3.2 Hz, 1H, H-2), 7.71 (d, J = 9.1 Hz, 1H, H-7), 8.04 (dd, J = 2.3, 9.1 Hz, 1H, H-6), 8.58 (d, J = 2.2 Hz, 1H, H-4); ^{13}C NMR (125 MHz, DMSO-d_6): δ = 28.97 (C-2'), 43.30 (C-1'), 48.00 (C-3'), 103.91 (C-3), 110.32 (C-7), 116.46 (C-6), 117.64 (C-4), 127.36 (C-9), 132.50 (C-2), 138.68 (C-5), 140.73 (C-5); IR (KBr): v = 2128 (m), 2101 (s, N_3), 2073 (m), 1613 (w), 1513 (m, NO_2), 1483 (w), 1455 (w), 1404 (w), 1331 (vs, NO_2), 1315 (s), 1302 (s), 1267 (m), 1176 (w), 1068 (m), 741 (s) cm^{-1}; elemental analysis: calcd (%) for $C_{11}H_{11}N_5O_2$ (245.24): C 53.87, H 4.52, N 28.56; found: C 53.77, H 4.65, N 28.32.

1-(4-Azidobutyl)-5-nitro-1H-indole (28d). NaN$_3$ (531 mg, 8.17 mmol) was added to a solution of **27d** (1.60 g, 5.38 mmol) in DMF (5 mL), and the resulting suspension was stirred at 55 °C. After 14 h, water (10 mL) was added, and the reaction mixture was extracted with EtOAc (3 × 20 mL). The organic layers were washed with water and brine (10 mL) and dried over Na$_2$SO$_4$. Silica gel chromatography (petroleum ether/EtOAc) gave **28d** (1.10 g, 79%) as a yellow solid. ^{1}H NMR (500 MHz, DMSO-d_6): δ = 1.43-1.50 (m, 2H, H-3'), 1.78-1.85 (m, 2H, H-2'), 3.31-3.38 (m, 2H, H-4'), 4.30 (t, J = 7.0 Hz, 2H, H-1'), 6.76 (d, J = 3.1 Hz, H-3), 7.68 (d, J = 3.2 Hz, H-2), 7.73 (d, J = 9.1 Hz, 1H, H-7), 8.03 (dd, J = 2.3, 9.1 Hz, 1H, H-6), 8.57 (d, J = 2.2 Hz, 1H, H-4); ^{13}C NMR (125 MHz, DMSO-d_6): δ = 25.63 (C-3'), 27.10 (C-2'), 45.44 (C-1'), 50.15 (C-4'), 103.70 (C-3), 110.40 (C-7), 116.37 (C-6), 117.64 (C-4), 127.32 (C-9), 132.55 (C-2), 138.67 (C-8), 140.66 (C-5); IR (KBr): v = 2089 (vs, N_3), 1514 (s, NO_2), 1479 (m), 1466 (w), 1453 (vw), 1402 (w), 1334 (vs, NO_2), 1319 (s), 1306 (s), 1267 (m), 1249 (m), 1233 (w), 1221 (vw), 1169 (vw), 1091 (vw), 1066 (m), 891 (m), 748 (vs) cm^{-1}; elemental analysis: calcd (%) for $C_{12}H_{13}N_5O_2$ (259.26): C 55.59, H 5.05, N 27.01; found C 55.66, H 5.20, N 26.81.

(5-Nitro-1H-indol-1-yl)methanol (29). 5-Nitro-1H-indole (**4**, 995 mg, 6.14 mmol) and K$_2$CO$_3$ (396 mg, 2.87 mmol) were dissolved in EtOH in a bomb tube. The solution was stirred at 60 °C for 5 min, then freshly prepared aq. methanal (8 mL, approx. 30%, preparation: 3.00 g paraformaldehyde and 0.901 g of K$_2$CO$_3$ were suspended in 10 mL H$_2$O and stirred at 60 °C until complete dissolution of the paraformaldehyde) were added. Stirring was continued at 60 °C for another 20 min. After concentration, the remains were redissolved

in EtOAc and adsorbed on silica gel. The adsorbed material was subjected to silica gel chromatography (petroleum ether/EtOAc) to afford **29** (784 mg, 66%) as a yellow solid. ^{1}H NMR (500 MHz, CD_3OD): δ = 5.62 (s, 2H, H-1'), 6.70 (d, J = 2.7 Hz, 1H, H-3), 7.50 (d, J = 3.3 Hz, 1H, H-2), 7.63 (d, J = 9.1 Hz, 1H, H-7), 8.08 (dd, J = 2.2, 9.1 Hz, 1H, H-6), 8.52 (d, J = 2.2 Hz, 1H, H-4); ^{13}C NMR (125 MHz, CD_3OD): δ = 70.45 (C-1'), 105.21 (C-3), 111.17 (C-7), 117.95 (C-6), 118.54 (C-4), 129.92 (C-9), 132.41 (C-2), 140.12 (C-8), 143.16 (C-5); IR (KBr): v = 3486 (vs, OH), 1609 (w), 1580 (vw), 1512 (s, NO_2), 1466 (m), 1399 (w), 1331 (vs, NO_2), 1279 (s), 1206 (w), 1147 (vw), 1100 (w), 1073 (w), 1040 (s), 988 (vw), 894 (vw), 814 (vw), 763 (vw), 744 (s), 722 (vw) cm^{-1}; elemental analysis: calcd (%) for $C_9H_8N_2O_3$ (192.17): C 56.25, H H 4.20, N 14.58; found: C 56.14; H 4.21; N 14.60.

1-(Azidomethyl)-5-nitro-1*H*-indole (28a). To a solution of **29** (770 mg, 4.01 mmol) in anhydrous THF (13 mL) were added $MeSO_2Cl$ (0.312 mL, 4.01 mmol) and Et_3N (1.1 mL, 8.02 mmol) at -15 °C under argon. After 10 min, the ice bath was removed and stirring was continued for 1 h. Then 15-crown-5 (0.397 mL, 2.01 mmol) and NaN_3 (521 mg, 8.02 mmol) were added to the solution. After another 5 h, the solvent was removed and the crude mixture was dissolved in EtOAc (75 mL) and H_2O (50 mL). The two phases were separated, and the organic phase was washed with brine (50 mL). The aqueous phase was extracted with EtOAc (2 × 50 mL). The combined organic layers were dried over Na_2SO_4, and the solvent was removed under reduced pressure. Silica gel chromatography (petroleum ether/EtOAc) gave **28a** (297 mg, 34%) as yellow crystals. ^{1}H NMR (500 MHz, $CDCl_3$): δ = 5.51 (s, 2H, H-1'), 6.77 (d, J = 3.3 Hz, 1H, H-3), 7.34 (d, J = 3.3 Hz, 1H, H-2), 7.49 (d, J = 9.0 Hz, 1H, H-7), 8.20 (dd, J = 2.2, 9.1 Hz, 1H, H-6), 8.61 (d, J = 2.1 Hz, 1H, H-4); ^{13}C NMR (125 MHz, $CDCl_3$): δ = 61.56 (C-1'), 106.03 (C-3), 109.68 (C-7), 118.43 (C-6), 118.50 (C-4), 128.73 (C-9), 130.71 (C-2), 138.88 (C-8), 142.84 (C-5); IR (KBr): v = 3101 (vw), 2924 (vw), 2118 (m, N_3), 2092 (m, N_3), 1612 (w), 1583 (vw), 1509 (s, NO_2), 1480 (m), 1451 (m), 1401 (vw), 1336 (vs, NO_2/N_3), 1287 (vs, N_3), 1266 (m), 1231 (m), 1208 (w), 1179 (m), 1147 (w), 1076 (w), 1065 (w), 1029 (vw), 934 (vw), 906 (w), 876 (w), 821 (w), 745 (s) cm^{-1}; elemental analysis: calcd (%) for $C_9H_7N_5O_2$ (217.18): C 49.77, H 3.25, N 32.25; found: C 49.59; H 3.28; N 32.46.

3-(Azidomethyl)-5-nitro-1*H*-indole (32a). To a suspension of **31**[S5] (752 mg, 3.91 mmol) in

toluene (10 mL) were added diphenyl phosphoryl azide (1.0 mL, 4.69 mmol) and dropwise at -10 °C DBU (0.7 mL, 4.69 mmol) under argon. The mixture was allowed to warm to rt, and 5 mL THF were added leading to the formation of two phases. The reaction was continued under vigorous stirring for 18 h. After removal of the THF *in vacuo*, EtOAc (80 mL) was added to the reaction mixture, and the organic phases were washed with satd aq. $NaHCO_3$ (2 × 40 mL), 0.5 M aq. HCl (40 mL), satd aq. $NaHCO_3$ (40 mL) and brine (40 mL). The aqueous layers were extracted with EtOAc (2 × 80 mL), and the organic phase was dried over Na_2SO_4. Silica gel chromatography (DCM) and subsequent crystallization from DCM afforded **32a** as yellow crystals (658 mg, 78%). ^{1}H NMR (500 MHz, DMSO-d_6): δ = 4.70 (s, 2H, H-1'), 7.60 (d, *J* = 9.0 Hz, 1H, H-7), 7.75 (s, 1H, H-2), 8.05 (dd, *J* = 1.8, 8.9 Hz, 1H, H-6), 8.65 (s, 1H, H-4), 11.90 (s, 1H, NH); ^{13}C NMR (125 MHz, DMSO-d_6): δ = 45.16 (C-1'), 111.57 (C-3), 112.38 (C-7), 115.76 (C-4), 117.07 (C-6), 125.88 (C-9), 129.50 C-2), 139.53 (C-8), 140.88 (C-5); IR (KBr): *v* = 3257 (m, NH), 2117 (vs, N_3), 1625 (w), 1580 (w), 1551 (m), 1515 (s, NO_2), 1472 (m), 1456 (m), 1436 (m), 1376 (w), 1331 (vs, N_3/ NO_2), 1261 (m), 1224 (m), 1196 (m), 1128 (w), 1113 (m), 1102 (m), 1045 (w), 976 (w), 939 (vw), 920 (vw), 894 (m), 863 (w), 836 (m), 816 (m), 782 (w), 769 (w), 751 (m), 735 (m), 686 (m), 631 (m), 613 (w), 563 (m), 559 (m) cm^{-1}; elemental analysis: calcd (%) for $C_9H_7N_5O_2$ (217.18): C 49.77, H 3.25, N 32.25; found: C 49.73, H 3.27, N 32.14.

General procedure C for the synthesis of triazoles. Alkyne (1.0 eq.) and azide (1.3 eq.) were dissolved in ^{t}BuOH/H$_2$O/THF (1:1:1, approx. 0.015 M) under argon, and the solution was degassed in an ultrasound bath for 20 min. Degassed 0.1 M aq. Na-L-ascorbate (0.5 eq.) and 0.1 M aq. CuSO$_4$·5 H$_2$O (0.25 eq.) were added, and the mixture was stirred at rt for 1-4 h until full conversion as indicated by MS. The solvent was removed *in vacuo*, the residue was redissolved in H$_2$O/MeCN (1:1 + 1-2 drops of Et$_3$N), filtrated (PTFE membrane filter) and purified by preparative HPLC-MS (H$_2$O/MeCN + 0.1% HCO$_2$H). All triazoles were isolated as yellow solids.

(1*R*,3*R*,4*R*,5*S*)-3-[2-*O*-Benzoyl-3-*O*-((1*S*)-1-carboxy-2-cyclohexyl-ethyl)-(β-D-galactopyranosyl)oxy]-4-[(α-L-fucopyranosyl)oxy]-5-methyl-*N*-({1-[(6-nitro-1*H*-indol-3-yl)methyl]-1*H*-1,2,3-triazol-4-yl}methyl)cyclohexanecarboxamide (33). Prepared according to general procedure C from **26a** (8.4 mg, 10.8 μmol), **28a** (3.6 mg, 16.6 μmol),

Na-L-ascorbate (54 µL, 5.4 µmol) and CuSO$_4$·5 H$_2$O (27 µL, 2.7 µmol). Yield: 10.1 mg (94%). [α]$_D^{20}$ -58.0 (*c* 0.32, MeOH); ^{1}H NMR (500 MHz, CD$_3$OD): δ = 0.55 (m, 1H, Cy), 0.61-0.73 (m, 3H, Cy), 0.91 (m, 1H, Cy), 1.06 (d, *J* = 6.4 Hz, 3H, Me), 1.10-1.27 (m, 3H, Cy, H-6a, H-2a), 1.26-1.45 (m, 8H, Fuc-H6, 4Cy, Lac-H3a), 1.46-1.65 (m, 4H, Lac-H3b, H-6b, Cy, H-5), 2.11 (m, 1H, H-2b), 2.22 (m, 1H, H-1), 3.10 (t, *J* = 9.6 Hz, 1H, H-4), 3.54 (t, *J* = 5.8 Hz, 1H, Gal-H5), 3.59-3.68 (m, 2H, Gal-H3, H-3), 3.68-3.80 (m, 4H, Fuc-H2, -H4, Gal-H6), 3.85 (dd, *J* = 3.2, 10.3 Hz, 1H, Fuc-H3), 3.95 (m, 1H, Gal-H4), 4.02 (m, 1H, Lac-H2), 4.30 (t, *J* = 5.3 Hz, 2H, H-1'), 4.64 (d, *J* = 8.0 Hz, 1H, Gal-H1), 4.92-5.00 (m, 2H, Fuc-H1, -H5), 5.42 (t, *J* = 8.9 Hz, 1H, Gal-H2), 6.79 (d, *J* = 3.3 Hz, 1H, Ind-H3), 6.84, 6.88 (A, B of AB, *J* = 14.8 Hz, 1H, H-1"), 7.40 (t, *J* = 7.7 Hz, 2H, C$_6$H$_5$), 7.55 (t, *J* = 7.4 Hz, 1H, C$_6$H$_5$), 7.72 (d, *J* = 3.3 Hz, 1H, Ind-H2), 7.88 (d, *J* = 9.1 Hz, 1H, Ind-H7), 8.02 (s, 3H, C$_6$H$_5$, H-3'), 8.14 (dd, *J* = 2.1, 9.1 Hz, 1H, Ind-H6), 8.19 (t, *J* = 5.4 Hz, 1H, NH), 8.54 (d, *J* = 2.0 Hz, 1H, Ind-H4); ^{13}C NMR (125 MHz, CD$_3$OD): δ = 16.73 (Fuc-C6), 19.22 (Me), 26.55, 26.72, 27.29, 33.10, 34.19, 35.00 (6 Cy), 35.09 (C-2), 35.45 (C-1'), 37.48 (C-6), 39.31 (C-5), 42.84 (Lac-C3), 42.95 (C-1), 59.70 (C-1"), 62.76 (Gal-C6), 67.71 (2C, Gal-C4, Fuc-C5), 70.28 (Fuc-C2), 71.39 (Fuc-C3), 72.98 (Gal-C2), 73.95 (Fuc-C4), 75.95 (Gal-C5), 78.25 (Lac-C2), 79.70 (C-3), 83.00 (C-4), 83.69 (Gal-C3), 100.44 (Fuc-C1), 100.47 (Gal-C1), 106.81 (Ind-C3), 111.48 (Ind-C7), 118.74 (Ind-C6), 118.78 (Ind-C4), 123.94 (C-3'), 129.69 (2C, C$_6$H$_5$), 130.10 (Ind-C9), 130.86, 131.52 (3C, C$_6$H$_5$), 132.58 (Ind-C2), 134.33 (C$_6$H$_5$), 140.07 (Ind-C8), 143.86 (Ind-C5), 146.95 (C-2'), 166.85 (*C*OPh), 176.93 (CONH), 179.38 (COOH); IR (KBr): *v* = 3430 (vs, OH), 2927 (s), 2846 (w), 1723 (s, C=O), 1648 (m, C=O), 1616 (w), 1584 (vw), 1520 (m), 1476 (vw), 1450 (m), 1403 (w), 1337 (vs, NO$_2$), 1314 (m), 1273 (s), 1226 (w), 1170 (w), 1114 (s), 1092 (s), 1073 (vs), 1040 (s), 999 (w), 966 (vw), 766 (w), 746 (w), 713 (m) cm^{-1}; HR-MS: *m/z*: calcd for C$_{48}$H$_{62}$N$_6$O$_{17}$ [M+Na]$^+$: 1017.4064; found: 1017.4067.

(1*R*,3*R*,4*R*,5*S*)-3-[2-*O*-Benzoyl-3-*O*-((1*S*)-1-carboxy-2-cyclohexyl-ethyl)-(β-D-galactopyranosyl)oxy]-4-[(α-L-fucopyranosyl)oxy]-5-methyl-*N*-(2-{1-[(6-nitro-1*H*-indol-3-yl)methyl]-1*H*-1,2,3-triazol-4-yl}ethyl)cyclohexanecarboxamide (34). Prepared according to general procedure C from **26b** (10.4 mg, 13.1 µmol), **28a** (4.3 mg, 19.8 µmol), Na-L-ascorbate (66 µL, 6.6 µmol) and CuSO$_4$·5 H$_2$O (33 µL, 3.3 µmol). Yield: 8.8 mg (66%). [α]$_D^{20}$ -67.5 (*c* 0.23, MeOH); ^{1}H NMR (500 MHz, CD$_3$OD): δ = 0.54 (m, 1H, Cy), 0.59-0.71 (m, 3H, Cy), 0.85-0.99 (m, 2H, Cy, H-6a), 1.02 (d, *J* = 6.5 Hz, 3H, Me), 1.09 (m,

1H, H-2a), 1.17-1.37 (m, 8H, Fuc-H6, 5 Cy), 1.37-1.45 (m, 2H, Lac-H3a, H-6b), 1.46-1.62 (m, 3H, Lac-H3b, H-5, Cy), 2.06-2.12 (m, 2H, H-2, H-1), 2.76 (t, J = 7.0 Hz, 2H, H-2'), 3.08 (t, J = 9.5 Hz, 1H, H-4), 3.55 (t, J = 5.8 Hz, 1H, Gal-H5), 3.59-3.66 (m, 2H, Gal-H3, H-3), 3.69-3.81 (m, 4H, Fuc-H2, -H4, Gal-H6), 3.86 (dd, J = 3.2, 10.3 Hz, 1H, Fuc-H3), 3.96 (m, 1H, Gal-H4), 4.01 (m, 1H, Lac-H2), 4.66 (d, J = 8.0 Hz, 1H, Gal-H1), 4.93-5.01 (m, 2H, Fuc-H1, -H5), 5.43 (t, J = 8.9 Hz, 1H, Gal-H2), 6.78 (A of AB, J = 14.8 Hz, 1H, H-1"a), 6.81 (d, J = 3.3 Hz, 1H, Ind-H3), 6.85 (B of AB, J = 14.7 Hz, 1H, H-1"b), 7.44 (t, J = 7.7 Hz, 2H, C_6H_5), 7.53 (t, J = 7.4 Hz, 1H, C_6H_5), 7.67 (d, J = 3.4 Hz, 1H, Ind-H2), 7.84 (s, 1H, H-4'), 7.88 (d, J = 9.1 Hz, 1H, Ind-H7), 8.05 (d, J = 7.7 Hz, 2H, C_6H_5), 8.16 (dd, J = 2.0, 9.1 Hz, 1H, Ind-H6), 8.57 (d, J = 2.0 Hz, 1H, Ind-H4); ^{13}C NMR (125 MHz, CD_3OD): δ = 16.74 (Fuc-C6), 19.18 (Me), 26.41, 26.54, 26.72 (2 Cy, C-2'), 27.28, 33.11, 34.21 35.10 (4 Cy), 35.35 (C-2'), 37.26 (C-6), 39.24 (C-5), 39.66 (C-1'), 42.88, 43.08 (Lac-C3, C-1), 59.63 (C-1"), 62.78 (Gal-C6), 67.71 (Gal-C4, Fuc-C5), 70.31 (Fuc-C2), 71.42 (Fuc-C3), 73.05 (Gal-C2), 73.98 (Fuc-C4), 76.00 (Gal-C5), 78.33 (Lac-C2), 79.87 (C-3), 82.91 (C-4), 83.69 (Gal-C3), 100.44 (Fuc-C1), 100.62 (Gal-C1), 106.92 (Ind-C3), 111.49 (Ind-C7), 118.78 (Ind-C6), 118.84 (Ind-C4), 123.30 (C-4'), 129.73 (2C, C_6H_5), 130.06 (Ind-C9), 130.93, 131.62 (3C, C_6H_5), 132.52 (Ind-C2), 134.36 (C_6H_5), 140.09 (Ind-C8), 143.89 (Ind-C5), 147.06 (C-3'), 166.81 (COPh), 176.99 (CONH), 179.82 (COOH); IR (KBr): v = 3429 (vs, OH), 2927 (s), 2853 (w), 1722 (s, C=O), 1648 (m, C=O), 1616 (w), 1584 (vw), 1520 (m), 1476 (vw), 1450 (m), 1403 (w), 1337 (vs, NO_2), 1317 (s), 1273 (s), 1224 (w), 1169 (w), 1114 (s), 1095 (s), 1073 (vs), 1034 (s), 1000 (vw), 966 (vw), 760 (vw), 746 (w), 713 (m) cm^{-1}; HR-MS: m/z: calcd for $C_{49}H_{64}N_6O_{17}$ [M+Na]$^+$: 1031.4220; found: 1031.4218.

(1R,3R,4R,5S)-3-[2-O-Benzoyl-3-O-((1S)-1-carboxy-2-cyclohexyl-ethyl)-(β-D-galactopyranosyl)oxy]-4-[(α-L-fucopyranosyl)oxy]-5-methyl-N-(3-{1-[(5-nitro-1H-indol-1-yl)methyl]-1H-1,2,3-triazol-4-yl}propyl)cyclohexanecarboxamide (35). Prepared according to general procedure C from **26c** (9.7 mg, 12.0 μmol), **28a** (3.9 mg, 18.0 μmol), Na-L-ascorbate (60 μL, 6.0 μmol) and $CuSO_4 \cdot 5\ H_2O$ (30 μL, 3.0 μmol). Yield: 7.5 mg (61%). [α]$_D^{20}$ -42.3 (c 0.72, MeOH); ^1H NMR (500 MHz, CD_3OD): δ = 0.54 (m, 1H, Cy), 0.59-0.71 (m, 4H, 4 Cy), 0.90 (m, 1H, Cy), 1.09 (d, J = 6.5 Hz, 3H, Me), 1.11-1.25 (m, 3H, Cy, H-6a, H-2a), 1.25-1.36 (m, 7H, 4 Cy, Fuc-H6), 1.41 (m, 1H, Lac-H3a), 1.45-1.60 (m, 3H, Lac-H3b, Cy, H-6b), 1.64 (m, 1H, H-5), 1.67-1.74 (m, 2H, H-2'), 2.10 (m, 1H, H-2b), 2.21 (m, 1H, H-1), 2.60 (t, J = 7.5 Hz, 2H, H-3'), 3.04-3.10 (m, 2H, H-1'), 3.13 (t, J = 9.6 Hz, 1H,

H-4), 3.56 (t, J = 5.9 Hz, 1H, Gal-H5), 3.62-3.81 (m, 6H, Gal-H3, -H6, H-3, Fuc-H2, -H4), 3.86 (dd, J = 3.2, 10.3 Hz, 1H, Fuc-H3), 3.96 (d, J = 2.5 Hz, 1H, Gal-H4), 4.02 (d, J = 6.9 Hz, 1H, Lac-H2), 4.66 (d, J = 8.0 Hz, 1H, Gal-H1), 4.95-5.00 (m, 2H, Fuc-H1, -H5), 5.42 (m, 1H, Gal-H2), 6.81 (m, 1H, Ind-H3), 6.85 (s, 2H, H-1"), 7.24-7.29, 7.30-7.35 (m, 3H, C_6H_5), 7.69-7.76 (m, 2H, NH, Ind-H2), 7.90 (m, 1H, Ind-H7), 7.94 (s, 1H, H-5'), 7.96-7.99 (m, 2H, C_6H_5), 8.15 (m, 1H, Ind-H6), 8.56 (m, 1H, Ind-H4); ^{13}C NMR (125 MHz, CD$_3$OD): δ = 16.70 (Fuc-C6), 19.24 (Me), 23.46 (C-3'), 26.52, 26.70, 27.26 (3 Cy), 30.12 (C-2'), 33.12, 34.19, 35.05 (3 Cy), 35.52 (C-2), 37.38 (C-6), 39.30, 39.42 (C-5, C-1'), 42.78 (Lac-C3), 43.37 (C-1), 59.70 (C-1"), 62.77 (Gal-C6), 67.71, 67.76 (Gal-C4, Fuc-C5), 70.33 (Fuc-C2), 71.42 (Fuc-C3), 73.04 (Gal-C2), 73.97 (Fuc-C4), 75.99 (Gal-C5), 78.28 (Lac-C2), 79.91 (C-3), 82.98 (C-4), 83.61 (Gal-C3), 100.45 (Fuc-C1), 100.63 (Gal-C1), 106.81 (Ind-C3), 111.47 (Ind-C7), 118.80, 118.81 (Ind-C4, -C6), 123.10 (C-5'), 129.58 (Ind-C9), 130.11, 130.76, 131.48 (5C, C_6H_5), 132.58 (Ind-C2), 134.21 (C_6H_5), 140.11 (Ind-C8), 143.89 (Ind-C5), 149.16 (C-4'), 166.76 (COPh), 177.05 (CONH); HR-MS: m/z: calcd for $C_{50}H_{66}N_6O_{17}$ [M+Na]$^+$: 1045.4377; found: 1045.4376.

(1R,3R,4R,5S)-3-[2-O-Benzoyl-3-O-((1S)-1-carboxy-2-cyclohexyl-ethyl)-(β-D-galactopyranosyl)oxy]-4-[(α-L-fucopyranosyl)oxy]-5-methyl-N-(4-{1-[(6-nitro-1H-indol-3-yl)methyl]-1H-1,2,3-triazol-4-yl}butyl)cyclohexanecarboxamide (36). Prepared according to general procedure C from **26d** (10.6 mg, 13.4 μmol), **28a** (4.4 mg, 20.3 μmol), Na-L-ascorbate (67 μL, 6.7 μmol) and CuSO$_4$·5 H$_2$O (34 μL, 3.4 μmol). Yield: 11.3 mg (81%). [α]$_D^{20}$ -53.2 (c 1.13, MeOH); ^{1}H NMR (500 MHz, CD$_3$OD): δ = 0.47-0.70 (m, 4H, 4 Cy), 0.89 (m, 1H, Cy), 1.08 (d, J = 6.4 Hz, 3H, Me), 1.11-1.24 (m, 3H, Cy, H-6a, H-2a), 1.25-1.32 (m, 4H, 4 Cy), 1.34 (d, J = 6.5 Hz, 3H, Fuc-H6), 1.37-1.68 (m, 9H, Lac-H3, H-2', H-6, H-3', H-5, Cy), 2.10 (m, 1H, H-2b), 2.20 (m, 1H, H-1), 2.66 (t, J = 7.5 Hz, 2H, H-4'), 3.06 (t, J = 7.0 Hz, 2H, H-1'), 3.13 (t, J = 9.6 Hz, 1H, H-4), 3.58 (t, J = 5.9 Hz, 1H, Gal-H5), 3.63-3.70 (m, 2H, Gal-H3, H-3), 3.75 (s, 4H, Fuc-H2, -H4, Gal-H6), 3.86 (dd, J = 3.2, 10.3 Hz, 1H, Fuc-H3), 3.96 (d, J = 2.0 Hz, 1H, Gal-H4), 4.02 (dd, J = 2.5, 9.7 Hz, 1H, Lac-H2), 4.69 (d, J = 8.0 Hz, 1H, Gal-H1), 4.95-5.02 (m, 2H, Fuc-H1, -H5), 5.43 (t, J = 8.9 Hz, 1H, Gal-H2), 6.79 (d, J = 3.3 Hz, 1H, Ind-H3), 6.83 (s, 2H, H-1"), 7.36-7.41, 7.51-7.56 (m, 3H, C_6H_5), 7.72 (d, J = 3.4 Hz, 1H, Ind-H2), 7.88 (d, J = 9.1 Hz, 1H, Ind-H7), 7.95 (s, 1H, H-6'), 7.99-8.03 (m, 2H, C_6H_5), 8.14 (dd, J = 2.1, 9.1 Hz, 1H, Ind-H6), 8.55 (d, J = 2.1 Hz, 1H, Ind-H4); ^{13}C NMR (125 MHz, CD$_3$OD): δ = 16.74 (Fuc-C6), 19.24 (Me), 25.67 (C-4'), 26.51,

26.67, 27.24 (3 Cy), 27.43 (C-3'), 29.67 (C-2'), 33.08, 34.13, 35.03 (3 Cy), 35.38 (C-2), 37.46 (C-6), 39.32 (C-5), 39.75 (C-1'), 42.75 (Lac-C3), 43.31 (C-1), 59.65 (C-1''), 62.73 (Gal-C6), 67.70, 67.75 (Gal-C4, Fuc-C5), 70.30 (Fuc-C2), 71.41 (Fuc-C3), 73.00 (Gal-C2), 73.96 (Fuc-C4), 75.95 (Gal-C5), 77.96 (Lac-C2), 79.82 (C-3), 83.02 (C-4), 83.63 (Gal-C3), 100.45 (Fuc-C1), 100.50 (Gal-C1), 106.78 (Ind-C3), 111.43 (Ind-C7), 118.77 (Ind-C6), 118.82 (Ind-C4), 122.98 (C-6'), 129.65 (2C, C_6H_5), 130.07 (Ind-C9), 130.84, 131.52 (3C, C_6H_5), 132.59 (Ind-C2), 134.34 (C_6H_5), 140.07 (Ind-C8), 143.83 (Ind-C5), 149.56 (C-5'), 166.79 (COPh), 176.95 (CONH), 178.88 (COOH); IR (KBr): ν = 3436 (vs, OH), 2927 (s), 2852 (w), 1725 (m, C=O), 1647 (m, C=O), 1616 (w), 1583 (vw), 1520 (m), 1476 (vw), 1450 (m), 1402 (w), 1384 (w), 1336 (s, NO_2), 1315 (m), 1271 (m), 1223 (w), 1167 (w), 1114 (m), 1072 (s), 1040 (s), 999 (w), 966 (vw), 763 (vw), 746 (w), 712 (w) cm^{-1}; HR-MS: m/z: calcd for $C_{51}H_{68}N_6O_{17}$ [M+Na]$^+$: 1059.4533; found: 1059.4531.

(1R,3R,4R,5S)-3-[2-O-Benzoyl-3-O-((1S)-1-carboxy-2-cyclohexyl-ethyl)-(β-D-galactopyranosyl)oxy]-4-[(α-L-fucopyranosyl)oxy]-5-methyl-N-({1-[2-(5-nitro-1H-indol-1-yl)ethyl]-1H-1,2,3-triazol-4-yl}methyl)cyclohexanecarboxamide (37). Prepared according to general procedure C from **26a** (15.0 mg, 19.3 μmol), **28b** (5.5 mg, 23.8 μmol), Na-L-ascorbate (96 μL, 9.6 μmol) and CuSO$_4$·5 H$_2$O (76 μL, 7.6 μmol). Yield: 12.9 mg (66%). [α]$_D^{20}$ -53.0 (c 1.09, MeOH); ^{1}H NMR (500 MHz, CD$_3$OD): δ = 0.55 (m, 1H, Cy), 0.61-0.72 (m, 3H, Cy), 0.91 (d, J = 11.6 Hz, 1H, Me), 1.12-1.25 (m, 3H, Cy, H-6a, H-2a), 1.25-1.37 (m, 7H, Fuc-H6, 4 Cy), 1.41 (m, 1H, Lac-H3a), 1.45-1.61 (m, 3H, Lac-H3b, H-6b, Cy), 1.66 (m, 1H, H-5), 2.10 (m, 1H, H-2b), 2.20 (m, 1H, H-1), 3.14 (t, J = 9.6 Hz, 1H, H-4), 3.59 (t, J = 6.0 Hz, 1H, Gal-H5), 3.64 (dd, J = 2.9, 9.7 Hz, 1H, Gal-H3), 3.66-3.82 (m, 5H, H-3, Fuc-H2, -H4, Gal-H6), 3.87 (dd, J = 3.3, 10.3 Hz, 1H, Fuc-H3), 3.94-4.01 (m, 2H, Gal-H4, Lac-H2), 4.15-4.18 (m, 2H, H-1'), 4.70 (d, J = 8.1 Hz, 1H, Gal-H1), 4.75 (t, J = 5.3 Hz, 2H, H-2''), 4.78-4.83 (m, 2H, H-1''), 4.97 (t, J = 5.1 Hz, 2H, Fuc-H1, -H5), 5.43 (dd, J = 8.3, 9.5 Hz, 1H, Gal-H2), 6.68 (d, J = 2.9 Hz, Ind-H3), 7.19 (d, J = 9.1 Hz, Ind-H7), 7.23 (d, J = 3.3 Hz, 1H, Ind-H2), 7.37 (s, 1H, H-3'), 7.38-7.44, 7.54-7.60 (m, 3H, C$_6$H$_5$), 7.96-8.03 (m, 3H, Ind-H6, C$_6$H$_5$), 8.06 (t, J = 5.3 Hz, 1H, NH), 8.50-8.54 (m, 1H, Ind-H4); ^{13}C NMR (125 MHz, CD$_3$OD): δ = 16.74 (Fuc-C6), 19.25 (Me), 26.54, 26.69, 27.27, 33.11, 34.17 (5 Cy), 35.05 (C-2), 35.09 (C-1'), 35.32 (Cy), 37.51 (C-6), 39.31 (C-5), 42.81 (Lac-C3), 42.91 (C-1), 47.53 (C-2''), 51.43 (C-1''), 62.74 (Gal-C6), 67.72 (2C, Gal-C4, Fuc-C5), 70.32 (Fuc-C2), 71.41 (Fuc-C3), 72.99 (Gal-C2), 73.97 (Fuc-C4), 75.95 (Gal-C5), 78.09 (Lac-C2), 79.78 (C-

3), 83.01 (C-4), 83.73 (Gal-C3), 100.46 (Fuc-C1), 100.52 (Gal-C1), 105.73 (Ind-C3), 110.25 (Ind-C7), 117.99 (Ind-C6), 118.71 (Ind-C4), 124.91 (C-3'), 129.18 (Ind-C9), 129.70, 130.88, 131.54 (5C, C_6H_5), 132.55 (Ind-C2), 134.32 (C_6H_5), 140.46 (Ind-C8), 142.89 (Ind-C5), 146.55 (C-2'), 166.84 (COPh), 176.74 (CONH), 179.18 (COOH); IR (KBr): v = 3435 (vs, OH), 2927 (m), 2852 (w), 1721 (m, C=O), 1643 (m, C=O), 1583 (w), 1516 (w), 1449 (w), 1402 (w), 1383 (w), 1335 (s, NO_2), 1272 (m). 1215 (vw), 1166 (w), 1111 (m), 1095 (m), 1073 (s), 1032 (m), 966 (vw), 897 (vw), 804 (vw), 776 (vw), 765 (vw), 744 (w), 713 (w) cm^{-1}; HR-MS: m/z: calcd for $C_{49}H_{64}N_6O_{17}$ [M+Na]$^+$: 1031.4220; found: 1031.4222.

(1R,3R,4R,5S)-3-[2-O-Benzoyl-3-O-((1S)-1-carboxy-2-cyclohexyl-ethyl)-(β-D-galactopyranosyl)oxy]-4-[(α-L-fucopyranosyl)oxy]-5-methyl-N-(2-{1-[2-(5-nitro-1H-indol-1-yl)ethyl]-1H-1,2,3-triazol-4-yl}ethyl)cyclohexanecarboxamide (38). Prepared according to general procedure C from **26b** (15.3 mg, 19.3 μmol), **28b** (5.8 mg, 25.0 μmol), Na-L-ascorbate (116 μL, 11.6 μmol) and $CuSO_4 \cdot 5$ H_2O (52 μL, 5.2 μmol). Yield: 15.7 mg (79%). [α]$_D^{20}$ -88.2 (c 0.29, MeOH); ^{1}H NMR (500 MHz, CD$_3$OD): δ = 0.55 (m, 1H, Cy), 0.61-0.73 (m, 3H, 3 Cy), 0.90 (m, 1H, Cy), 1.09 (d, J = 6.5 Hz, 3H, Me), 1.11-1.26 (m, 3H, H-2a, H-6a, Cy), 1.26-1.37 (m, 8H, 5 Cy, Fuc-H6), 1.42 (m, 1H, Lac-H3a), 1.45-1.61 (m, 3H, Lac-H3b, H-6, Cy), 1.65 (m, 1H, H-5), 2.10 (m, 1H, H-2), 2.18 (m, 1H, H-1), 2.61 (t, J = 7.4 Hz, 2H, H-2'), 3.09-3.19 (m, 3H, H-1', H-4), 3.56 (m, 1H, Gal-H5), 3.59-3.83 (m, 6H, Gal-H3, -H6, H-3, Fuc-H2, -H4), 3.87 (dd, J = 3.3, 10.3 Hz, 1H, Fuc-H3), 3.91-4.00 (m, 2H, Gal-H4, Lac-H2), 4.68 (d, J = 8.0 Hz, 1H, Gal-H1), 4.73-4.78 (m, 2H, H-2"), 4.78-4.82 (m, 2H, H-1"), 4.92-5.01 (m, 2H, Fuc-H1, -H5), 5.43 (m, 1H, Gal-H2), 6.70 (d, J = 3.2 Hz, 1H, Ind-H3), 7.24-7.28 (m, 2H, Ind-H2, -H7), 7.29 (s, 1H, H-4'), 7.40-7.46 (m, 2H, C_6H_5), 7.51-7.55 (m, J = 7.4 Hz, 1H, C_6H_5), 7.67 (t, J = 5.8 Hz, 1H, NH), 8.00 (dd, J = 2.2, 9.1 Hz, 1H, Ind-H6), 8.02-8.06 (m, 2H, C_6H_5), 8.52 (m, 1H, Ind-H4); ^{13}C NMR (125 MHz, CD$_3$OD): δ = 16.72 (Fuc-C6), 19.25 (Me), 26.35 (C-2'), 26.53, 26.70, 27.27, 33.15, 34.22, 35.07 (6 Cy), 35.31 (C-2), 37.38 (C-6), 39.29 (C-5), 40.03 (C-1'), 42.82 (Lac-C3), 43.20 (C-1), 47.50 (C-2"), 51.30 (C-1"), 62.78 (Gal-C6), 67.71, 67.77 (Gal-C4, Fuc-C5), 70.33 (Fuc-C2), 71.43 (Fuc-C3), 73.04 (Gal-C2), 73.96 (Fuc-C4), 76.00 (Gal-C5), 79.84 (C-3), 82.99 (C-4), 83.66 (Gal-C3), 100.41 (Fuc-C1), 100.57 (Gal-C1), 105.73 (Ind-C3), 110.26 (Ind-C7), 117.96 (Ind-C6), 118.74 (Ind-C4), 124.34 (C-4'), 129.20 (Ind-C9), 129.69, 129.74, 130.89 (5C, C_6H_5), 132.54 (Ind-C2), 134.32 (C_6H_5), 140.44 (Ind-C8), 142.97 (Ind-C5), 146.47 (C-3'), 166.82 (COPh), 176.94 (CONH); IR (KBr): v = 3418 (s, OH), 2926 (s), 2853 (m), 1722 (s, C=O),

1648 (m, C=O), 1619 (m), 1583 (w), 1517 (s), 1479 (w), 1451 (m), 1404 (w), 1334 (vs, NO_2), 1290 (m), 1271 (w), 1223 (w), 1166 (m), 1112 (s), 1095 (s), 1071 (vs), 1032 (s), 967 (w), 999 (m), 935 (vw), 897 (vw), 809 (vw), 778 (w), 766 (w), 747 (m), 712 (s), 677 (w), 593 (w) cm^{-1}; HR-MS: *m/z*: calcd for $C_{50}H_{66}N_6O_{17}$ [M-H+2Na]$^+$: 1067.4202; found: 1067.4207.

(1*R*,3*R*,4*R*,5*S*)-3-[2-*O*-Benzoyl-3-*O*-((1*S*)-1-carboxy-2-cyclohexyl-ethyl)-(β-D-galactopyranosyl)oxy]-4-[(α-L-fucopyranosyl)oxy]-5-methyl-*N*-(3-{1-[2-(5-nitro-1*H*-indol-1-yl)ethyl]-1*H*-1,2,3-triazol-4-yl}propyl)cyclohexanecarboxamide (39). Prepared according to general procedure C from **26c** (14.6 mg, 18.1 μmol), **28b** (5.5 mg, 23.8 μmol), Na-L-ascorbate (91 μL, 9.1 μmol) and CuSO$_4$·5 H$_2$O (45 μL, 4.5 μmol). Yield: 12.8 mg (68%). [α]$_D$ -51.0 (*c* 0.89, MeOH); ^{1}H NMR (500 MHz, CD$_3$OD): δ = 0.54 (m, 1H, Cy), 0.59-0.70 (m, 3H, 3 Cy), 0.89 (m, 1H, Cy), 1.11 (d, *J* = 6.5 Hz, 3H, Me), 1.14-1.36 (m, 10H, 5 Cy, H-6a, H-2a, Fuc-H6), 1.40 (m, 1H, Lac-H3a), 1.44-1.54 (m, 3H, Lac-H3b, H-2'), 1.54-1.62 (m, 2H, Cy, H-6b), 1.67 (m, 1H, H-5), 2.15 (m, 1H, H-2b), 2.23 (m, 1H, H-1), 2.47 (t, *J* = 7.4 Hz, 2H, H-3'), 2.86-2.93 (m, 2H, H-1'), 3.15 (t, *J* = 9.6 Hz, 1H, H-4), 3.59 (t, *J* = 5.8 Hz, 1H, Gal-H5), 3.65 (dd, *J* = 2.7, 9.7 Hz, 1H, Gal-H3), 3.67-3.82 (m, 5H, H-3, Fuc-H2, -H4, Gal-H6), 3.88 (dd, *J* = 3.3, 10.3 Hz, 1H, Fuc-H3), 3.94-3.99 (m, 2H, Gal-H4, Lac-H2), 4.72-4.78 (m, 3H, Gal-H1, H-2''), 4.79-4.83 (m, 2H, H-1''), 4.95-5.02 (m, 2H, Fuc-H1, -H5), 5.43 (dd, *J* = 8.4, 9.3 Hz, 1H, Gal-H2), 6.70 (d, *J* = 3.1 Hz, 1H, Ind-H3), 7.17 (d, *J* = 9.1 Hz, Ind-H7), 7.21 (s, 1H, H-5'), 7.33 (d, *J* = 3.3 Hz, 1H, Ind-H2), 7.49-7.54, 7.49-7.54 (m, 3H, C$_6$H$_5$), 7.96 (m, 1H, Ind-H6), 8.01-8.04 (m, 2H, C$_6$H$_5$), 8.50 (d, *J* = 2.2 Hz, 1H, Ind-H4); ^{13}C NMR (125 MHz, CD$_3$OD): δ = 16.73 (Fuc-C6), 19.27 (Me), 23.28 (C-3'), 26.54, 26.71, 27.30 (3 Cy), 30.26 (C-2'), 33.11, 34.24, 35.13 (3 Cy), 35.38 (C-2), 37.49 (C-6), 39.31, 39.36 (C-5, C-1'), 42.98 (Lac-C3), 43.32 (C-1), 47.51 (C-2''), 51.46 (C-1''), 62.87 (Gal-C6), 67.73, 67.76 (Gal-C4, Fuc-C5), 70.34 (Fuc-C2), 71.42 (Fuc-C3), 73.02 (Gal-C2), 73.97 (Fuc-C4), 76.03 (Gal-C5), 78.78 (Lac-C2)‡, 79.85 (C-3), 83.05 (C-4), 83.72 (Gal-C3), 100.44 (Fuc-C1), 100.56 (Gal-C1), 105.87 (Ind-C3), 110.18 (Ind-C7), 117.98 (Ind-C6), 118.73 (Ind-C4), 124.12 (C-5'), 129.11 (Ind-C9), 129.65, 130.85, 131.62 (5C, C$_6$H$_5$), 132.46 (Ind-C2), 134.25 (C$_6$H$_5$), 140.57 (Ind-C8), 142.88 (Ind-C5), 148.44 (C-4'), 166.82 (*C*OPh), 176.99 (CONH), 180.71 (COOH); IR (KBr): *v* = 3421 (s, OH), 2927 (m), 2852 (w), 1718 (m, C=O), 1646 (m, C=O), 1638 (m), 1620 (m), 1580 (w), 1517 (m), 1476 (w), 1429 (w), 1402 (w), 1383 (w), 1336 (vs, NO$_2$), 1270 (m), 1218 (w), 1166 (w), 1095 (s), 1070 (s), 1029 (s), 996 (m), 966 (w), 933 (vw), 894 (vw), 826 (vw), 809 (vw), 779 (vw), 771 (vw), 746 (w), 712 (w), 675 (vw),

589 (vw) cm^{-1}; HR-MS: *m/z*: calcd for $C_{51}H_{68}N_6O_{17}$ [M+H]$^+$: 1037.4714; found: 1037.4711.

(1*R*,3*R*,4*R*,5*S*)-3-[2-*O*-Benzoyl-3-*O*-((1*S*)-1-carboxy-2-cyclohexyl-ethyl)-(β-D-galactopyranosyl)oxy]-4-[(α-L-fucopyranosyl)oxy]-5-methyl-*N*-(4-{1-[2-(6-nitro-1*H*-indol-3-yl)ethyl]-1*H*-1,2,3-triazol-4-yl}butyl)cyclohexanecarboxamide (40). Prepared according to general procedure C from **26d** (10.2 mg, 12.9 μmol), **28b** (4.5 mg, 19.5 μmol), Na-L-ascorbate (64 μL, 6.4 μmol) and CuSO$_4$·5 H$_2$O (32 μL, 3.2 μmol). Yield: 11.5 mg (85%). [α]$_D^{20}$ -47.8 (*c* 1.10, MeOH); ^{1}H NMR (500 MHz, CD$_3$OD): *δ* = 0.54 (m, 1H, Cy), 0.59-0.71 (m, 3H, 3 Cy), 0.90 (m, 1H, Cy), 1.10 (d, *J* = 6.5 Hz, 3H, Me), 1.14-1.24 (m, 3H, Cy, H-6a, H-2a), 1.24-1.36 (m, 9H, Fuc-H6, 4 Cy, H-2'), 1.36-1.61 (m, 6H, H-3', Lac-H3b, H-6b, Cy), 1.66 (m, 1H, H-5), 2.13 (m, 1H, H-2), 2.24 (m, 1H, H-1), 2.50 (t, *J* = 7.3 Hz, 2H, H-4'), 2.96-3.07 (m, 2H, H-1'), 3.14 (t, *J* = 9.6 Hz, 1H, H-4), 3.57 (t, *J* = 5.7 Hz, 1H, Gal-H5), 3.64 (dd, *J* = 2.5, 9.7 Hz, 1H, Gal-H3), 3.66-3.82 (m, 5H, H-3, Fuc-H2, -H4, Gal-H6), 3.87 (dd, *J* = 3.2, 10.3 Hz, 1H, Fuc-H3), 3.96 (m, 1H, Gal-H4), 4.03 (m, 1H, Lac-H2), 4.71 (d, *J* = 8.0 Hz, 1H, Gal-H1), 4.74-4.78 (m, 2H, H-2''), 4.79-4.83 (m, 2H, H-1''), 4.95-5.01 (m, 2H, Fuc-H1, -H5), 5.43 (m, 1H, Gal-H2), 6.70 (d, *J* = 3.2 Hz, 1H, Ind-H3), 7.21 (d, *J* = 9.0 Hz, 1H, Ind-H7), 7.22 (s, 1H, H-6'), 7.29 (d, *J* = 3.2 Hz, 1H, Ind-H2), 7.43 (t, *J* = 7.7 Hz, 2H, C$_6$H$_5$), 7.58 (t, *J* = 7.4 Hz, 1H, C$_6$H$_5$), 7.97 (dd, *J* = 2.1, 9.1 Hz, 1H, Ind-H6), 8.02 (d, *J* = 7.6 Hz, 2H, C$_6$H$_5$), 8.52 (d, *J* = 2.1 Hz, 1H, Ind-H4); ^{13}C NMR (125 MHz, CD$_3$OD): *δ* = 16.72 (Fuc-C6), 19.24 (Me), 25.46 (C-4'), 26.49, 26.66, 27.24 (3 Cy), 27.59 (C-3'), 29.51 (C-2'), 33.08, 34.13, 35.02 (3 Cy), 35.32 (C-2), 37.52 (C-6), 39.34 (C-5), 39.79 (C-1'), 42.76 (Lac-C3), 43.27 (C-1), 47.49 (C-2''), 51.34 (C-1''), 62.72 (Gal-C6), 67.68 (Gal-C4), 67.73 (Fuc-C5), 70.29 (Fuc-C2), 71.39 (Fuc-C3), 72.95 (Gal-C2), 73.94 (Fuc-C4), 75.94 (Gal-C5), 77.98 (Lac-C2), 79.81 (C-3), 83.03 (C-4), 83.65 (Gal-C3), 100.44 (Fuc-C1), 100.47 (Gal-C1), 105.76 (Ind-C3), 110.21 (Ind-C7), 117.97 (Ind-C6), 118.69 82 (Ind-C4), 123.96 (C-6'), 129.12 (Ind-C9), 129.68, 130.84, 131.51 (5C, C$_6$H$_5$), 132.46 (Ind-C2), 134.34 (C$_6$H$_5$), 140.49 (Ind-C8), 142.87 (Ind-C5), 148.89 (C-5'), 166.79 (*C*OPh), 176.92 (CONH), 178.93 (COOH); IR (KBr): *v* = 3436 (vs, OH), 2927 (m), 2852 (w), 1725 (m, C=O), 1638 (m, C=O), 1584 (vw), 1516 (w), 1479 (vw), 1450 (w), 1383 (vw), 1335 (s, NO$_2$), 1269 (s), 1218 (w), 1166 (w), 1114 (m), 1071 (s), 1032 (m), 998 (w), 966 (vw), 746 (vw), 712 (w) cm^{-1}; HR-MS: *m/z*: calcd for $C_{52}H_{70}N_6O_{17}$ [M+H]$^+$: 1051.4870; found: 1051.4872.

(1*R*,3*R*,4*R*,5*S*)-3-[2-*O*-Benzoyl-3-*O*-((1*S*)-1-carboxy-2-cyclohexyl-ethyl)-(β-D-galactopyranosyl)oxy]-4-[(α-L-fucopyranosyl)oxy]-5-methyl-*N*-({1-[3-(5-nitro-1*H*-indol-1-yl)propyl]-1*H*-1,2,3-triazol-4-yl}methyl)cyclohexanecarboxamide (41). Prepared according to general procedure C from **26a** (12.0 mg, 15.4 μmol), **28c** (5.7 mg, 23.2 μmol), Na-L-ascorbate (77 μL, 7.7 μmol) and CuSO$_4$·5 H$_2$O (39 μL, 3.9 μmol). Yield: 13.5 mg (85%). [α]$_D^{20}$ -51.9 (*c* 1.15, MeOH); ^{1}H NMR (500 MHz, CD$_3$OD): δ = 0.50-0.72 (m, 4H, Cy), 0.90 (m, 1H, Cy), 1.08 (d, *J* = 6.4 Hz, 3H, Me), 1.13-1.25 (m, 3H, Cy, H-6a, H-2a), 1.24-1.37 (m, 7H, 4 Cy, Fuc-H6), 1.41 (m, 1H, Lac-H3a), 1.45-1.58 (m, 2H, Lac-H3b, Cy), 1.58-1.71 (m, 2H, H-6b, H-5), 2.16 (m, 1H, H-2b), 2.29 (m, 1H, H-1), 2.47 (p, *J* = 6.8 Hz, 2H, H-2"), 3.13 (t, *J* = 9.5 Hz, 1H, H-4), 3.56 (t, *J* = 5.8 Hz, 1H, Gal-H5), 3.61 (dd, *J* = 2.5, 9.7 Hz, 1H, Gal-H3), 3.65-3.82 (m, 5H, H-3, Fuc-H2, -H4, Gal-H6), 3.86 (dd, *J* = 3.3, 10.3 Hz, 1H, Fuc-H3), 3.95 (s, 1H, Gal-H4), 4.01 (d, *J* = 7.9 Hz, 1H, Lac-H2), 4.31 (t, *J* = 7.0 Hz, 2H, H-3"), 4.33 (s, 2H, H-1'), 4.39 (t, *J* = 6.7 Hz, 2H, H-1"), 4.67 (d, *J* = 8.0 Hz, 1H, Gal-H1), 4.93-4.99 (m, 2H, Fuc-H1, -H5), 5.43 (m, 1H, Gal-H2), 6.74 (d, *J* = 3.1 Hz, 1H, Ind-H3), 7.38-7.45 (m, 3H, Ind-H7, C$_6$H$_5$), 7.48 (d, *J* = 3.2 Hz, 1H, Ind-H2), 7.56 (m, 1H, C$_6$H$_5$), 7.75 (s, 1H, H-3'), 7.99-8.02 (m, 2H, C$_6$H$_5$), 8.07 (dd, *J* = 2.2, 9.1 Hz, 1H, Ind-H6), 8.20-8.24 (m, 1H, NH), 8.56 (d, *J* = 2.2 Hz, 1H, Ind-H4); ^{13}C NMR (125 MHz, CD$_3$OD): δ = 16.73 (Fuc-C6), 19.24 (Me), 26.53, 26.68, 27.26 (3 Cy), 31.48 (C-2"), 33.12, 34.18 (2 Cy), 35.04, 35.09 (Cy, C-2), 35.64 (C-1'), 37.51 (C-6), 39.34 (C-5), 42.77 (Lac-C3), 43.03 (C-1), 44.50 (C-3"), 49.85 (C-1"), 62.76 (Gal-C6), 67.72, 67.75 (Gal-C4, Fuc-C5), 70.31 (Fuc-C2), 71.41 (Fuc-C3), 72.98 (Gal-C2), 73.95 (Fuc-C4), 75.99 (Gal-C5), 77.98 (Lac-C2), 79.75 (C-3), 83.03 (C-4), 83.71 (Gal-C3), 100.43 (Fuc-C1), 100.47 (Gal-C1), 105.24 (Ind-C3), 110.69 (Ind-C7), 117.94 (Ind-C6), 118.84 (Ind-C4), 124.44 (C-3'), 129.36 (Ind-C9), 129.68, 130.87, 131.55 (5C, C$_6$H$_5$), 132.79 (Ind-C2), 134.30 (C$_6$H$_5$), 140.24 (Ind-C8), 142.85 (Ind-C5), 166.82 (*C*OPh), 176.96 (CONH); IR (KBr): *v* = 3429 (vs, OH), 2928 (m), 2852 (w), 1723 (m, C=O), 1643 (m, C=O), 1580 (vw), 1516 (m), 1479 (w), 1449 (w), 1402 (w), 1380 (w), 1335 (s, NO$_2$), 1269 (m), 1210 (w), 1163 (w), 1111 (m), 1070 (s), 1032 (m), 963 (w), 894 (vw), 768 (vw), 745 (w), 712 (w), 672 (w) cm^{-1}; HR-MS: *m/z*: calcd for C$_{50}$H$_{66}$N$_6$O$_{17}$ [M+H]$^+$: 1023.4557; found: 1023.4561.

(1*R*,3*R*,4*R*,5*S*)-3-[2-*O*-Benzoyl-3-*O*-((1*S*)-1-carboxy-2-cyclohexyl-ethyl)-(β-D-galactopyranosyl)oxy]-4-[(α-L-fucopyranosyl)oxy]-5-methyl-*N*-(2-{1-[3-(5-nitro-1*H*-indol-1-yl)propyl]-1*H*-1,2,3-triazol-4-yl}ethyl)cyclohexanecarboxamide (42). Prepared

according to general procedure C from **26b** (17.3 mg, 21.8 µmol), **28c** (7.0 mg, 28.5 µmol), Na-L-ascorbate (110 µL, 11.0 µmol) and $CuSO_4 \cdot 5\ H_2O$ (55 µL, 5.5 µmol). Yield: 14.4 mg (63%). $[\alpha]_D^{20}$ -60.4 (*c* 0.32 , MeOH); ^{1}H NMR (500 MHz, CD_3OD): $\delta = 0.49$-0.74 (m, 4H, 4 Cy), 0.90 (m, 1H, Cy), 1.05 (d, *J* = 6.5 Hz, 3H, Me), 1.07-1.25 (m, 3H, H-2a, H-6a, Cy), 1.26-1.37 (m, 7H, Fuc-H6, 4 Cy), 1.41 (m, 1H, Lac-H3a), 1.45-1.58 (m, 3H, Lac-H3b, H-6b, Cy), 1.64 (m, 1H, H-5), 2.11 (m, 1H, H-2b), 2.22 (m, 1H, H-1), 2.46 (p, *J* = 6.6 Hz, 2H, H-2"), 2.79 (t, *J* = 7.1 Hz, 2H, H-2'), 3.11 (t, *J* = 9.6 Hz, 1H, H-4), 3.32-3.41 (m, 2H, H-1'), 3.54 (t, *J* = 6.1 Hz, 1H, Gal-H5), 3.61 (dd, *J* = 2.8, 9.8 Hz, 1H, Gal-H3), 3.63-3.82 (m, 6H, H-3, Fuc-H1, -H4, Gal-H6), 3.85 (dd, *J* = 3.3, 10.3 Hz, 1H, Fuc-H3), 3.95 {d, *J* = 2.5 Hz, 1H, Gal-H4), 4.00 (m, 1H, Lac-H2), 4.30 (t, *J* = 6.9 Hz, 2H, H-3"), 4.37 (t, *J* = 6.8 Hz, 2H, H-1"), 4.66 (d, *J* = 8.0 Hz, 1H, Gal-H1), 4.93-5.00 (m, 2H, Fuc-H1, -H5), 5.42 (dd, *J* = 8.2, 9.5 Hz, 1H, Gal-H2), 6.73 (d, *J* = 3.0 Hz, 1H, Ind-H3), 7.41-7.53 (m, 4H, C_6H_5, Ind-H2, -H7), 7.58 (m, 1H, C_6H_5), 7.68 (s, 1H, H-4'), 7.81 (t, *J* = 5.3 Hz, 1H, NH), 8.02-8.06 (m, 2H, C_6H_5), 8.05 (d, *J* = 7.2 Hz, 1H, Ind-H6), 8.56 (d, *J* = 2.2 Hz, 1H, Ind-H4); ^{13}C NMR (125 MHz, CD_3OD): δ = 16.72 (Fuc-C6), 19.24 (Me), 26.53, 26.62, 26.71 (2 Cy, C-2'), 27.27 (Cy), 31.48 (C-2"), 33.15, 34.22, 35.07 (3 Cy), 35.26 (C-2), 37.52 (C-6), 39.31 (C-5), 39.94 (C-1'), 42.84 (Lac-C3), 43.23 (C-1), 44.60 (C-3"), 48.16 (C-1"), 62.80 (Gal-C6), 67.72, 67.77 (Gal-C4, Fuc-C5), 70.33 (Fuc-C2), 71.42 (Fuc-C3), 73.04 (Gal-C2), 73.96 (Fuc-C4), 76.01 (Gal-C5), 77.78 (Lac-C1), 79.77 (C-3), 82.98 (C-4), 83.69 (Gal-C3), 100.40 (Fuc-C1), 100.52 (Gal-C1), 105.21 (Ind-C3), 110.75 (Ind-C7), 117.92 (Ind-C6), 118.83 (Ind-C4), 123.83 (C-4'), 129.39 (Ind-C9), 129.72, 130.90, 131.62 (5C, C_6H_5), 132.84 (Ind-C2), 134.34 (C_6H_5), 140.25 (Ind-C8), 142.90 (Ind-C5), 146.71 (C-3'), 166.81 (*C*OPh), 177.01 (CONH); IR (KBr): v = 3431 (vs, OH), 2927 (s), 2852 (w), 1724 (s, C=O), 1644 (m,C=O), 1578 (w), 1516 (m), 1476 (w), 1451 (m), 1404 (w), 1334 (vs, NO_2), 1271 (s), 1220 (w), 1163 (m), 1109 (s), 1071 (vs), 1032 (s), 967 (w), 899 (vw), 807 (vw), 765 (w), 746 (m), 713 (m), 593 (w) cm^{-1}; HR-MS: *m/z*: calcd for $C_{51}H_{68}N_6O_{17}$ [M-H+2Na]$^+$: 1081.4358; found: 1081.4360.

(1*R*,3*R*,4*R*,5*S*)-3-[2-*O*-Benzoyl-3-*O*-((1*S*)-1-carboxy-2-cyclohexyl-ethyl)-(β-D-galactopyranosyl)oxy]-4-[(α-L-fucopyranosyl)oxy]-5-methyl-*N*-(3-{1-[3-(5-nitro-1*H*-indol-1-yl)propyl]-1*H*-1,2,3-triazol-4-yl}propyl)cyclohexanecarboxamide (43). Prepared according to general procedure C from **26c** (106 mg, 132 µmol), **28c** (48.0 mg, 196 µmol), Na-L-ascorbate (658 µL, 65.8 µmol) and $CuSO_4 \cdot 5\ H_2O$ (329 µL, 32.9 µmol). Yield: 125 mg (91%). $[\alpha]_D^{20}$ -53.1 (*c* 0.99, MeOH); ^{1}H NMR (500 MHz, CD_3OD): δ = 0.46-0.70 (m, 4H, 4

Cy), 0.87 (m, 1H, Cy), 1.11 (d, J = 6.5 Hz, 3H, Me), 1.14-1.36 (m, 10H, H-2a, H-6a, 5 Cy, Fuc-H6), 1.40 (m, 1H, Lac-H3a), 1.47 (m, 1H, Lac-H3b), 1.54 (m, 1H, Cy), 1.60 (dd, J = 2.5, 13.2 Hz, 1H, H-6b), 1.67 (m, 1H, H-5), 1.71-1.81 (m, 2H, H-2'), 2.15 (m, 1H, H-2b), 2.25 (ddd, J = 3.2, 8.0, 12.7 Hz, 1H, H-1), 2.49 (p, J = 6.8 Hz, 2H, H-2''), 2.65 (t, J = 7.4 Hz, 2H, H-3'), 3.05-3.19 (m, 3H, H-1', H-4), 3.57 (t, J = 6.1 Hz, 1H, Gal-H5), 3.64 (dd, J = 3.0, 9.7 Hz, 1H, Gal-H3), 3.66-3.83 (m, 5H, H-3, Fuc-H2, -H4, Gal-H6), 3.87 (dd, J = 3.3, 10.3 Hz, 1H, Fuc-H3), 3.96 (d, J = 2.4 Hz, 1H, Gal-H4), 4.00 (dd, J = 2.9, 9.8 Hz, 1H, Lac-H2), 4.32 (t, J = 6.9 Hz, 2H, H-3''), 4.40 (t, J = 6.7 Hz, 2H, H-1''), 4.70 (d, J = 8.1 Hz, 1H, Gal-H1), 4.95-5.01 (m, 2H, Fuc-H1, -H5), 5.43 (dd, J = 8.2, 9.6 Hz, 1H, Gal-H2), 6.72 (d, J = 2.9 Hz, 1H, Ind-H3), 7.34-7.38 (m, 2H, C_6H_5), 7.44-7.52 (m, 3H, Ind-H2, -H7, C_6H_5), 7.65 (s, 1H, H-5'), 7.98-8.02 (m, 2H, C_6H_5), 8.06 (dd, J = 2.2, 9.1 Hz, 1H, Ind-H6), 8.56 (d, J = 2.2 Hz, Ind-H4); ^{13}C NMR (125 MHz, CD$_3$OD): δ = 16.73 (Fuc-C6), 19.26 (Me), 23.54 (C-3'), 26.50, 26.67, 27.25 (3 Cy), 30.22 (C-2'), 31.41 (C-2''), 33.11, 34.18, 35.04 (3 Cy), 35.42 (C-2), 37.50 (C-6), 39.35, 39.48 (C-5, C-1'), 42.82 (Lac-C3), 43.35 (C-1), 44.64 (C-3''), 48.56 (C-1''), 62.79 (Gal-C6), 67.71, 67.77 (Gal-C4, Fuc-C5), 70.33 (Fuc-C2), 71.42 (Fuc-C3), 73.00 (Gal-C2), 73.96 (Fuc-C4), 75.99 (Gal-C5), 78.32 (Lac-C2), 79.85 (C-3), 83.03 (C-4), 83.67 (Gal-C3), 100.45 (Fuc-C1), 100.54 (Gal-C1), 105.21 (Ind-C3), 110.70 (Ind-C7), 117.90 (Ind-C6), 118.83 (Ind-C4), 123.54 (C-5'), 129.36 (Ind-C9), 129.65, 130.83, 131.56 (5C, C_6H_5), 132.81 (Ind-C2), 134.26 (C_6H_5), 140.24 (Ind-C8), 142.83 (Ind-C5), 148.51 (C-4'), 166.78 (*C*OPh), 177.04 (CONH), 179.26 (COOH); IR (KBr): v = 3433 (vs, OH), 2926 (m), 2852 (w), 1725 (m, C=O), 1638 (m, C=O), 1514 (w), 1449 (w), 1402 (w), 1383 (w), 1334 (m, NO$_2$), 1268 (m), 1213 (w), 1163 (w), 1111 (m), 1070 (s), 1032 (m), 996 (w), 963 (vw), 933 (vw), 897 (vw), 807 (vw), 777 (vw), 744 (w), 712 (w) cm^{-1}; HR-MS: *m/z*: calcd for C$_{52}$H$_{70}$N$_6$O$_{17}$ [M+Na]$^+$: 1073.4690; found: 1073.4684.

(1*R*,3*R*,4*R*,5*S*)-3-[2-*O*-Benzoyl-3-*O*-((1*S*)-1-carboxy-2-cyclohexyl-ethyl)-(β-D-galactopyranosyl)oxy]-4-[(α-L-fucopyranosyl)oxy]-5-methyl-*N*-({1-[4-(5-nitro-1*H*-indol-1-yl)butyl]-1*H*-1,2,3-triazol-4-yl}methyl)cyclohexanecarboxamide (44). Prepared according to general procedure C from **26a** (9.7 mg, 12.5 μmol), **28d** (4.2 mg, 16.2 μmol), Na-L-ascorbate (124 μL, 12.4 μmol) and CuSO$_4$·5 H$_2$O (62 μL, 6.2 μmol). Yield: 6.4 mg (49%). [α]$_D^{20}$ -57.0 (*c* 0.62, MeOH); ^{1}H NMR (500 MHz, CD$_3$OD): δ = 0.50-0.73 (m, 4H, Cy), 0.91 (m, 1H, Cy), 1.07 (d, J = 6.4 Hz, 3H, Me), 1.17 (m, 3H, Cy, H-6a, H-2a), 1.32 (m, 7H, 4 Cy, Fuc-H6), 1.42 (m, 1H, Lac-H3a), 1.50 (m, 1H, Lac-H3b), 1.54-1.69 (m, 3H, Cy, H-

6, H-5), 1.77-1.93 (m, 4H, H-3", H-2"), 2.15 (m, 1H, H-2), 2.26 (m, 1H, H-1), 3.12 (t, J = 9.5 Hz, 1H, H-4), 3.55 (t, J = 5.8 Hz, 1H, Gal-H5), 3.62 (dd, J = 2.9, 9.7 Hz, 1H, Gal-H3), 3.64-3.82 (m, 5H, H-3, Fuc-H2, -H4, Gal-H6), 3.86 (dd, J = 3.3, 10.3 Hz, 1H, Fuc-H3), 3.96 (m, 1H, Gal-H4), 4.01 (dd, J = 2.5, 9.6 Hz, 1H, Lac-H2), 4.26 (t, J = 6.8 Hz, 2H, H-4"), 4.31 (s, 2H, H-1'), 4.39 (t, J = 6.6 Hz, 2H, H-1"), 4.67 (d, J = 8.1 Hz, 1H, Gal-H1), 4.94-4.99 (m, 2H, Fuc-H1, -H5), 5.43 (m, 1H, Gal-H2), 6.71 (d, J = 3.2 Hz, 1H, Ind-H3), 7.41-7.47 (m, 3H, Ind-H7, C_6H_5), 7.52 (d, J = 9.1 Hz, 1H, Ind-H2), 7.58 (m, 1H, C_6H_5), 7.72 (s, 1H, H-3'), 8.02-8.05 (m, 2H, C_6H_5), 8.07 (dd, J = 2.2, 9.1 Hz, 1H, Ind-H6), 8.55 (d, J = 2.1 Hz, 1H, Ind-H4); ^{13}C NMR (125 MHz, CD$_3$OD): δ = 16.73 (Fuc-C6), 19.23 (Me), 26.54, 26.70, 27.28 (3 Cy), 28.16, 28.48 (C-2", C-3"), 33.13, 34.20 (2 Cy), 35.06, 35.10 (Cy, C-2), 35.58 (C-1'), 37.44 (C-6), 39.31 (C-5), 42.83 (Lac-C3), 42.97 (C-1), 46.81 (C-4"), 50.70 (C-1"), 62.78 (Gal-C6), 67.72, 67.76 (Gal-C4, Fuc-C5), 70.31 (Fuc-C2), 71.41 (Fuc-C3), 73.00 (Gal-C2), 73.96 (Fuc-C4), 75.99 (Gal-C5), 78.29 (Lac-C2), 79.76 (C-3), 83.00 (C-4), 83.72 (Gal-C3), 100.43 (Fuc-C1), 100.50 (Gal-C1), 104.94 (Ind-C3), 110.76 (Ind-C7), 117.80 (Ind-C6), 118.81 (Ind-C4), 124.19 (C-3'), 129.27 (Ind-C9), 129.71, 130.89, 131.59 (5C, C_6H_5), 132.79 (Ind-C2), 134.33 (C_6H_5), 140.27 (Ind-C8), 142.72 (Ind-C5), 146.16 (C-2'), 166.85 (*C*OPh), 176.90 (CONH), 179.31 (COOH); IR (KBr): v = 3431 (vs, OH), 2927 (m), 2852 (m), 1725 (m, C=O), 1639 (m, C=O), 1580 (w), 1516 (m), 1479 (w), 1448 (w), 1402 (w), 1383 (w), 1334 (s, NO$_2$), 1271 (m), 1111 (m), 1071 (s), 1032 (m), 999 (vw), 966 (vw), 933 (vw), 897 (vw), 837 (vw), 804 (vw), 768 (vw), 746 (vw), 713 (w), 667 (vw), 593 (vw) cm^{-1}; HR-MS: *m/z*: calcd for $C_{51}H_{68}N_6O_{17}$ [M-H+2Na]$^+$: 1081.4353; found: 1081.4342.

(1*R*,3*R*,4*R*,5*S*)-3-[2-*O*-Benzoyl-3-*O*-((1*S*)-1-carboxy-2-cyclohexyl-ethyl)-(β-D-galactopyranosyl)oxy]-4-[(α-L-fucopyranosyl)oxy]-5-methyl-*N*-(2-{1-[4-(5-nitro-1*H*-indol-1-yl)butyl]-1*H*-1,2,3-triazol-4-yl}ethyl)cyclohexanecarboxamide (45). Prepared according to general procedure C from **26b** (14.0 mg, 17.7 μmol), **28d** (6.1 mg, 23.5 μmol), Na-L-ascorbate (252 μL, 25.2 μmol) and CuSO$_4$·5 H$_2$O (125 μL, 12.5 μmol). Yield: 9.3 mg (50%). [α]$_D^{20}$ -60.1 (*c* 0.86, MeOH); ^{1}H NMR (500 MHz, CD$_3$OD): δ = 0.49-0.72 (m, 4H, 4 Cy), 0.90 (m, 1H, Cy), 1.06 (d, J = 6.5 Hz, 3H, Me), 1.08-1.26 (m, 3H, Cy, H-6a, H-2a), 1.26-1.36 (m, 7H, 4 Cy, H-6), 1.40 (m, 1H, Lac-H3), 1.46-1.59 (m, 3H, Lac-H3, H-6b, Cy), 1.63 (m, 1H, H-5), 1.77-1.91 (m, 4H, H-3", H-2"), 2.12 (m, 1H, H-2b), 2.19 (m, 1H, H-1), 2.76 (t, J = 7.2 Hz, 2H, H-2'), 3.11 (t, J = 9.6 Hz, 1H, H-4), 3.32 (m, 1H, H-1') 3.56 (m, 1H, Gal-H5), 3.61-3.81 (m, 6H, Gal-H3, -H6, H-3, Fuc-H2, -H4), 3.86 (dd, J = 3.3, 10.3 Hz, 1H,

Fuc-H3), 3.95 (d, J = 2.3 Hz, 1H, Gal-H4), 4.03 (dd, J = 2.8, 9.8 Hz, 1H, Lac-H1), 4.27 (t, J = 6.7 Hz, 2H, H-1"), 4.36 (t, J = 6.4 Hz, 2H, H-1"), 4.68 (d, J = 8.1 Hz, 1H, Gal-H1), 4.94 (d, J = 4.0 Hz, 1H, Fuc-H1), 4.98 (m, 1H, Fuc-H5), 5.43 (dd, J = 8.3, 9.5 Hz, 1H, Gal-H2), 6.71 (dd, J = 0.5, 3.2 Hz, 1H, Ind-H3), 7.43-7.47 (m, 3H, C_6H_5, Ind-H2), 7.52-7.58 (m, 2H, Ind-H7, C_6H_5), 7.64 (s, 1H, H-4'), 8.03-8.09 (m, 3H, C_6H_5, Ind-H6), 8.56 (d, J = 2.2 Hz, 1H, Ind-H4); ^{13}C NMR (125 MHz, CD_3OD): δ = 16.74 (Fuc-C6), 19.24 (Me), 26.53, 26.59, 26.70 (3C, 2 Cy, C-2'), 27.27 (Cy), 28.11 (C-3"), 28.50 (C-2"), 33.12, 34.18, 35.05 (3 Cy), 35.27 (C-2), 37.46 (C-6), 39.31 (C-5), 39.97 (C-1'), 42.80 (Lac-C3), 43.22 (C-1), 46.85 (C-2"), 50.61 (C-1"), 62.75 (Gal-C6), 67.70, 67.74 (Gal-C4, Fuc-C5), 70.31 (Fuc-C2), 71.42 (Fuc-C3), 73.02 (Gal-C2), 73.96 (Fuc-C4), 75.98 (Gal-C5), 78.07 (Lac-C2), 79.79 (C-3), 83.00 (C-4), 83.68 (Gal-C3), 100.43 (Fuc-C1), 100.51 (Gal-C1), 104.93 (Ind-C3), 110.78 (Ind-C7), 117.79 (Ind-C6), 118.84 (Ind-C4), 123.58 (C-4'), 129.29 (Ind-C9), 129.73, 130.91, 131.58 (5C, C_6H_5), 132.88 (Ind-C2), 134.36 (C_6H_5), 140.24 (Ind-C8), 142.72 (Ind-C5), 146.35 (C-3'), 166.81 (COPh), 176.99 (CONH), 179.14 (COOH); IR (KBr): v = 3414 (vs, OH), 2927 (s), 2852 (m), 1722 (s, C=O), 1648 (m, C=O), 1610 (w), 1580 (w), 1515 (m), 1479 (w), 1450 (m), 1404 (w), 1334 (vs), 1272 (s), 1215 (w), 1163 (m), 1112 (s), 1072 (vs), 1032 (s, NO_2), 967 (w), 897 (vw), 807 (vw), 768 (w), 747 (m), 713 (m), 675 (w), 628 (w), 593 (w) cm^{-1}; HR-MS: m/z: calcd for $C_{52}H_{70}N_6O_{17}$ [M+H]$^+$: 1051.4870; found: 1051.4868.

(1R,3R,4R,5S)-3-[2-O-Benzoyl-3-O-((1S)-1-carboxy-2-cyclohexyl-ethyl)-(β-ᴅ-galactopyranosyl)oxy]-4-[(α-ʟ-fucopyranosyl)oxy]-5-methyl-N-(3-{1-[4-(5-nitro-1H-indol-1-yl)butyl]-1H-1,2,3-triazol-4-yl}propyl)cyclohexanecarboxamide (46). Prepared according to general procedure C from **26c** (12.0 mg, 14.9 µmol), **28d** (5.8 mg, 22.4 µmol), Na-ʟ-ascorbate (74 µL, 7.4 µmol) and $CuSO_4 \cdot 5\ H_2O$ (37 µL, 3.7 µmol). Yield: 9.4 mg (59%). [α]$_D^{20}$ -53.1 (c 0.82, MeOH); ^1H NMR (500 MHz, CD_3OD): δ = 0.49-0.70 (m, 4H, 4 Cy), 0.89 (m, 1H, Cy), 1.10 (d, J = 6.4 Hz, 3H, Me), 1.14-1.37 (m, 10H, H-2a, H-6a, 5 Cy, Fuc-H6), 1.40 (dd, J = 9.1, 11.8 Hz, 1H, Lac-H3a), 1.45-1.62 (m, 3H, Lac-H3b, Cy, H-6b), 1.66 (m, 1H, H-5), 1.70-1.78 (m, 2H, H-2'), 1.78-1.93 (m, 4H, H-3", H-2"), 2.15 (m, 1H, H-2b), 2.25 (m, 1H, H-1), 2.63 (t, J = 7.4 Hz, 2H, H-3'), 3.03-3.19 (m, 3H, H-1', H-4), 3.57 (t, J = 5.9 Hz, 1H, Gal-H5), 3.64 (dd, J = 2.8, 9.7 Hz, 1H, Gal-H3), 3.66-3.83 (m, 5H, H-3, Fuc-H2, -H4, Gal-H6), 3.87 (dd, J = 3.2, 10.3 Hz, 1H, Fuc-H3), 3.95-4.03 (m, 2H, Gal-H4, Lac-H2), 4.28 (t, J = 6.8 Hz, 2H, H-4"), 4.38 (t, J = 6.6 Hz, 2H, H-1"), 4.70 (d, J = 8.0 Hz, 1H, Gal-H1), 4.95-5.02 (m, 2H, Fuc-H1, -H5), 5.43 (m, 1H, Gal-H2), 6.70 (d, J = 2.8 Hz, 1H,

Ind-H3), 7.33-7.40 (m, 2H, C$_6$H$_5$), 7.44 (d, J = 3.2 Hz, 1H, Ind-H2), 7.46-7.54 (m, 2H, C$_6$H$_5$, Ind-H7), 7.63 (s, 1H, H-5'), 7.98-8.04 (m, 2H, C$_6$H$_5$), 8.06 (dd, J = 2.2, 9.1 Hz, 1H, Ind-H6), 8.55 (d, J = 2.2 Hz, 1H, Ind-H4); ^{13}C NMR (125 MHz, CD$_3$OD): δ = 16.73 (Fuc-C6), 19.26 (Me), 23.53 (C-3'), 26.52, 26.69, 27.27 (3 Cy), 28.11, 28.47 (C-2'', C-3''), 30.23 (C-2'), 33.12, 34.20, 35.07 (3 Cy), 35.44 (C-2), 37.48 (C-6), 39.34, 39.45 (C-5, C-1'), 42.86 (Lac-C3), 43.34 (C-1), 46.87 (C-2''), 50.61 (C-1''), 62.81 (Gal-C6), 67.71, 67.76 (Gal-C4, Fuc-C5), 70.33 (Fuc-C2), 71.42 (Fuc-C3), 73.02 (Gal-C2), 73.97 (Fuc-C4), 76.00 (Gal-C5), 78.36 (Lac-C2), 79.87 (C-3), 83.01 (C-4), 83.67 (Gal-C3), 100.44 (Fuc-C1), 100.58 (Gal-C1), 104.90 (Ind-C3), 110.78 (Ind-C7), 117.78 (Ind-C6), 118.82 (Ind-C4), 123.35 (C-5'), 129.31 (Ind-C9), 129.65, 130.83, 131.57 (5C, C$_6$H$_5$), 132.89 (Ind-C2), 134.26 (C$_6$H$_5$), 140.26 (Ind-C8), 142.71 (Ind-C5), 148.45 (C-4'), 166.78 (*C*OPh), 177.03 (CONH), 179.61 (COOH); IR (KBr): ν = 3436 (vs, OH), 2926 (w), 2852 (vw), 1723 (w, C=O), 1632 (m, C=O), 1512 (w), 1451 (w), 1383 (w), 1334 (m, NO$_2$), 1270 (m), 1210 (vw), 1166 (vw), 1111 (m), 1070 (m), 1032 (m), 996 (vw), 966 (vw), 744 (w), 711 (w) cm^{-1}; HR-MS: *m/z*: calcd for C$_{53}$H$_{72}$N$_6$O$_{17}$ [M+Na]$^+$: 1087.4846; found: 1087.4848.

(1*R*,3*R*,4*R*,5*S*)-3-[2-*O*-Benzoyl-3-*O*-((1*S*)-1-carboxy-2-cyclohexyl-ethyl)-(β-D-galactopyranosyl)oxy]-4-[(α-L-fucopyranosyl)oxy]-5-methyl-*N*-({1-[2-(6-nitro-1*H*-indol-3-yl)ethyl]-1*H*-1,2,3-triazol-4-yl}methyl)cyclohexanecarboxamide (47). Prepared according to general procedure C from **26a** (9.2 mg, 11.8 μmol), **32b** (3.6 mg, 15.6 μmol), Na-L-ascorbate (118 μL, 11.8 μmol) and CuSO$_4$·5 H$_2$O (59 μL, 5.9 μmol). Yield: 2.5 mg (21%). [α]$_D^{20}$ -62.7 (*c* 0.26, MeOH); ^{1}H NMR (500 MHz, CD$_3$OD): δ = 0.48-0.71 (m, 4H, 4 Cy), 0.90 (m, 1H, Cy), 1.10 (t, J = 7.0 Hz, 3H, Me), 1.13-1.24 (m, 3H, H-2a, H-6a, Cy), 1.24-1.36 (m, 7H, 4 Cy, Fuc-H6), 1.41 (m, 1H, Lac-H3a), 1.49 (m, 1H, Lac-H3b), 1.53-1.61 (m, 2H, Cy, H-6b), 1.65 (m, 1H, H-5), 2.15 (m, 1H, H-2b), 2.25 (m, 1H, H-1), 3.14 (t, J = 9.6 Hz, 1H, H-4), 3.41 (t, J = 6.7 Hz, 2H, H-2''), 3.57 (t, J = 5.9 Hz, 1H, Gal-H5), 3.61 (dd, J = 2.9, 9.7 Hz, 1H, Gal-H3), 3.65-3.82 (m, 5H, H-3, Fuc-H2, -H4, Gal-H6), 3.87 (dd, J = 3.3, 10.3 Hz, 1H, Fuc-H3), 3.93-3.98 (m, 2H, Gal-H4, Lac-H2), 4.27 (s, 2H, H-1'), 4.66-4.71 (m, 3H, H-1'', Gal-H1), 4.94-5.00 (m, 2H, Fuc-H1, -H5), 5.42 (dd, J = 8.2, 9.6 Hz, 1H, Gal-H2), 7.21 (s, 1H, Ind-H2), 7.41-7.46 (m, 3H, C$_6$H$_5$, Ind-H7), 7.57 (m, 1H, C$_6$H$_5$), 7.66 (s, 1H, H-3'), 8.01-8.05 (m, 3H, Ind-H6, C$_6$H$_5$), 8.30 (d, J = 2.1 Hz, 1H, Ind-H4); ^{13}C NMR (125 MHz, CD$_3$OD): δ = 16.72 (Fuc-C6), 19.26 (Me), 26.54, 26.72, 27.09 (3 Cy), 27.30 (C-2''), 33.12, 34.24 (2 Cy), 35.12, 35.16 (Cy, C-2), 35.54 (C-1'), 37.39 (C-6), 39.32 (C-5), 42.95, 42.98 (C-

1, Lac-C3), 52.36 (C-1"), 62.85 (Gal-C6), 67.74, 67.75 (Gal-C4, Fuc-C5), 70.33 (Fuc-C2), 71.41 (Fuc-C3), 73.02 (Gal-C2), 73.96 (Fuc-C4), 76.03 (Gal-C5), 79.11 (Lac-C2), 79.79 (C-3), 83.03 (C-4), 83.75 (Gal-C3), 100.44 (Fuc-C1), 100.54 (Gal-C1), 112.57 (Ind-C7), 114.78 (Ind-C3), 116.40 (Ind-C4), 117.99 (Ind-C6), 124.51 (C-3'), 127.90, 127.98 (Ind-C2, -C9), 129.69, 130.89, 131.60, 134.30 (6C, C_6H_5), 141.03 (Ind-C8), 142.51 (Ind-C5), 146.17 (C-2'), 166.86 (*C*OPh), 176.85 (CONH); IR (KBr): v = 3435 (vs, OH), 2925 (w), 2852 (vw), 1720 (w, C=O), 1632 (m, C=O), 1517 (vw), 1451 (vw), 1383 (w), 1333 (m), 1268 (w), 1163 (w), 1076 (m), 1032 (m, NO_2), 966 (vw), 711 (vw), 675 (vw), 587 (vw) cm^{-1}; HR-MS: *m/z*: calcd for $C_{49}H_{64}N_6O_{17}$ [M+Na][+]: 1031.4220; found: 1031.4223.

(1*R*,3*R*,4*R*,5*S*)-3-[2-*O*-Benzoyl-3-*O*-((1*S*)-1-carboxy-2-cyclohexyl-ethyl)-(β-ᴅ-galactopyranosyl)oxy]-4-[(α-ʟ-fucopyranosyl)oxy]-5-methyl-*N*-(2-{1-[2-(6-nitro-1*H*-indol-3-yl)ethyl]-1*H*-1,2,3-triazol-4-yl}ethyl)cyclohexanecarboxamide (48). Prepared according to general procedure C from **26b** (15.2 mg, 19.2 μmol), **32b** (5.9 mg, 25.5 μmol), Na-ʟ-ascorbate (96 μL, 9.6 μmol) and $CuSO_4 \cdot 5$ H_2O (48 μL, 4.8 μmol). Yield: 13.7 mg (70%). $[α]_D^{20}$ -53.9 (*c* 1.04, MeOH); ^{1}H NMR (500 MHz, CD_3OD): $δ$ = 0.50-0.73 (m, 4H, 4 Cy), 0.90 (m, 1H, Cy), 1.08 (d, *J* = 6.5 Hz, 3H, Me), 1.10-1.26 (m, 3H, H-6a, H-2a, Cy), 1.26-1.37 (m, 8H, 5 Cy, Fuc-H6), 1.41 (m, 1H, Lac-H3a), 1.46-1.58 (m, 3H, Lac-H3b, Cy, H-6b), 1.64 (m, 1H, H-5), 2.11 (m, 1H, H-2), 2.20 (m, 1H, H-1), 2.72 (t, *J* = 7.2 Hz, 2H, H-2'), 3.12 (t, *J* = 9.6 Hz, 1H, H-4), 3.24-3.29 (m, 2H, H-1'), 3.41 (t, *J* = 6.7 Hz, 2H, H-2"), 3.54 (t, *J* = 5.9 Hz, 1H, Gal-H5), 3.61 (dd, *J* = 3.0, 9.7 Hz, 1H, Gal-H3), 3.67 (ddd, *J* = 4.7, 9.3, 11.6 Hz, 1H, H-3), 3.70-3.81 (m, 4H, Fuc-H2, -H4, Gal-H6), 3.86 (dd, *J* = 3.3, 10.3 Hz, 1H, Fuc-H3), 3.94 (d, *J* = 2.4 Hz, 1H, Gal-H4), 4.01 (dd, *J* = 3.1, 9.7 Hz, 1H, Lac-H2), 4.64-4.69 (m, 3H, Gal-H1, H-1"), 4.93-4.99 (m, 2H, Fuc-H1, -H5), 5.42 (dd, *J* = 8.2, 9.6 Hz, 1H, Gal-H2), 7.22 (s, 1H, Ind-H2), 7.41-7.48 (m, 3H, Ind-H7, C_6H_5), 7.54 (m, 1H, C_6H_5), 7.60 (s, 1H, H-4'), 7.99-8.05 (m, 3H, Ind-H6, C_6H_5), 8.09 (s, 1H, NH), 8.30 (d, *J* = 2.2 Hz, 1H, Ind-H4); ^{13}C NMR (125 MHz, CD_3OD): $δ$ = 16.71 (Fuc-C6), 19.24 (Me), 26.47, 26.53, 26.70 (2 Cy, C-2'), 27.12, 27.26 (Cy, C-2"), 33.14, 34.18, 35.04 (3 Cy), 35.29 (C-2), 37.43 (C-6), 39.31 (C-5), 39.96 (C-1'), 42.77 (Lac-C3), 43.22 (C-1), 52.34 (C-1"), 62.76 (Gal-C6), 67.71, 67.77 (Gal-C4, Fuc-C5), 70.32 (Fuc-C2), 71.42 (Fuc-C3), 73.02 (Gal-C2), 73.96 (Fuc-C4), 75.97 (Gal-C5), 78.06 (Lac-C2), 79.83 (C-3), 83.01 (C-4), 83.67 (Gal-C3), 100.42 (Fuc-C1), 100.53 (Gal-C1), 112.58 (Ind-C7), 114.82 (Ind-C3), 116.36 (Ind-C4), 117.99 (Ind-C6), 124.01 (C-4'), 127.93, 127.95 (Ind-C2, -C9), 129.73, 130.88, 131.55, 134.37 (6C, C_6H_5), 140.99 (Ind-

C8), 142.53 (Ind-C5), 146.19 (C-3'), 166.83 (COPh), 176.99 (CONH), 178.96 (COOH); IR (KBr): v = 3431 (vs, OH), 2927 (m), 2852 (w), 1721 (m, C=O), 1647 (m, C=O), 1545 (w), 1522 (w), 1471 (w), 1450 (w), 1380 (w), 1334 (s, NO$_2$), 1272 (m), 1221 (w), 1163 (w), 1097 (s), 1079 (s), 1029 (m), 999 (w), 963 (vw), 809 (vw), 785 (vw), 741 (vw), 712 (w), 678 (w) cm^{-1}; HR-MS: m/z: calcd for C$_{50}$H$_{66}$N$_6$O$_{17}$ [M+Na]$^+$: 1045.4377; found: 1045.4375.

(1R,3R,4R,5S)-3-[2-O-Benzoyl-3-O-((1S)-1-carboxy-2-cyclohexyl-ethyl)-(β-D-galactopyranosyl)oxy]-4-[(α-L-fucopyranosyl)oxy]-5-methyl-N-(3-{1-[2-(6-nitro-1H-indol-3-yl)ethyl]-1H-1,2,3-triazol-4-yl}propyl)cyclohexanecarboxamide (49). Prepared according to general procedure C from **26c** (14.5 mg, 18.0 μmol), **32b** (6.3 mg, 27.2 μmol), Na-L-ascorbate (90 μL, 9.0 μmol) and CuSO$_4$·5 H$_2$O (45 μL, 4.5 μmol). Yield: 10.3 mg (55%). [α]$_D^{20}$ -32.3 (c 0.31, MeOH); ^{1}H NMR (500 MHz, CD$_3$OD): δ = 0.46-0.71 (m, 4H, 4 Cy), 0.88 (m, 1H, Cy), 1.11 (d, J = 6.5 Hz, 3H, Me), 1.14-1.37 (m, 10H, H-2a, H-6a, 5 Cy, Fuc-H6), 1.41 (m, 1H, Lac-H3a), 1.45-1.56 (m, 2H, Lac-H3b, Cy), 1.60 (m, 1H, H-6b), 1.62-1.74 (m, 3H, H-5, H-2'), 2.15 (m, 1H, H-2b), 2.25 (m, 1H, H-1), 2.53-2.64 (m, 2H, H-3'), 2.95-3.11 (m, 2H, H-1'), 3.15 (t, J = 9.4 Hz, 1H, H-4), 3.41 (t, J = 6.5 Hz, 2H, H-2''), 3.55-3.65 (m, 2H, Gal-H3, -H5), 3.66-3.83 (m, 5H, H-3, Fuc-H2, -H4, Gal-H6), 3.87 (dd, J = 2.8, 10.3 Hz, 1H, Fuc-H3), 3.90-4.04 (m, 2H, Gal-H4 Lac-H2), 4.61-4.74 (m, 3H, Gal-H1, H-1''), 4.95-5.01 (m, 2H, Fuc-H1, -H5), 5.43 (m, 1H, Gal-H2), 7.23 (s, 1H, Ind-H2,), 7.35-7.45 (m, 3H, Ind-H7, C$_6$H$_5$), 7.51 (m, 1H, C$_6$H$_5$), 7.58 (s, 1H, H-5'), 7.99-8.05 (m, 3H, Ind-H6, C$_6$H$_5$), 8.23 (d, J = 2.1 Hz, 1H, Ind-H4); ^{13}C NMR (125 MHz, CD$_3$OD): δ = 16.72 (Fuc-C6), 19.28 (Me), 23.50 (C-3'), 26.50, 26.71 (2 Cy), 27.09 (C-2''), 27.28 (Cy), 30.12 (C-2'), 33.12, 34.38, 35.13 (3 Cy), 35.41 (C-2), 37.45 (C-6), 39.34, 39.40 (C-1', C-5), 43.33 (2C, Lac-C3, C-1), 52.54 (C-1''), 62.88 (Gal-C5), 67.73 (2C, Fuc-C5, Gal-C4), 70.33 (Fuc-C2), 71.41 (Fuc-C3), 73.08 (Gal-C2), 73.97 (Fuc-C4), 76.26 (Lac-C2), 79.84 (C-3), 83.03 (C-4), 83.70 (Gal-C3), 100.43 (Fuc-C1), 100.59 (Gal-C1), 112.55 (Ind-C7), 114.91 (Ind-C3), 116.35 (Ind-C4), 117.93 (Ind-C6), 123.98 (C-5'), 127.99 (2C, Ind-C2, -C9), 129.66, 130.85, 131.59, 134.27 (6C, C$_6$H$_5$), 140.96 (Ind-C8), 142.49 (Ind-C5), 148.09 (C-4'), 166.82 (COPh), 177.03 (CONH); IR (KBr): v = 3434 (vs, OH), 2926 (m), 282 (w), 1720 (w, C=O), 1631 (m, C=O), 1547 (w), 1520 (w), 1468 (w), 1449 (w), 1380 (w), 1333 (m, NO$_2$), 1268 (m), 1169 (w), 1161 (w), 1097 (m), 1074 (m), 1032 (m), 999 (w), 712 (w) cm^{-1}; HR-MS: m/z: calcd for C$_{51}$H$_{68}$N$_6$O$_{17}$ [M+Na]$^+$: 1059.4533; found: 1059.4528.

(1R,3R,4R,5S)-3-[2-O-Benzoyl-3-O-((1S)-1-carboxy-2-cyclohexyl-ethyl)-(β-D-galactopyranosyl)oxy]-4-[(α-L-fucopyranosyl)oxy]-5-methyl-N-({1-[3-(6-nitro-1H-indol-3-yl)propyl]-1H-1,2,3-triazol-4-yl}methyl)cyclohexanecarboxamide (50). Prepared according to general procedure C from **26a** (14.4 mg, 11.8 μmol), **32c** (6.8 mg, 27.7 μmol), Na-L-ascorbate (186 μL, 18.6 μmol) and CuSO$_4$·5 H$_2$O (92 μL, 9.2 μmol). Yield: 12.9 mg (68%). [α]$_D^{20}$ -54.1 (c 0.3, MeOH); ^{1}H NMR (500 MHz, CD$_3$OD): δ = 0.47-0.71 (m, 4H, 4 Cy), 0.88 (m, 1H, Cy), 1.09 (d, J = 6.4 Hz, 3H, Me), 1.12-1.44 (m, 11 H, H-2a, H-6a, 5 Cy, Lac-H3a), 1.49 (m, 1H, Lac-H3b), 1.52-1.70 (m, 4H, 2 Cy, H-6b, H-5), 2.16 (m, 1H, H-2b), 2.26-2.36 (m, 3H, H-1, H-2"), 2.82 (t, J = 7.5 Hz, 2H, H-3"), 3.13 (t, J = 9.5 Hz, 1H, H-4), 3.53-3.58 (m, 2H, Gal-H3, -H5), 3.65-3.81 (m, 5H, H-3, Fuc-H2, -H4, Gal-H6), 3.84-3.90 (m, 2H, Fuc-H3, Gal-H4), 3.94 (s, 1H, Lac-H2), 4.31-4.41 (m, 2H, H-1'), 4.46 (t, J = 6.8 Hz, 2H, H-1"), 4.65 (d, J = 8.1 Hz, 1H, Gal-H1), 4.93-4.98 (m, 2H, Fuc-H1, -H5), 5.41 (dd, J = 8.5, 9.3 Hz, 1H, Gal-H2), 7.30 (s, 1H, Ind-H2), 7.38-7.44 (m, 2H, C$_6$H$_5$), 7.46 (d, J = 9.0 Hz, 1H, Ind-H7), 7.55 (m, 1H, C$_6$H$_5$), 7.82 (s, 1H, H-3'), 7.98-8.02 (m, 2H, C$_6$H$_5$), 8.04 (dd, J = 2.2, 9.0 Hz, 1H, Ind-H6), 8.47 (d, J = 2.1 Hz, 1H, Ind-H4); ^{13}C NMR (125 MHz, CD$_3$OD): δ = 16.72 (Fuc-C6), 19.24 (Me), 22.56 (C3"), 26.53, 26.74, 27.33 (3 Cy), 31.89 (C-2"), 33.10, 34.29 (3C, 3 Cy), 35.14, 35.20 (Cy, C-2), 35.63 (C-1'), 37.49 (C-6), 39.33 (C-5), 43.04 (Lac-C3), 43.14 (C-1), 50.86 (C-1"), 62.92 (Gal-C6), 67.71, 67.74 (Gal-C4, Fuc-C5), 70.33 (Fuc-C2), 71.40 (Fuc-C3), 72.99 (Gal-C2), 73.96 (Fuc-C4), 76.01 (Gal-C5), 79.76 (C-3), 83.02 (C-4), 83.76 (Gal-C3), 100.41 (Fuc-C1), 100.55 (Gal-C1), 112.53 (Ind-C7), 116.55 (Ind-C4), 117.68 (Ind-C3), 117.93 (Ind-C6), 124.35 (C-3'), 127.11 (Ind-C2), 127.95 (Ind-C9), 129.66, 130.87, 131.65, 134.24 (6C, C$_6$H$_5$), 141.25 (Ind-C8), 142.29 (Ind-C5), 166.84 (COPh), 176.98 (CONH); IR (KBr): v = 3433 (vs, OH), 2925 (m), 2852 (w), 1722 (m, C=O), 1631 (m, C=O), 1520 (w), 1468 (w), 1451 (w), 1383 (w), 1333 (m, NO$_2$), 1270 (m), 1210 (w), 1163 (w), 1108 (m), 1074 (m), 1029 (m), 966 (vw), 892 (vw), 807 (vw), 776 (vw), 738 (vw), 712 (w), 672 (vw) cm^{-1}; HR-MS: m/z: calcd for C$_{50}$H$_{66}$N$_6$O$_{17}$ [M+Na]$^+$: 1045.4377; found: 1045.4381.

(1R,3R,4R,5S)-3-[2-O-Benzoyl-3-O-((1S)-1-carboxy-2-cyclohexyl-ethyl)-(β-D-galactopyranosyl)oxy]-4-[(α-L-fucopyranosyl)oxy]-5-methyl-N-(2-{1-[3-(6-nitro-1H-indol-3-yl)propyl]-1H-1,2,3-triazol-4-yl}ethyl)cyclohexanecarboxamide (51). Prepared according to general procedure C from **26b** (15.8 mg, 20.0 μmol), **32c** (6.9 mg, 28.1 μmol), Na-L-ascorbate (100 μL, 10.0 μmol) and CuSO$_4$·5 H$_2$O (50 μL, 5.0 μmol). Yield: 14.1 mg

(68%). $[\alpha]_D^{20}$ -59.7 (*c* 1.22, MeOH); ^{1}H NMR (500 MHz, CD$_3$OD): δ = 0.50-0.72 (m, 4H, 4 Cy), 0.89 (m, 1H, Cy), 1.00 (d, *J* = 6.5 Hz, 3H, Me), 1.04-1.25 (m, 3H, H-2a, H-6a, Cy), 1.26-1.36 (m, 7H, 4 Cy, Fuc-H6), 1.40 (m, 1H, Lac-H3a), 1.45-1.62 (m, 4H, Lac-H3b, Cy, H-6b, H-5), 2.12 (m, 1H, H-2b), 2.20 (tt, *J* = 3.2, 12.7 Hz, 1H, H-1), 2.24-2.34 (m, 2H, H-2"), 2.77-2.85 (m, 4H, H-2', H-3"), 3.06 (t, *J* = 9.6 Hz, 1H, H-4), 3.39 (t, *J* = 7.0 Hz, 2H, H-1'), 3.52 (t, *J* = 6.0 Hz, 1H, Gal-H5), 3.59 (dd, *J* = 2.8, 9.7 Hz, 1H, Gal-H3), 3.64 (ddd, *J* = 4.6, 9.1, 11.6 Hz, 1H, H-3), 3.69-3.81 (m, 4H, Fuc-H2, -H4, Gal-H6), 3.85 (dd, *J* = 3.3, 10.3 Hz, 1H, Fuc-H3), 3.93 (d, *J* = 2.1 Hz, 1H, Gal-H4), 3.98 (dd, *J* = 2.5, 9.6 Hz, 1H, Lac-H2), 4.36-4.47 (m, 2H, H-1"), 4.64 (d, *J* = 8.1 Hz, 1H, Gal-H1), 4.92 (m, 1H, Fuc-H1), 4.96 (q, *J* = 6.4 Hz, 1H, Fuc-H5), 5.42 (dd, *J* = 8.2, 9.6 Hz, 1H, Gal-H2), 7.30 (s, 1H, Ind-H2), 7.43-7.50 (m, 3H, Ind-H7, C$_6$H$_5$), 7.58 (m, 1H, C$_6$H$_5$), 7.70 (s, 1H, H-4'), 8.01-8.09 (m, 3H, C$_6$H$_5$, Ind-H6), 8.49 (d, *J* = 2.1 Hz, 1H, Ind-H4); ^{13}C NMR (125 MHz, CD$_3$OD): δ = 16.73 (Fuc-C6), 19.17 (Me), 22.58 (C-3"), 26.53, 26.55, 26.71 (2 Cy, C-2'), 27.29 (Cy), 31.85 (C-2"), 33.12, 34.24, 35.12 (3 Cy), 35.30 (C-2), 37.43 (C-6), 39.25 (C-5), 39.87 (C-1'), 42.95 (Lac-C3), 43.17 (C-1), 50.75 (C-1"), 62.84 (Gal-C6), 67.72, 67.73 (Gal-C4, Fuc-C5), 70.31 (Fuc-C2), 71.41 (Fuc-C3), 73.03 (Gal-C2), 73.95 (Fuc-C4), 75.97 (Gal-C5), 78.36 (Lac-C2), 79.77 (C-3), 83.01 (C-4), 83.72 (Gal-C3), 100.39 (Fuc-C1), 100.54 (Gal-C1), 112.53 (Ind-C7), 116.59 (Ind-C4), 117.69 (Ind-C3), 117.93 (Ind-C6), 123.79 (C-4'), 127.12 (Ind-C2), 127.94 (Ind-C9), 129.74, 130.91, 131.63, 134.36 (6C, C$_6$H$_5$), 141.23 (Ind-C8), 142.30 (Ind-C5), 146.29 (C-3'), 166.84 (*C*OPh), 177.00 (CONH); IR (KBr): v = 3430 (vs, OH), 2927 (m), 2852 (w), 1720 (m, C=O), 1647 (m, C=O), 1547 (w), 1520 (w), 1471 (w), 1450 (w), 1333 (s, NO$_2$), 1272 (m), 1221 (w), 1163 (w), 1097 (s), 1078 (s), 1029 (m), 999 (w), 966 (vw), 809 (vw), 778 (vw), 738 (vw), 712 (w), 678 (vw) cm^{-1}; HR-MS: *m/z*: calcd for C$_{51}$H$_{68}$N$_6$O$_{17}$ [M+H]$^+$: 1037.4714; found: 1037.4714.

(1*R*,3*R*,4*R*,5*S*)-3-[2-*O*-Benzoyl-3-*O*-((1*S*)-1-carboxy-2-cyclohexyl-ethyl)-(β-D-galactopyranosyl)oxy]-4-[(α-L-fucopyranosyl)oxy]-5-methyl-*N*-(3-{1-[3-(6-nitro-1*H*-indol-3-yl)propyl]-1*H*-1,2,3-triazol-4-yl}propyl)cyclohexanecarboxamide (52). Prepared according to general procedure C from **26c** (11.6 mg, 14.4 µmol), **32c** (5.3 mg, 21.6 µmol), Na-L-ascorbate (72 µL, 7.2 µmol) and CuSO$_4$·5 H$_2$O (36 µL, 3.6 µmol). Yield: 9.5 mg (63%). $[\alpha]_D^{20}$ -47.6 (*c* 0.87, MeOH); ^{1}H NMR (500 MHz, CD$_3$OD): δ = 0.46-0.67 (m, 4H, 4 Cy), 0.85 (m, 1H, Cy), 1.10 (d, *J* = 6.4 Hz, 3H, Me), 1.13-1.44 (m, 11H, H-2a, H-6a, 5 Cy, Fuc-H6, Lac-H3a), 1.50 (m, 1H, Lac-H3b), 1.58 (m, 1H, H-6b), 1.66 (m, 1H, H-5), 1.75-1.84

(m, 2H, H-2'), 2.15 (m, 1H, H-2b), 2.25 (dd, J = 3.5, 13.0 Hz, 1H, H-1), 2.29-2.39 (m, 2H, H-2''), 2.66-2.72 (m, 2H, H-3'), 2.82 (t, J = 7.4 Hz, 2H, H-3''), 3.06-3.23 (m, 3H, H-1', H-4), 3.55-3.65 (m, 2H, Gal-H3, -H5), 3.65-3.84 (m, 5H, H-3, Fuc-H2, -H4, Gal-H6), 3.87 (dd, J = 3.2, 10.3 Hz, 1H, Fuc-H3), 3.96 (s, 2H, Lac-H2, Gal-H4), 4.45 (t, J = 6.8 Hz, 2H, H-1''), 4.69 (d, J = 8.0 Hz, 1H, Gal-H1), 4.92-5.03 (m, 2H, Fuc-H1, -H5), 5.42 (m, 1H, Gal-H2), 7.30 (s, 1H, Ind-H2), 7.34-7.38 (m, 2H, C_6H_5), 7.45 (d, J = 9.0 Hz, 1H, Ind-H7), 7.50 (m, 1H, C_6H_5), 7.74 (s, 1H, H-5'), 7.98-8.02 (m, 2H, C_6H_5), 8.04 (dd, J = 2.1, 9.0 Hz, 1H, Ind-H6), 8.47 (m, 1H, Ind-H4); ^{13}C NMR (125 MHz, CD$_3$OD): δ = 16.72 (Fuc-C6), 19.25 (Me), 22.55 (C-3''), 23.63 (C-3'), 26.46, 26.67, 27.25 (3 Cy), 30.31 (C-2'), 31.86 (C-2''), 33.08, 34.19, 35.07 (3 Cy), 35.47 (C-2), 37.41 (C-6), 39.32 (C-5), 39.54 (C-1'), 42.88 (Lac-C3), 43.36 (C-1), 50.80 (C-1''), 62.82 (Gal-C6), 67.71, 67.73 (Gal-C4, Fuc-C5), 70.34 (Fuc-C2), 71.42 (Fuc-C3), 72.99 (Gal-C2), 73.97 (Fuc-C4), 75.99 (Gal-C5), 78.69 (Lac-C2), 79.89 (C-3), 83.03 (C-4), 83.70 (Gal-C3), 100.44 (Fuc-C1), 100.58 (Gal-C1), 112.51 (Ind-C7), 116.55 (Ind-C4), 117.69 (Ind-C3), 117.89 (Ind-C6), 123.54 (C-5'), 127.11 (Ind-C2), 127.96 (Ind-C9), 129.64, 130.83, 131.55, 134.27 (6C, C_6H_5), 141.22 (Ind-C8), 142.25 (Ind-C5), 148.53 (C-4'), 166.79 (COPh), 177.05 (CONH); IR (KBr): v = 3431 (vs, OH), 2927 (m), 2852 (w), 1720 (s, C=O), 1631 (m, C=O), 1547 (w), 1517 (w), 1471 (w), 1450 (w), 1383 (w), 1332 (s, NO$_2$), 1270 (m), 1213 (w), 1166 (w), 1106 (s), 1073 (s), 1032 (m), 996 (w), 963 (vw), 807 (vw), 774 (vw), 741 (vw), 712 (w), 669 (vw) cm^{-1}; HR-MS: m/z: calcd for C$_{52}$H$_{70}$N$_6$O$_{17}$ [M+H]$^+$: 1051.4870; found: 1051.4870.

***tert*-Butyl *N*-[1-(3-bromopropyl)-1*H*-indol-5-yl]carbamate (53).** Nitroindole **27c** (700 mg, 2.50 mmol) and PtO$_2$ (35 mg, 5% w/w) were suspended in a solution of Boc$_2$O (1.76 g, 8.06 mmol) in EtOH (23 mL) under argon. The flask was flushed with H$_2$, and the solution was stirred under H$_2$ (1 atm) at rt for 45 min. Then another 35 mg of PtO$_2$ was added and stirring was continued for 30 min. The mixture was filtrated (PTFE membrane filter) and the solvent was removed *in vacuo*. The residue was dissolved in EtOAc (100 mL) and washed with 0.5 M aq. HCl (50 mL), satd aq. NaHCO$_3$ (50 mL) and brine (50 mL). The organic layer was dried over Na$_2$SO$_4$, and the solvent was removed under reduced pressure. After purification by silica gel chromatography (petroleum ether/EtOAc), **53** (637 mg, 72%) was obtained as a pale yellow oil, which eventually crystallized and turned pink after 24 h at -18 °C. ^{1}H NMR (500 MHz, CD$_3$OD): δ = 1.50 (s, 9H, C(CH$_3$)$_3$), 2.28 (p, J = 6.4 Hz, 2H, H-2'), 3.28 (m, 2H, H-3'), 4.27 (t, J = 6.5 Hz, 2H, H-1'), 6.35 (dd, J = 0.6, 3.1 Hz, 1H, H-3), 7.10 (dd, J = 1.3,

8.7 Hz, 1H, H-6), 7.16 (d, J = 3.1 Hz, 1H, H-2), 7.30 (d, J = 8.8 Hz, 1H, H-7), 7.57 (bs, 1H, H-4); ^{13}C NMR (125 MHz, CD$_3$OD): δ = 28.80 (C(*CH$_3$*)$_3$), 31.16 (C-3'), 34.31 (C-2'), 45.05 (C-1'), 80.44 (*C*(CH$_3$)$_3$), 102.08 (H-3), 110.37 (C-7), 112.84 (C-6), 116.67 (C-4), 129.81 (C-2), 130.26 (C-9), 132.41 (C-8), 134.36 (C-5), 156.27 (CO); IR (KBr): ν = 2972 (w) 2932 (w), 1695 (vs, C=O), 1625 (vw), 1584 (m), 1532 (s), 1509 (m), 1490 (s), 1447 (m), 1441 (m), 1392 (m), 1367 (s), 1334 (m), 1312 (vw), 1295 (m), 1287 (m), 1261 (m), 1232 (s), 1163 (vs), 1092 (vw), 1053 (m), 1027 (vw), 889 (vw), 863 (vw), 825 (vw), 802 (vw), 756 (w), 726 (w), 623 (vw), 563 (vw) cm^{-1}; elemental analysis: calcd (%) for C$_{16}$H$_{21}$BrN$_2$O$_2$ (353.25): C 54.40, H 5.99, N 7.93; found: C 54.29, H 5.97, N 7.86.

tert-Butyl *N*-[1-(3-azidopropyl)-1*H*-indol-5-yl]carbamate (54). To a solution of **53** (570 mg, 1.61 mmol) in anhydrous DMF (15 mL), NaN$_3$ (528 mg, 8.12 mmol) was added at rt. After 2 h, H$_2$O (50 mL) was added to the reaction mixture, and the aqueous layer was extracted with EtOAc (100 mL). The organic layer was washed with satd aq NaHCO$_3$ and brine, and dried over Na$_2$SO$_4$. After removal of the solvent under reduced pressure, the crude product was purified by silica gel chromatography (petroleum ether/EtOAc) to afford **54** (458 mg, 90%) as yellowish crystals. ^{1}H NMR (500 MHz, CD$_3$OD): δ = 1.52 (s, 9H, C(CH$_3$)$_3$), 2.02 (p, J = 6.6 Hz, 2H, H-2'), 3.22 (t, J = 6.5 Hz, 2H, H-3'), 4.22 (t, J = 6.7 Hz, 2H, H-1'), 6.37 (d, J = 3.1 Hz, 1H, H-3), 7.13 (dd, J = 1.4, 8.7 Hz, 1H, H-6), 7.16 (d, J = 3.0 Hz, 1H, H-2), 7.30 (d, J = 8.8 Hz, 1H, H-7), 7.59 (bs, 1H, H-4); ^{13}C NMR (125 MHz, CD$_3$OD): δ = 28.80 (C(*CH$_3$*)$_3$), 30.51 (C-2'), 44.02 (C-1'), 49.54 (C-3'), 80.40 (*C*(CH$_3$)$_3$), 102.01 (H-3), 110.27 (C-7), 112.79 (C-6), 116.63 (C-4), 129.72 (C-2), 130.20 (C-9), 132.32 (C-8), 134.38 (C-5), 156.24 (CO); IR (KBr): ν = 2976 (w), 2930 (w), 2873 (vw), 2099 (vs, N$_3$), 1697 (s, C=O), 1625 (vw), 1584 (w), 1529 (m), 1510 (m), 1489 (s), 1450 (m), 1440 (m), 1392 (w), 1366 (m), 1334 (w), 1286 (m), 1236 (m), 1159 (s), 1096 (vw), 1085 (vw), 1051 (w), 1051 (m), 1026 (w) cm^{-1}; elemental analysis: calcd (%) for C$_{16}$H$_{21}$N$_5$O$_2$ (315.37): C 60.94, H 6.71, N 22.21; found: C 61.04, H 6.70, N 22.17.

1-(3-Azidopropyl)-1*H*-indol-5-amine (55). A solution of **54** (408 mg, 1.29 mmol) in DCM (40 mL) was treated with trifluoroacetic acid (3 mL) at rt for 30 min. Then, the solvent was removed *in vacuo*, and the mixture was co-evaporated with toluene. The residue was dissolved in EtOAc (50 mL), the organic layer was washed with satd aq. NaHCO$_3$ and brine

(30 mL), and the aqueous layers were extracted with EtOAc (50 mL). The combined organic phases were dried over Na_2SO_4 and concentrated under reduced pressure. The residue was purified by silica gel chromatography (DCM/MeOH, 10:1) to give **55** (239 mg, 86%) as a mixture with inseparable by-products. ^{1}H NMR (500 MHz, CD_3OD): δ = 1.93-1.99 (m, 3H, H-2'), 3.15 (t, J = 6.4 Hz, 3H, H-3'), 4.08 (t, J = 6.6 Hz, 2H, H-1'), 6.24 (d, J = 3.0 Hz, 1H, H-3), 6.62 (dd, J = 2.1, 8.6 Hz, 1H, H-6), 6.86 (d, J = 1.9 Hz, 1H, H-4), 6.92 (d, J = 3.0 Hz, 1H, H-2), 7.07 (d, J = 8.6 Hz, 1H, H-7).

N-[1-(3-Azidopropyl)-1H-indol-5-yl]acetamide (56). To a solution of **55** (43 mg, 0.200 mmol) in DCM (2 mL) were added Et_3N (28 μL, 0.200 mmol) and Ac_2O (18 μL, 0.200 mmol), and the solution was stirred for 3 h. The solvents were removed *in vacuo* and the residue was purified by silica gel chromatography (DCM/EtOAc) to give **56** (44 mg, 86%) as a mixture with inseparable by-products. ^{1}H NMR (500 MHz, $CDCl_3$): δ = 1.92-1.96 (m, 2H, H-2'), 2.07 (s, 3H, Ac), 3.12 (t, J = 6.3 Hz, 2H, H-3'), 4.09 (t, J = 6.6 Hz, 2H, H-1'), 6.35 (d, J = 3.1 Hz, 1H, H-3), 6.98 (d, J = 3.1 Hz, 1H, H-2), 7.14-7.16 (m, 2H, H-6, H-7), 7.70 (s, 1H, H-4); ^{13}C NMR (125 MHz, $CDCl_3$): δ = 24.38 (Ac), 29.35 (C-2'), 43.14 (C-1'), 48.33 (C-3'), 101.72 (C-3), 109.33 (C-7), 113.41 (C-4), 116.48 (C-6), 128.71, 128.72 (C-2, C-9), 130.38 (C-8), 133.42 (C-5), 168.85 (CO); ESI-MS: m/z: calcd for $C_{13}H_{15}N_5O$ [M+Na][+]: 280.12; found: 280.20.

(1R,3R,4R,5S)-3-[2-O-Benzoyl-3-O-((1S)-1-carboxy-2-cyclohexyl-ethyl)-(β-D-galactopyranosyl)oxy]-4-[(α-L-fucopyranosyl)oxy]-5-methyl-N-(3-{1-[3-(5-acetamido-1H-indol-1-yl)propyl]-1H-1,2,3-triazol-4-yl}propyl)cyclohexanecarboxamide (57). Prepared according to general procedure C from **26c** (11.6 mg, 14.4 μmol), **56** (13 mg, 22.3 μmol), Na-L-ascorbate (72 μL, 7.2 μmol) and $CuSO_4·5 H_2O$ (36 μL, 3.6 μmol). Yield: 11.0 mg (73%). $[\alpha]_D^{20}$ -49.4 (c 0.83, MeOH); ^{1}H NMR (500 MHz, CD_3OD): δ = 0.52 (m, 1H, Cy), 0.57-0.70 (m, 3H, 3 Cy), 0.88 (m, 1H, Cy), 1.10 (d, J = 6.4 Hz, 3H, Me), 1.13-1.36 (m, 8H, H-2a, H-6a, 5 Cy, Fuc-H6), 1.40 (m, 1H, Lac-H3a), 1.48 (m, 1H, Lac-H3b), 1.51-1.61 (m, 2H, H-6b, Cy), 1.66 (m, 1H, H-5), 1.73-1.80 (m, 2H, H-2'), 2.10-2.15 (m, 4H, H-2b, Ac), 2.25 (m, 1H, H-1), 2.42 (p, J = 6.7 Hz, 2H, H-2''), 2.65 (t, J = 7.5 Hz, 2H, H-3'), 3.06-3.18 (m, 3H, H-1', H-4), 3.55 (m, 1H, Gal-H5), 3.60 (dd, J = 2.8, 9.7 Hz, 1H, Gal-H3), 3.65-3.81 (m, 5H, H-3, Fuc-H2, -H4, Gal-H6), 3.86 (dd, J = 3.2, 10.3 Hz, 1H, Fuc-H3), 3.94 (d, J = 2.1

Hz, 1H, Gal-H4), 4.00 (dd, J = 2.3, 9.6 Hz, 1H, Lac-H2), 4.20 (t, J = 6.7 Hz, 2H, H-3"), 4.32 (t, J = 6.8 Hz, 2H, H-1"), 4.67 (d, J = 8.0 Hz, 1H, Gal-H1), 4.94-5.01 (m, 2H, Fuc-H1, -H5), 5.42 (m, 1H, Gal-H2), 6.42 (m, 1H, Ind-H3), 7.18-7.28 (m, 3H, Ind-H2, -H6, -H7), 7.33-7.41, 7.47-7.52 (m, 3H, C$_6$H$_5$), 7.60 (s, 1H, H-5'), 7.77 (m, 1H, Ind-H4), 7.99-8.03 (m, 2H, C$_6$H$_5$); ^{13}C NMR (125 MHz, CD$_3$OD): δ = 16.74 (Fuc-C6), 19.25 (Me), 23.54 (Ac), 23.67 (C-3'), 26.50, 26.68, 27.25 (3 Cy), 30.23 (C-2'), 31.61 (C-2"), 33.07, 34.14, 35.05 (3 Cy), 35.43 (C-2), 37.43 (C-6), 39.33, 39.47 (C-5, C-1'), 42.81 (Lac-C3), 43.30 (C-1), 44.14 (C-3"), 48.66 (C-1"), 62.76 (Gal-C6), 67.70 (2C, Gal-C4, Fuc-C5), 70.28 (Fuc-C2), 71.39 (Fuc-C3), 72.95 (Gal-C2), 73.96 (Fuc-C4), 75.95 (Gal-C5), 78.15 (Lac-C2), 79.80 (C-3), 83.03 (C-4), 83.65 (Gal-C3), 100.47 (Fuc-C1), 100.50 (Gal-C1), 102.48 (Ind-C3), 110.34 (Ind-C7), 114.12 (Ind-C4), 117.20 (Ind-C6), 123.59 (C-5'), 129.68 (2C, C$_6$H$_5$), 129.97 (Ind-C9), 130.11 (Ind-C2), 130.83 (2C, C$_6$H$_5$), 131.52, 131.94 (Ind-C5, C$_6$H$_5$), 134.32 (C$_6$H$_5$), 134.78 (Ind-C8), 147.95 (C-4'), 166.76 (*C*OPh), 171.50 (*C*OCH$_3$), 177.04 (*C*ONH), 178.70 (*C*OOH); IR (KBr): v = 3422 (vs, OH), 2927 (s), 2853 (m), 1725 (s, C=O), 1651 (s, C=O), 1603 (m), 1587 (m), 1548 (m), 1488 (m), 1450 (m), 1401 (w), 1373 (m), 1337 (m), 1316 (m), 1271 (vs), 1113 (vs), 1076 (vs), 1033 (s), 1000 (w), 874 (vw), 804 (w), 762 (w), 762 (w), 713 (m), 675 (w) cm^{-1}; HR-MS: *m/z*: calcd for C$_{54}$H$_{74}$N$_6$O$_{16}$ [M+H]$^+$: 1063.5234; found: 1063.5234.

(1*R*,3*R*,4*R*,5*S*)-3-[2-*O*-Benzoyl-3-*O*-((1*S*)-1-carboxy-2-cyclohexyl-ethyl)-(β-D-galactopyranosyl)oxy]-4-[(α-L-fucopyranosyl)oxy]-5-methyl-*N*-(3-{1-[3-(5-amino-1*H*-indol-1-yl)propyl]-1*H*-1,2,3-triazol-4-yl}propyl)cyclohexanecarboxamide (58). A mixture of nitroindole **43** (8.5 mg, 8.1 µmol), PtO$_2$ (2 mg, cat.) and morpholine (5 µL) in MeOH was stirred at rt under an H$_2$ atmosphere (1 atm). Completion of the reaction was indicated by discoloration of the solution and confirmed by MS after 30 min. The catalyst was removed via filtration through a PTFE membrane filter, and the solution was concentrated *in vacuo*. Purification by preparative HPLC-MS (H$_2$O/MeCN + 0.1% HCO$_2$H) gave **58** (4.5 mg, 54%) as a colorless solid. [α]$_D^{20}$ -59.1 (*c* 0.45, MeOH); ^{1}H NMR (500 MHz, CD$_3$OD): δ = 0.39-0.65 (m, 4H, 4 Cy), 0.82 (m, 1H, Cy), 1.04 (d, J = 5.8 Hz, 3H, Me), 1.09-1.36 (m, 11H, H-2a, H-6a, 5 Cy, Fuc-H6, Lac-H3a), 1.43 (t, J = 11.9 Hz, 1H, Lac-H3b), 1.47-1.55 (m, 2H, H-6b, Cy), 1.60 (m, 1H, H-5), 1.70-1.78 (m, 2H, H-2'), 2.09 (m, 1H, H-2), 2.19 (t, J = 11.8 Hz, 1H, H-1), 2.35-2.44 (m, 2H, H-2"), 2.62 (t, J = 7.0 Hz, 2H, H-3'), 3.02-3.16 (m, 3H, H-1', H-4), 3.47-3.54 (m, 2H, Gal-H3, -H5), 3.60-3.80 (m, 6H, H-3, Fuc-H2, -H4, Gal-H6, Lac-H2), 3.83 (m, 1H, Fuc-H3), 3.89 (s, 1H, Gal-H4), 4.20 (t, J = 6.5 Hz, 2H, H-3"), 4.30 (t, J = 6.3 Hz, 2H,

H-1"), 4.62 (d, J = 8.1 Hz, 1H, Gal-H1), 4.89-4.97 (m, 2H, Fuc-H1, -H5), 5.37 (t, J = 8.7 Hz, 1H, Gal-H2), 6.41 (s, 1H, Ind-H3), 6.95 (m, 1H, Ind-H6), 7.27 (s, 1H, Ind-H2), 7.29-7.37 (m, 4H, C_6H_5, Ind-H4, -H7), 7.44 (t, J = 7.1 Hz, 1H, C_6H_5), 7.60 (s, 1H, H-5'), 7.97 (d, J = 7.5 Hz, 2H, C_6H_5); ^{13}C NMR (125 MHz, CD_3OD): δ = 16.75 (Fuc-C6), 19.26 (Me), 23.54 (C-3'), 26.53, 26.77, 27.34 (3 Cy), 30.15 (C-2'), 31.60 (C-2"), 33.05, 34.33, 35.26 (3 Cy), 35.50 (C-2), 37.39 (C-6), 39.26 (C-5), 39.41 (C-1'), 43.27 (2C, Lac-C3, C-1), 44.28 (C-3"), 48.66 (C-1"), 63.02 (Gal-C6), 67.70, 67.78 (Gal-C4, Fuc-C5), 70.28 (Fuc-C2), 71.36 (Fuc-C3), 73.07 (Gal-C2), 73.94 (Fuc-C4), 76.10 (Gal-C5), 79.74 (C-3), 79.89 (Lac-C2), 83.02 (C-4), 83.66 (Gal-C3), 100.46 (Fuc-C1), 100.62 (Gal-C1), 102.22 (Ind-C3), 111.54 (Ind-C4), 112.92 (Ind-C6), 115.87 (Ind-C7), 123.58 (C-5'), 129.63 (2C, C_6H_5), 130.84, 130.87 (C_6H_5, Ind-H2), 131.68 (Ind-C8), 134.19 (C_6H_5), 135.30 (Ind-C5), 148.45 (C-4'), 166.78 (COPh), 177.05 (CONH), 181.91 (COOH); IR (KBr): v = 3431 (vs, OH), 2926 (m), 2853 (w), 1722 (w), 1643 (m), 1603 (m), 1584 (m), 1555 (w), 1492 (w), 1451 (w), 1406 (w), 1384 (w), 1365 (w), 1348 (w), 1316 (w), 1273 (m), 1222 (vw), 1167 (w), 1118 (m), 1096 (m), 1079 (s), 1031 (m), 1000 (w), 967 (vw), 804 (vw), 768 (vw), 713 (m) cm^{-1}; HR-MS: m/z: calcd for $C_{52}H_{72}N_6O_{15}$ $[M+H]^+$: 1021.5128; found: 1021.5159.

HRMS data for the target compounds:

Table S1. HRMS data for the target compounds.

Compound	Formula	HRMS [m/z]	
		calcd	found
3	$C_{37}H_{53}O_{16}$	753.3339 [M-H]⁻	753.3331 [M-H]⁻
18•	$C_{48}H_{74}N_3O_{17}{}^{•}$	987.4910 [M+Na]⁺	987.4920 [M+Na]⁺
26b	$C_{40}H_{57}NO_{15}$	814.3620 [M+Na]⁺	814.3620 [M+Na]⁺
33	$C_{48}H_{62}N_6O_{17}$	1017.4064 [M+Na]⁺	1017.4067 [M+Na]⁺
34	$C_{49}H_{64}N_6O_{17}$	1031.4220 [M+Na]⁺	1031.4218 [M+Na]⁺
35	$C_{50}H_{66}N_6O_{17}$	1045.4377 [M+Na]⁺	1045.4376 [M+Na]⁺
36	$C_{51}H_{68}N_6O_{17}$	1059.4533 [M+Na]⁺	1059.4531 [M+Na]⁺
37	$C_{49}H_{64}N_6O_{17}$	1031.4220 [M+Na]⁺	1031.4222 [M+Na]⁺
38	$C_{50}H_{66}N_6O_{17}$	1067.4202 [M-H+2Na]⁺	1067.4207 [M-H+2Na]⁺
39	$C_{51}H_{68}N_6O_{17}$	1037.4714 [M+H]⁺	1037.4711 [M+H]⁺
40	$C_{52}H_{70}N_6O_{17}$	1051.4870 [M+H]⁺	1051.4872 [M+H]⁺
41	$C_{50}H_{66}N_6O_{17}$	1023.4557 [M+H]⁺	1023.4561 [M+H]⁺
42	$C_{51}H_{68}N_6O_{17}$	1081.4358 [M-H+2Na]⁺	1081.4360 [M-H+2Na]⁺
43	$C_{52}H_{70}N_6O_{17}$	1073.4690 [M+Na]⁺	1073.4684 [M+Na]⁺
44	$C_{51}H_{68}N_6O_{17}$	1081.4353 [M-H+2Na]⁺	1081.4342 [M-H+2Na]⁺
45	$C_{52}H_{70}N_6O_{17}$	1051.4870 [M+H]⁺	1051.4868 [M+H]⁺
46	$C_{53}H_{72}N_6O_{17}$	1087.4846 [M+Na]⁺	1087.4848 [M+Na]⁺
47	$C_{49}H_{64}N_6O_{17}$	1031.4220 [M+Na]⁺	1031.4223 [M+Na]⁺
48	$C_{50}H_{66}N_6O_{17}$	1045.4377 [M+Na]⁺	1045.4375 [M+Na]⁺
49	$C_{51}H_{68}N_6O_{17}$	1059.4533 [M+Na]⁺	1059.4528 [M+Na]⁺
50	$C_{50}H_{66}N_6O_{17}$	1045.4377 [M+Na]⁺	1045.4381 [M+Na]⁺
51	$C_{51}H_{68}N_6O_{17}$	1037.4714 [M+H]⁺	1037.4714 [M+H]⁺
52	$C_{52}H_{70}N_6O_{17}$	1051.4870 [M+H]⁺	1051.4870 [M+H]⁺
57	$C_{54}H_{74}N_6O_{16}$	1063.5234 [M+H]⁺	1063.5234 [M+H]⁺
58	$C_{52}H_{72}N_6O_{15}$	1021.5128 [M+H]⁺	1021.5159 [M+H]⁺

Compound purity:

Compound purity was determined on an Agilent 1100 HPLC apparatus with UV detection (190-410 nm). A linear gradient (5% B → 95% B over 25 min; A: Water + 0.1% formic acid; B: acetonitrile + 0.1% formic acid) was used, and the absorption was measured at a wavelength of 250 or 350 nm. Column: Waters Atlantis dC18, 3 μm, 4.6 × 75 mm.

Table S2. HPLC data for the target compounds

Compound	Formula	Retention [min]	Detection [nm]	Purity [%]
33	$C_{48}H_{62}N_6O_{17}$	14.150	350	95.3
34	$C_{49}H_{64}N_6O_{17}$	14.000	350	95.4
35	$C_{50}H_{66}N_6O_{17}$	14.017	350	94.5
36	$C_{51}H_{68}N_6O_{17}$	14.367	350	95.5
37	$C_{49}H_{64}N_6O_{17}$	14.483	350	97.2
38	$C_{50}H_{66}N_6O_{17}$	14.500	350	96.2
39	$C_{51}H_{68}N_6O_{17}$	14.583	350	96.3
40	$C_{52}H_{70}N_6O_{17}$	14.000	350	97.0
41	$C_{50}H_{66}N_6O_{17}$	14.317	350	96.1
42	$C_{51}H_{68}N_6O_{17}$	15.033	350	95.1
43	$C_{52}H_{70}N_6O_{17}$	14.267	350	97.3
44	$C_{51}H_{68}N_6O_{17}$	14.633	350	95.1
45	$C_{52}H_{70}N_6O_{17}$	15.283	350	96.5
46	$C_{53}H_{72}N_6O_{17}$	14.517	350	98.9
47	$C_{49}H_{64}N_6O_{17}$	13.517	350	99.4
48	$C_{50}H_{66}N_6O_{17}$	13.550	350	> 99.5
49	$C_{51}H_{68}N_6O_{17}$	13.617	350	95.0
50	$C_{50}H_{66}N_6O_{17}$	13.883	350	98.9
51	$C_{51}H_{68}N_6O_{17}$	13.717	350	> 99.5
52	$C_{52}H_{70}N_6O_{17}$	13.767	350	96.1
57	$C_{54}H_{74}N_6O_{16}$	12.483	250	95.2
58	$C_{52}H_{72}N_6O_{15}$	11.117	250	95.8

References

[S1] B. Ernst, B. Wagner, G. Baisch, A. Katopodis, T. Winkler and R. Öhrlein, *Can. J. Chem.* **2000**, *78*, 892-904.

[S2] I. MacInnes, J. C. Walton, *J. Chem. Soc., Perkin Trans. 2* **1987**, *8*, 1077-1082.

[S3] M. Pullagurla, M. Dukat, B. L. Roth, V. Setola, B. A. Glennon, *Med. Chem. Res.* **2005**, *14*, 1-18.

[S4] (a) Y. W. Li, T. J. Marks, *J. Am. Chem. Soc.* **1996**, *118*, 9295-9306; (b) Y. Li, P.-F. Fu, T. J. Marks, *Organometallics* **1994**, *13*, 439-440.

[S5] S. Shelke, B. Cutting, X. Jiang, H. Koliwer-Brandl, D. S. Strasser, S. Kelm, O. Schwardt, B. Ernst, *Angew. Chem. Int. Ed.* **2010**, *49*, 5721-5725.

3. Results and Discussion (continued)

For a simple representation of the linker pattern and the nitroindole attachment point, the naming convention shown in Figure 3-1 is used in the following sections.
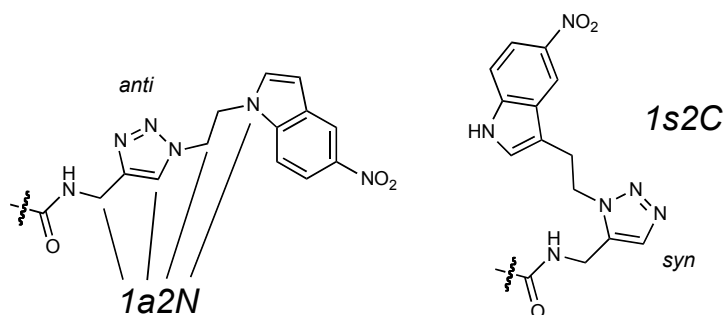
Figure 3-1. Naming convention for the linker pattern of triazole–nitroindole antagonists.

3.1. Failed approaches to the synthesis of alkyne amides

As mentioned in Section 2, the synthesis of alkyne amides *via* direct aminolysis suffered from low yields caused by low reaction rate and excessive byproduct formation. Before the eventual discovery that the cHex carboxyl group of diacid **P24** can be selectively activated, different reaction conditions and synthetic strategies had been evaluated unsuccessfully. Here, an overview of the different attempts is given.

3.1.1. Stability of alkyne amines

The direct aminolysis approach mainly suffered from the low stability and reactivity of the alkyne amines. The low stability furthermore aggravated the synthesis of these amines and required careful adaption of the reaction conditions. Generally, unprotected alkyne amines were found to be very unstable even at room temperature, which was indicated by coloration of the originally colorless solutions. For unprotected alkyne amines, the stability appeared to decrease with increasing chain length, while an inverse relationship was observed for TMS-protected alkyne amines. Here, stability was lowest for the propargyl amine derivative, which had to be stored at -80 °C to delay its decomposition.
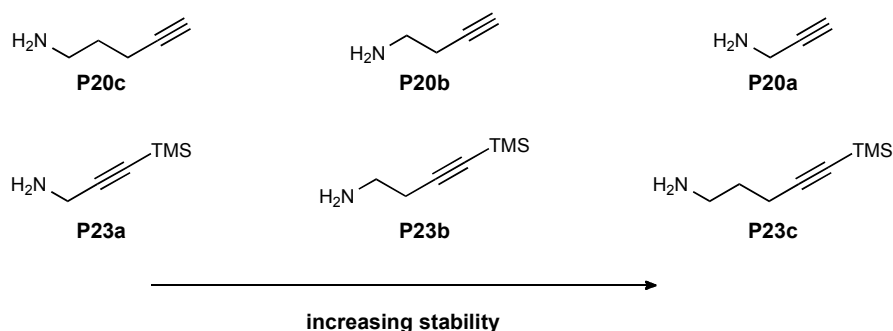
Figure 3-2. Stability of alkyne amines with respect to chain length.

3.1.2. Direct aminolysis *via* TMS-protected alkyne amines

Different catalysts or activators were tested for their ability to accelerate the direct aminolysis (Figure 3-3). DMAP and cyanide (194) were used as nucleophilic catalysts. Also tetraethyleneglcole (TEG), which was described as a catalyst stabilizing the transition state of the aminolysis reaction (195), was investigated. Furthermore, amines can be converted to dimethylaluminium amides ($\rightarrow$ Weinreb reagent) (196), which increases their nucleophilicity. In this work, a relatively stable DABCO-$(AlMe_3)_2$ ("DABAL-Me_3") (197) complex was used as a source of trimethylaluminium.

However, the reaction rate was not sufficiently increased by any of the conditions, and the desired amides could only be obtained with low yields.
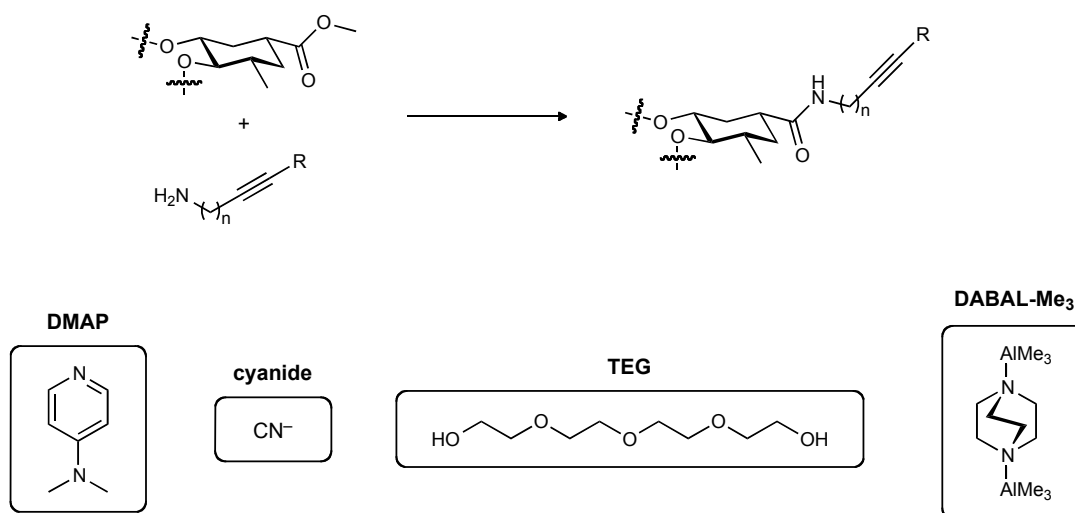
Figure 3-3. Catalysts and activators used in the direct aminolysis of the methyl ester **P3** to the corresponding alkyne amides.

Table 3-1. Illustrative examples of reaction conditions used for the direct aminolysis.

catalyst/activator	conditions	n	R	yield
DMAP	amine as solvent, µw: 120 °C, 3 h	1	H	traces
cyanide	amine excess, DMF, µw: 100 °C, 6 h	2	TMS	approx. 8%
TEG/DMAP	amine/TEG 3:1, µw: 100 °C, 8 h	2	TMS	2% diamide: 24%
TEG/DMAP	amine/TEG 3:1, 70 °C, 48 h	2	TMS	< 18%
DABAL-Me$_3$	amine excess, THF, µw: 100-130 °C, 2.5 h	2	TMS	traces

3.1.3. Direct aminolysis *via* (1-(2-(5-nitro-1*H*-indol-1-yl)ethyl)-1*H*-1,2,3-triazol-4-yl)methanamine

To circumvent the inherent instability and low reactivity of alkyne amines, an alternative route for direct aminolysis was investigated (Scheme 3-1). Besides the increased stability, amine **32** was also expected to be more nucleophilic due to the absence of the electron-withdrawing alkyne group. However, the solubility of **32** was limited, and it could not be used in as large an excess like the liquid alkyne amines. Thus, product **P37** was formed only in trace amounts under various reaction conditions.
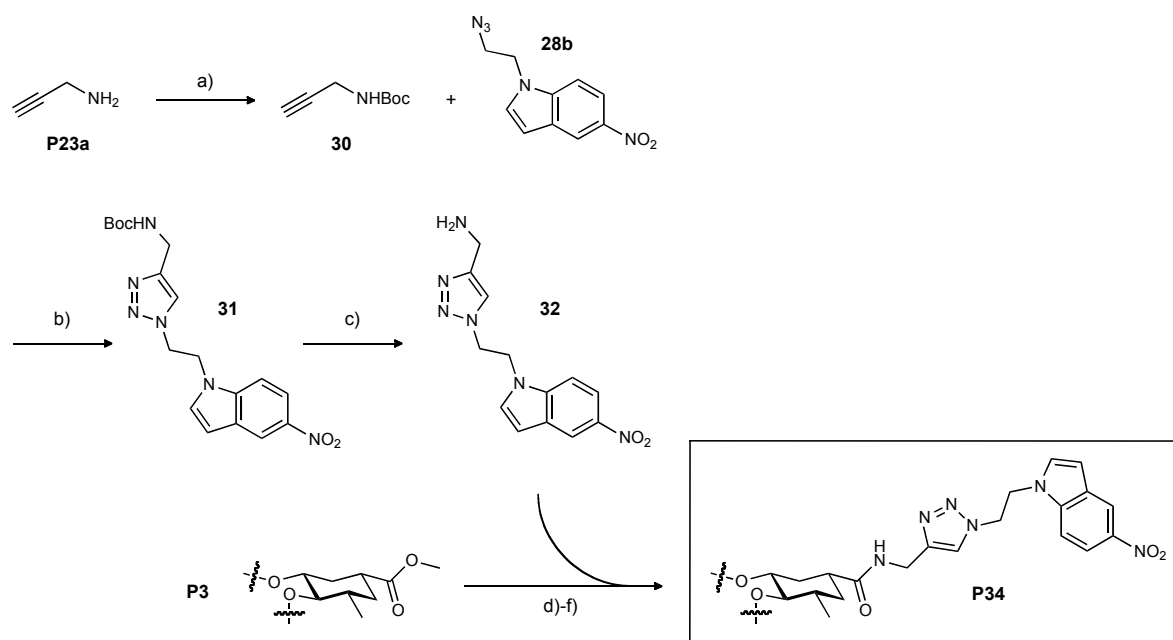
Scheme 3-1. a) Di-*tert*-butyldicarbonate, DMAP, Et$_3$N, CH$_2$Cl$_2$, 0 °C, 3 h, 46%; b) Na-L-ascorbate, CuSO$_4$·5H$_2$O, *t*BuOH/H$_2$O/MeCN 9:2:2, r.t., 15 h, 100%; c) TFA, 30 min, 96%; d) DABAL-Me$_3$, THF, µW: 100 °C, 30 min, < 2%; e) DABAL-Me$_3$, THF/DMF 4:1, µW: 70-90 °C, 6 h; f) NaH, THF/DMF 1:1, 70 °C, 6 h.

3.1.4. Alkyne ethers as a possible alternative for alkyne amides

As shown in Scheme 3-2, an alternative synthetic strategy for the synthesis of alkyne ethers instead of amides was suggested. However, test reactions revealed similar stability and reactivity problems as encountered in the direct aminolysis approach. Furthermore, some uncertainty was associated with the benzyl–pivaloate protecting group exchange on the sterically restricted fucose. Thus, this alternative was not considered any further.
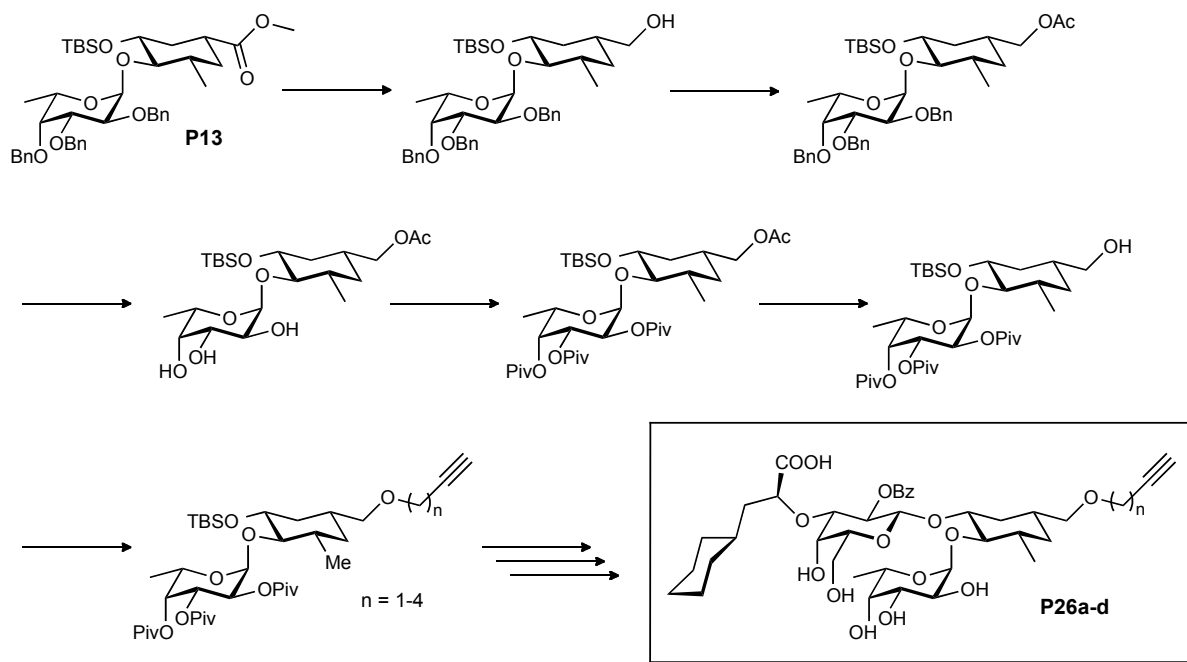

Scheme 3-2. Alternative approach for the synthesis of alkyne ethers.

3.2. Studies on physicochemical parameters

3.2.1. Observation of micelle formation in ITC and Biacore assays

The triazole–nitroindole antagonists are comprised of a polar carbohydrate-mimetic and a hydrophobic linker part (Figure 3-4A), *i.e.* they have an amphiphilic structure. This property became first evident during the preparation of these antagonists, where the compounds formed opalescent films on aqueous surfaces or tended to form aggregates in aqueous solutions. Also in biological assays, the unusual properties of the triazole–nitroindole antagonists were recognized: Figure 3-4B shows Biacore sensorgrams of sequential blank injections, which were carried out after a single injection of **P38** at a concentration of 62.5 μM. The intensity and characteristic shape of the signal (up to 40 resonance units) indicated that significant amounts of the compound had remained within the instrument after the first injection. Furthermore, in an isothermal titration calorimentry (ITC) experiment with

P38 (Figure 3-4C), an endothermic process was superimposed on the exothermic ligand binding process.
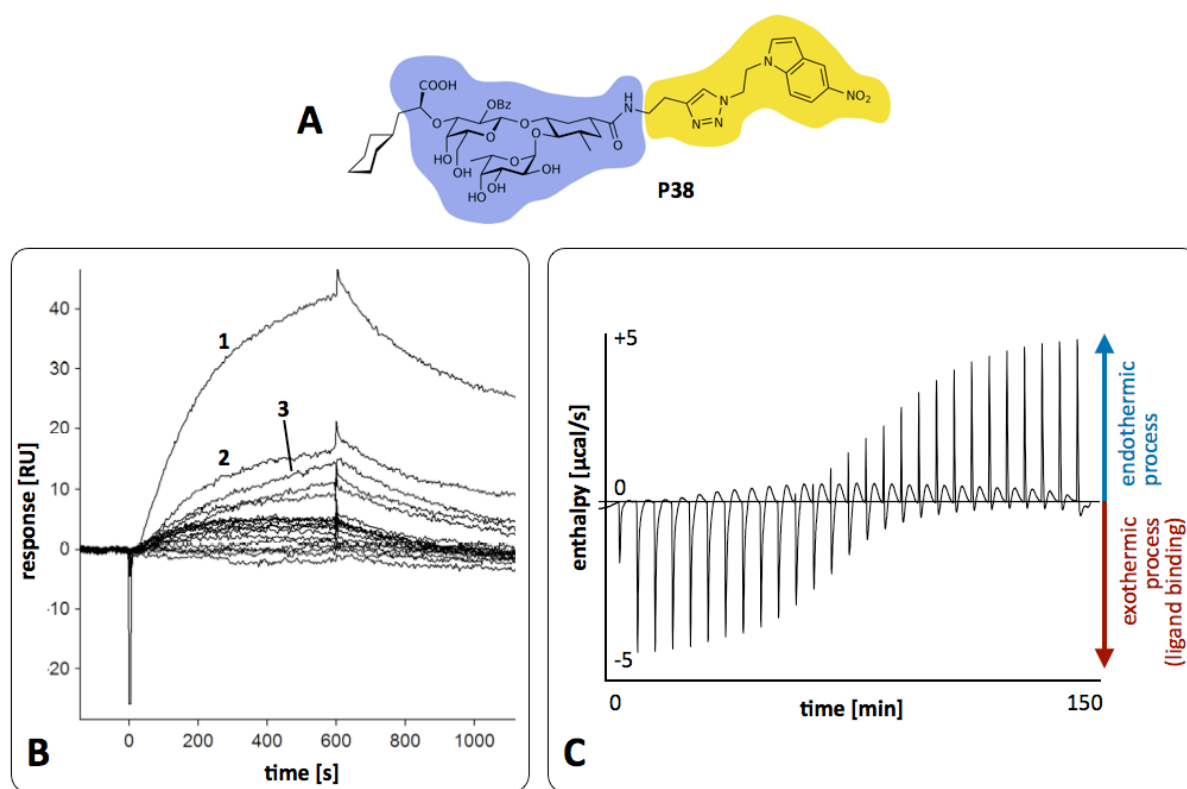

Figure 3-4. A) **P38**; blue: hydrophilic carbohydrate-mimetic part; yellow: hydrophobic linker part. B) Biacorre soensorgrams; 1-3: serial blank injections after one injection of **P38** at a concentration of 62.5 μM. Experiment performed by Céline Weckerle. C) ITC enthalpogram of **P38** (ligand 1.6 mM titrated into E-selectin/IgG 84 μM) showing an exothermic binding process. Experiment performed by Katrin Lemme.

Amphiphilic properties are common to many drugs. Apart from the effects in biological assays as described above, amphiphilicity is of considerable importance *in vivo*. Drug toxicity, for example, may arise from the incorporation of amphiphilic molecules into membranes, where they can lead to membrane disruption or alteration of other membrane properties (198, 199). Besides toxicity, gastrointestinal absoprtion (200), blood–brain barrier permeation (201), and P-glycoprotein substrate avidity (202) correlate with amphiphilicity.

Based on these considerations and given the difficulties encountered during compound characterization, it was decided to investigate the physicochemical properties of the triazole–nitroindole antagonists and derivatives thereof.

3.2.2. Chemical modifications to reduce surface activity

P43, the most potent antagonist identified by Biacore (Section 2) was chosen for the investigation of structural modifications, which are summarized in Figure 3-5.
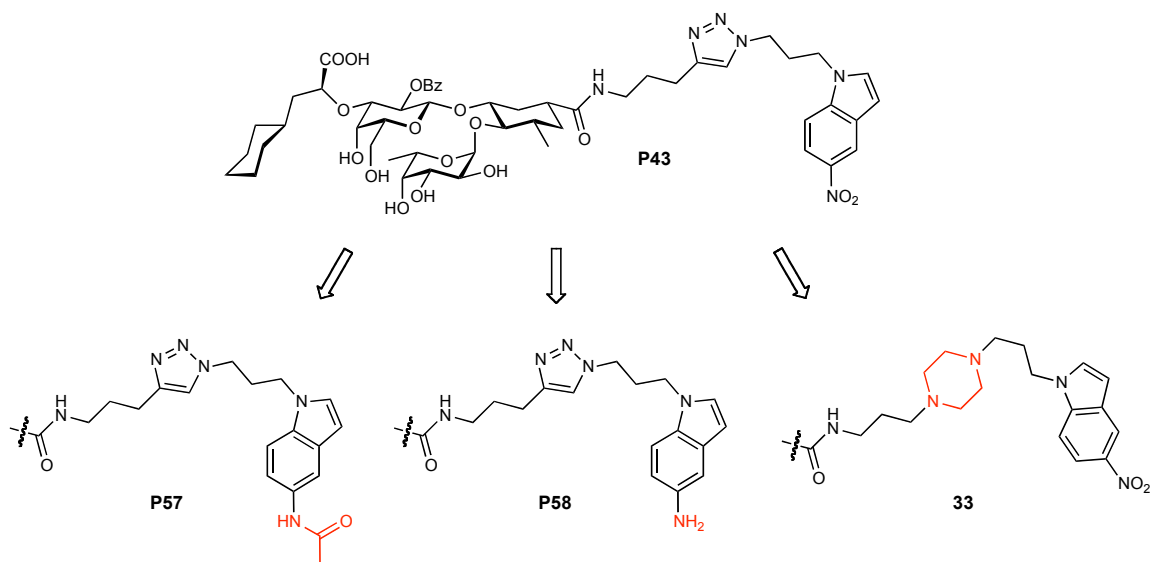
Figure 3-5. Modifications to **P43** for lowering the CMC.

3.2.2.1. Modifications of the nitro group

As described in Section 2, amine and acetamide derivatives of **P43** were synthesized to elucidate the effect of these functional groups on binding affinity.

Yet, these modifications may also influence CMC, as the corresponding indole fragments have a markedly reduced logP and the aminoindole even a potentially charged basic group (Figure 3-6) (203).

log P	2.5	0.85	1.1
pK_a	–	4.9	–

Figure 3-6. Calculated logP (and pK_a) values for 5-nitroindole, 5-aminoindole, and *N*-(indol-5-yl)acetamide.

3.2.2.2. Replacement of the triazole

While the use of triazole as a linking heterocycle made sense against the background of the *in situ* click approach, it is not necessarily the best choice with respect to the binding and physicochemical properties of the nitroindolyl antagonists.

Piperazine, a common motif of many marketed drug molecules, was considered as an alternative linking heterocycle. It is more hydrophilic (logD$_7$ = -1.2, logP = -0.2; calculated for 1,4-dimethylpiperazine) than triazole (logD$_7$ = logP = -0.4; calculated for 1,4-dimethyl-1H-1,2,3-triazole) and expected to be (partly) protonated at physiological pH (pK_a of alkylated piperazine $\approx$ 9) (203). Thus, the substitution of triazole with piperazine was expected to increase the solubility/CMC of the molecule.

Furthermore, a pair of piperazinyl- and bromine-substituted ligands could in priniple be used for an alternative *in situ* click experiment (see *e.g.* (204, 205)). While E-selectin did not have an accelerating effect on triazole formation, this may be the case for a different type of reaction such as a nucleophilic substitution. However, bioorthogonality may be arguable in this case because a bromide could react with nucleophilic amino acid side chains of E-selectin.

As Figure 3-7 shows, the distance between the attachment points in piperazine and triazole differ by only 0.5 Å. Given that linkers with 4 to 6 methylene groups led to high-affinity antagonists (Section 2), it is reasonable to assume that such a modification may be tolerated. However, piperazine may add some flexibility to the linker and thus have different requirements for linker length and pattern.
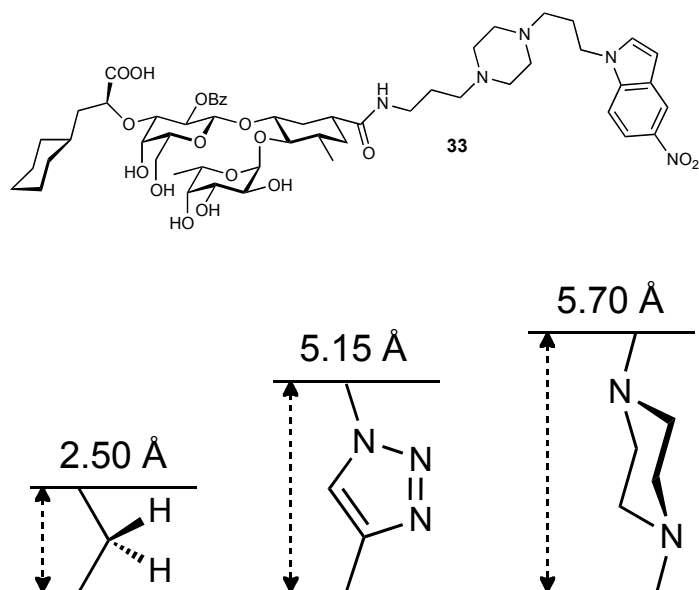
Figure 3-7. Use of piperazine as linking heterocycle.

3.2.2.3. Synthesis of the piperazinyl antagonist

The synthesis of piperazinyl antagonist **33** started from commercial 5-nitroindole, which was alkylated using dibromopropane to yield **P27c**. This was coupled to commercial 3-(piperazin-1-yl)propan-1-ol with quantitative yield to give **34**. Using DPPA, the alcohol was converted to the azide in one step (→ **35**), and reduction gave amine **36**, which was coupled to diacid **P24** using the previously described conditions for the synthesis of alkyne amides (Section 2).
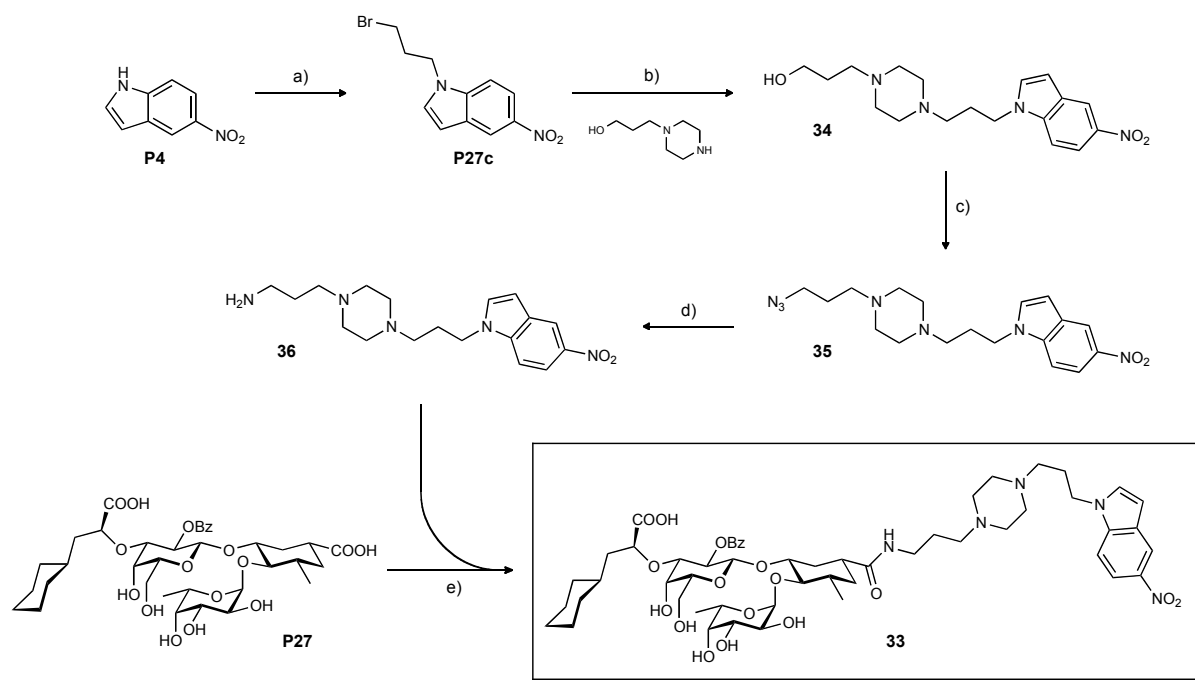
Scheme 3-3. a) 1,3-dibromopropane, KOH, DMF, r.t.,17 h, 46% (28% of the starting material were recovered); b) Et₃N, DMF, r.t., 2 h, 100%; c) DPPA, DBU, THF, r.t., 24 h, 79%; d) PPh₃, THF/H₂O, r.t., 3 h, 78%; e) HOBt, HBTU, DIPEA, DMF, r.t., 3 h, 34%.

3.2.2.4. Determination of binding affinities by Biacore

As discussed in Section 2, nitroindole substitution in **P43** is accompanied by an affinity loss. For the substitution of triazole by piperazine, K_D was increased approximately 4-fold.

Table 3-2. Affinities of **P57**, **P58**, and **33** determined by Biacore (steady state response fit to a 1:1 binding model). Measurements performed by Céline Weckerle.

Analyte	K_D [µM]
P57	0.544
P58	0.186
33	0.110

3.2.2.5. Determination of physicochemical and pharmacokinetic parameters

The physicochemical and pharmacokinetic parameters were determined on the PADMET platform (206) by Matthias Wittwer and Simon Kleeb.

Critical micelle concentration

The results of the surface activity measurements are summarized in Table 3-3. All antagonists are expected to have CMCs in the range of 1 to 10 mM and show beginning surface activity (SA) at concentrations of 4 to 30 μM. The increase of surface pressure with increasing ligand concentrations is most pronounced for **P45** and least pronounced for **P35**. As, in **P45** and **P35**, the linker parts attached to the nitroindole are the longest and the shortest in the series, respectively, CMC may depend on the length of this part. All CMC values are in a range commonly seen in marketed drugs (198, 200). The values for the beginning of SA, but potentially also the CMC, are in a concentration relevant for biological assays (see above). Although the amount of molecules in surface interfaces is usually small compared to the amount found in solution, caution may be indicated when performing measurements at concentrations in these ranges.

Surprisingly, antagonist **33** appeared to exhibit stronger surface activity than all other antagonists, despite the presence of two nitrogens in the linker, of which at least one is expected to be protonated at the slightly acidic pH ($= 6.5$) of the experiment.

Figure 3-9 indicates a trend towards lower surface activity if the nitroindole is replaced by an acetamide (**P57**) or by an amine (**P58**).

Table 3-3. Critical micelle concentration and begin of surface activity measured at pH 6.5. The antagonists are ordered by increasing linker length. In brackets, the linker patter and the indole substituents are indicated.

Compound	CMC	begin of SA
P41 (1a3N)	1-10 mM	> 8 μM
P35 (3a1N)	1-10 mM	> 16 μM
P38 (2a2N)	> 1 mM	> 8 μM
P51 (2a3C)	1-10 mM	> 16 μM
P45 (2a4N)	> 1 mM	> 8 μM
P43 (3a3N)	> 1 mM	> 8 μM
P57 (3a3N, NHAc)	> 1 mM	> 10 μM
P58 (3a3N, NH$_2$)	> 1 mM	> 30 μM
33 (3pip3N)	approx. 1 mM	approx. 4 μM
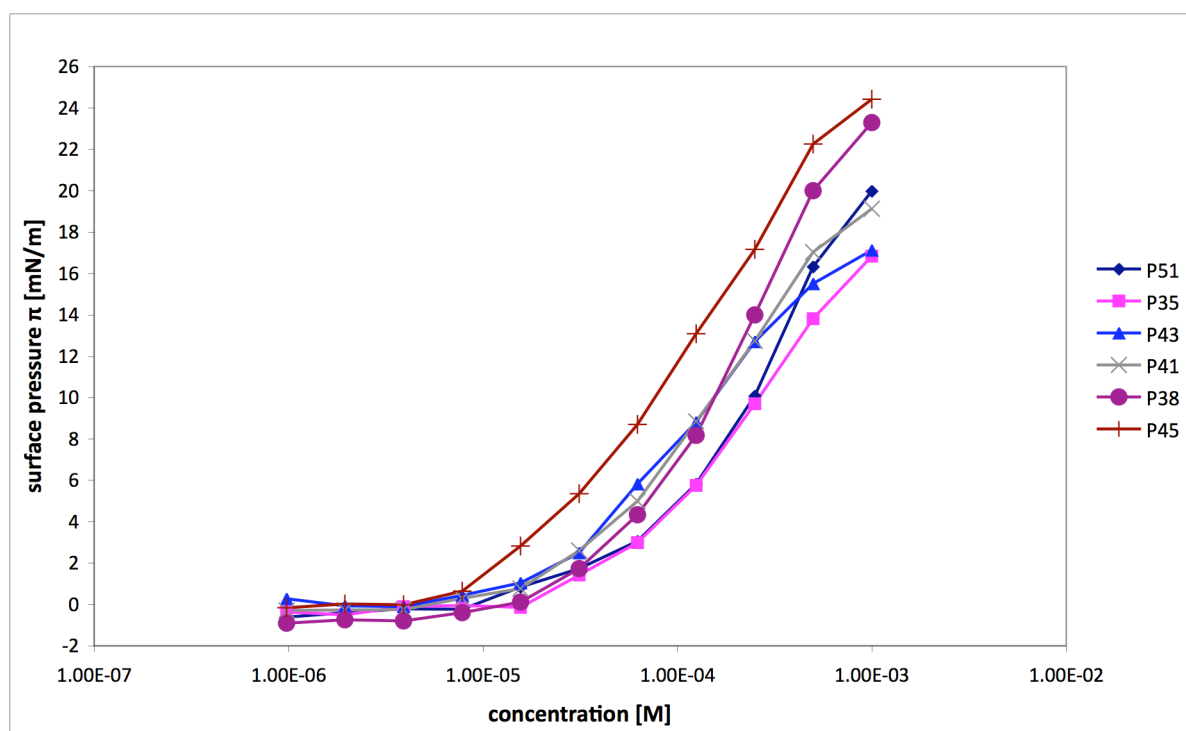
Figure 3-8. CMC measurement curves of triazole–nitroindole antagonists.
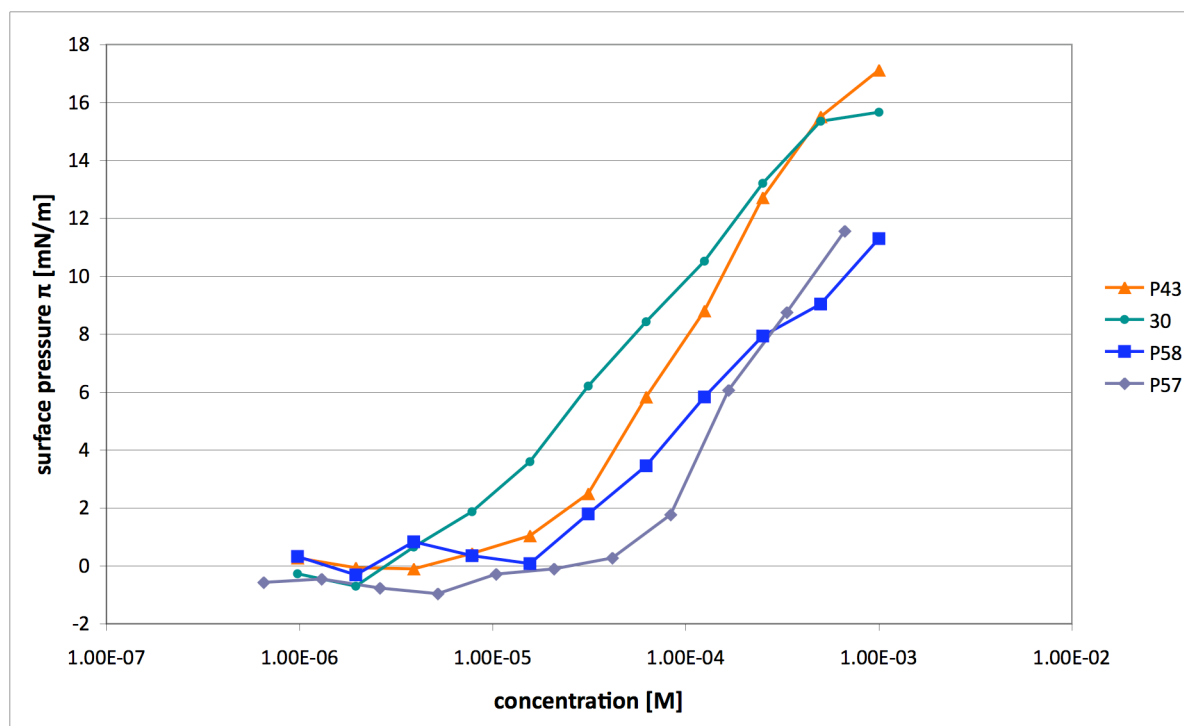
Figure 3-9. CMC measurement curves of **P43** and its derivatives.

PAMPA, logD, and plasma protein binding

Table 3-4 shows the results of the PAMPA (207, 208), $logD_{7.4}$, and plasma protein binding measurements. Due to the difficult analysis of this compound class (*e.g.* the occurrence of nonlinear calibration curves, *cf.* Section 3.6.4.5), the data are of qualitative rather than quantitative nature (209).

None of the compounds showed permeation in the PAMPA assay (permeation can be expected for $log P_e$ values above -5.7 or membrane retention above 80 %Mm/M). Yet, with decreasing pH, some membrane enrichment (PAMPA %Mm/M) of **P43** was observed.

The $logD_{7.4}$ was similar for all compounds except **P45**. Its logD was remarkable 1.2 units higher than the one of its isomer **P43**, *i.e.* its concentration in the octanol phase was approx. 10 times higher than the one of **P43**.

Antagonists **P43**, **P57**, **P58** are reasonably well soluble. However, the substitution of triazole by piperazine (→ **33**) led to a strong decrase of solubility by a factor of at least seven.

With values in the range 88 to 97%, the extent of plasma protein binding (PPB) is high. This may contribute to a prolonged plasma half-life resulting from reduced excretion and/or metabolism (87). At the same time displacement of the ligand from plasma proteins by a competing ligand (*e.g.* acetylsalicylic acid) may be clinically relevant (210).

Table 3-4. PAMPA parameters, logD$_{7.4}$, solubility, and plasma protein binding (PPB) of triazole–nitroindole antagonists; n.p.: no permeation; n.r.: no retention.

Compound	PAMPA log P$_e$		PAMPA %Mm/M		logD$_{7.4}$	Solubility [µg/mL], (pH)	PPB %
P45 (2a4N)	n.p.		pH 5: n.r. pH 6.2: n.r. pH 7.4: n.r.		2.42	not determined	89
P51 (2a3C)	n.p.		pH 5: n.r. pH 6.2: n.r. pH 7.4: n.r.		1.25	not determined	97
P41 (1a3N)	n.p.		pH 5: 8.7 pH 6.2: 19 pH 7.4: n.r.		1.83	not determined	94
P43 (3a3N)	n.p.		pH 5: 41.5 pH 6.2: 20.5 pH 7.4: n.r.		1.22	> 2400 (6.27)	92
P57 (3a3N, NH$_2$)	pH 5: n.p. pH 6.2: n.p. pH 7.4: -8.4		pH 5: n.r. pH 6.2: n.r. pH 7.4: n.r.		1.20	> 2000 (6.37)	91
P58 (3a3N, NHAc)	n.p.		n.r.		1.60	> 3000 (6.53)	88
33 (3pip3N)	–		–		–	340 (6.61)	–

pK_a determination of 33

This experiment is in progress. Preliminary results allowed the to identify three pK_as, corresponding to the three ionizable groups of **33**.

3.2.2.6. Discussion and conclusions

In general, none of the antagonists tested exhibited particularly favorable pharmakokinetic properties. For example, passive absorption from the gastrointestinal tract cannot be expected based on the PAMPA measurements. The replacement of the nitro group had a small effect on surface activity, whereas other parameters were not strongly affected. The solubility of antagonists **P43**, **P57**, and **P58** was good. A pronounced reduction of solubility was observed for **33**, but the value of 340 µg/mL is still in an acceptable range (211). This, as well as the

trend to a lower CMC, contradicts the expectation that the introduction of polarity to the linker would have a beneficial influence on these properties. Considering the carboxyl group of **33** and the definition of the isoelectric point (p*I*) given by Equation 6,

$$pI = \frac{pK_{a1} + pK_{a2}}{2} \tag{6}$$

it is evident that **33** is zwitterionic at the pH (≈ 6.5) of the CMC and solubility measurements (pK_a of piperazine ≈ 9, pK_a of carboxyl group ≈ 4). Thus, the molecule's net charge is zero, leading to large crystal lattice energies and thus to a high tendency to aggregate. The high polarity further implies that passive diffusion through membranes would probably be low (212).

Phospholipidosis, the excessive accumulation of phospholipids in lysosomes, is a (reversible) effect exerted by cationic amphiphilic drugs (CADs) (213). Most commonly, the CADs inducing phospholipidosis share a hydrophobic ring structure to which a side chain with a charged cationic amine group is attached (213, 214). As Figure 3-10 illustrates, **33** has typical features of a CAD inducing phospholipidosis.

Without implying significancy, it is further noteworthy that amiodarone (Figure 3-10) induces *QT* prolongation *via* blockade of hERG (215). hERG-blocking compounds are, in a very simplified view, characterized by one or two hydrophobic moieties attached to a positively charged nitrogen (216) – structural features that are also found in **33**. Blocking of the hERG channel is a highly disfavored property of drug leads, as it is associated to sudden death caused by cardiac arrest (215).
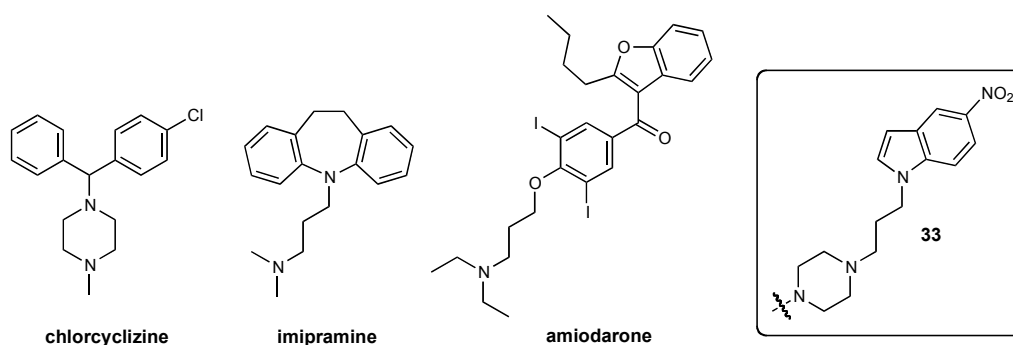
Figure 3-10. Structure of **33** and some CADs inducing phospholipidosis. Besides inducing phospholipidosis, amiodarone is an inducer of *QT* prolongation.

Although the clinical implications of phospholipidosis are uncertain and there is a considerable number of marketed and experimental drugs inducing this condition, its possible

association with toxic or unwanted effects have given it the status of an adverse finding from a regulatory perspective (214).

Given the above results and considerations, the piperazine moiety in **33** cannot be regarded as a suitable replacement for the triazole moiety in **P43**. The loss of affinity caused by replacing the triazole by piperazine further implies that the triazole is well suited for the binding to E-selectin. Yet, from the present data it is not evident whether this is a result of altered linker flexibility, differences in polarity or other structural differences. Further insights could be achieved by by STD NMR studies to elucidate whether some parts of the linker are in contact with E-selectin.

3.3. Synthesis of antagonists for an inversed Biacore assay

As illustrated in Section 1.5.1, usually, the target protein is immobilized in a Biacore experiment. To verify this setup, derivatives **37** (derived from the first-site antagonist **P3**) and **P38** (derived from the high-affinity triazole–nitroindole antagonist **P43**) carrying an ethyleneglycole linker with a terminal amine were synthesized. These antagonists can be immobilized on a Biacore chip *via* standard amine coupling (133), allowing to perform an "inversed" Biacore experiment. Also the free aromatic amine group of **P58** was used for immobilizing this ligand directly Figure 3-11.
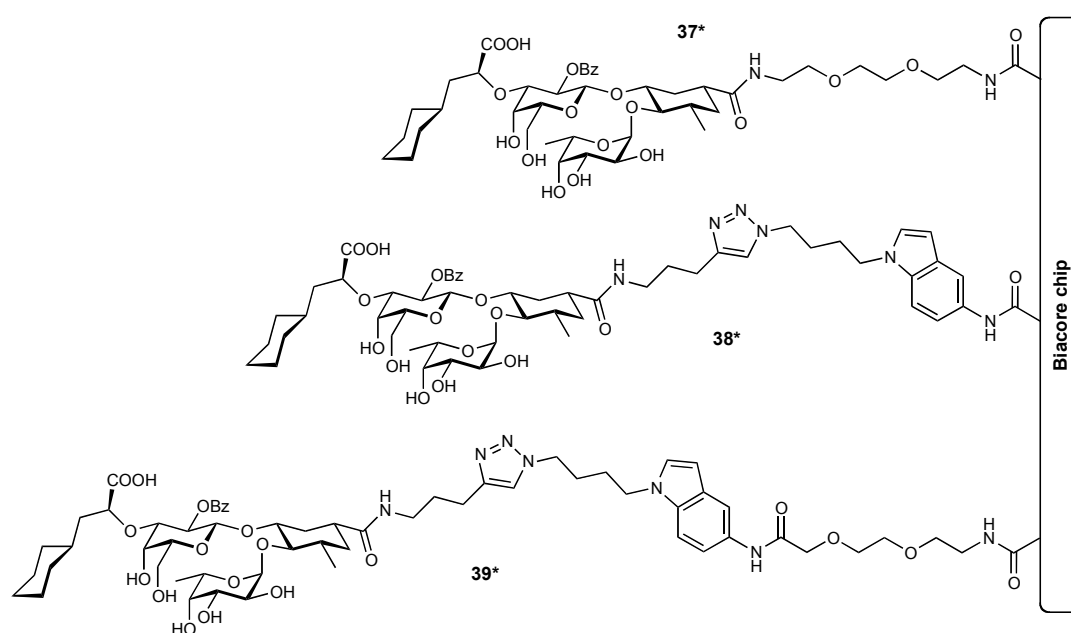
Figure 3-11. Schematic representation of ligands immobilized on a Biacore chip.

3.3.1. Synthesis

Derivative **37** was obtained *via* direct aminolysis of methyl ester **P3**, which gave the amine in satisfactory yields (40%) (Scheme 3-3).

The synthesis of derivative **P38** started from indole amine **P34** (see Section 2). NHS ester **P36** was coupled to the indole amine, which was then used in the CuAAC with alkyne **P26c**. After *in situ* removal of the Fmoc protecting group, the free amine (**P38**) was obtained (Scheme 3-5).
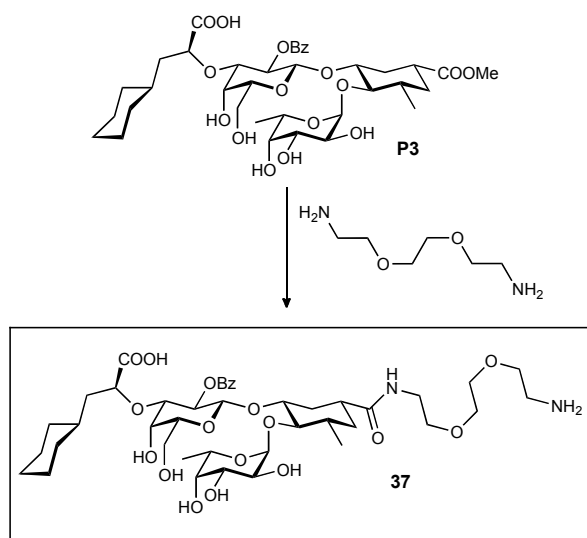
Scheme 3-4. 2-2'-(Ethylenedioxy)bis-(ethylamine)/DMF 1:1, 65-70 °C, 2 d, 40%.
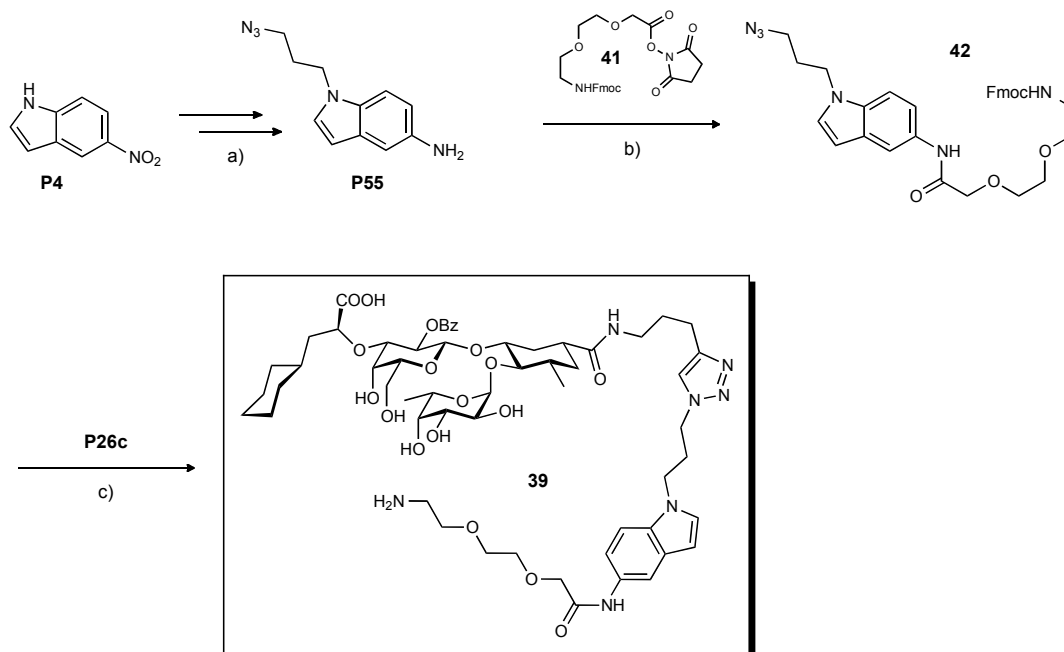
Scheme 3-5. a) The synthesis of **P34** is described in Section 2; b) NHS ester **P36**, DMF, r.t., 17 h, approx. 50%; c) 1) Alkyne **P26c**, Na-L-ascorbate, CuSO₄·5H₂O, ᵗBuOH/H₂O/THF, r.t., 40 min; 2) piperidine, r.t., 3 h, 66%.

3.3.2. Biacore analysis

The Biacore analysis war performed by Céline Weckerle (133). As Table 3-5 shows, first-site ligand **37** gave identical results in the standard and in the reversed assay. The range of K_Ds given resulted from different etanolamine·HCl (EA) concentrations used for the inactivation of residual activated NHS esters on the Biacore chip surface (ligand/EA ratios: 1:1, 1:10, 1:50, 1:100). Binding kinetics were not affected by the new setup (data not shown). However,

as can be seen from Figure 3-12 the response was by magnitudes higher when E-selectin was in solution, which is a result of the large mass differences between E-selectin and **37**.

The finding for **37** could not be reproduced with the triazole–nitroindole derivatives **P38** and **P58**: Upon immobilization, their estimated K_Ds increased to the one-digit micromolar range.

Table 3-5. K_Ds determined in a conventional Biacore assay (**37**, **P38**, **P57**, **P58**) and in the inversed Biacore assay (**37***, **P38***, **P58***).

Compound	K_D[a] [µM], **free**	K_D[b] [µM], **immobilized**
37/37*	6.0	4.4-8.9[c]
P38/ P38*	0.36	8.2[d]
P58/P58*	0.19	7.8[e]
P57	0.54	–

a) Protein used: dimeric E-selectin (E-selectin/IgG); b) protein used: monomeric E-selectin (LecEGF_CR2); c) the K_D range is a result of different etanolamine·HCl concentrations used for the inactivation of residual activated NHS esters on the Biacore chip surface; d) ligand/EA: 1:100; e) ligand/EA: 1:50.

For **37**, the reverse assay was performed using dimeric E-selectin (E-selectin/IgG) as well. Using this setup, two binding events were observed. The first binding occurred in the micromolar ($K_{D,1}$ = 12.1 µM), and the second in the nanomolar range ($K_{D,2}$ = 320 nM). This result suggested that, for reverse assays, the monomeric form of the protein should be used preferably.
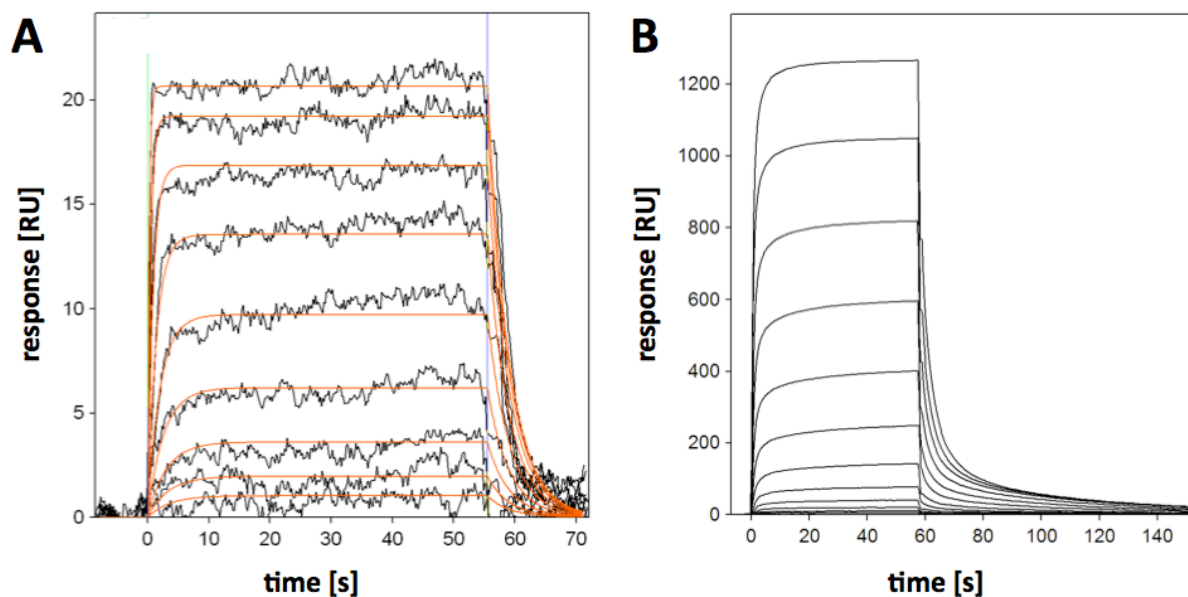
Figure 3-12. Sensorgrams of **37** in the normal experimental setup (A) and in the reversed assay (B). Adapted from (133).

3.3.3. Discussion and conclusions

Given that the affinities of **P58*** and **33*** were similar to the ones of the first-site antagonists, the immobilization apparently prevented the binding of the triazole–indole moiety, while the interaction with the tetrasaccharide part was still possible. An alternative strategy for ligand immobilization (Figure 3-13) may provide further insights.
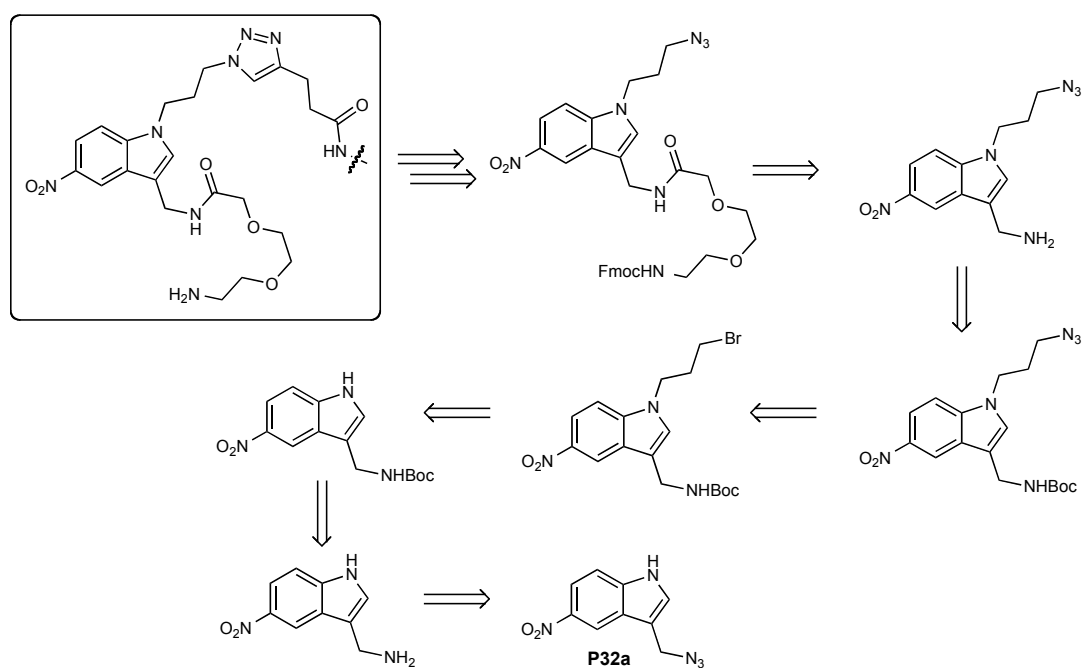
Figure 3-13. Alternative synthetic strategy for ligand immobilization.

3.4. The influence of linker length on linker flexibility

In **P33** and **P34**, the NMR signals of the CH$_2$ group linking the triazole and the nitroindole moiety differed significantly from the signal in **P35** and **P36**. In the former cases, the protons gave two doublets, in the latter a singlet was observed. This indicates that rotation around the bonds linking the triazole and the nitroindole is restricted in **P33** and **P34**. Interestingly, the amide–triazole part of the linker seems to determine the rotational freedom of the nitroindole, as it is the only difference between the molecules. Currently, there are no additional NMR data describing this phenomenon, and aggregate formation resulting in restricted linker flexibility cannot be excluded. However, the present finding is in agreement with the observation that retention times and rates of *syn/anti* triazole formation are also influenced by the linker lengths (*cf.* Section 3.6.5).
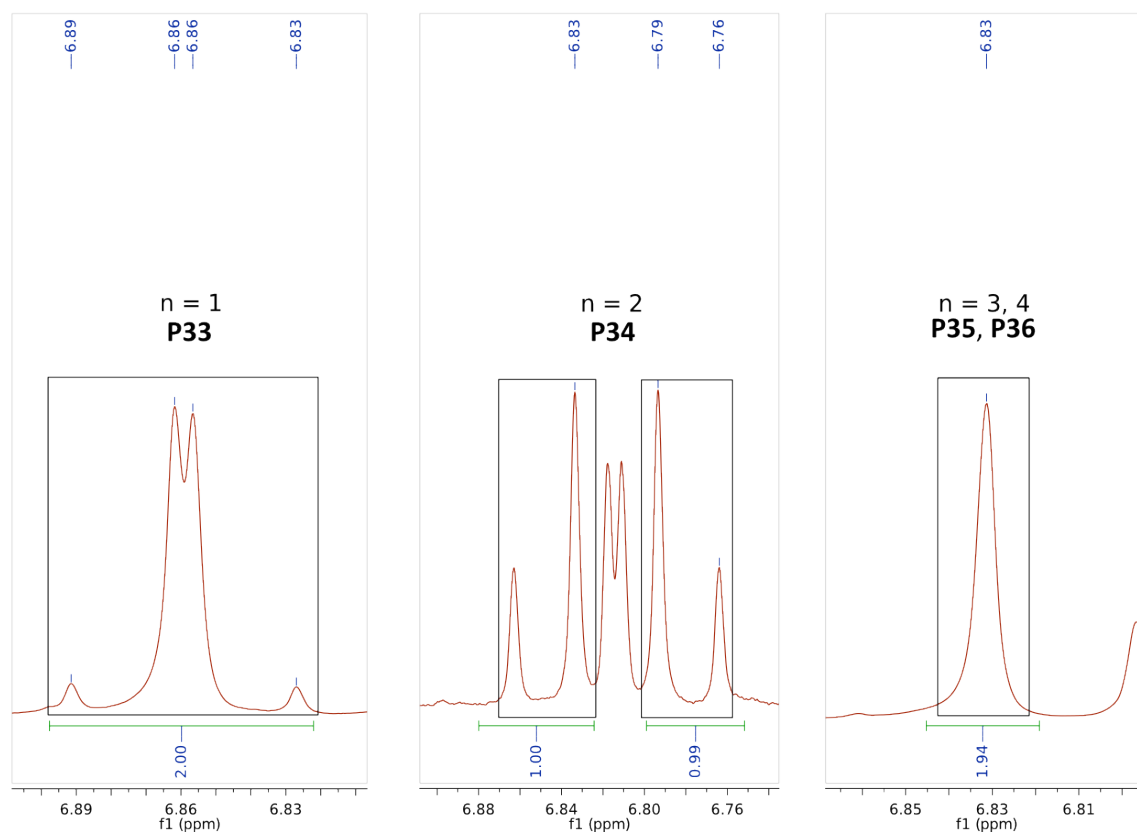
Figure 3-14. NMR signals of the CH$_2$ group linking the triazole and the nitroindole in **P33** (left), **P34** (middle; note: the doublet at 6.82 ppm corresponds to the proton at position 3 of the nitroindole) and **P36** (right; peak in **P35** is a singlet as well). The spectra were recorded in deuterated methanol.

3.4.1. Spontaneous deuteration of P57 and P58

Spontaneous proton–deuteron exchange at room temperature was observed at the 3-position of the nitroindole moiety of **P57**. As shown in Figure 3-15, leaving **P57** in MeOH-d4 for estimated 2 d leads to almost complete exchange of the 3-proton by deuterium.
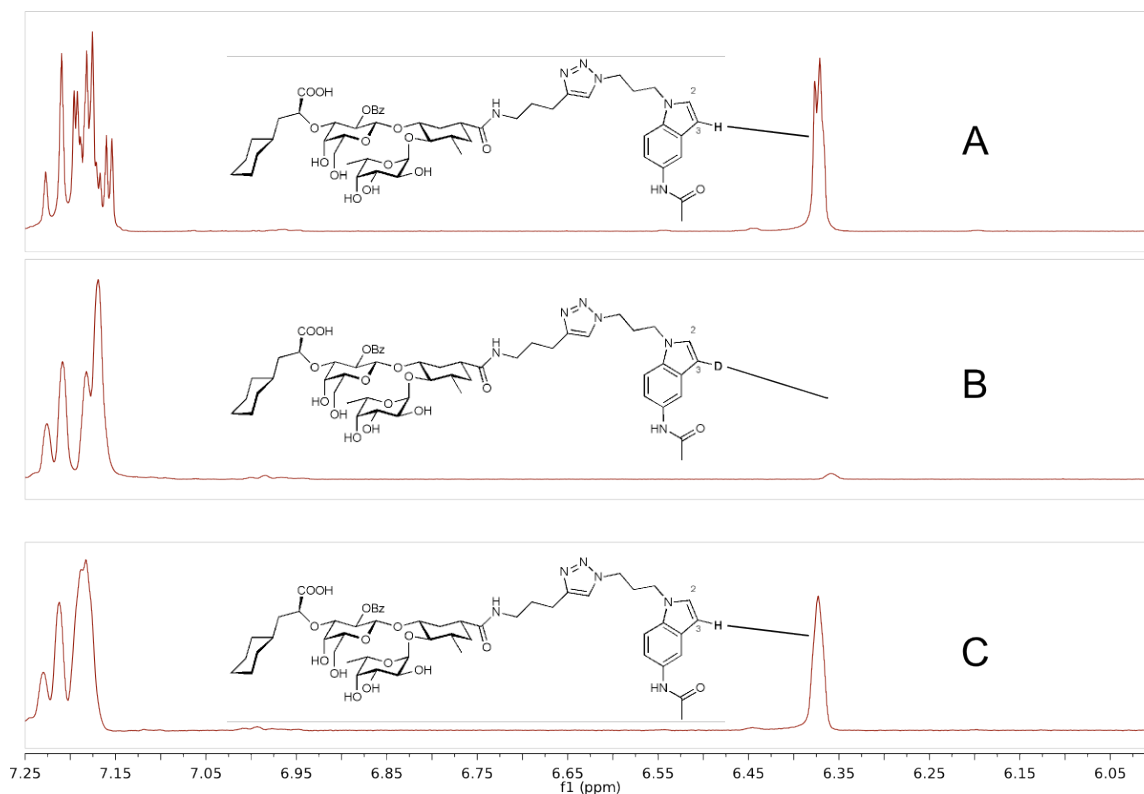
Figure 3-15. Spontaneous exchange of **P58**'s nitroindole 3-proton at r.t. by a deuteron and *vice versa*. A) Initial ^{1}H spectrum in MeOH-d4, recorded within approx. 1 h after dissolution of the sample; B) spectrum recorded after the sample had been left in MeOH-d4 for estimated 2 d; C) spectrum recorded after stirring of **P58** in MeOH for 48 h.

As the marked upfield shift of the 3-proton indicates (note that all other aromatic protons appear at > 7.15 ppm), the electron density at the 3-carbon is increased due to the +M effect of the 1-nitrogen. This is confirmed by DFT calculations (performed by Martin Smiesko; Figure 3-16) and is, for example, exploited in the Vilsmeier formylation, which occurs selectively at the 3 position (*cf.* Section 2).
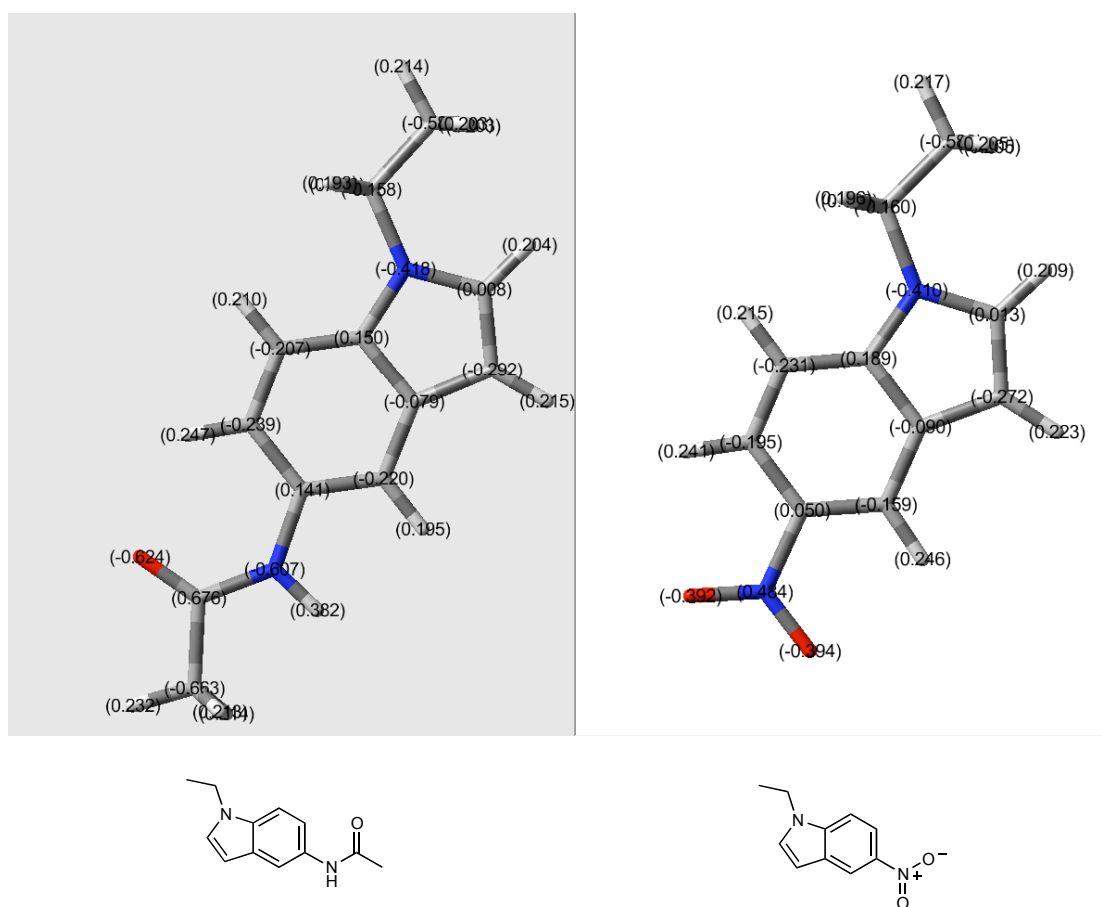
Figure 3-16. Electron densities in the indole acetamide (left) and the nitroindole (right) derivative. 3-carbon in the acetamide: -0.292; 3-carbon in the nitro compound: -0.272. Experimental parameters: DFT: B3LYP/6-J11++6(dip); charge population analysis; gas phase optimization.

Mass spectra showed the same phenomenon to occur in the indole amine derivative **P58**, too. It was not observed in the nitro derivatives, albeit a systematic investigation has not been performed.

3.5. A theoretical approach to the design of an *in situ* click experiment

3.5.1. Background

Similar to the myelin associated glycoprotein (MAG), E-selectin represents a borderline case for the application of the *in situ* click methodology (160). The sLe^x binding site lies at the surface of E-selectin, and Figure 3-17 shows that the linker alkyne and azides will likely be exposed to the solvent during an *in situ* click experiment. This is somewhat in contrast to the first *in situ* click experiments of Sharpless and coworkers, where the click reaction took place within the spatially restricted active sites of enzymes. However, the most recent *in situ* click experiment performed by Heath, Sharpless, and coworkers (183) may be comparable to the E-selectin and MAG cases. It started from a low-affinity peptide fragment ($K_D \approx 500$ μM) and led to the formation of antibody-like ligands that do not interfere with enzyme activity.
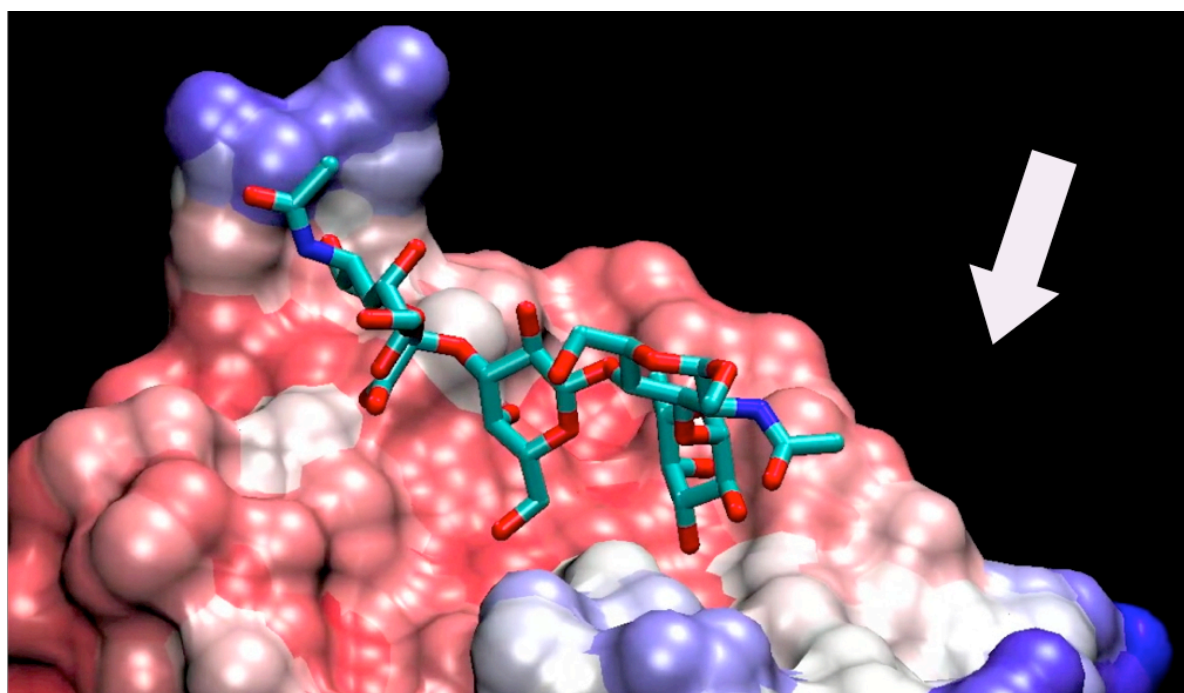
Figure 3-17. E-selectin cocrystallized with sLe^x (pdb code: 1G1T). The arrow indicates the expected approximate location of the second-site ligand relative to the first-site ligand. Image created by Gianluca Rossato, Institute of Molecular Pharmacy, University of Basel.

In the present case, the binding of the first- and second-site ligands is characterized by low affinities (K_Ds of approx. 1 μM and estimated 5 mM, respectively) and the half-life times of the protein–ligand complex are distinctively short (133). Although high substrate affinities are not generally required for supramolecular catalysis (*e.g.* (188, 189)), there may be some consequences of low substrate affinity. Namely, proteins (unlike synthetic supramolecular

catalysts) are usually available only in limited quantities and concentrations, and thus achieving sufficiently high concentrations of ternary complex $L_1 \cdot P \cdot L_2$ (L_1, L_2: first- and second-site ligand; P: protein) for the detection of triazole formation may be aggravated. [$L_1 \cdot P \cdot L_2$] can be increased by increasing the ligand concentration but this will be accompanied by a faster background reaction due to the higher amounts of unbound ligand. Indeed, spontaneous triazole formation was readily detected in some preliminary experiments. Eventually, the question was raised in which way the experimental conditions have to be optimized for detecting the protein-mediated triazole formation, *i.e.* for the kinetic discriminitation of specifically and spontaneously formed triazoles. In lack of a systematic theoretical discussion of these aspects in literature, an attempt to rationalize the choice of experimental conditions for *in situ* click experiments is presented in the following section.

3.5.2. Free and bound ligand

The extent of ligand binding is an important parameter for the determination of suitable conditions for an experiment, as will be outlined in the following.

Figure 3-18 (blue and red lines) illustrates the consequences of the low affinities of first- and second-site ligand for the fraction of unbound ligand. Due to the low affinity of the second-site ligand (estimated K_D = 5 mM) (160), the vast majority of second-site ligand remains in solution, independent of the concentration of the ligand added. For the first-site ligand, the fraction of free ligand remains low up to concentrations of about 75 µM but then increases more steeply. Thus, increasing the concentration of first-site ligand above 75 µM will mainly increase the concentration of free ligand.

The green lines in Figure 3-18 show the fraction of protein bound to both ligands simultaneously. As illustrated by the black rectangle, the fraction of protein bound to both ligands cannot exceed 15% due to the solubility limit of the second-site ligands. This is of relevance because the concentration of ternary complex is related to the speed of protein-mediated triazole formation (*cf.* Equation 7 in Section 3.5.3) and because the protein-assisted triazole formation is not a truly catalytic process if it leads to high-affinity ligands. These may eventually block the binding site and thus cancel the rate-accelerating effect of the protein.
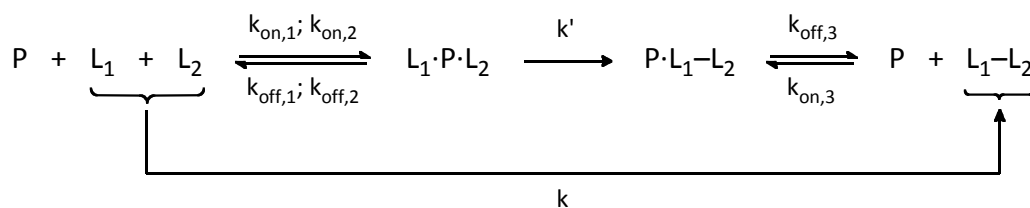
Taken together, Figure 3-18 suggests that there is a practical concentration window for performing an *in situ* click experiment and that the expected concentration of ternary complex is rather low. The consequences of this are further discussed in Section 3.5.3.
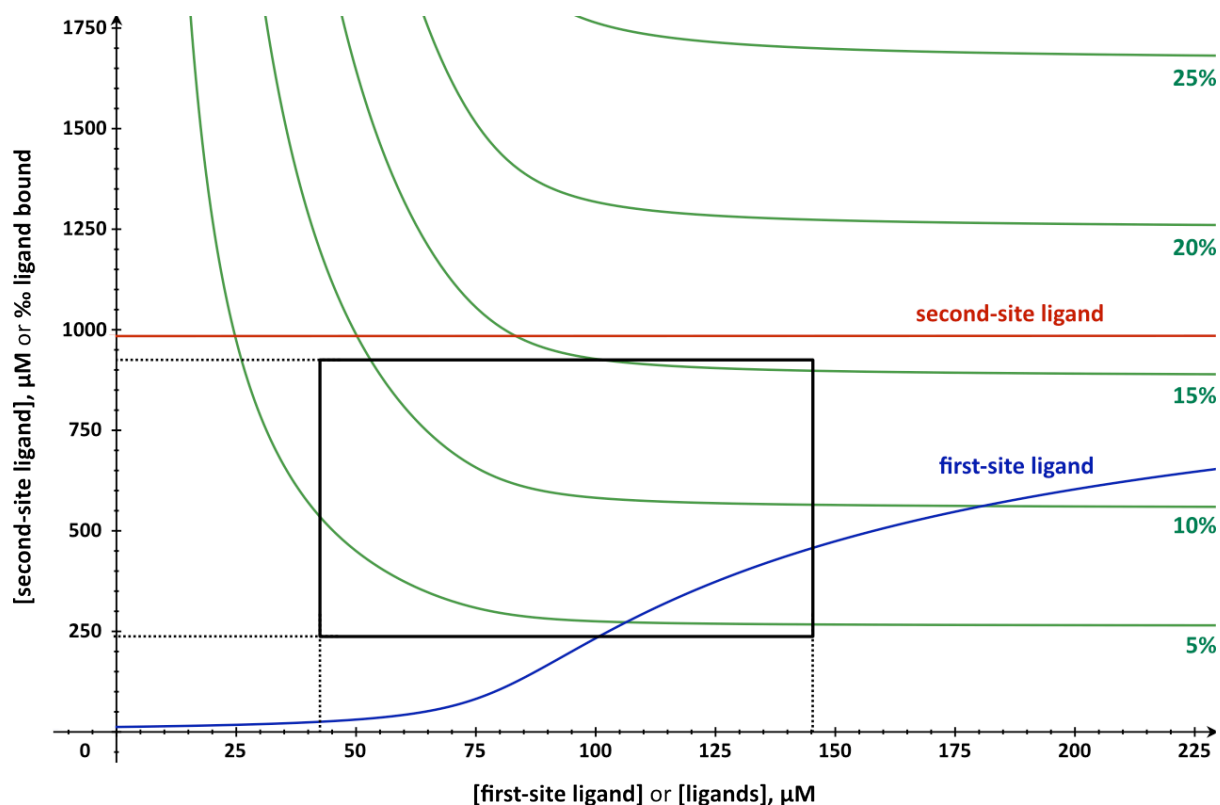
Figure 3-18. Green curves: percentages of protein bound to first- *and* second-site ligand in relation to the concentrations of first- and second-site ligand. Rectangle: accessible concentration range for the *in situ* click experiment. Blue and red curves: fraction of free first- and second-site ligand (in ‰) relative to the concentration of ligand added. Values calculated using Equations 11 and 13 with the following values: $K_D(L_1) = 1$ µM; $K_D(L_2) = 5$ mM; [P] = 80 µM.

3.5.3. Reaction kinetics

In the *in situ* click experiment, triazoles are formed *via* a protein-assisted as well as a spontaneous reaction pathway (Figure 3-19), as a significant amount of first- and second-site ligands will *not* be bound to E-selectin. Furthermore, spontaneous triazole formation will occur in the control samples containing bovine serum albumin (BSA) or buffer. To be able to detect the triazoles formed in the protein-assisted reaction, the speed v' of this reaction must be higher than the speed of the spontaneous reaction (v). Therefore, the concentrations of the ligands should be chosen in a way that leads to sufficiently high concentrations of ternary complex (*cf.* Section 3.5.2) and at the same time keeps the concentrations of free ligands as low as possible.

$$P \; + \; \underbrace{L_1 \; + \; L_2} \; \underset{k_{off,1};\, k_{off,2}}{\overset{k_{on,1};\, k_{on,2}}{\rightleftharpoons}} \; L_1 \cdot P \cdot L_2 \; \xrightarrow{\;\; k' \;\;} \; P \cdot L_1 - L_2 \; \underset{k_{on,3}}{\overset{k_{off,3}}{\rightleftharpoons}} \; P \; + \; \underbrace{L_1 - L_2}$$

$$\xrightarrow{\;\;\;\;\; k \;\;\;\;\;}$$

Figure 3-19. Reaction pathways (protein mediated and spontaneous) for triazole formation in an *in situ* click experiment. P: protein; L_1: first-site ligand; L_2: second-site ligand; $L_1 \cdot P \cdot L_2$: ternary complex; $P \cdot L_1 - L_2$: complex of protein with newly formed ligand; k: rate constant of spontaneous reaction; k': rate constant of protein-assisted reaction; k_{on}, k_{off}: association and dissociation rate constants.

In the target-templated click reaction, azide, alkyne, and the template form a ternary complex. With both reactants bound to a common scaffold, the intermolecular reaction now has the characteristics of an intramolecular one. Thus, the initial rate v' of protein-mediated triazole formation can be described by first-order kinetics (191):

$$v' = k' \, [L_1 \cdot P \cdot L_2] \tag{7}$$

This equation is only valid if $k_{on,1}$, $k_{on,2}$ and $k_{off,3} > k'$. While $k_{on,1}$ and $k_{on,2}$ are expected to fulfill this condition, $k_{off,2}$ may become rate-limiting if a high-affinity ligand $L_1 - L_2$ is formed in the process. Accordingly, Equation 7 only applies to the beginning of an experiment.

Spontaneous triazole formation is subject to second-order kinetics, *i.e.* its rate depends on the concentration of azide and alkyne. Assuming that the spontaneous reaction takes place only for free ligand ($L_{1,f}$ and $L_{2,f}$) in the E-selectin or a control sample, we obtain:

$$v = k \, [L_1]_f [L_2]_f \tag{8}$$

Because the rate of triazole formation is very slow at room temperature ($\rightarrow [L]_{tot} \gg$ [triazole]) (177, 188, 189) we can assume that $[L_1]_f$ and $[L_2]_f$ remain constant during an *in situ* click experiment.

As mentioned, for the detection of triazoles formed with the assistance of protein, the protein-mediated reaction must be faster than the spontaneous reaction, *i.e.* v' > v or:

$$k' \, [L_1 \cdot P \cdot L_2] > k \, [L_1]_f [L_2]_f \tag{9}$$

Or, upon rearrangement:

$$\frac{k'}{k} > \frac{[L_1]_f [L_2]_f}{[L_1 \cdot P \cdot L_2]} = EM_{min} \tag{10}$$

Equation 10 allows the quantitative comparison of different experimental setups by evaluating the ratio $[L_1]_f [L_2]_f/[L_1 \cdot P \cdot L_2]$, which should be kept as low as possible. The ratio k'/k, or effective molarity (EM), is commonly used for quantifying the catalytic efficiency of supramolecular systems. It has the unit M and corresponds to the concentration of one of the reactants required for the pseudo-first-order *inter*molecular reaction to proceed with the same rate like the reaction in the presence of the supramolecular catalyst (191). Hence, the ratio $[L]_f [L_2]_f/[L_1 \cdot P \cdot L_2]$ corresponds to the minimal EM value (EM_{min}) required for detecting triazoles formed in the protein-assisted reaction. Besides its usefulness for experimental optimization, the minimally required EM value can also be used to compare the present system to other supramolecular systems described in literature (*cf.* Section 3.5.5).

To calculate the concentrations of free ligand, the fraction of bound ligand ($x_{L,b}$) is determined (217). (Note: Divided by 2, the numerator in Equation 11 corresponds to the concentration of ligand–protein complex $[L_i \cdot P]$. For the following calculations, a 1:1 binding mode is assumed.):

$$x_{P,b} = \frac{K_D + [P]_{tot} + [L]_{tot} - \sqrt{(K_D + [P]_{tot} + [L]_{tot})^2 - 4\,[L]_{tot}[P]_{tot}}}{2\,[L]_{tot}} \qquad (11)$$

Which leads to Equation 12 for the concentration of free ligand:

$$[L]_f = (1 - x_{L,b})\,[L]_{tot} \qquad (12)$$

Likewise, the concentration of ternary complex is calculated. Equation 14 shows that a high protein concentration is desireable for the *in situ* click experiment.

$$x_{P,b} = \frac{K_D + [P]_{tot} + [L]_{tot} - \sqrt{(K_D + [P]_{tot} + [L]_{tot})^2 - 4\,[L]_{tot}[P]_{tot}}}{2\,[P]_{tot}} \qquad (13)$$

$$[L_1 \cdot P \cdot L_2] = x_{P,b,1} \cdot x_{P,b,2} \cdot [P]_{tot} \qquad (14)$$

These equations were used to evaluate suitable experimental conditions, as outlined in the following section.

### 3.5.4. Determination of suitable experimental conditions

As mentioned, the minimal EM_{min} and the the concentration of ternary complex are crucial for a succesful *in situ* click experiment. Figure 3-20 shows how these parameters depend on the concentration of first-site ligand. As already indicated in Figure 3-18, increasing the

concentration of first-site ligand above approx. 60 μM leads to steep increase of EM_{min}, whereas the concentration of ternary complex is not further increased. In contrast to this, an increase of protein concentration leads to both a reduction of the EM_{min} values and increased concentrations of ternary complex. Consequently, adding the protein in excess is expected to be beneficial, as, theoretically, this would allow to keep most of the first-site ligand protein-bound.
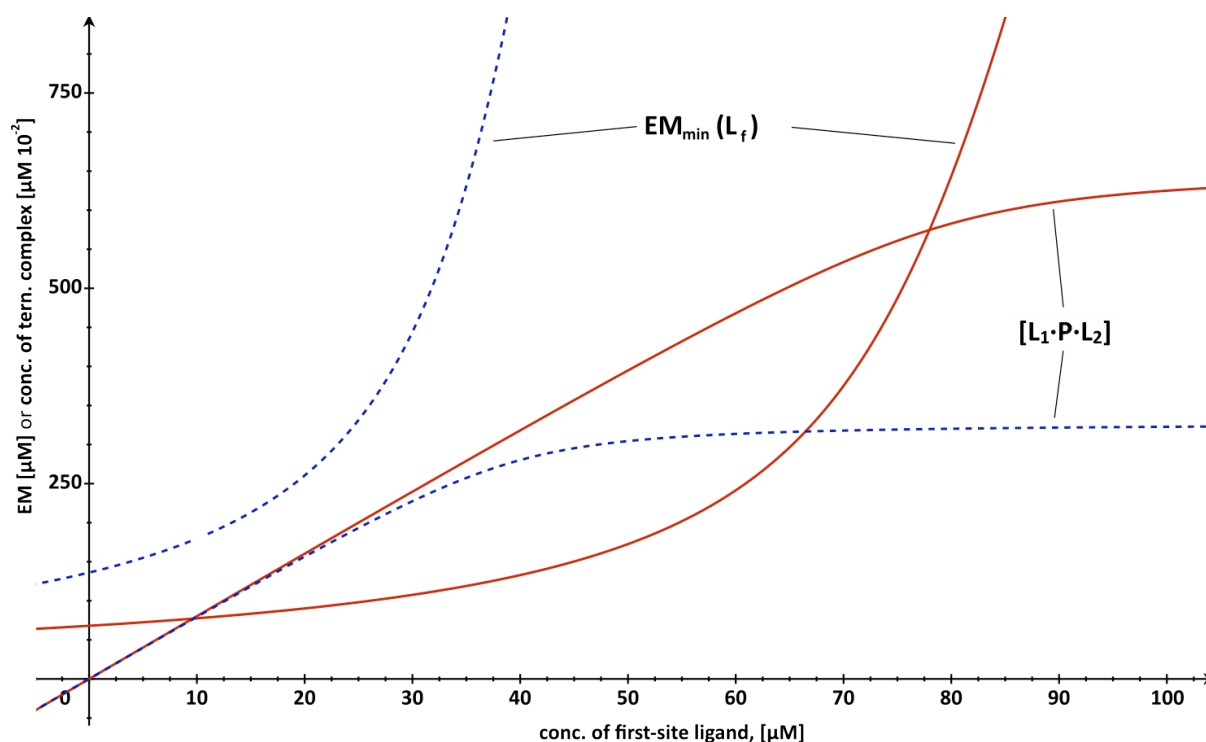
Figure 3-20. Plot of $[L_1 \cdot P \cdot L_2]$ (unit: μM $\times 10^{-2}$; calculated using Equation 14) and $EM_{min}(L_f)$ (unit: μM; calculated using Equations 12 and 14; L_f: free ligand in the sample containing active protein) relative to the concentration of first-site ligand. Red lines: protein concentration of 80 μM; dashed blue lines: protein concentration of 40 μM. Concentration of second-site ligand: 450 μM.

Figure 3-21 illustrates that changes of $[L_2]$ (straight lines) have a much smaller influence on EM_{min} and $[L_1 \cdot P \cdot L_2]$ than changes of $[L_1]$ (dotted lines). Therefore, the concentration of first-site ligand must be adjusted more carefully than the one of the second-site ligand.
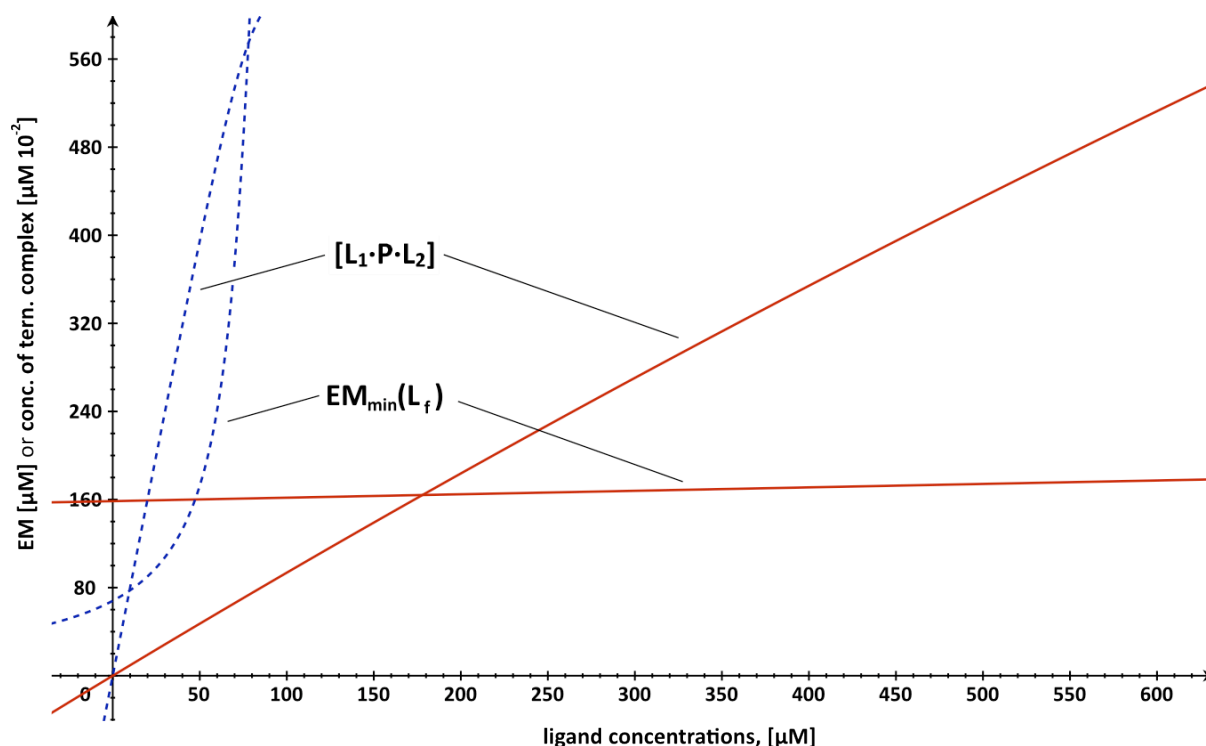
Figure 3-21. Comparison of the effect of [L₁] (dashed blue lines) and [L₂] (red lines) on [L₁·P·L₂] (unit: μM ×10⁻²) and EM$_{min}$(L$_f$). For the calculations (*cf.* Figure 3-20), either the value of [L₁] or [L₂] was kept constant. [L₁] = 50 μM; [L₂] = 450 μM.

Figure 3-21 shows the EM$_{min}$ values for the differentiation of a protein-mediated reaction *within* the reaction vessel containing active protein. This situation corresponds to a multi-component experiment, where a mixture of substrates is investigated. However, when comparing the active protein sample to the control samples, the situation is different, because there the ligands are not protein-bound and therefore the rate of spontaneous triazole formation is higher in the control samples. Figure 3-22 shows the EM$_{min}$ values required for a differentiation of active protein (→ EM$_{min}$(L$_f$)) and control (→ EM$_{min}$(L$_{tot}$)) samples. For the calculation of EM$_{min}$(L$_{tot}$), the total ligand concentration is divided by the concentration of ternary complex (Equation 15):

$$EM_{min}(L_{tot}) = \frac{[L_1]_{tot}[L_2]_{tot}}{[L_1 \cdot P \cdot L_2]} \tag{15}$$
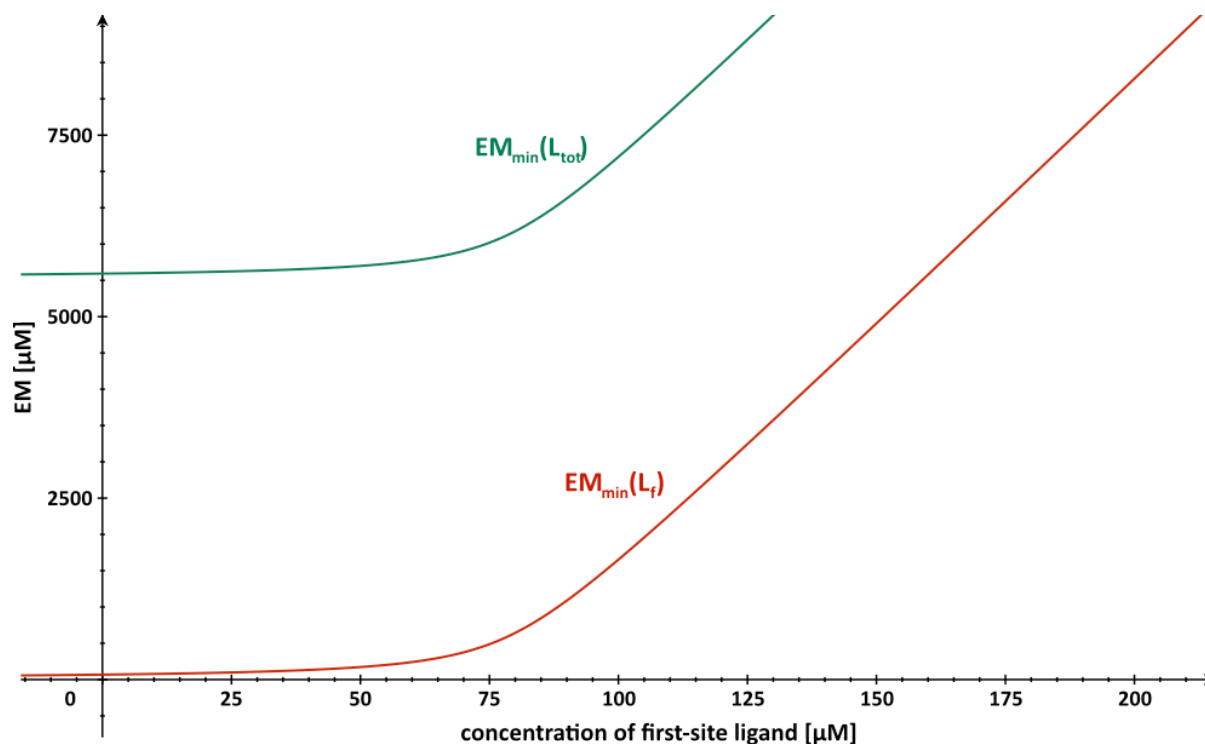
Figure 3-22. Comparison of EM_{min} values for the active protein sample ($EM_{min}(L_f)$, red) and for the control samples ($EM_{min}(L_{tot})$, green); $[L_2] = 450$ μM.

As $EM_{min}(L_{tot})$ is more than a factor of 30 higher than $EM_{min}(L_f)$, multicomponent experiments are considered beneficial in terms of the detectability of specifically formed triazoles.

In such an experiment there is, however, competition for the binding site between the different ligands, which causes a drop of $[L_1 \cdot P \cdot L_2]$ and an increase of $EM_{min}(L_f)$. In the following, a way of estimating the extent of this effect is described.

As the concentration of second-site ligands has a much smaller influence on the relevant parameters (*cf.* Figure 3-18 and Figure 3-21), it should be beneficial to perform the *in situ* click experiment with different second-site ligands. Given that there is a maximal *total* nitroindole concentration (The solubility of a ternary mixture of nitroindoles (**P28c, P28d, P28b**) in HEPES buffer + 5% DMSO was found to be < 675 μM.) and that the different nitroindoles compete for the binding site, the ratio of free to bound second-site ligand can be estimated as follows (n: number of nitroindole components; $x_{n,i}(P)$: fraction of protein bound to ligand **i** with n nitroindole components; $x_{n,i}(L_f)$: fraction of free ligand **i** for n nitroindole components):

With n second-site ligands, the *total* concentration of a ligand **i** is reduced by a factor n due to the total solubility limit. Thus, $x_{n,i}(P)$ is reduced by a factor of approximately n (assuming a

linear relationship between concentration and ligand binding, which is realistic in the case of the nitroindoles). Additionally, there is competition for the binding site, which reduces $x_{n,i}(P)$ by another factor of n (assuming identical K_Ds for all ligands).

$$x_{n,i}(P) \approx \frac{x_{1,i}(P)}{n^2} \tag{16}$$

With n second-site ligands, the concentration of a ligand **i** *in solution* is reduced by a factor n due to the total solubility limit. As the binding affinity of the second-ligand is very low, the fraction of bound ligand can be neglected here.

$$x_{n,i}(L_f) \approx \frac{x_{1,i}(L_f)}{n} \tag{17}$$

Upon rearrangement, we obtain the following relationship:

$$\frac{x_{n,i}(L_f)}{x_{n,i}(P)} \approx n \frac{x_{1,i}(L_f)}{x_{1,i}(P)} \tag{18}$$

Equation 18 indicates that the ratio of free to bound ligand becomes less favorable with an increasing number of components, and hence EM_{min} increases as well. For example, doubling the number of components will double the ratio of free ligand fraction to bound protein fraction.

3.5.5. Discussion

The findings of the previous section were used to calculate the EM_{min} for different ligand concentrations. For comparison, the EM_{min} of Sharpless' *in situ* click experiments and of Mock's cucurbituril studies were determined (Table 3-6).

Table 3-6. Calculated EM_{min} values and concentrations of ternary complex ($[L_1 \cdot P \cdot L_2]$) for different proteins and for cucurbituril. A: E-selectin; B: acetylcholinesterase (AChE); range of K_Ds given in (177), highest value chosen for calculation; C: AChE (179); D: AChE (180); E: carbonic anhydrase II; $K_{D,2}$: "high micromolar affinities and above" (181); F: HIV-1 protease; $K_{D,1}$: $IC_{50} > 100$ μM, $K_{D,2}$: IC_{50} = 4.2 μM (184); G: cucurbit[6]uril; range of concentrations given in (189), intermediate values chosen for calculation. All values are in μM.

	A1	A2	A3	B	C	D	E	F	G
[L$_1$]	500	50	50	30	4.6	4.6	60	500	60'000
[L$_2$]	450	450	450	66	24	24	400	100	12'000
$K_{D,1}$	1.0	1.0	1.0	0.1	0.018	0.023	0.037	150	650
$K_{D,2}$	5'000	5'000	5'000	100	1.1	34	500	4.2	2'500
[P]	80	80	40	1.0	1.0	1.0	30	15	5'000
[L$_1$·P·L$_2$]	8.4	4.0	3.0	0.4	0.9	0.4	13	11	3'784
EM$_{min}$(L$_f$)	28'659	172	1'890	4'820	87	203	889	3'827	118'897
EM$_{min}$(L$_{tot}$)	34'604	5'699	7'391	5'015	116	265	1'836	4'570	190'276

With EM_{min} values differing by factor of 167 and 6, cases A1 and A2 demonstrate the importance of selecting appropriate ligand concentrations: For the detection of a catalytic effect, the rate of protein-mediated triazole formation needs to be substantially higher in case A1 than in case A2. As illustrated by A3, reducing the protein concentration by a factor of 2 leads to an increase of EM_{min} by factors of 11 and 1.2.

For the optimized conditions in case A2, $EM_{min}(L_f)$ is 33 times smaller than $EM_{min}(L_{tot})$. In other words, in an ISC experiment with multiple components it is easier to detect a specific effect of E-selectin. However, as Equation 18 shows, multicomponent reactions have less favorable ratios of free ligand to ligand-bound protein, which also lowers $EM_{min}(L_f)$. Therefore, the number of components should be limited for first proof-of-concept experiments.

Cases B to F correspond to experiments of Sharpless and Mock, where actually a catalytic effect of the supramolecular template (a protein or cucurbituril) was observed. The EM_{min} values of these experiments are similar to or in some cases even considerably higher than the ones obtained in A2. Therefore, the conditions chosen in A2 should be suitable for an *in situ* click experiment, provided that E-selectin is a sufficiently efficient supramolecular catalyst.

In a review of 16 different supramolecular catalysts in two-substrate reactions, Mandolini found EM values ranging from 10^{-3} to 10^{4} M (191). As the EM_{min} in Table 3-6 range from 10^{-5} to 10^{-2} M, it appears that, in general, supramolecular catalysts are quite likely efficient enough to allow detection of protein-mediated product formation in setups as used here. Interestingly, the most efficient supramolecular catalysts in this analysis mediated the (regiospecific) cycloaddition of an alkyne and an azide. The previously mentioned cucurbituril (see above) exhibited an EM as high as 16'000 M, and for a different encapsulation system catalyzing the cycloaddition between phenylacetylene and phenylazide (218), an EM of 120 M was found. Tight encapsulation of the substrates is a common feature of these two supramolecular systems and may explain their high catalytic efficiency. Menger suggested a "spatiotemporal prinicple" to rationalize the rate acceleration in intramolecular reactions (219). According to this principle, *"the rate of reaction between functionalities A and B is proportional to the time that A and B reside within a critical distance"*. Consequently, the high EMs observed in two examples mentioned above may result from the host system's ability to hold the substrates together in critical distance for a sufficient amount of time.

3.5.6. Conclusions

In this analysis, the kinetics of spontaneous and protein-mediated triazole formation were investigated on a theoretical basis. A new paramenter (EM_{min}) that allows the evaluation and comparison of different experimental conditions, was introduced and was used to optimally adjust ligand and protein concentrations for an ISC experiment. Furthermore, single and multicomponent reactions were compared with respect to the fractions of free ligand, and it was shown that EM_{min} values become less favorable with increasing numbers of components.

The EM_{min} values obtained for the experiments with E-selectin are within the range of the values obtained for experiments from literature. Provided E-selectin can act as a supramolecular catalyst of triazole formation the conditions chosen should thus be suitable for the detection of a catalytic effect.
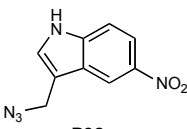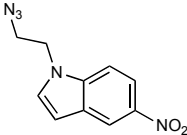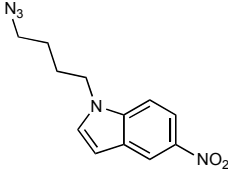
3.6. *In situ* click experiments

3.6.1. Preliminary experiments

3.6.1.1. Solubility of second-site ligands

Before starting the *in situ* click (ISC) experiments, the solubility of several fragments was roughly estimated by visually assessing precipitation of the nitroindoles from a buffer solution with 5% DMSO (Table 3-7). The actual solubility is expected to be lower than these values, which was suggested by the findings presented in Section 3.6.6.1.

Table 3-7. Approximate upper concentration limits in buffer (10 mM HEPES, 150 mM NaCl, 1 mM CaCl$_2$, pH 7.4) containing 5% DMSO.

compound	solubility [mM]
P32a	< 1
P28b	< 0.625
P28d	< 0.625

3.6.1.2. Fragmentation of triazole antagonists/Determination of the linker pattern

In a multicomponent ISC experiment, many different products may be formed (Scheme 3-6). Ideally, their structure should be assignable directly after the HPLC-MS run, which is aggravated by the fact that, depending on the alkyne–azide mixture, several isomers of identical mass can be formed.
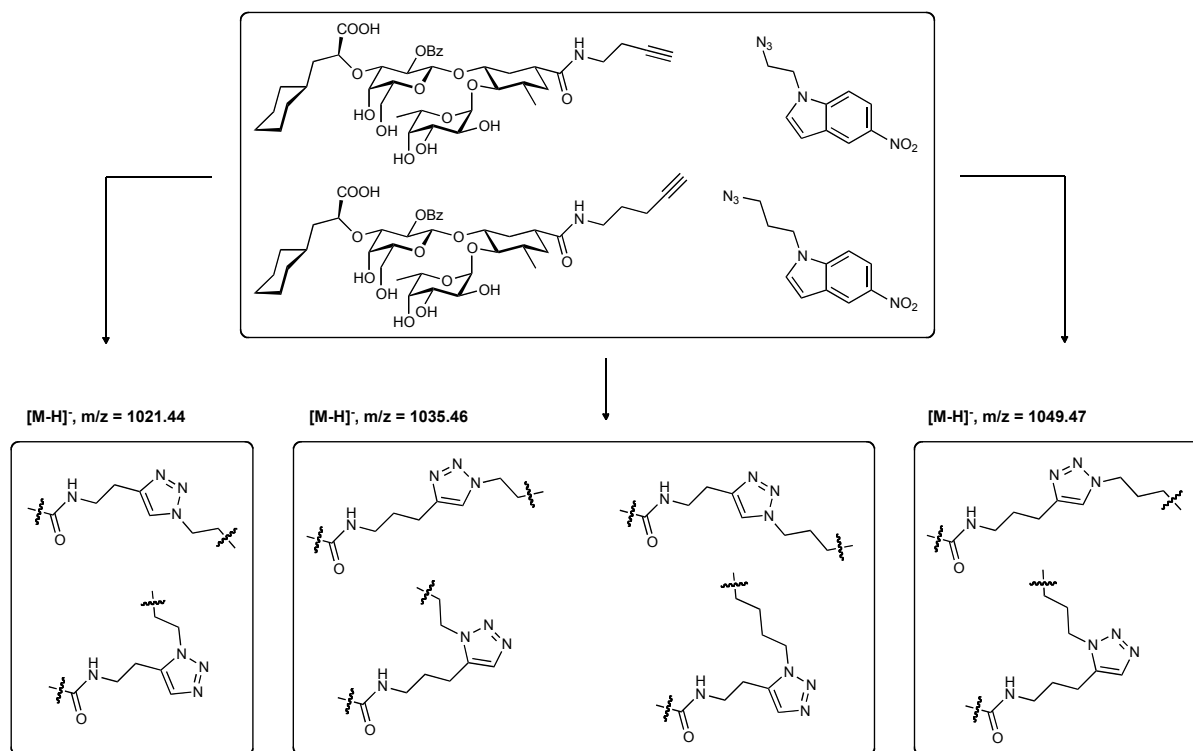
Scheme 3-6. Possible products formed from the reaction of alkynes **P26b** and **P26c** with azides **P28b** and **P28c**.

One way of structure assignment consists of comparing the observed retention times to the ones of known triazoles. This is quite straightforward as the synthesis of the triazoles can be performed on analytical scale (*cf.* Section 3.6.5). Due to the different spatial arrangement of the substituents in *syn* and *anti* triazoles, these may be well differentiable based on retention times (177), which is expected to be more difficult for ligand isomers where just the position of the triazole moieties differs (*e.g.* in the triazoles with m/z = 1035.5 in Scheme 3-6). As a solution to this, Ernst and coworkers (160) used HPLC-MS/MS to generate fragment ions characteristic for a certain linker pattern.

Following this approach, a product ion scan in the negative ionization mode (*cf.* Figure 1-27) revealed two characteristic fragments of **P38** (m/z = 413.2, m/z = 249.1) containing information about the linker pattern (Scheme 3-7). In single reaction monitoring mode, optimal fragmentor voltages and collision energies for fragmentation were determined (Table 3-8 and Figure 3-23). About 3 times higher maximal signal intensities were found for the fragment with m/z = 413.2.

Table 3-8. Optimized fragmentor voltages and collision energies for **P38**.

	positive mode	negative mode
fragmentor voltage [V]	170	290-300
collision energy [V]	n.d.	m/z 413.2: 50 m/z 249.1: 70
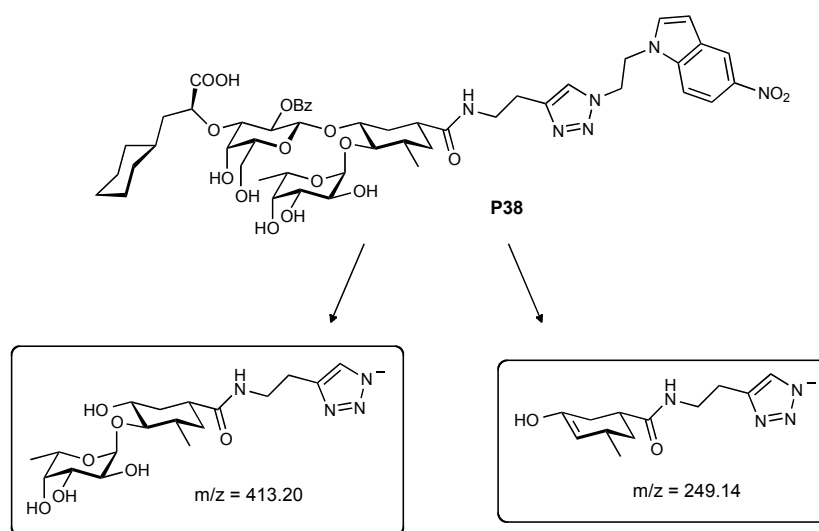
Scheme 3-7. MS/MS experiment with **P38**. Fragmentation of the precursor ion **P38** (m/z = 1021.5, negative mode) at a fragmentor voltage of 290 V and at collision energies of 70 V (top) and 50 V (bottom).
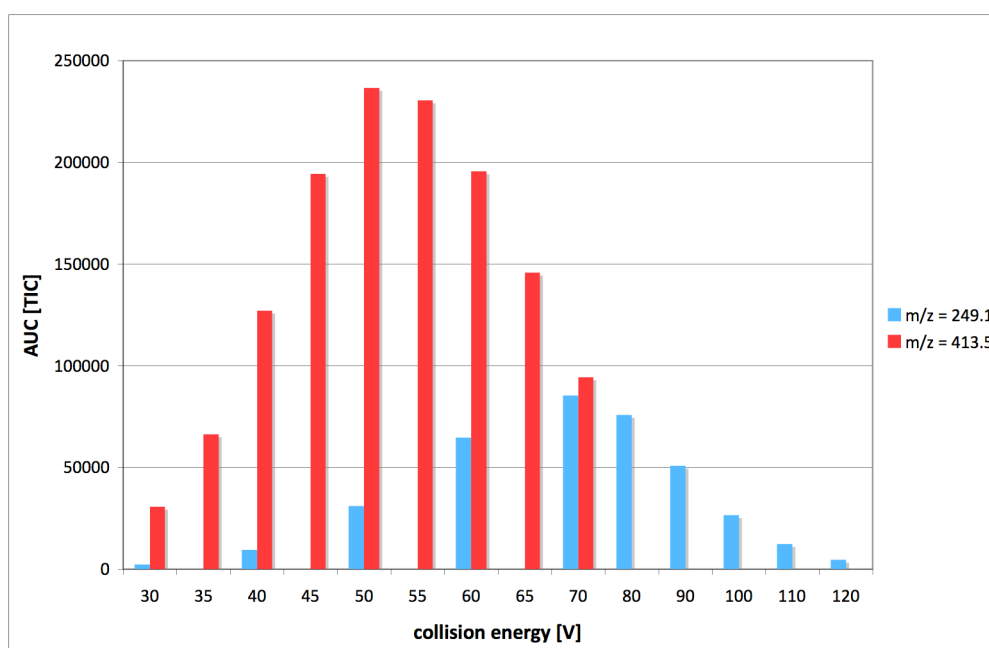
Figure 3-23. Abundancy of product ions with m/z = 249.1 and m/z = 413.5 plotted against different collision energies.

3.6.2. Experimental setup of *in situ* click experiments

Further experimental details are given in Section 5.1.2.

3.6.2.1. Sample preparation

Figure 3-24 shows the typical workflow of an *in situ* click (ISC) experiment. As the required protein concentrations were high (40-80 µM), the reaction volume was restricted to 50 µL, allowing 5 measurements per experiment. The reactions were shaken at 20 °C and not at 37 °C as previously reported (160, 177, 179-181, 183, 184) to prevent the evaporation of water, which aggravates sustaining stable experimental conditions and may have led to protein denaturation due to concentration of the solutions. For the MS measurements, 10 µL of sample were pipetted into 40 µL of water + 0.1% HCOOH, and the mixture was subsequently analyzed by HPLC-MS. This dilution step was introduced to reduce pipetting errors caused by the small liquid volumes.
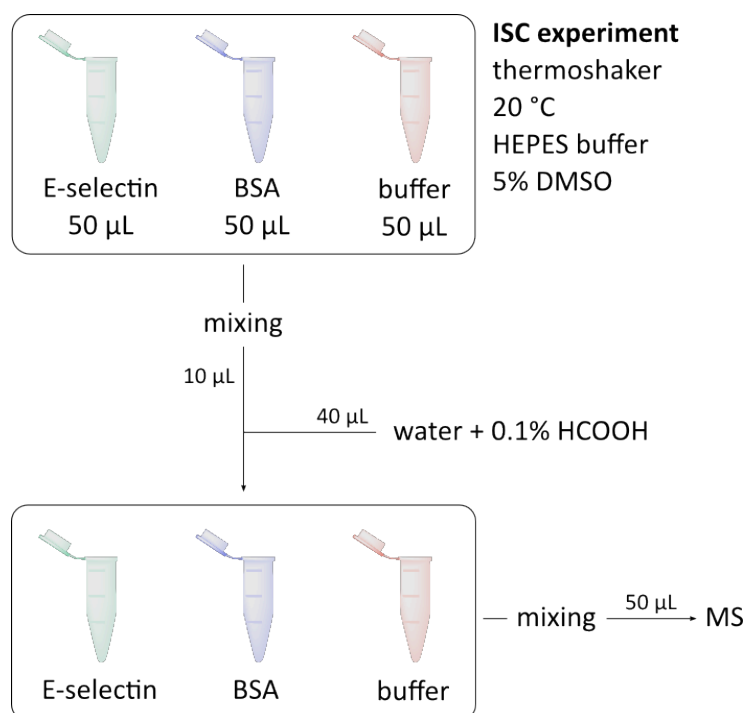
Figure 3-24. Schematic representation of the standard sample preparation before injection into the MS. HEPES buffer: HEPES 10 mM (pH 7.4), NaCl 150 mM, CaCl$_2$ 1 mM.

The suitability of this sample workup procedure is demonstrated by experiments described in Section 3.6.5.8.

3.6.2.2. HPLC-MS method

Figure 3-25 summarizes the HPLC-MS method used for the analysis of the samples.

The MS was run in negative ionization mode. While sensitivity would have been higher in the positive ionization mode, it was found that the selectivity in the positive mode was insufficient, leading to a frequent occurrence of nonspecific signals. Single ion monitoring was used (*cf.* Figure 1-27E) to increase both sensitivity and selectivity.

As a control, the starting materials were monitored along with the triazoles, the first-site ligands by MS and the second-site ligands using the diode array detector (DAD). The MS analysis was restricted to separate time windows where the elution of the starting materials and the triazoles occurred. The use of separate time windows reduces the wear and unnecessary contamination of the MS and increases sensitivity. Additionaly, for enhanced sensitivity in the time window for triazole detection, the electron multiplier voltage (Δ EMV) was set to 1000 V (higher values of Δ EMV correspond to higher sensitivity).
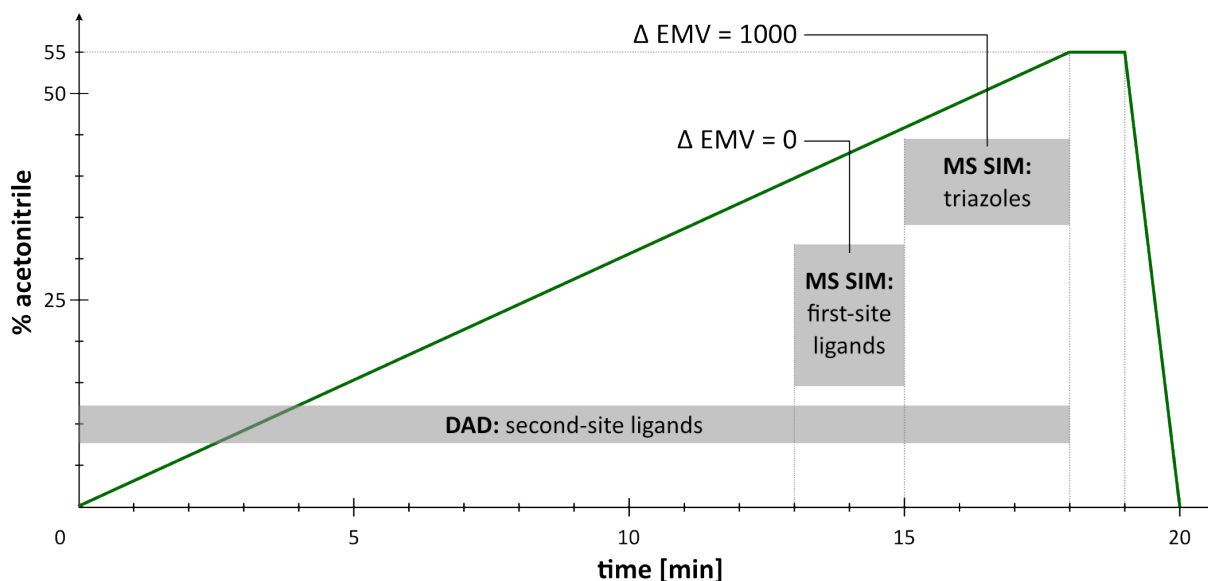
Figure 3-25. Schematic representation of the standard HPLC-MS method used for the analysis of ISC and ISCtest experiments. Green line: gradient (percent of acetonitrile + 0.1% HCOOH in the eluent); the grey squares represent time windows during which the indicated detection method was used; DAD: diode array detector; MS SIM: mass spectrometry, single ion monitoring; EMV: electron multiplier voltage.

3.6.3. *In situ* click experiments

The components of the ISC experiments were chosen based on the Biacore affinity ranking of the *anti* triazole antagonists (133) to detect possible differences in the rate of triazole formation that may result from differences in preorganization between more and less potent

ligands. *I.e.*, alkynes and azides leading to *anti* antagonists with a $K_D > 89$ nM and *anti* antagonists with a $K_D < 89$ nM were preferentially chosen. Furthermore, the components were selected to result in products with different mass or in the least possible number of products with identical mass.

In the following sections, representative chromatograms of the ISC experiments are shown. For each experiment, a rationale and a short discussion is given.

3.6.3.1. *In situ* click experiment 1 (ISC1)
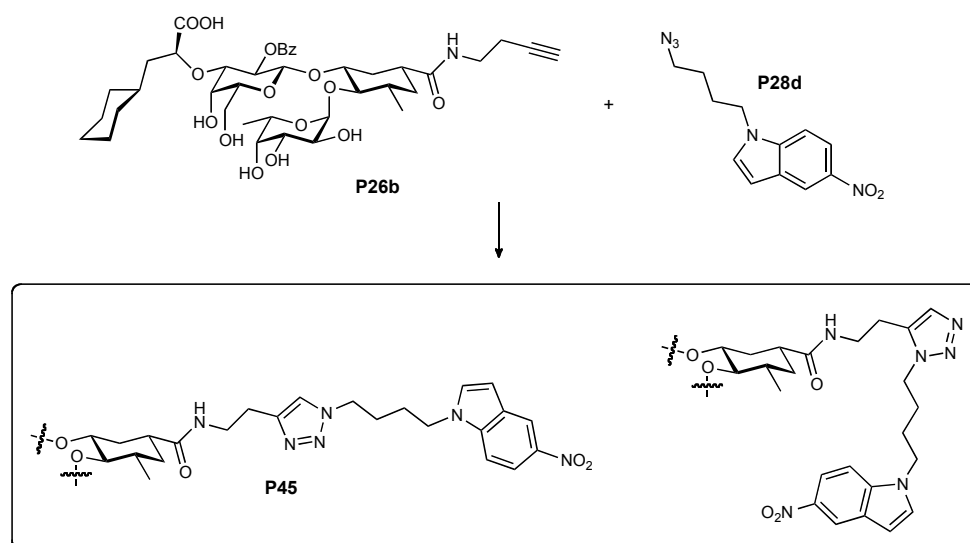
Scheme 3-8. ISC1: P26b: 50 μM; P28d: 450 μM; protein: 81 μM; 20 °C.

Rationale:

The protein-mediated reaction between **P26b** and **P28d** may lead to formation of the high-affinity *anti* triazole **P45** ($K_D = 49$ nM).

Discussion and conclusions:

There was no accelerated triazole formation in the E-selectin sample. The cycloaddition proceeded faster in the two samples containing protein. The *syn* and *anti* isomers appear to have identical retention times.

reference (P45)

P45

ISC1a
E-selectin
192 h
m/z = 1049.5

ISC1b
BSA
192 h
m/z = 1049.5

ISC1c
buffer
192 h
m/z = 1049.5
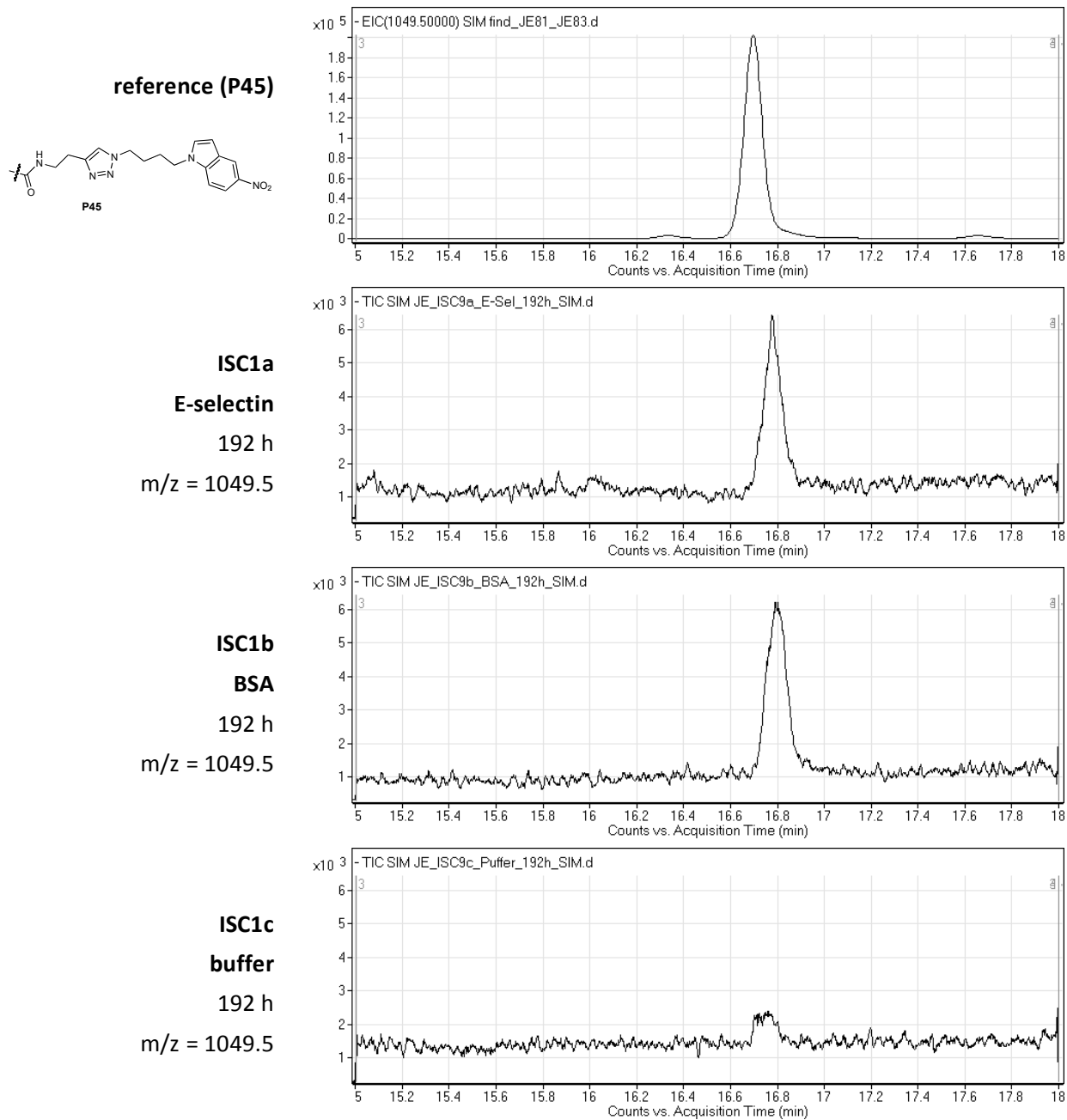
Figure 3-26. Representative chromatograms of ISC1.

3.6.3.2. *In situ* click experiment 2 (ISC2)
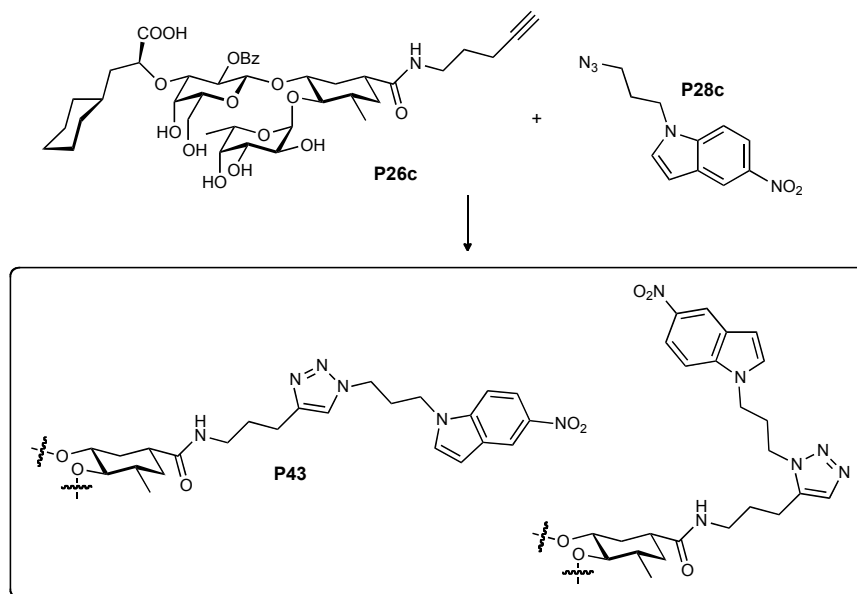
Scheme 3-9. ISC2: **P26c**: 50 µM; **P28c**: 450 µM; **protein**: 80 µM; 20 °C.

Rationale:

The protein-mediated reaction between **P26c** and **P28c** may lead to formation of the high-affinity *anti* triazole antagonist **P43** (K_D = 30 nM).

Discussion and conclusions:

There was no accelerated triazole formation in the E-selectin sample. Interestingly, only in the BSA sample detectable amounts of triazole were formed.

reference (P43)

ISC2a

E-selectin

79 h

m/z = 1049.6

ISC2b

BSA

79 h

m/z = 1049.6

ISC2c

buffer

79 h

m/z 1049.6
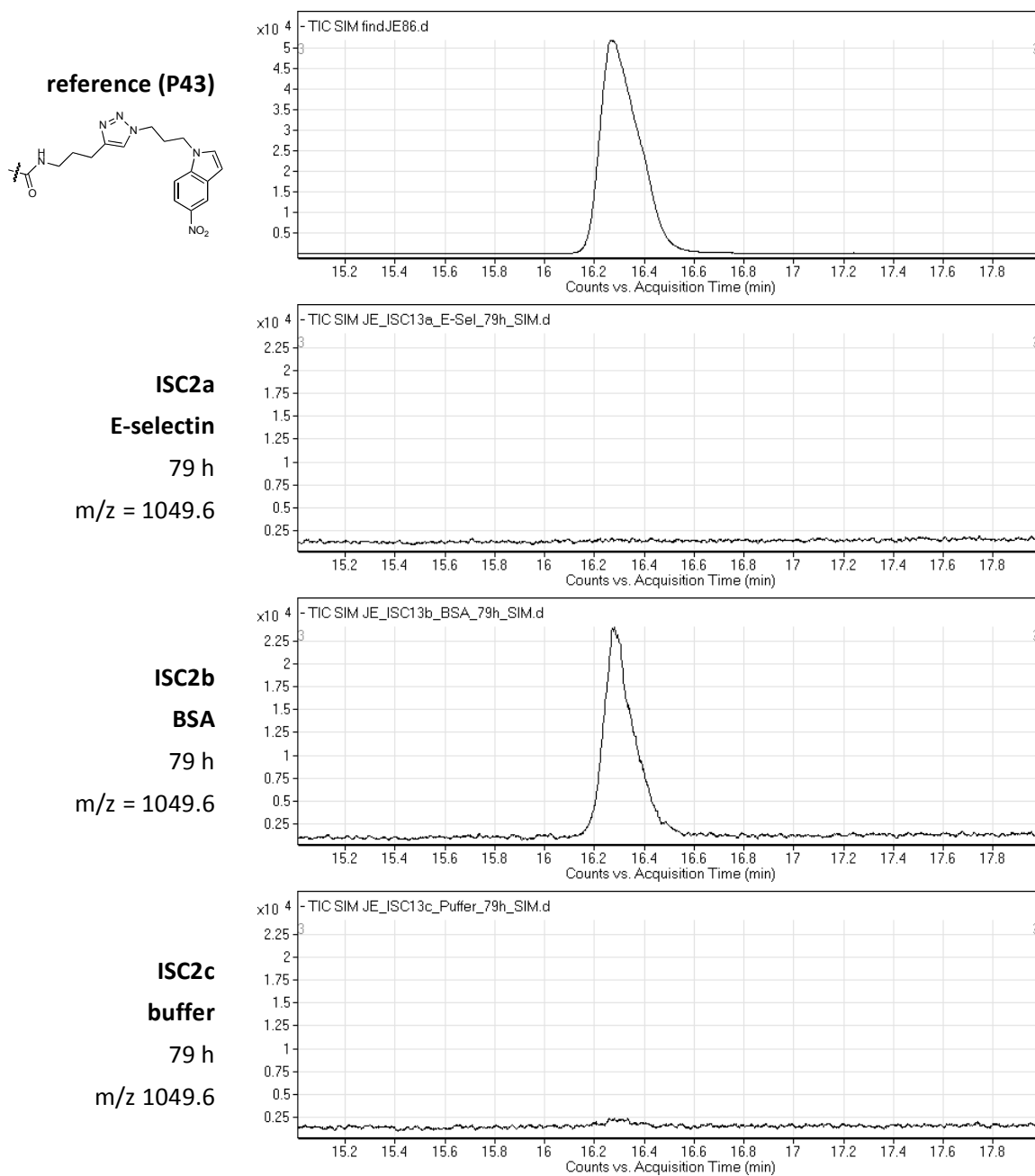
Figure 3-27. Representative chromatograms of ISC2. Note: The peak tailing in the reference chromatogram was caused by a worn pre-column.

3.6.3.3. *In situ* click experiment 3 (ISC3)
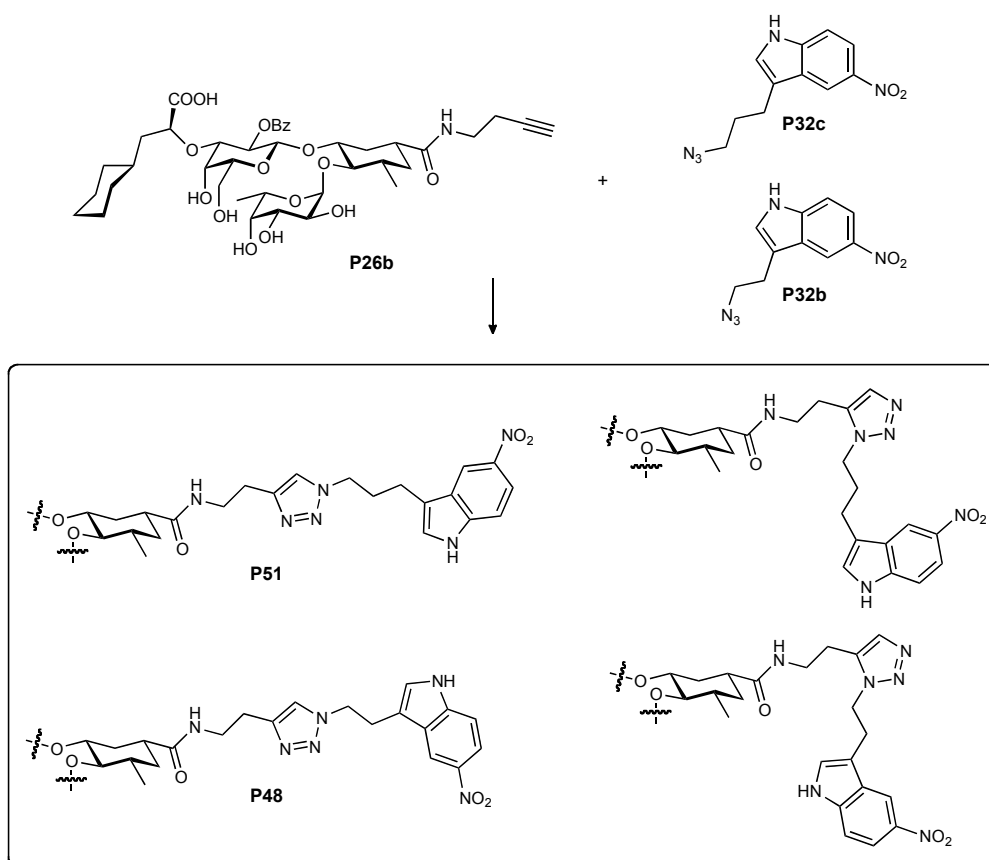
Scheme 3-10. ISC3: **P26b**: 50 µM; **P32b**: 250 µM; **P32c**: 250 µM; protein: 80 µM; 20 °C.

Rationale:

In ISC3, *anti* triazole antagonist **P51** (K_D = 50 nM) may be formed preferentially over *anti* triazole antagonist **P48** (K_D > 89 nM).

Conclusions:

In none of the samples, any triazoles were detected at a significant level. Thus, in this experiment, no catalytic effect of E-selectin could be shown.
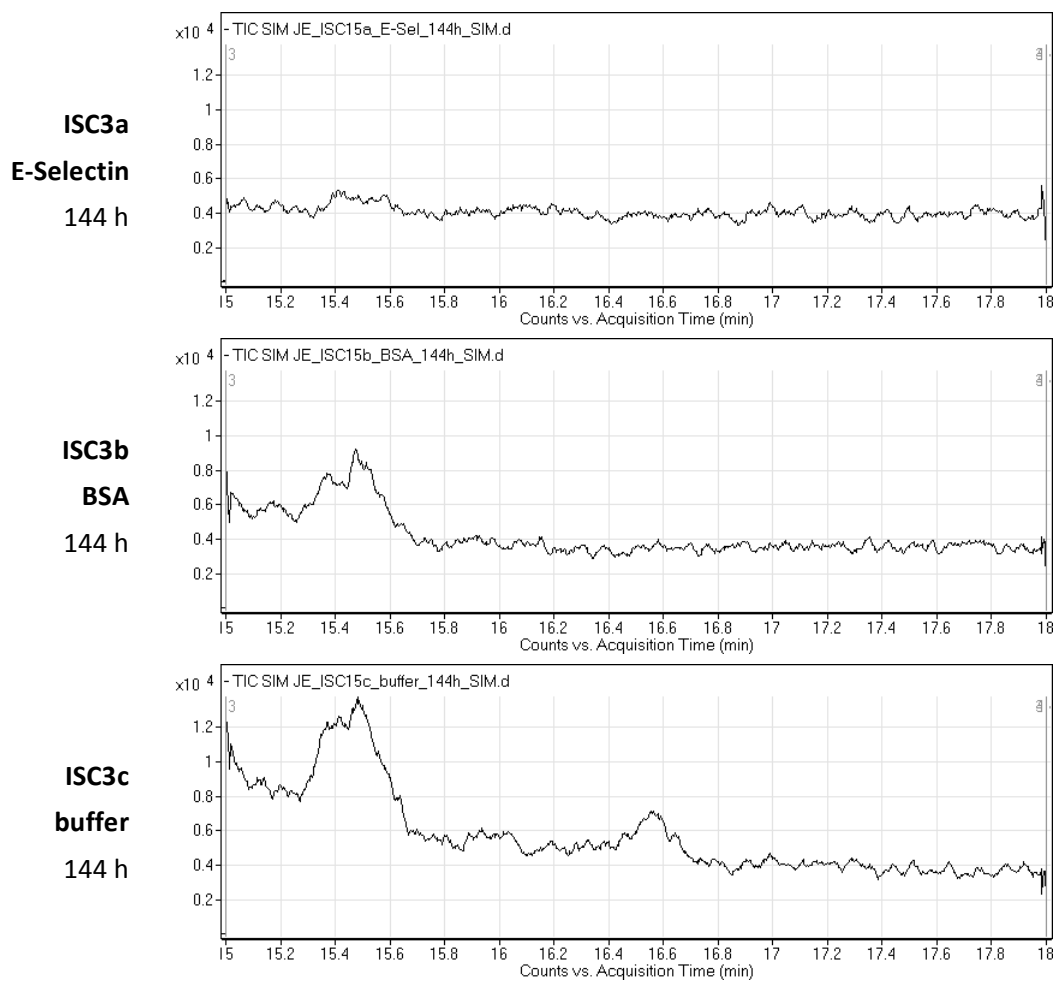
Figure 3-28. Representative chromatograms of ISC3.

154

3.6.3.4. *In situ* click experiment 4 (ISC4)
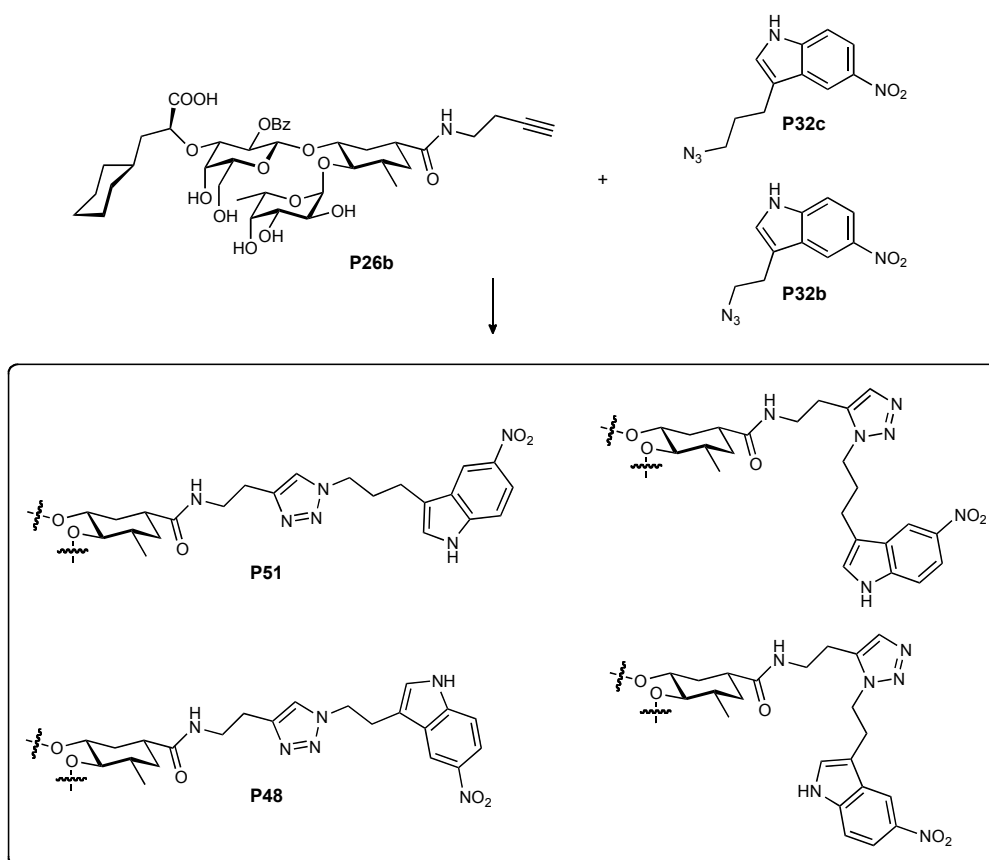
Scheme 3-11. ISC4: **P26b**: 500 μM; **P32b**: 250 μM; **P32c**: 250 μM; protein: 80 μM; 20 °C.

Rationale:

The components of ISC4 were the same as in ISC3. However, a higher concentration of first-site ligand (500 μM instead of 50 μM) due to the low signal intensity observed in ISC3.

Conclusions:

As can be seen from Figure 3-29, the bovine serum albumin (BSA) sample shows a slightly different peak pattern than the E-selectin and buffer samples, and the rate of triazole formation is considerably higher. As the peak patterns of the buffer and the E-selectin sample are identical, this experiment does not indicate any specific effect of E-selectin. According to the reference chromatogram from ISCtest8, the two peaks correspond to the *syn* and *anti* isomers of the 2s/a3C series.
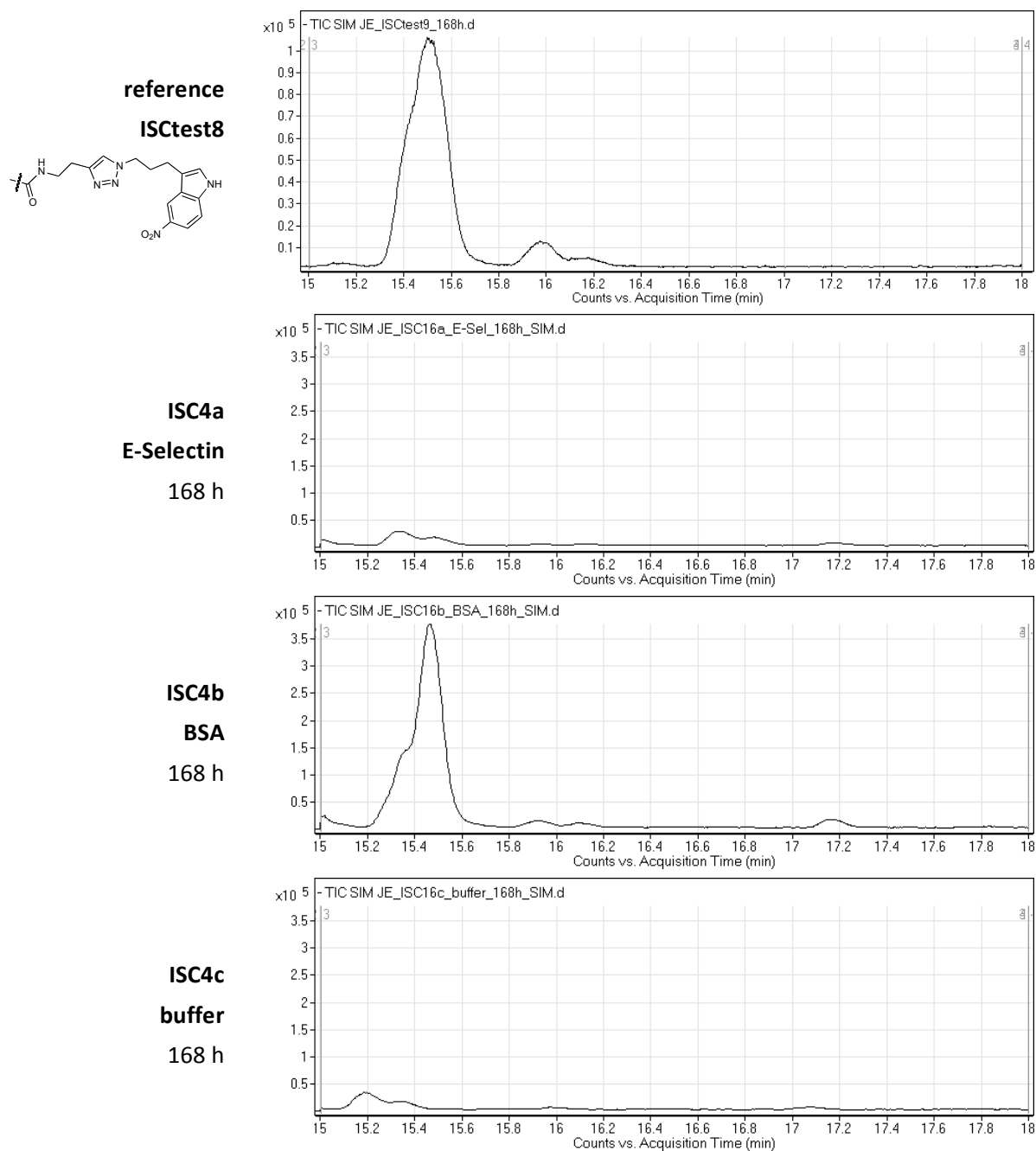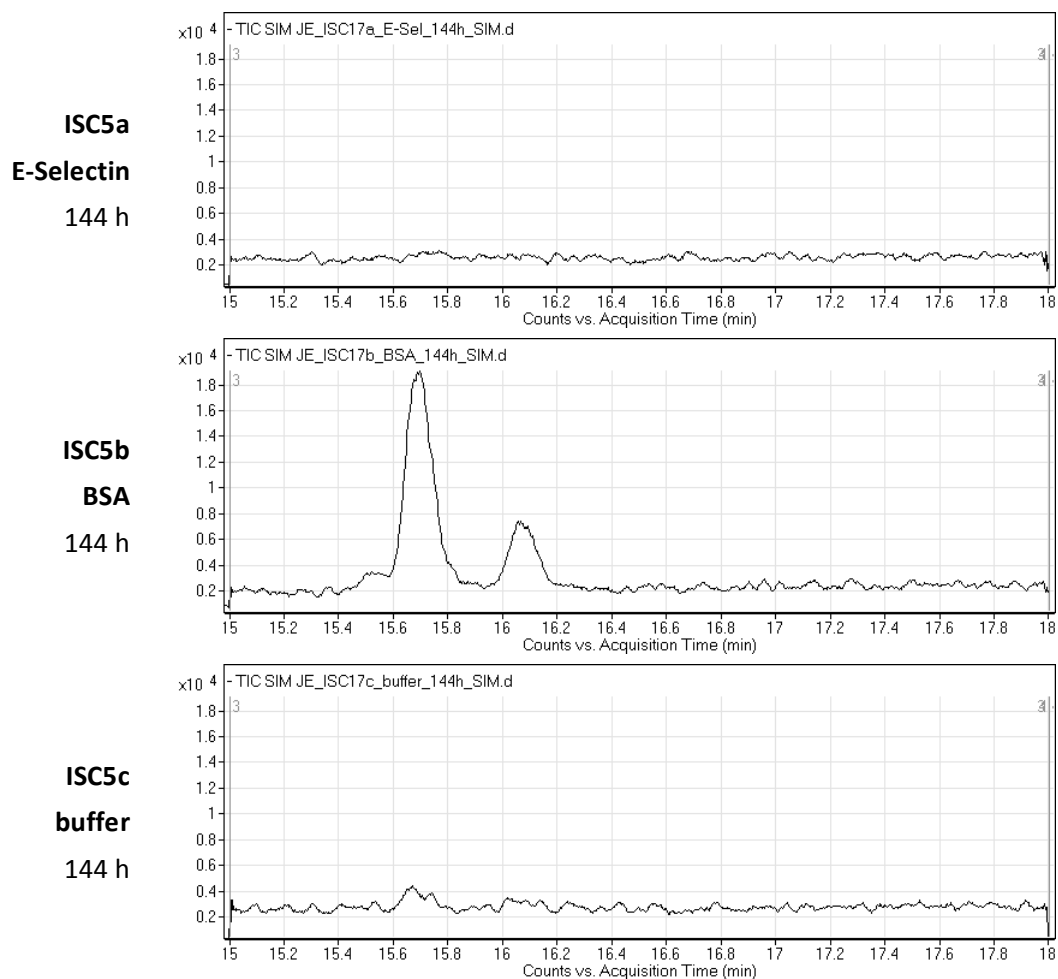
Figure 3-29. Representative chromatograms of ISC4.

3.6.3.5. *In situ* click experiment 5 (ISC5)
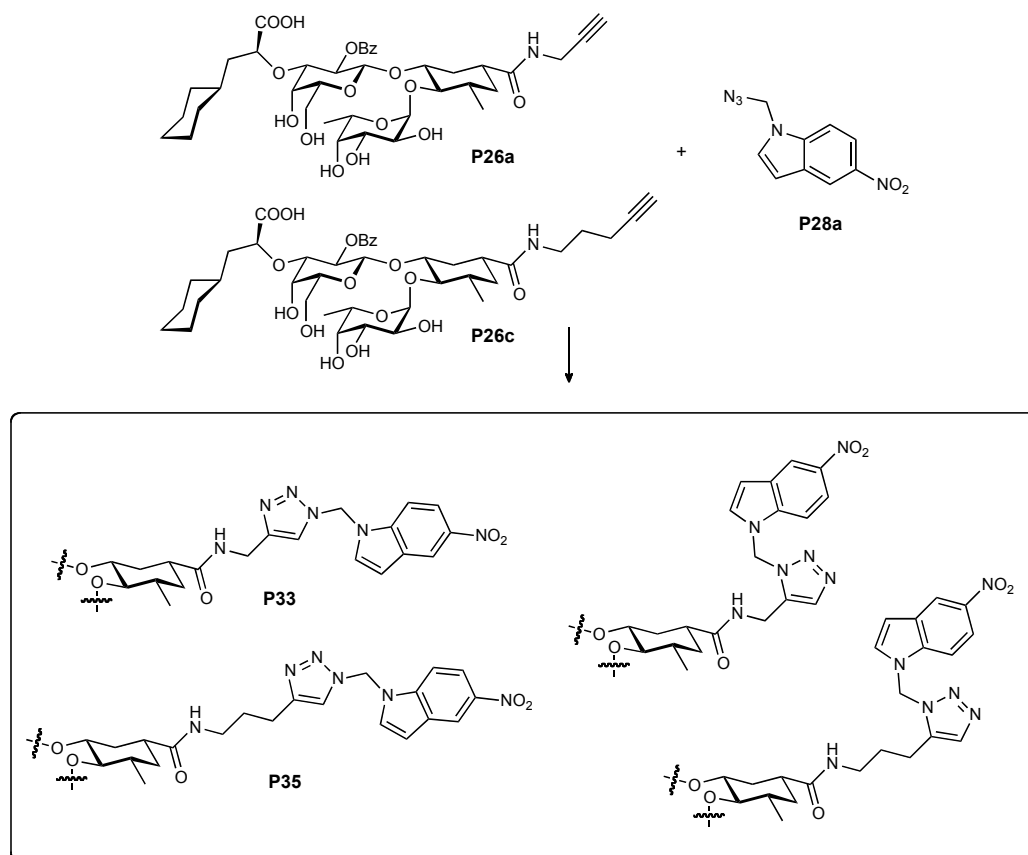
Scheme 3-12. ISC5: **P26c**: 50 μM; **P26a**: 50 μM; **P28a**: 500 μM; protein: 80 μM; 20 °C.

Rationale:

In contrast to the other ISC experiments, only one second-site but two first-site ligands were used here. As discussed previously (Section 3.5.4), this setup is actually expected to be less favorable because it leads to higher concentrations of unbound ligand, which in turn increases the rate of spontaneous triazole formation.

The combination of fragments may again lead to a high-affinity (**P51**, K_D = 89 nM) and a lower-affinity (**P33**, K_D > 89 nM) *anti* triazole ligand.

Conclusions:

Only in the BSA sample some triazole formation was detected. No reference compound or experiment is available for ISC5.

Figure 3-30. Representative chromatograms of ISC5.

3.6.3.6. *In situ* click experiment 6 (ISC6)
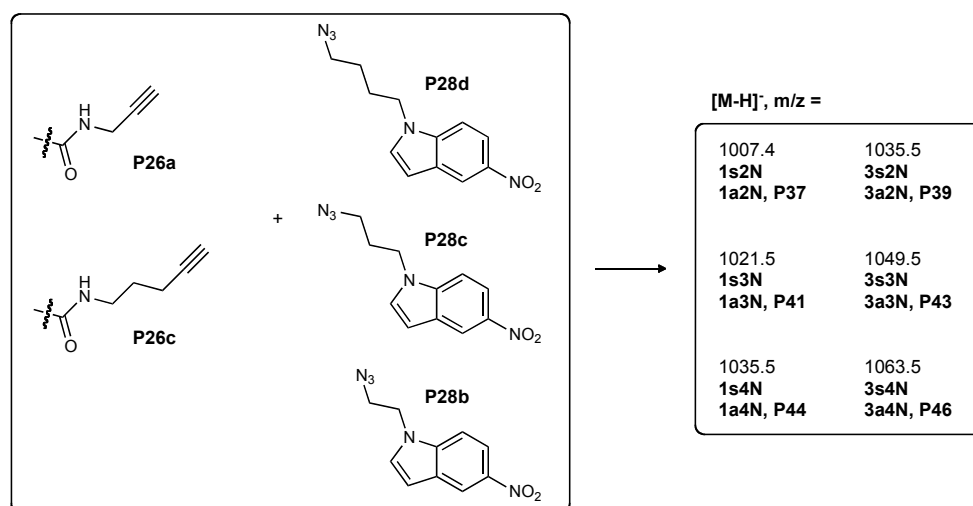
Scheme 3-13. ISC6: **P26a**: 50 μM; **P26c**: 50 μM; **P28b**: 400 μM; **P28c**: 400 μM; **P28d**: 400 μM; protein: 80 μM; 20 °C.

Rationale:

Because previous ISC experiments had shown that BSA is not a neutral control sample compared to buffer, an additional control sample containing E-selectin + 3 mM EDTA was used in ISC6. By complexing Ca^{2+} from the E-selectin binding site, EDTA should eliminate binding to the first site, which is calcium-dependent. ISC6 was the first experiment involving more than three fragments. Here, 12 different combinations of first- and second-site ligands with 5 different masses can be formed. Among these, there are two high-affinity *anti* triazole antagonists (**P41**, $K_D = 57$ nM; **P43**, $K_D = 30$ nM).

Discussion and conclusions:

Figure 3-31 shows the chromatograms covering all possible masses ($\rightarrow$ total ion count [TIC] traces). An inspection of the extracted chromatograms ($\rightarrow$ single mass traces) revealed that the trace for m/z = 1035.5 accounts for most of the signals in the TIC trace (Figure 3-32).

Peaks **A** and **B** are a result of non-specific signal, as confirmed by a test experiment (ISCtest1), where an identical pattern was observed. The test experiment further showed that peak group **C** corresponds to the triazoles formed from alkyne **P26c** and azide **P28b**, and peak **D** to triazoles from **P26a** and **P28d**. Concluding from the fact that peak group **C** and peak **D** were *not* observed in both E-selectin, but in the BSA and buffer samples, E-selectin did not have a catalytic effect on triazole formation in this experiment. As previously, the rate of triazole formation was highest in the BSA sample.

In ISC6 and ISC7, a strong variation of retention times was observed between the measurements taken at different time points (see Figure 3-33 for an example from ISC6; data for ISC7 not shown). ISCtest1 revealed that this was most probably caused by a worn out pre-column (Figure 3-42).
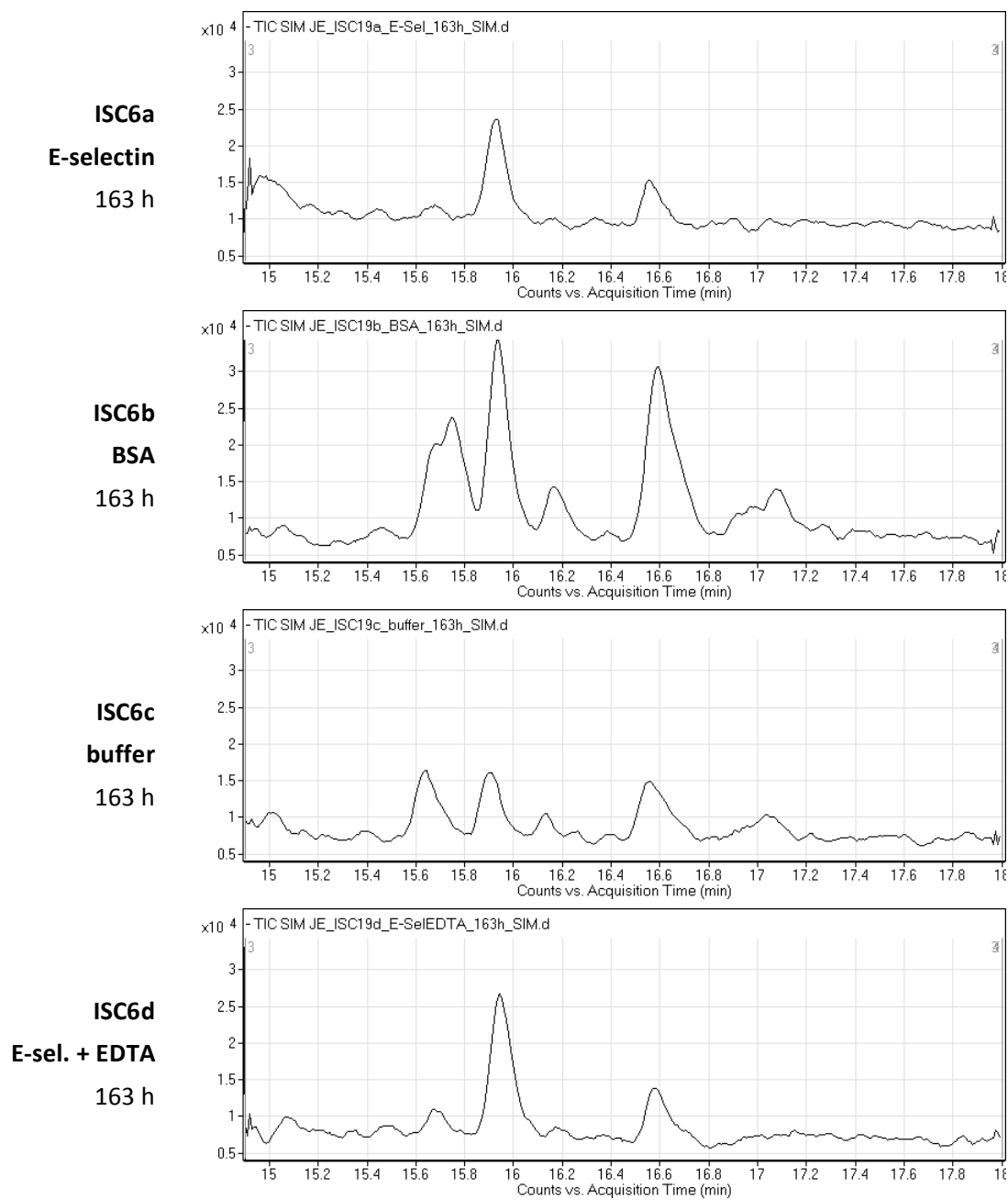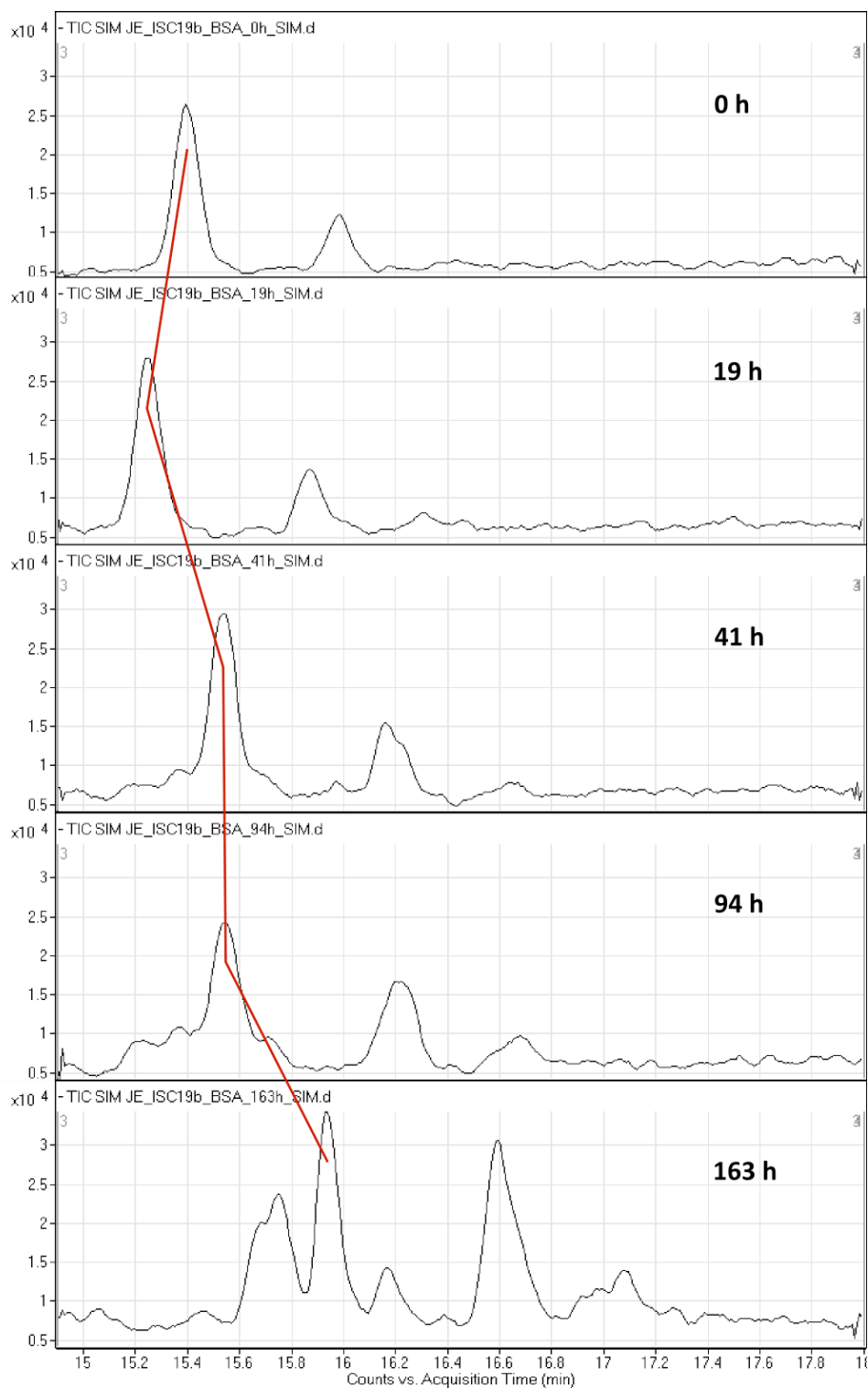
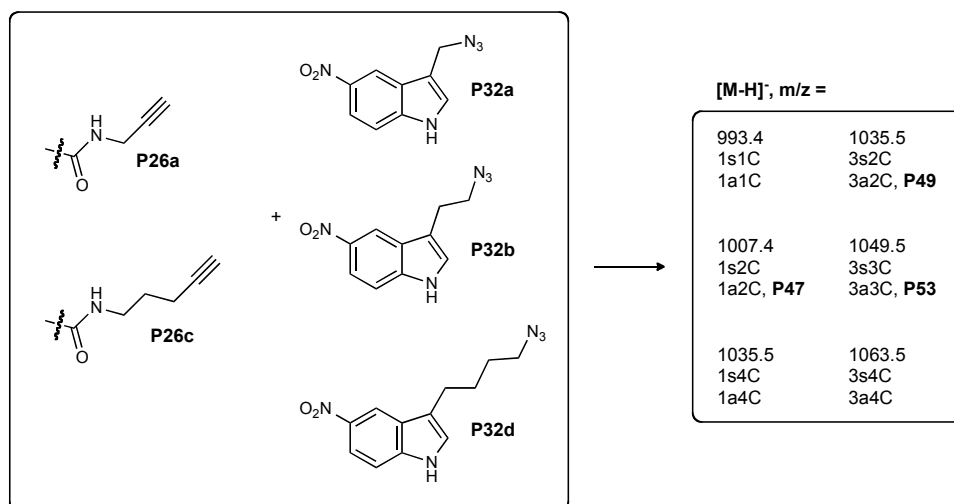**Figure 3-31.** Representative chromatograms of ISC6 (TIC trace).
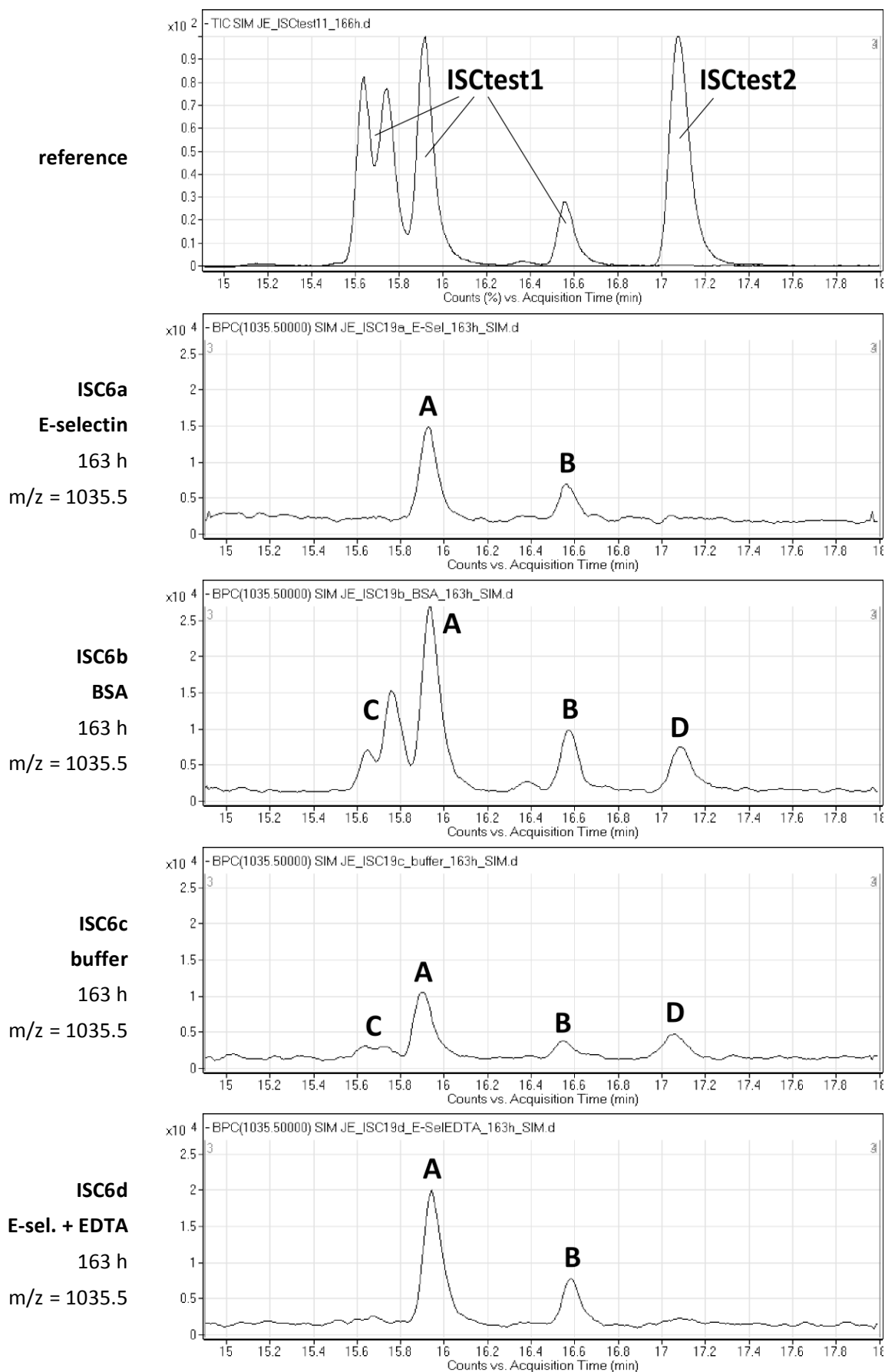
Figure 3-32. Representative chromatograms of ISC6 (single-mass trace for m/z = 1035.5).

Figure 3-33. Variations of retention times in ISC6 caused by a worn out pre-column.

3.6.3.7. *In situ* click experiment 7 (ISC7)

Scheme 3-14. ISC7: **P26a**: 50 μM; **P26c**: 50 μM; **P32a**: 250 μM; **P32b**: 250 μM; **P32d**: 250 μM; protein: 80 μM; 20 °C.

Rationale:

Like ISC6, ISC7 included 5 fragments. The nitroindole second-site ligands were all *C*-alkylated to cover three so far untapped linker combinations. The nitroindole concentration was reduced from 400 to 250 μM due to the low solubility of the nitroindoles.

Conclusions:

Similar to ISC6, the signals in the TIC trace essentially corresponded to the single mass trace for m/z = 1035.5. Again, nonspecific signals (peaks **B** and **C**, Figure 3-35) were observed, indicated by the fact that peaks **B** and **C** were detected already in the samples analyzed immediately after starting the experiment. Triazole formation (peak group **A**) was fastest in the BSA sample, and no specific effect of E-selectin could be demonstrated.
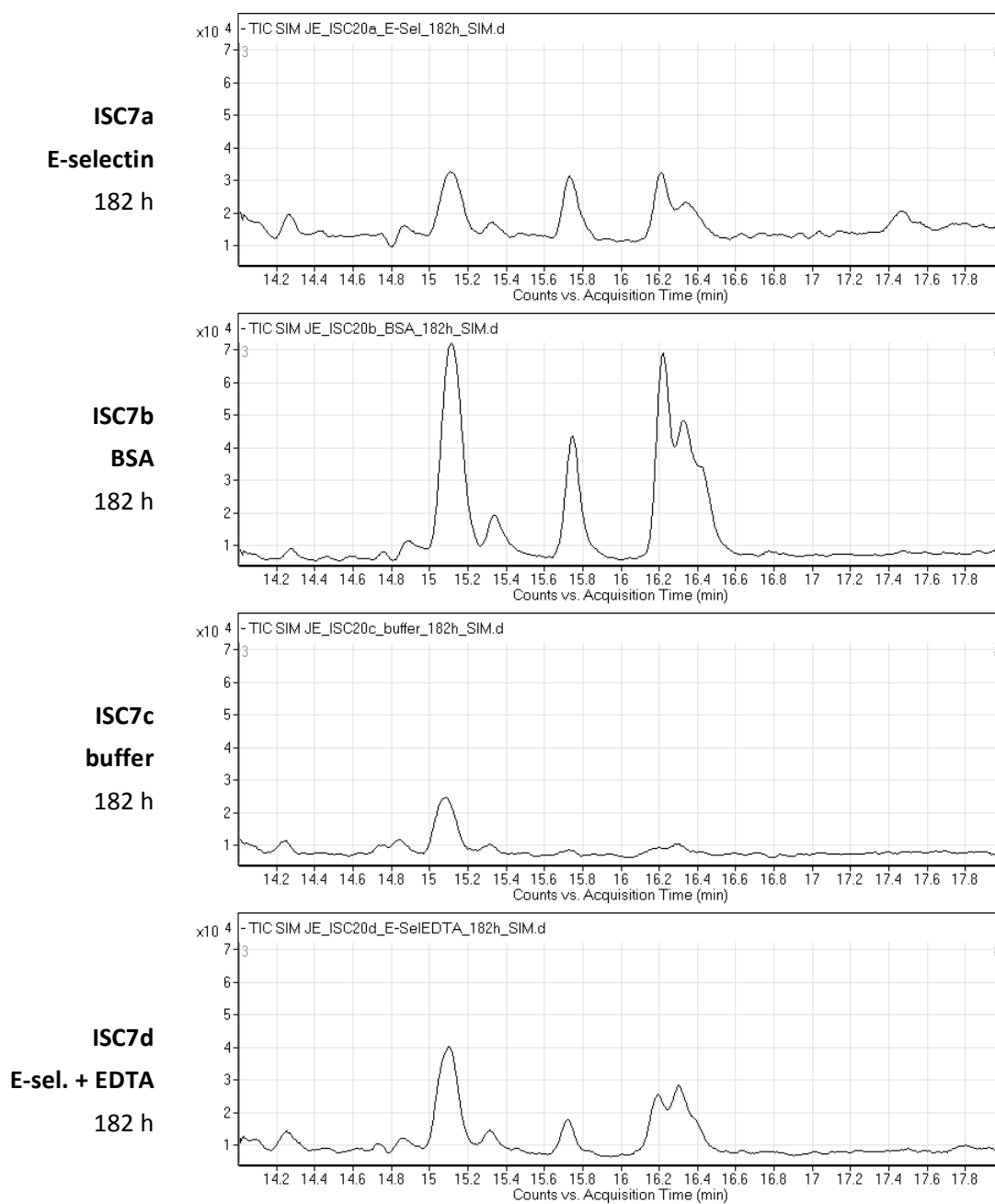
**Figure 3-34.** Representative chromatograms of ISC7 (TIC trace).
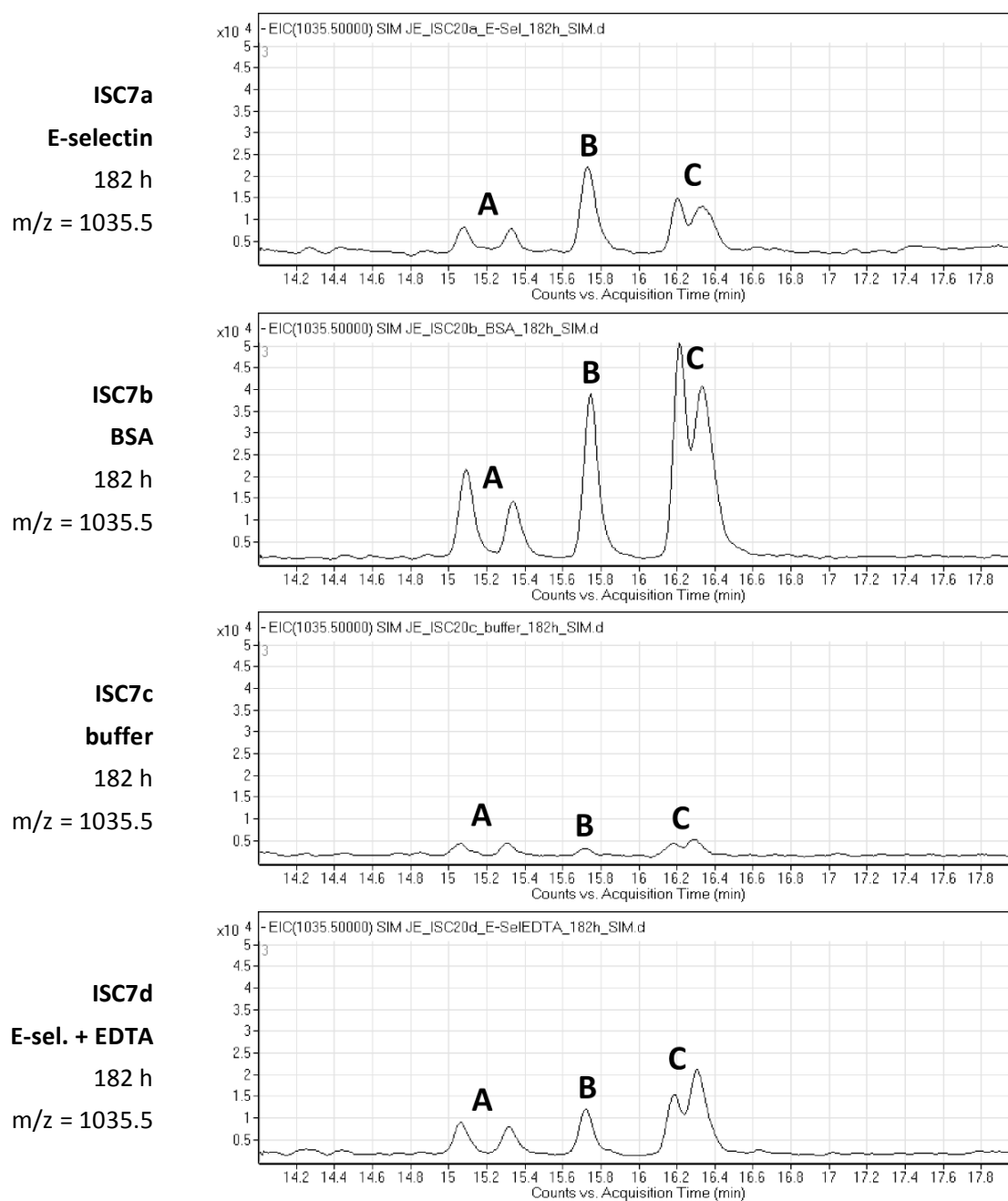
Figure 3-35. Representative chromatograms of ISC7 (single-mass trace for m/z = 1035.5).

3.6.4. ISC experiments with contaminated E-selectin

The appereance of some peaks at unexpected retention times and *apparently* positive results in some ISC experiments eventually led to the identification of impurities in 4 batches of E-selectin. In the following these experiments and the screening of different protein batches for contaminations are outlined.

3.6.4.1. *In situ* click experiment 8 (ISC8)
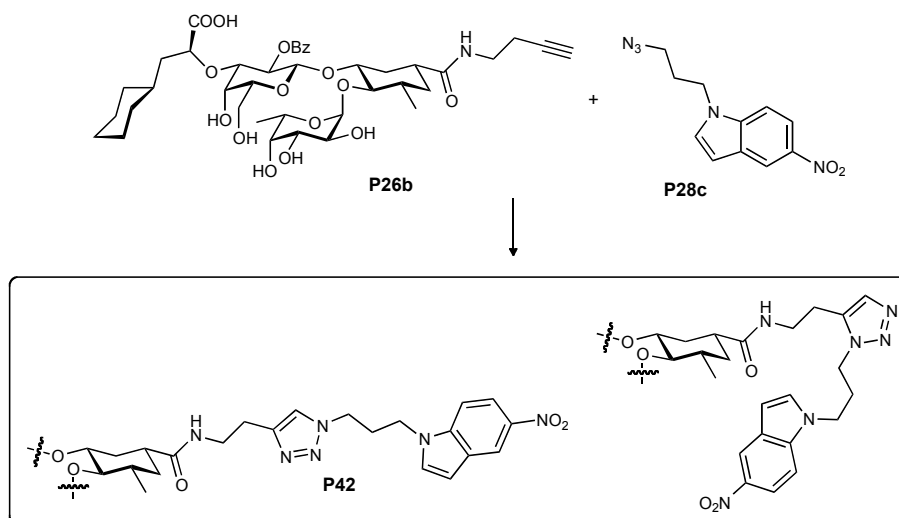
Scheme 3-15. ISC8: **P26b**: 50 µM; **P28c**: 600 µM; **protein**: 41 µM (E-selectin protein code: 0001/AC/3/2/KL/090721); 20 °C.

Rationale:

This experiment was performed to investigate the effect of E-selectin on triazole formation for a ligand pair that may lead to an *anti* triazole antagonist of intermediate affinity ($K_D >$ 89 nM).

Discussion and conclusions:

The injection of a native sample from the E-selectin batch showed that the apparently higher amount of triazole in the BSA sample was the result of a contamination with **P42**. Peak **A** is the result of a nonspecific signal, as the intensity remained constant over time. Furthermore, no corresponding peak was found in the test experiment
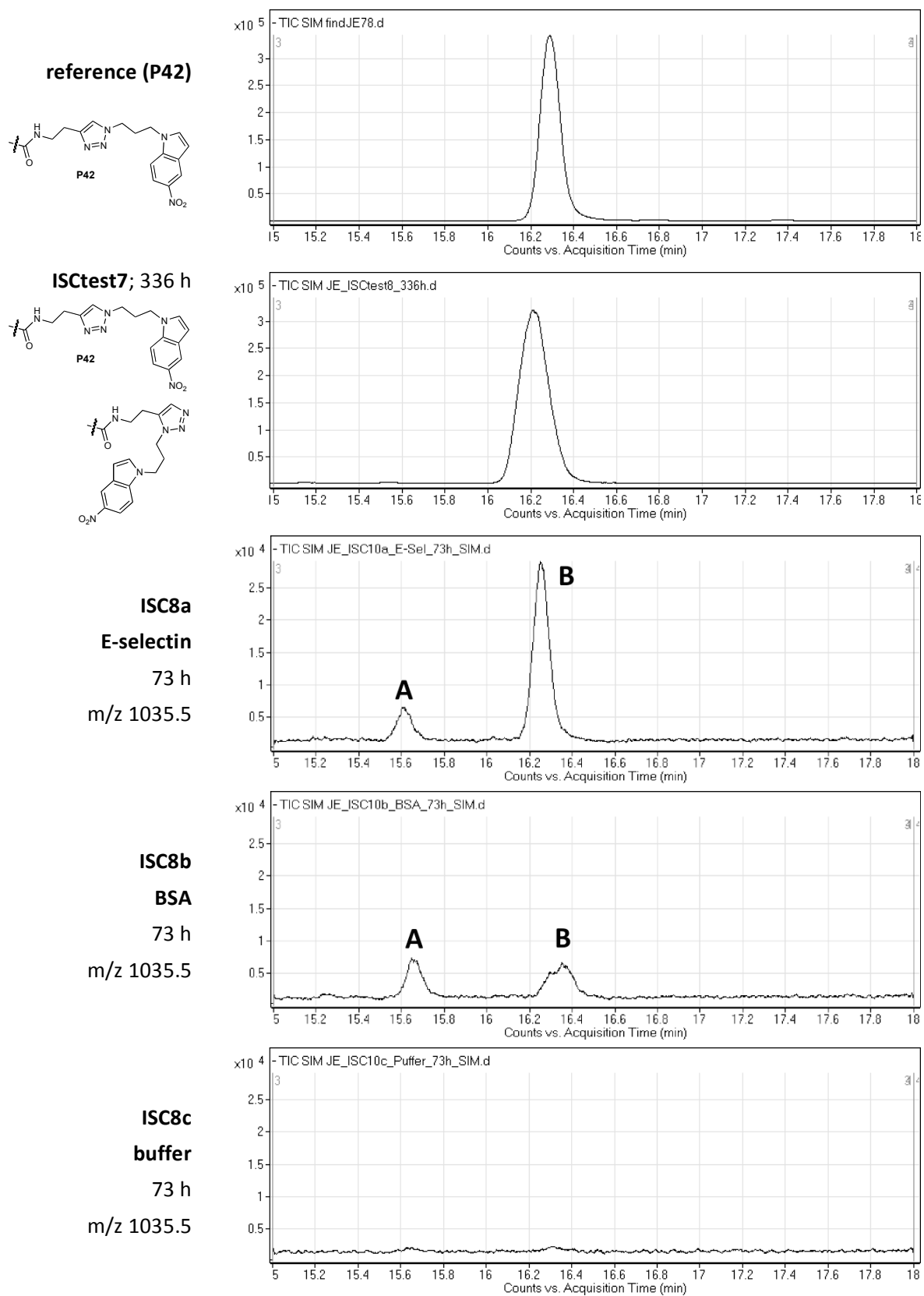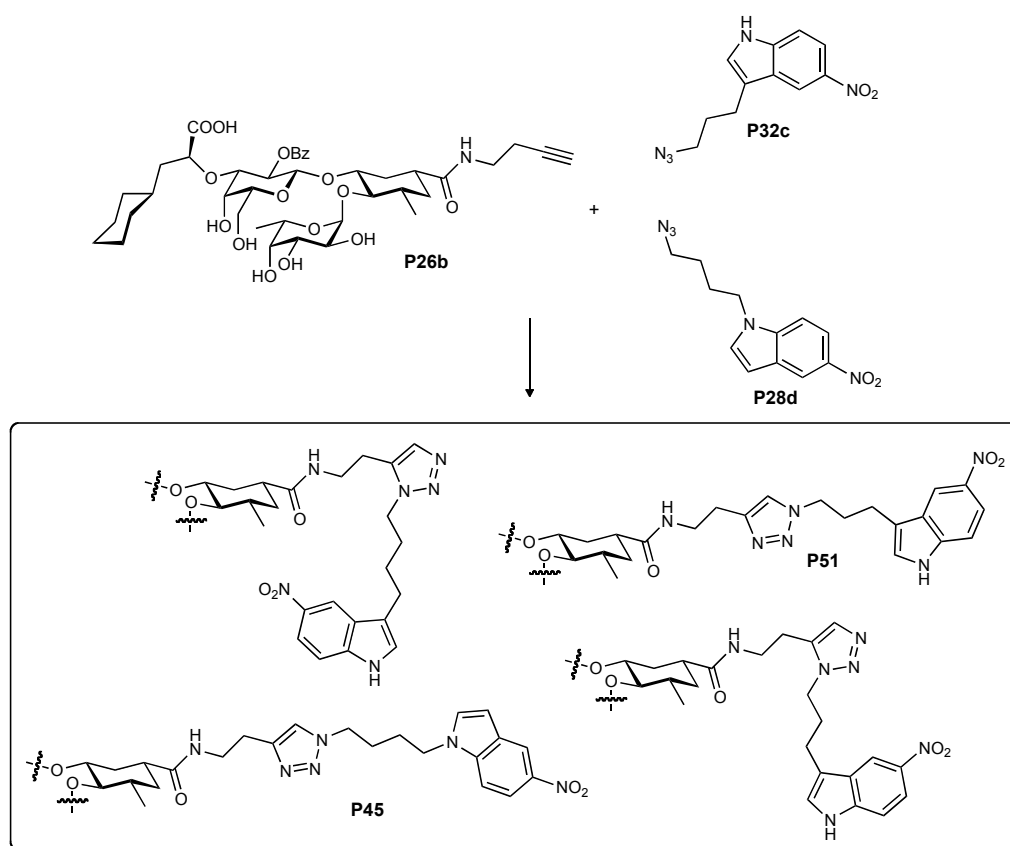
Figure 3-36. Representative chromatograms of ISC8.

3.6.4.2. *In situ* click experiment 9 (ISC9)

Scheme 3-16. ISC9: **P26b**: 50 μM; **P28d**: 250 μM; **P32c**: 250 μM; **protein**: 80 μM ((E-selectin protein code: 0001/AC/3/2/KL/090721); 20 °C.

Rationale:

ISC9 was a multicomponent reaction intended to lead to *anti* triazole ligands with high (**P45**) and lower (**P51**) affinity to E-selectin. The choice of components was based on the erroneous ranking of **P51** as the weakest E-selectin ligand. In fact, **P45** and **P51** have identically high affinities (K_Ds of 49 and 50 nM).

Discussion and conclusion:

In all measurements, a single peak was observed in the E-selectin sample, whose retention time did not match the peaks found in the corresponding test experiments (ISCtest6 and ISCtest8) but corresponded to the one of **P42**. The peak was also detected in the native E-selectin batch, indicating that the latter was contaminated with traces of **P42**. The contamination most probably resulted from using re-purified E-selectin hat had previously been used in experiments involving **P42**.

Triazole formation was faster in the BSA sample than in the buffer sample. It remains unclear why no spontaneously formed triazoles could be detected in the E-selectin sample. Yet, the

absence of any signal in the E-selectin sample indicates that there was no catalytic effect of E-selectin.
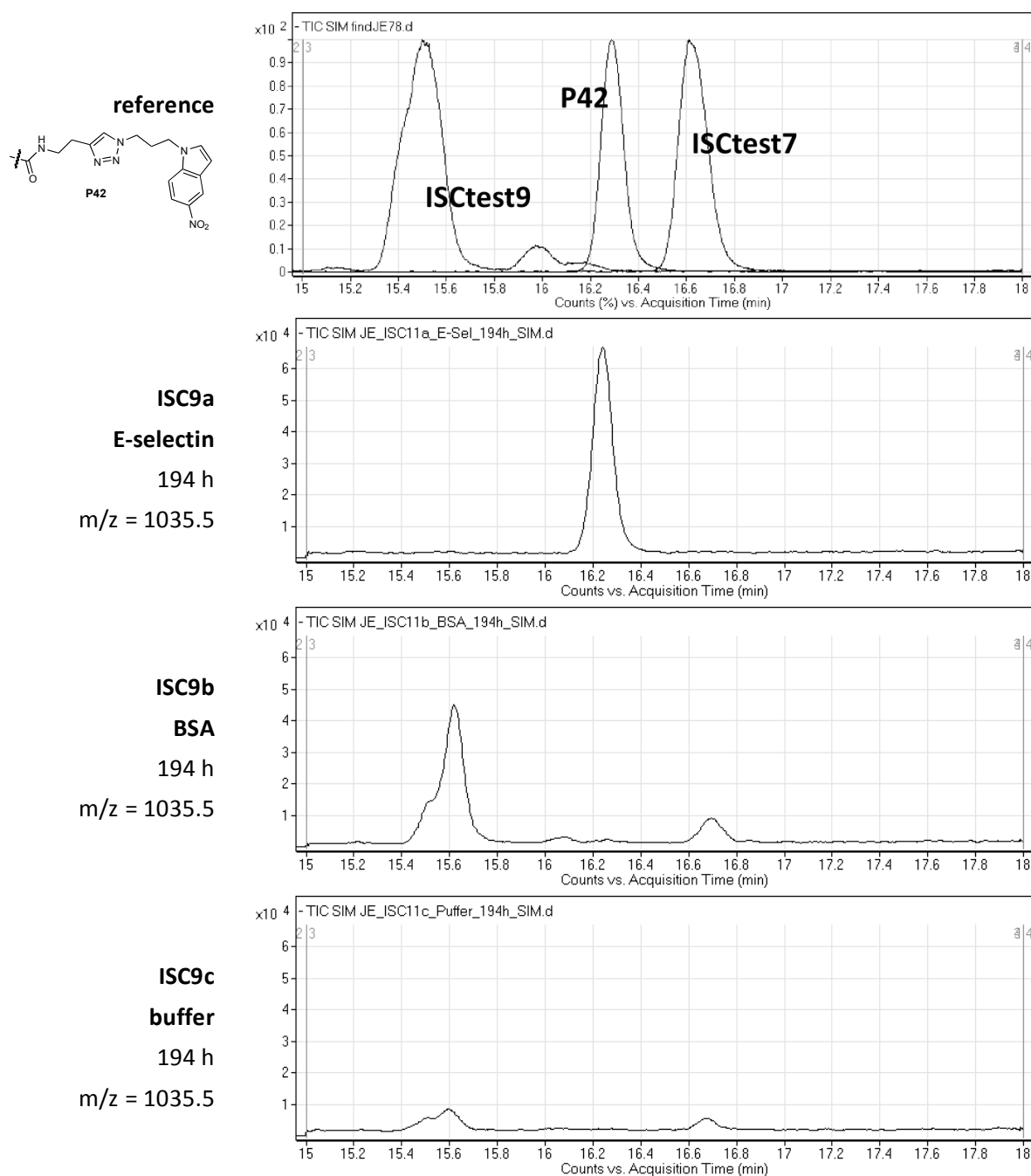
Figure 3-37. Representative chromatograms of ISC9.

3.6.4.3. *In situ* click experiment 10 (ISC10)
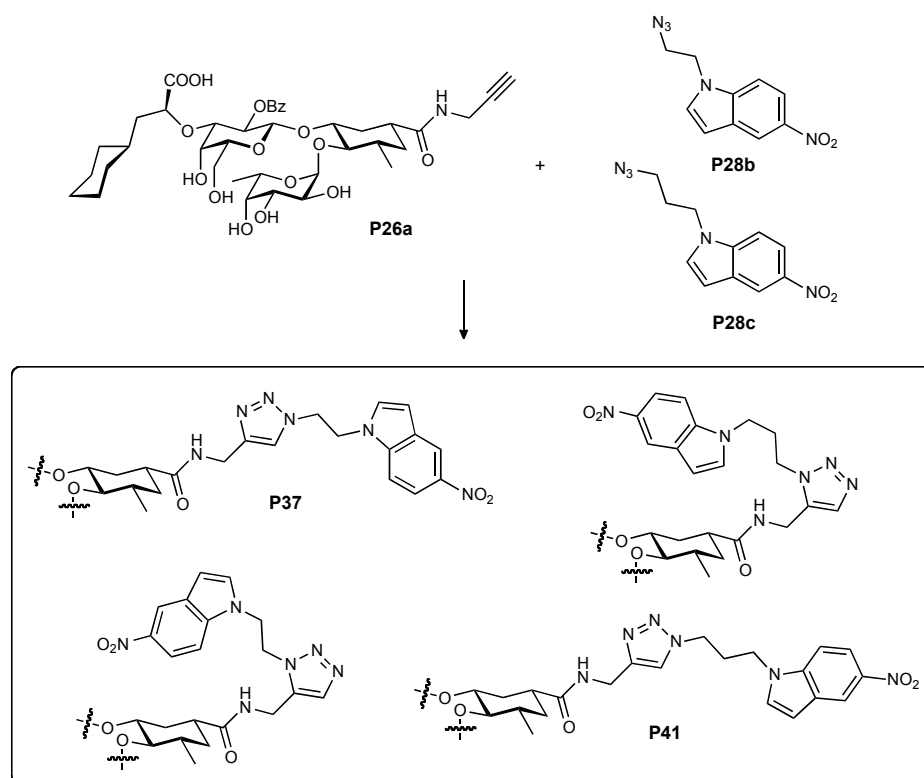
Scheme 3-17. ISC10: **P26a**: 50 µM; **P28b**: 250 µM; **P28c**: 250 µM; **protein**: 80 µM (E-selectin protein code: 0001/AC/4/2/KL/091006); 20 °C.

Rationale:

ISC10 was a multicomponent experiment potentially leading to *anti* triazole ligands with high (**P41**, K_D = 57 nM) and lower (**P37**, K_D > 89 nM) affinity to E-selectin.

Discussion and conclusion:

In ISC9, an intense peak, which did not match the reference (**P41**) or the peaks found in the corresponding test experiment (ISCtest6), was observed in the E-selectin sample (Figure 3-38). The peak's retention time was identical to the one of **P38**, and it was detected in the native E-selectin batch, indicating that the latter was contaminated with **P38**.

The other peaks corresponding to 1s/a2N and 1s/a3N triazoles were of comparable intensities in all samples, which indicates that there was no catalytic effect of E-selectin.

Note: Figure 3-38 shows that the retention times of the reference compound **P38** and **P41** differ by almost 0.8 min. Considering that these isomers differ only by the position of the triazole moiety, this finding is quite remarkable and fits in with the observations made in ISCtest5 (Section 3.6.5.4).
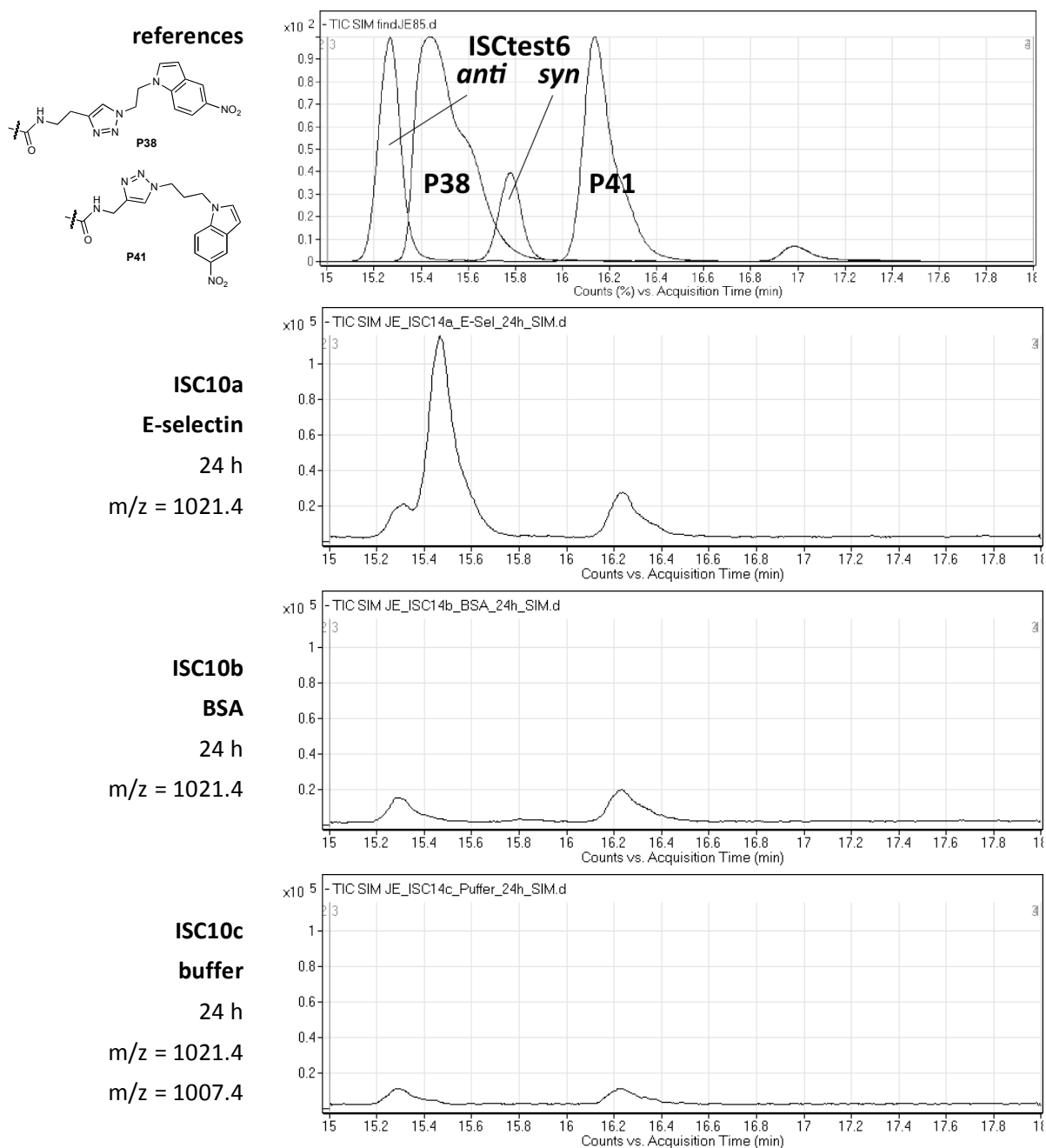
Figure 3-38. Chromatograms of ISC10 after 24 h. Spontaneously formed triazoles in the E-selectin sample were only detected in the measurement after 24 h.
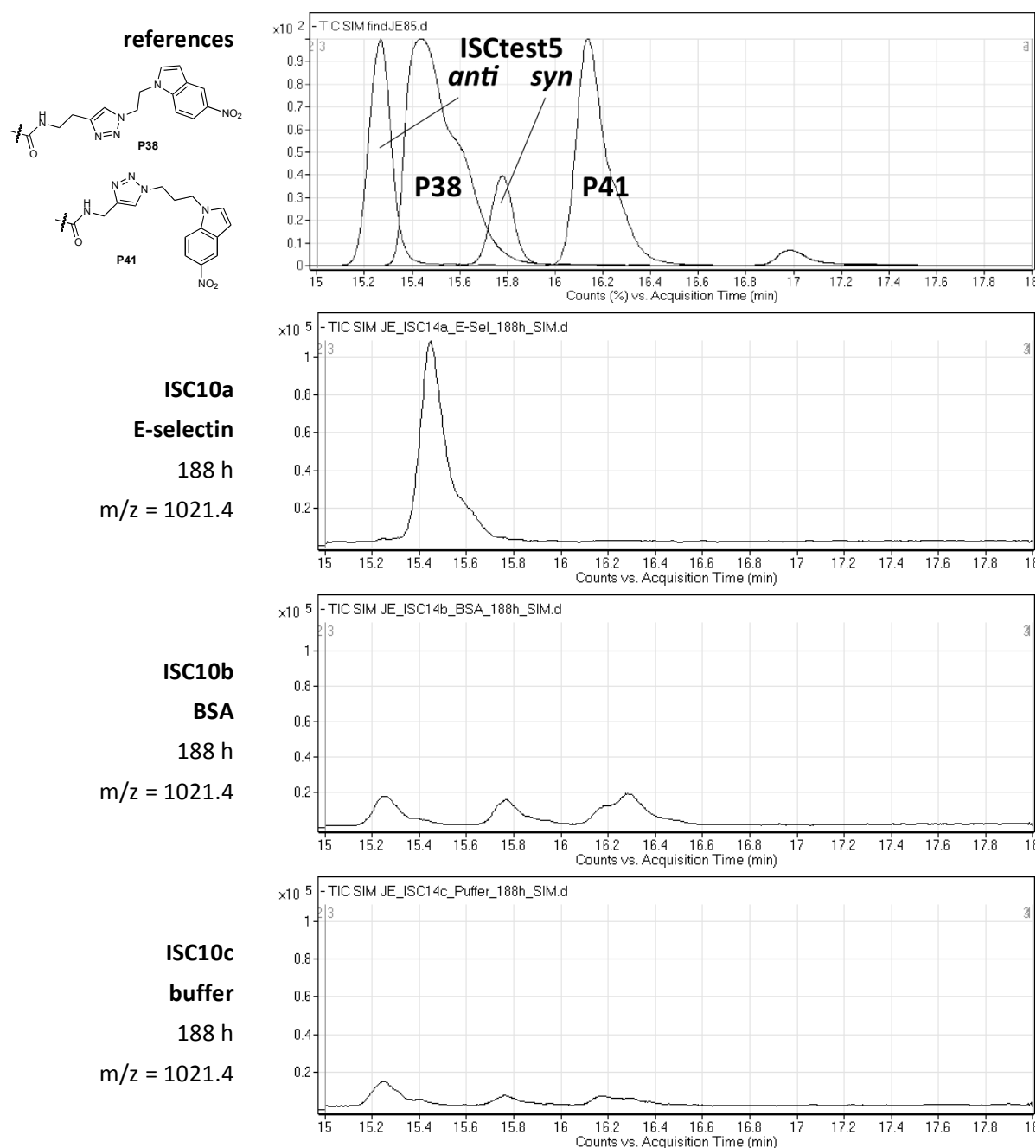
Figure 3-39. Chromatograms of ISC10 after 188 h. Spontaneously formed triazole could not be detectd in the E-selectin sample.

3.6.4.4. Investigation of protein batches containing recycled protein

The contaminated protein batches (0001/AC/4/2/KL/091006 and 0001/AC/3/2/KL/090721) identified in the ISC experiments contained recycled E-selectin that had been used for some NMR and ITC analysis of **P38** and **P45**. Therefore, it was presumed that the recycling procedure had failed in fully removing these antagonists and that other batches containing recycled E-selectin were contaminated as well. Relevant protein batches were scanned in single ion mode for m/z ratios corresponding to the triazole–nitroindole antagonists (m/z =

993.4, 1007.5, 1021.5, 1035.5, 1049.6) and three tetrasaccharide mimics (**BW69669** (m/z = 599.6), **DS41-15** (m/z = 613.7), **DS41-49** (m/z = 717.8)) (131), which had also been analyzed with subsequently recycled E-selectin. None of the tetrasaccharide mimics was detected in any of the E-selectin batches. But, as Figure 3-40 shows, traces of **P38** and, in one case, **P42** were detected in samples containing recycled protein. In a batch (0001/AC/0/1/KL/081117) containing only freshly produced protein, no contaminations were found, further supporting the assumption that the detected contaminations originated from recycled protein.
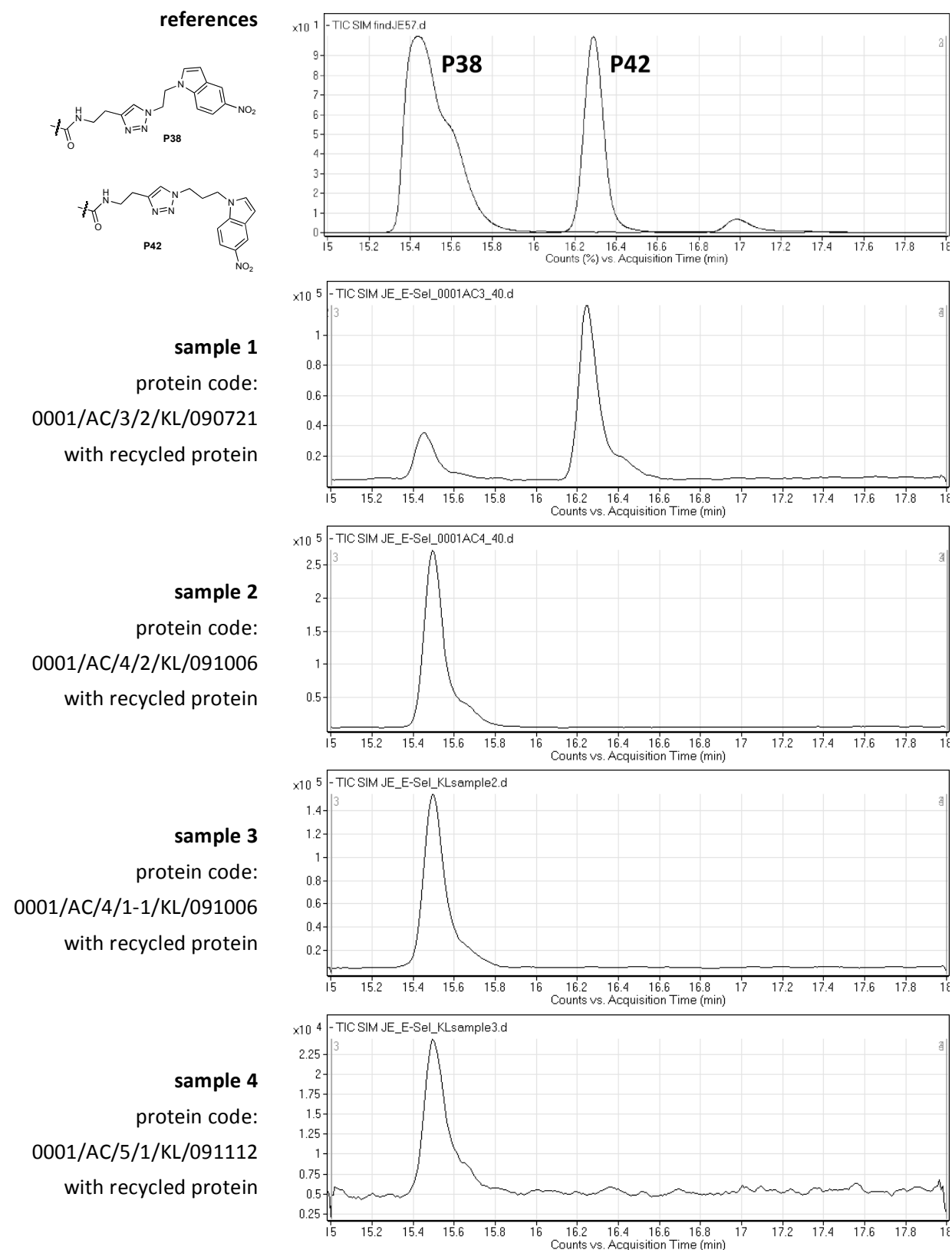
Figure 3-40. MS analysis of different protein batches.

3.6.4.5. Influence of the contaminations on experimental outcomes

The presence of an E-selectin antagonist (**P42**: $K_D > 89$ nM) in a protein sample could corrupt ISC experiments or biological assays where competition for the sLe^x binding site may occur. Thus, the concentration of **P42** in sample 1 (Figure 3-40) was estimated *via* a linear calibration curve (Figure 3-41). The observed relationship between concentration and the MS signal was nonlinear, a property common to the triazole–nitroindole antagonists (209).

Using the linear calibration curve shown in Figure 3-41, the concentration of **P42** in protein sample 1 was estimated to be roughly 0.5 µM. Assuming a K_D of 100 nM for **P42**, no more than 0.5% of the protein in the undiluted protein batch are expected to be ligand-bound. Considering this, a relevant influence on measurements performed with contaminated E-selectin appears improbable. Accordingly, the conclusions from ISC9 and ISC10 remain valid. *I.e.*, E-selectin did not have a catalytic effect on the cycloaddition of the alkynes and azides investigated in these experiments.
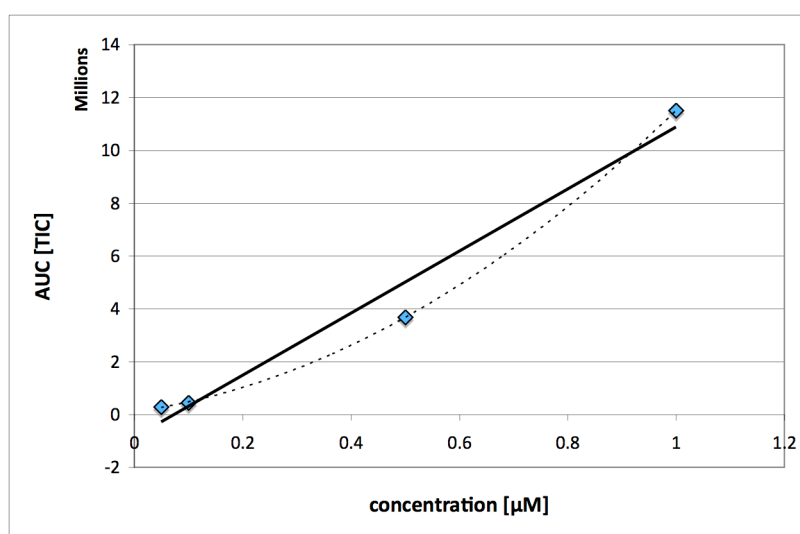
Figure 3-41. Calibration curve for **P42**. Measured concentrations: 0.05 µM, 0.1 µM, 0.5 µM, and 1 µM. A nonlinear relationship between concentration and MS signal was observed. Linear calibration curve: $y = 10^7 \cdot x - 862040$; $R^2 = 0.9698$.

Nevertheless, E-selectin that has been in contact with the triazole–nitroindole antagonists should not be recycled, or the recycling procedure should be adapted to ensure complete removal of these antagonists.

Based on the above results, the concentrations of spontaneously formed nitroindolyl ligands in the ISC experiments are expected to be in the two-digit nM range.

3.6.5. *In situ* click test experiments

A series of test experiments was performed to gain insight into spontaneous triazole formation. In particular, the information gained from these experiments was useful as a reference for the *in situ* click experiments.

3.6.5.1. In situ click test experiment 1 and 2 (ISCtest1 and ISCtest2)
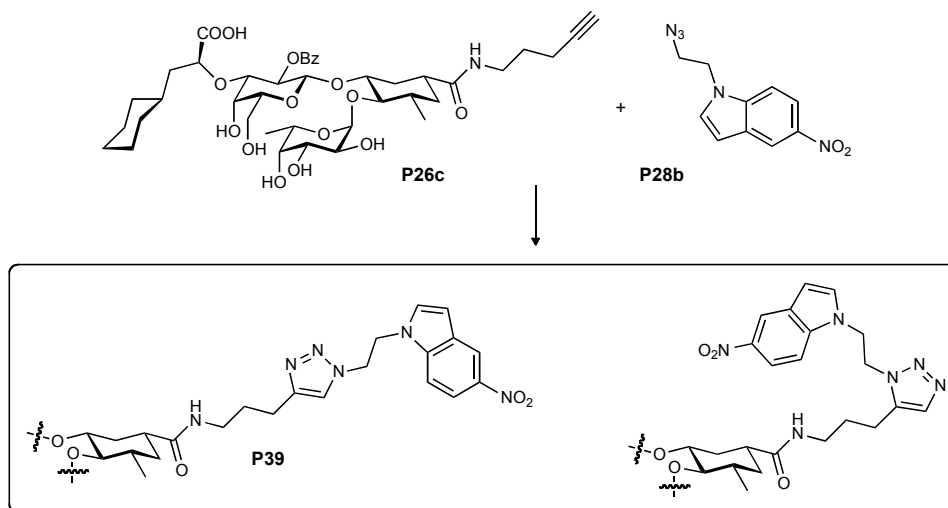
Scheme 3-18. ISCtest1: **P26c**: 500 μM; **P28b**: 500 μM; 37 °C.
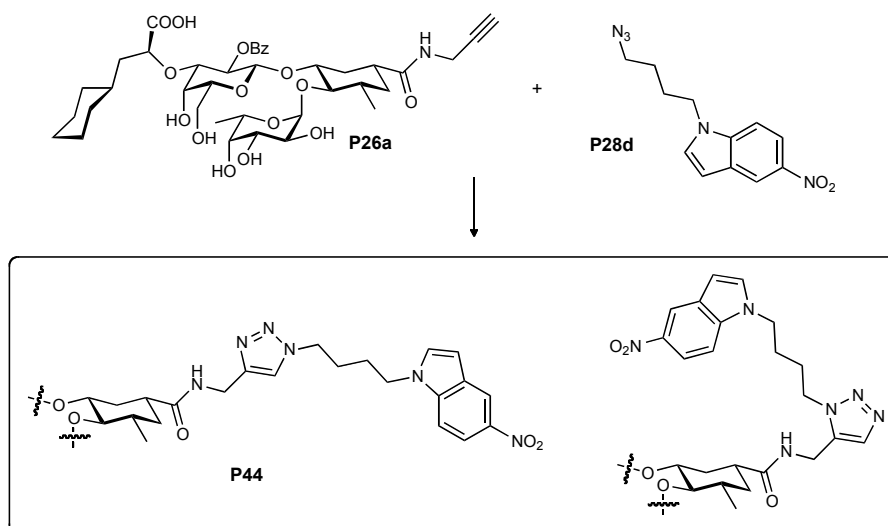
Scheme 3-19. ISCtest2: **P26a**: 500 μM; **P28d**: 500 μM; 37 °C.

Rationale:

These test experiments were performed for the identification of the peaks observed in ISC6. Peaks **A**, **B**, and **C** from ISCtest1 and peak **D** from ISCtest2 corresponded to the one in ISC6.

Discussion and conclusions:

Peaks **A** and **B** were already present after 3 h, which indicates that they are non-specific. This is further confirmed by the fact that only the area under the curve (AUC) of peak **C** increases over time (Figure 3-43). The shifts of retention times, as also illustrated in Figure 3-32, were caused by a worn out pre-column.
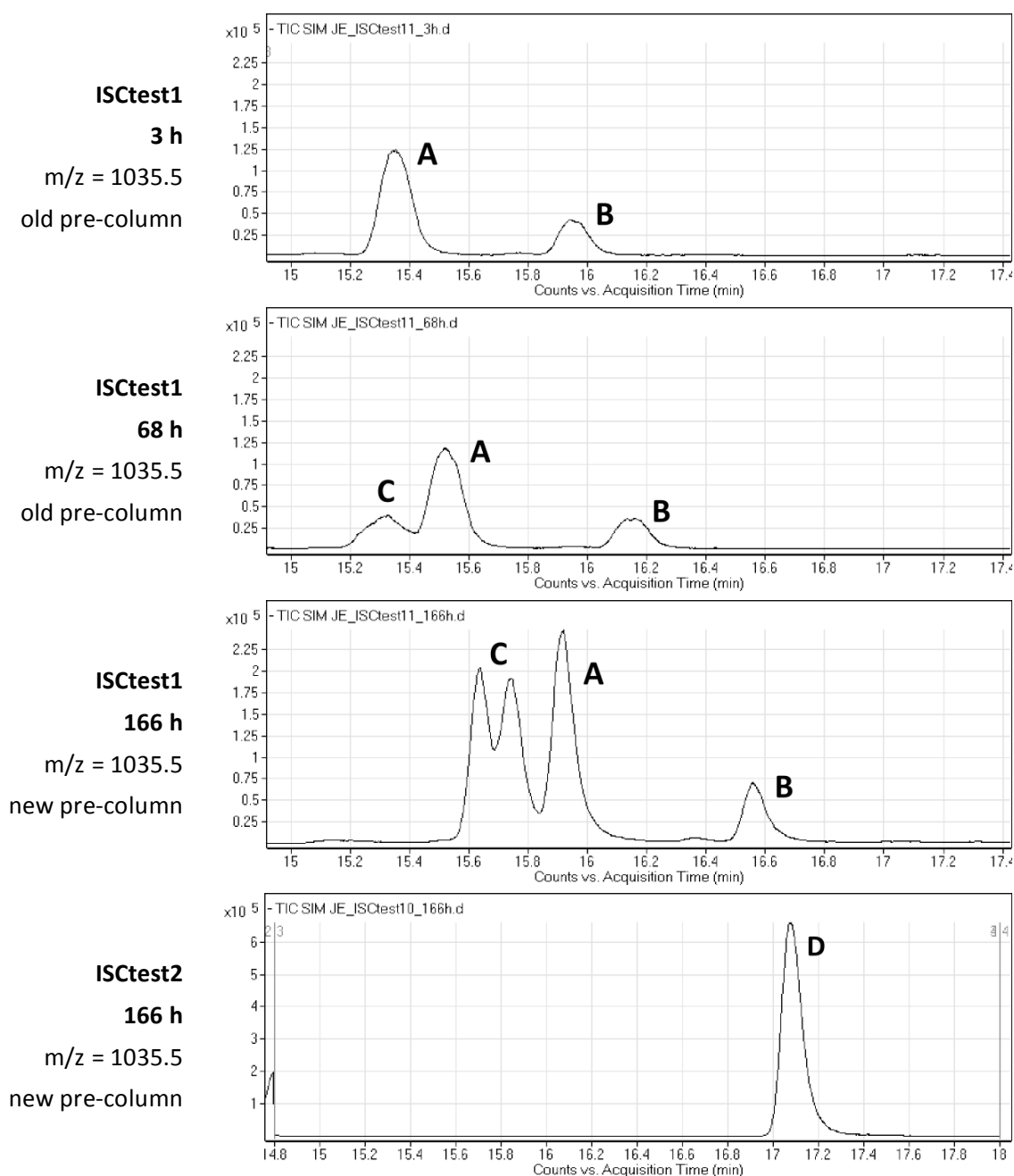
Figure 3-42. Representative chromatograms of ISCtest1 and ISCtest2.
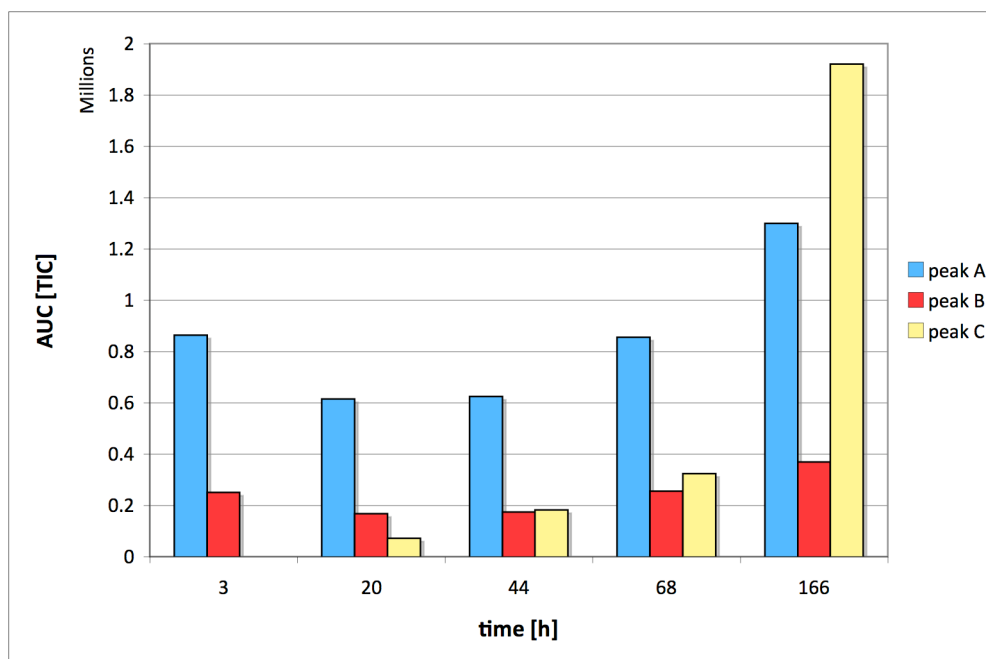
Figure 3-43. Peak intensities (AUCs) of ISCtest1.

3.6.5.2. The influence of EDTA: ISCtest3
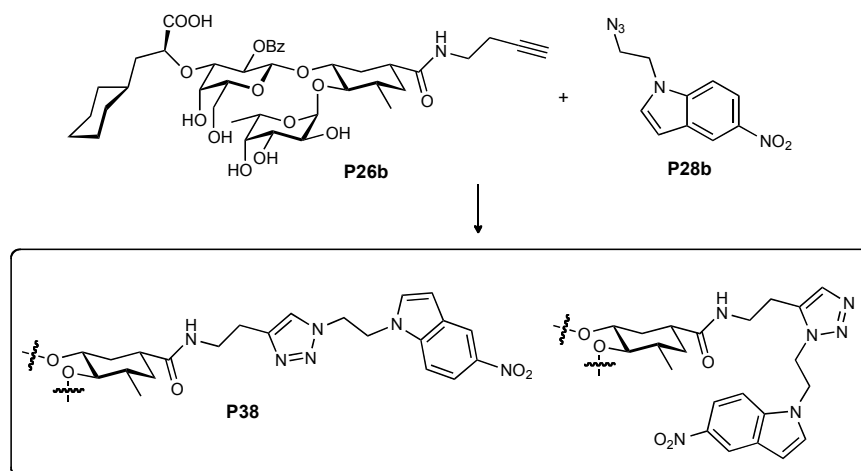
Scheme 3-20. ISCtest3a: **P26b**: 500 μM; **P28b**: 600 μM; 37 °C; ISCtest3b: + EDTA 10 mM.

Rationale:

ISCtest3 was performed to investigate the influence of EDTA on triazole formation, as EDTA was used in a control sample (ISC6 and ISC7).

Discussion and conclusions:

Interestingly, the rate of triazole formation was somewhat lower in the presence of EDTA. This result led to the speculation, that traces of copper may have been present in the sample,

causing a small catalytic effect. Although the effect was small, the influence of Cu^{2+} on triazole formation was investigated in an additional experiment (ISCtest3):
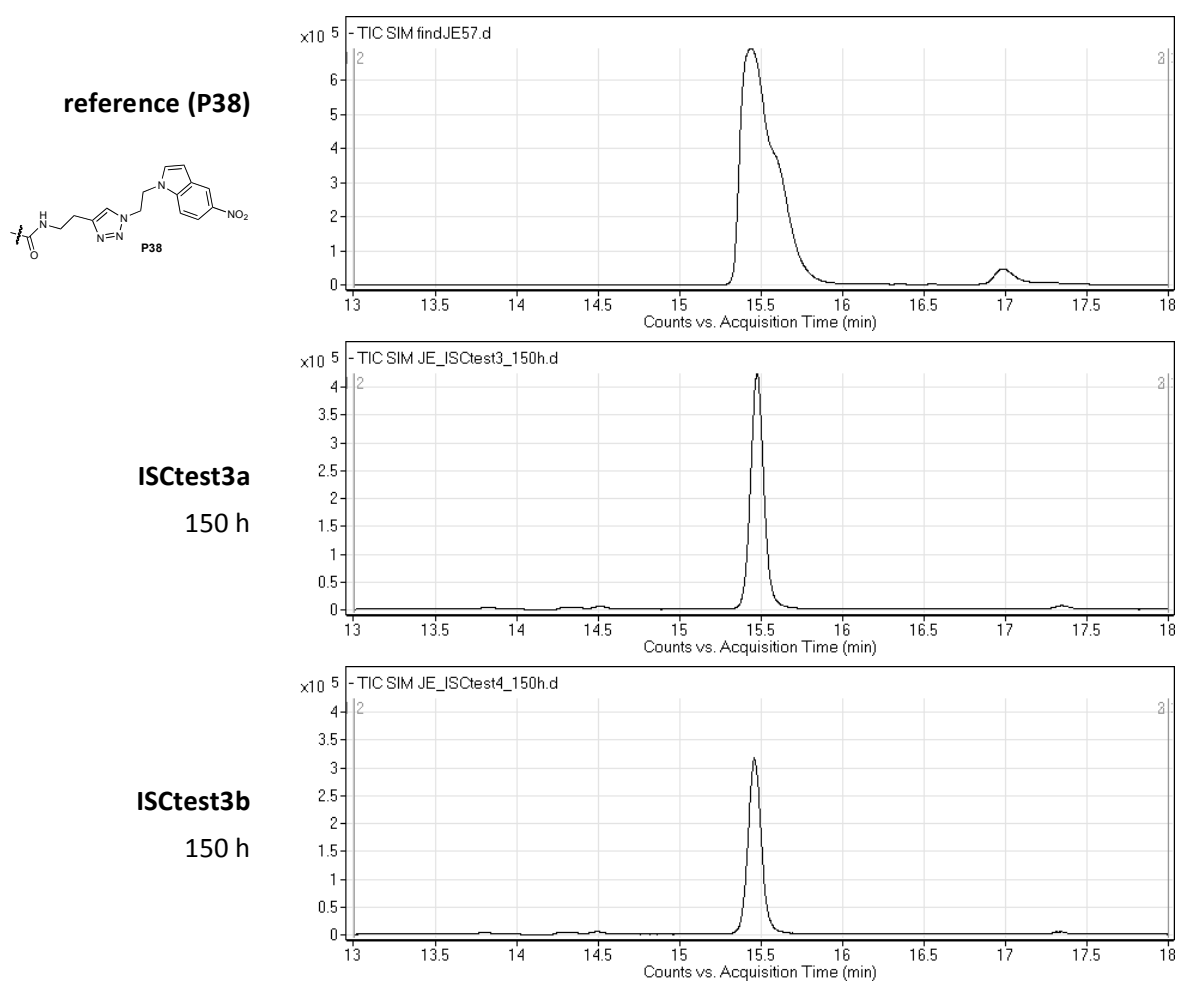
Figure 3-44. Representative chromatograms of ISCtest3.
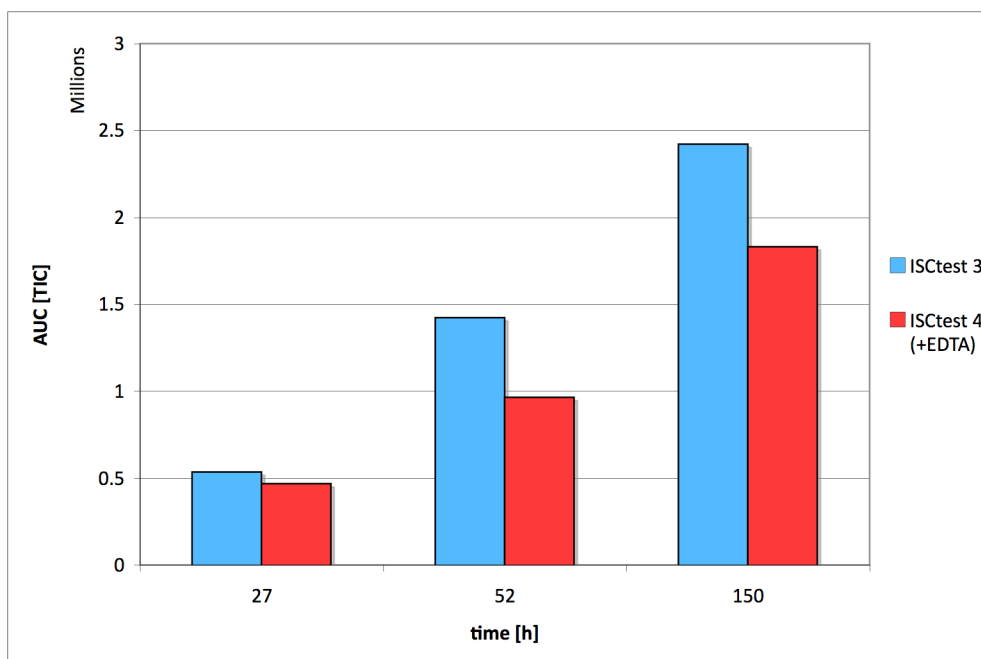
Figure 3-45. Comparison of the peak intensities (AUCs) of ISCtest3a and 3b.

3.6.5.3. The influence of Cu^{2+}: ISCtest4
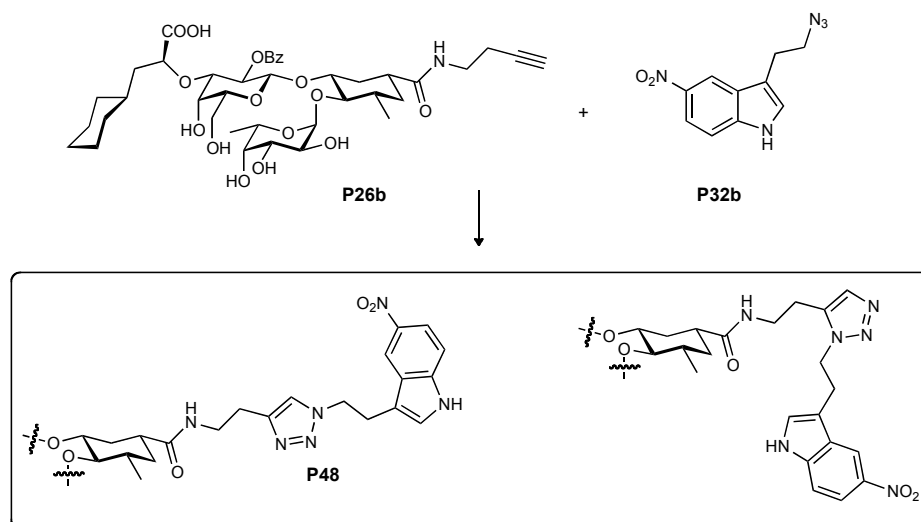
Scheme 3-21. ISCtest4a: **P26b**: 500 μM; **P32b**: 600 μM; 5% DMSO; 37 °C; ISCtest4b: + $CuSO_4 \cdot 5H_2O$ (5 mM).

Rationale:

In ISCtest3, EDTA was shown to reduce the rate of triazole formation. As EDTA is capable of complexing Cu^{2+} ions, one may attribute this effect to the removal of traces of catalytically active Cu^{I} species. To validate this hypothesis, the rate of triazole formation was investigated in the presence of a high concentration (5 mM) of Cu^{2+}.

Discussion and conclusions:

Figure 3-46 and Figure 3-47 show that the addition of $CuSO_4 \cdot 5H_2O$ indeed accelerated the formation of the *anti* triazole. After 3 d, its concentration was approximately 6-fold higher in the sample containing Cu^{2+} than in the reference sample, while the concentration of *syn* triazoles was essentially unchanged. Given the large amounts of $CuSO_4 \cdot 5H_2O$ added, it is not expected that possible traces of copper would have a major impact on the outcome of *in situ* click experiments.
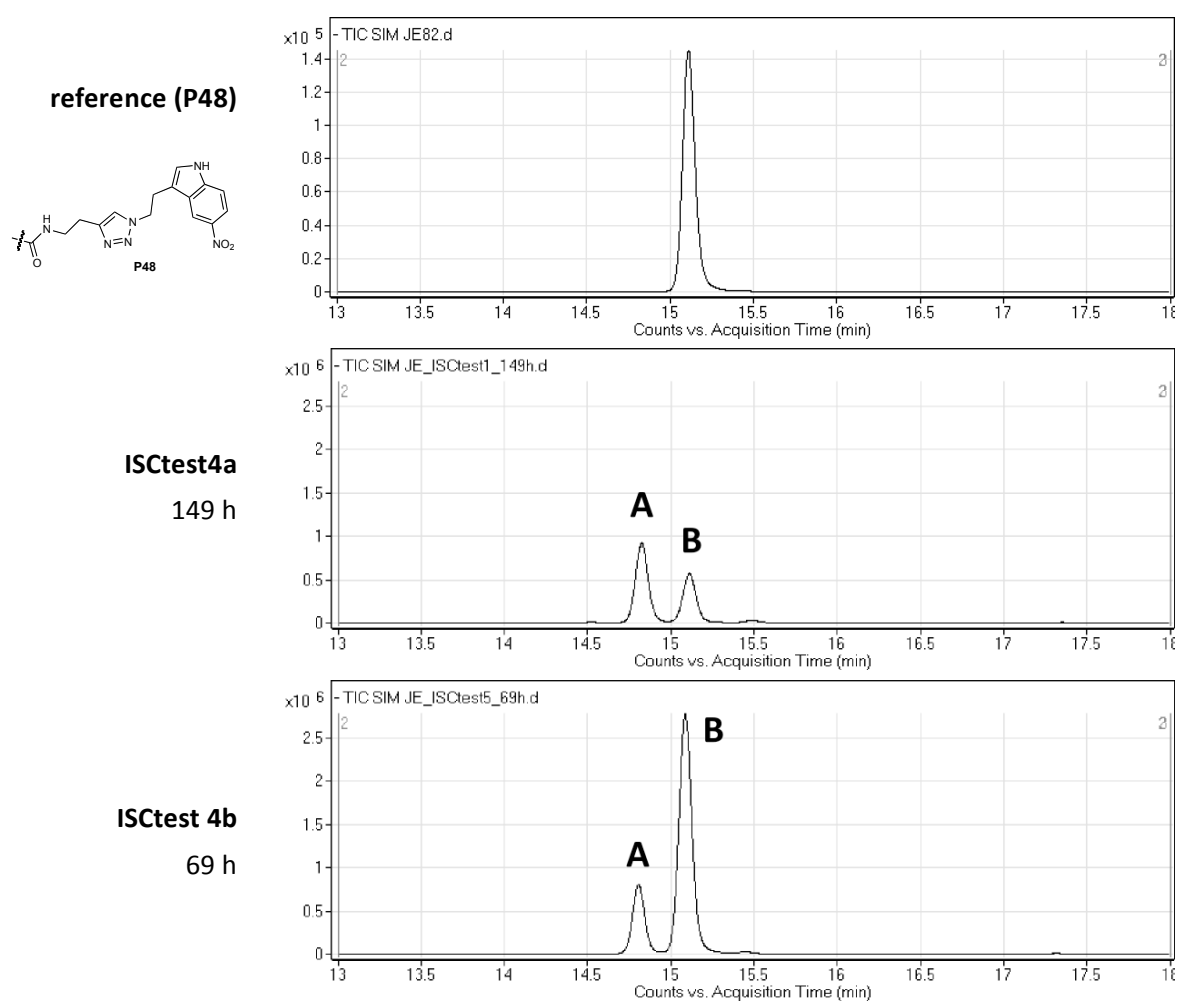
Figure 3-46. Representative chromatograms of ISCtest4a and 4b.
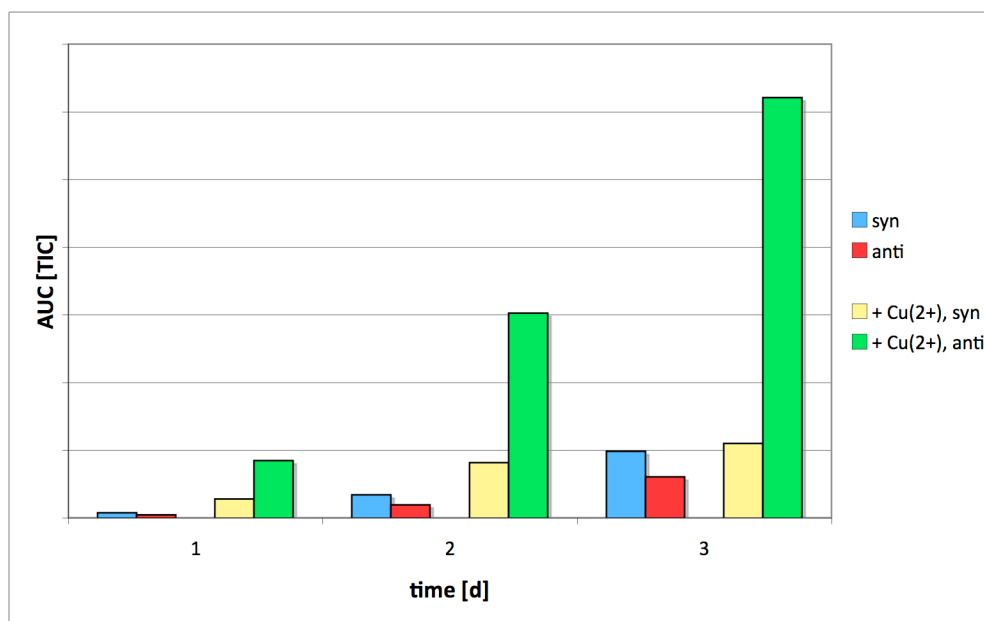
**Figure 3-47.** Comparison of the peak intensities (AUC) of ISCtest4a and 4b.

3.6.5.4. *In situ* click test experiment 5 (ISCtest5)
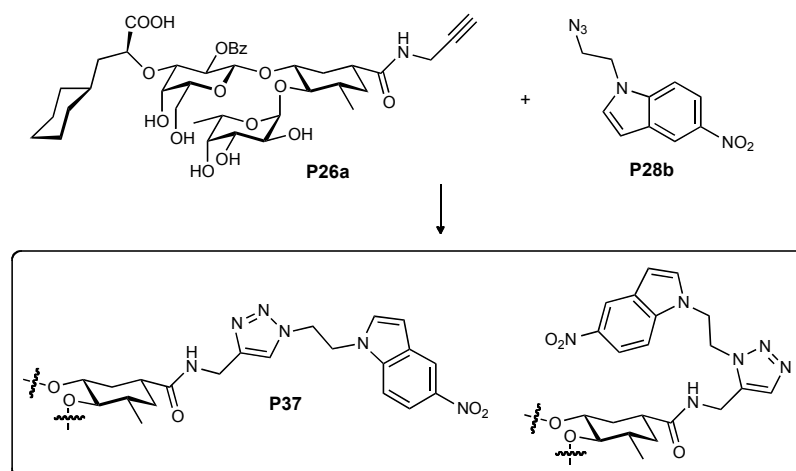
Scheme 3-22. ISCtest5: **P26b**: 500 μM; **P28b**: 600 μM; 5% DMSO; 37 °C.

Rationale:

As Figure 3-44 from ISCtest3 shows, the 2s/a2N isomers have identical retention times, resulting in a sharp single peak in the chromatogram. Thus, ISCtest5 was performed to investigate the separation behaviour of 1s/a2N isomers.

Discussion and conclusions:

In contrast to the 2s/a2N isomer, the 1s/a2N isomers are well separable using the standard gradient. Interestingly, the retention time of the 1s2N triazole is higher than the ones of the

182

2s/a2N isomers, despite the shorter linker. The comparison of these results to ISCtest4, where 2s/a2C triazoles were analyzed, revealed an inversed elution behavior of *syn* and *anti* isomers. Additionally, in ISCtest5, the formation of *anti* triazole was faster than *syn* triazole formation, while it was the other way round in ISCtest4.

These and other ($\rightarrow$ Section 3.6.4.3) findings indicate that conformational aspects may be important for this antagonist class: small structural changes can apparently lead to relatively strong effects on the elution behavior and even seem to influence the selectivity of the alkyne–azide cycloaddition.
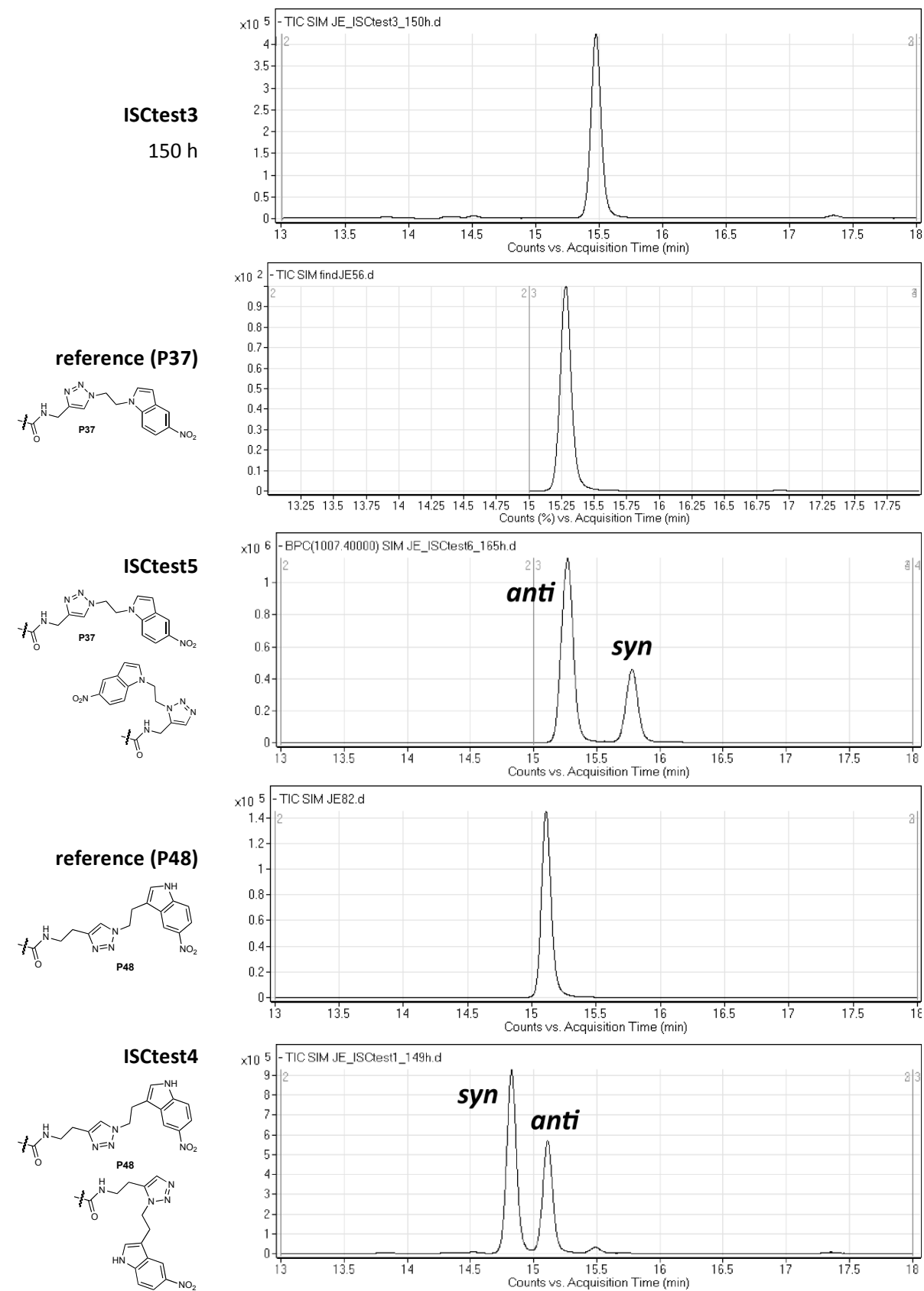
Figure 3-48. Representative chromatograms of ISCtest5.
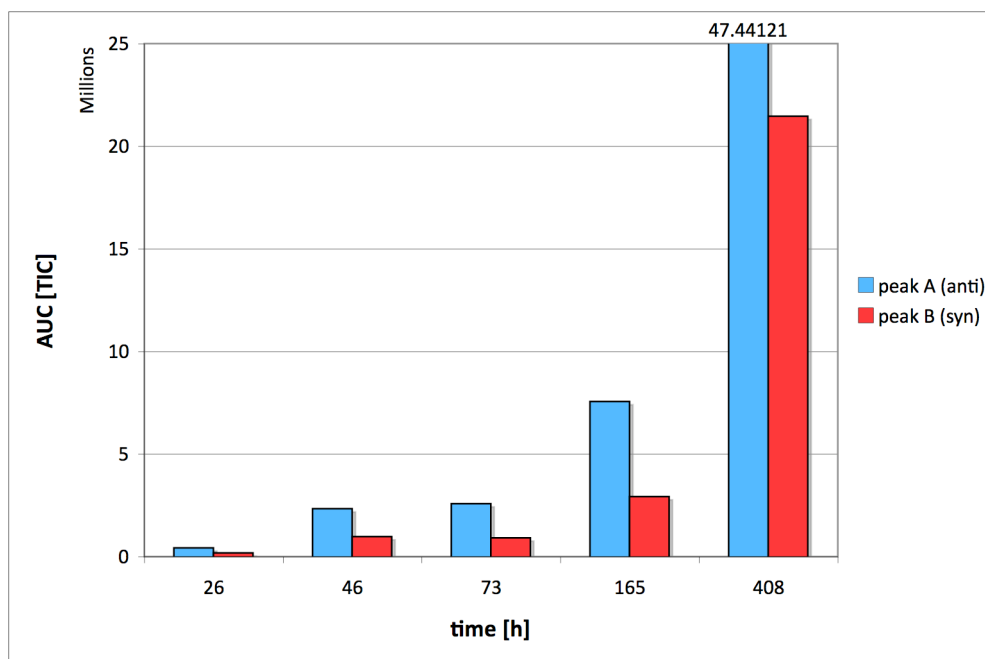
Figure 3-49. Peak intensities (AUC) of ISCtest5.

3.6.5.5. *In situ* click test experiment 6 (ISCtest6)
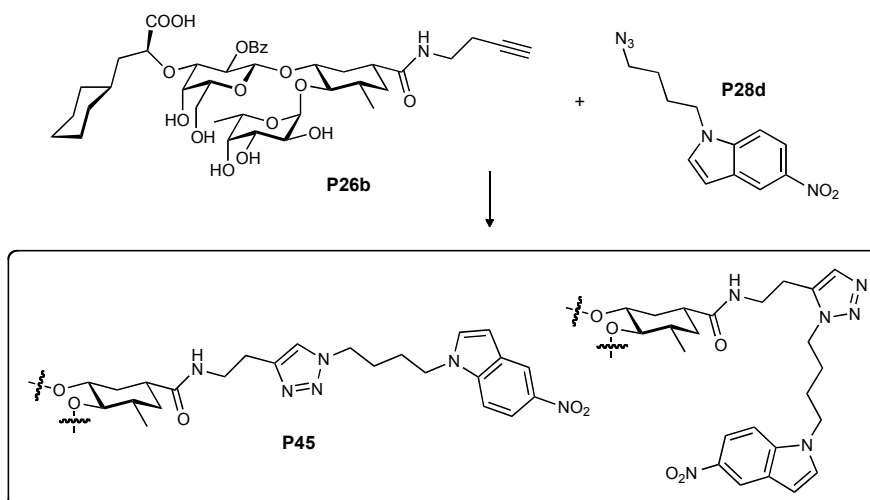
Scheme 3-23. ISCtest6: **P26b**: 500 µM; **P28d**: 600 µM; 5% DMSO; 37 °C.

Rationale:

ISCtest6 was performed to investigate the separation behaviour of the 2s/aN isomers and as a reference for the ISC experiments.

Discussion and conclusions:

The 2s/a4N isomers were not separable using the standard chromatographic method for the ISC experiments.
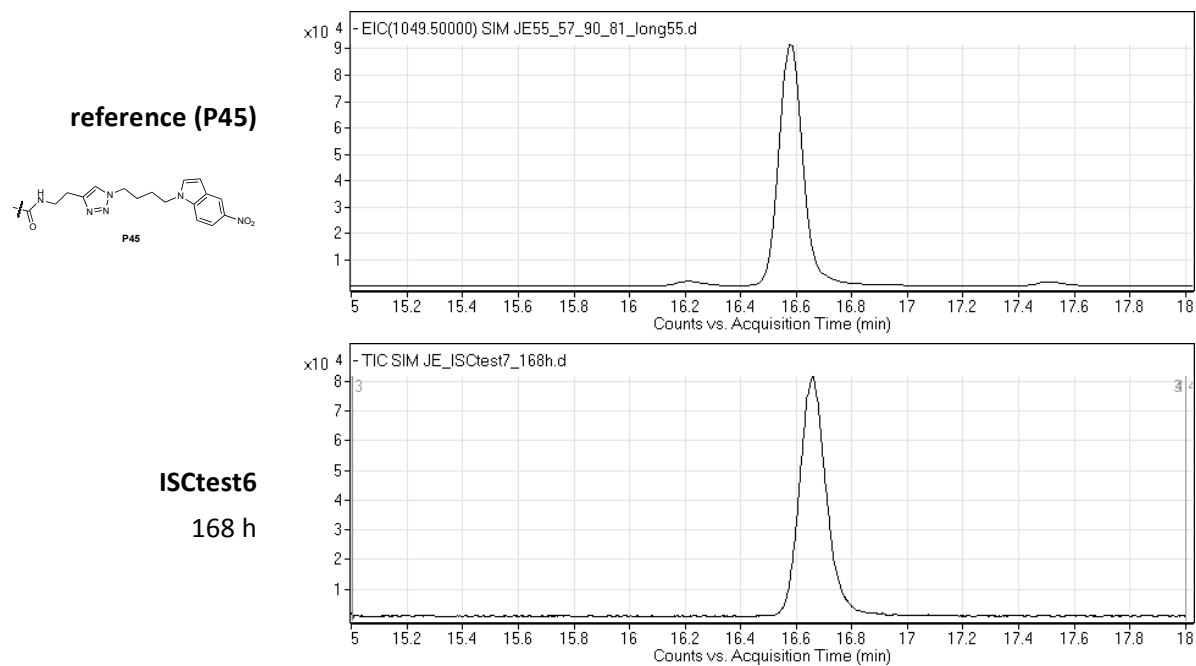
Figure 3-50. Representative chromatograms of ISCtest6.
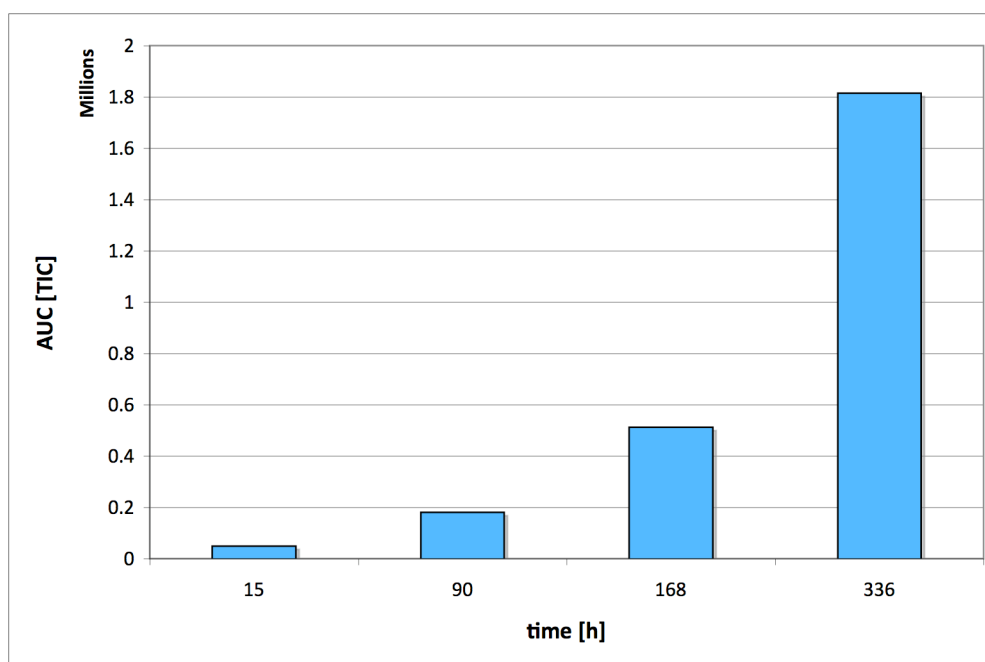
Figure 3-51. Peak intensities (AUC) of ISCtest6.

3.6.5.6. *In situ* click test experiment 7 (ISCtest7)
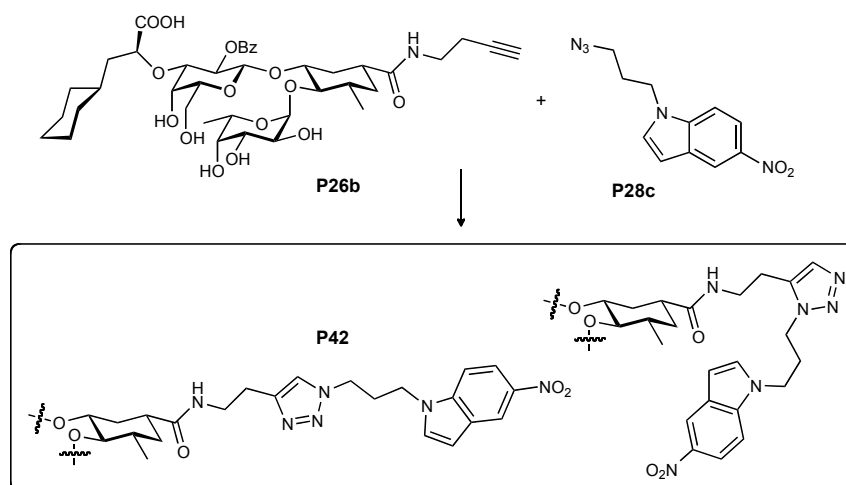
Scheme 3-24. ISCtest7: **P26b**: 500 mᴍ; **P28c**: 600 mᴍ; 5% DMSO; 37 °C.

Rationale:

ISCtest7 was performed to investigate the separation behaviour of the 2s/a3N isomers and as a reference for the ISC experiments.

Discussion and conclusions:

The 2s/a3N isomers are not separable using the standard chromatographic method for the ISC experiments.
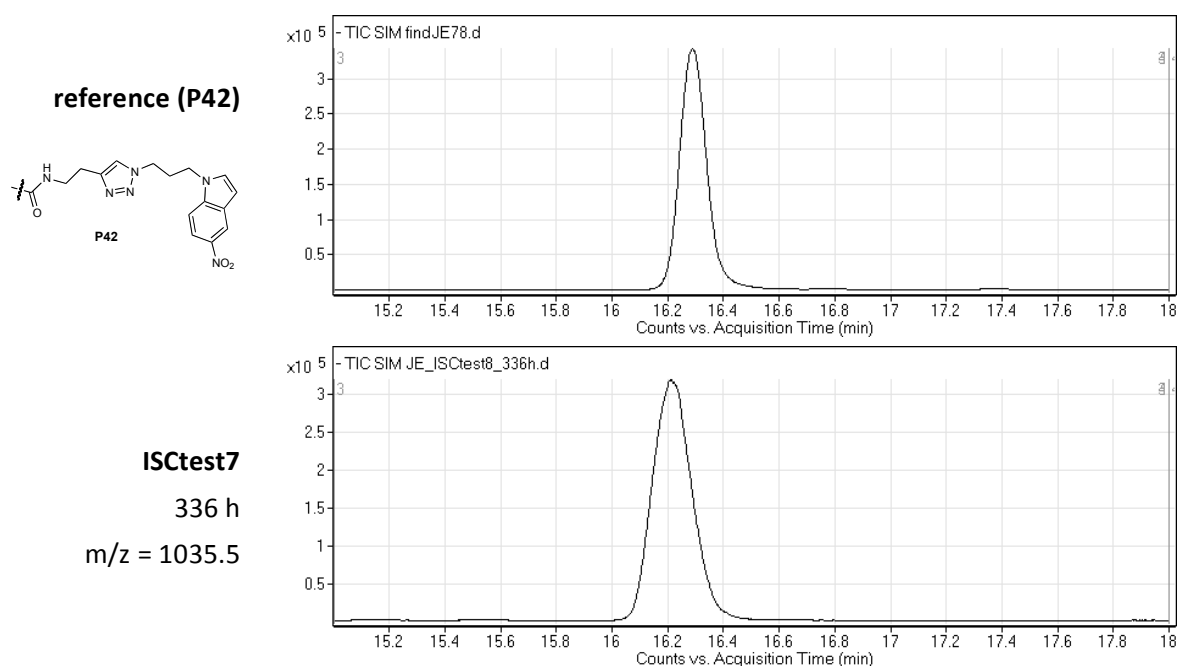
Figure 3-52. Representative chromatograms of ISCtest7.
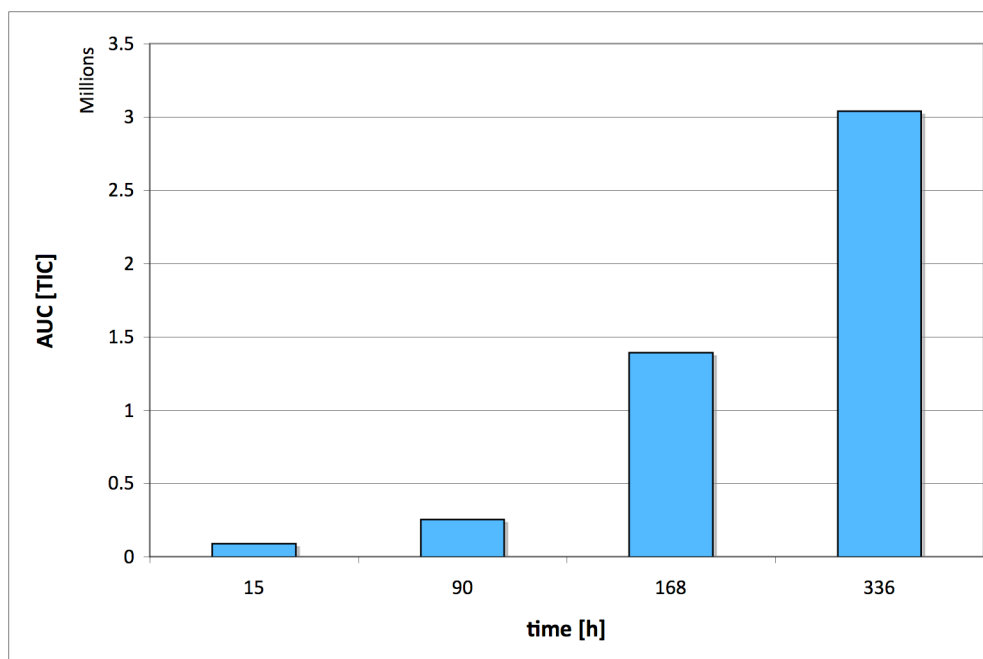
Figure 3-53. Peak intensities (AUC) of ISCtest7.

3.6.5.7. *In situ* click test experiment 8 (ISCtest8)
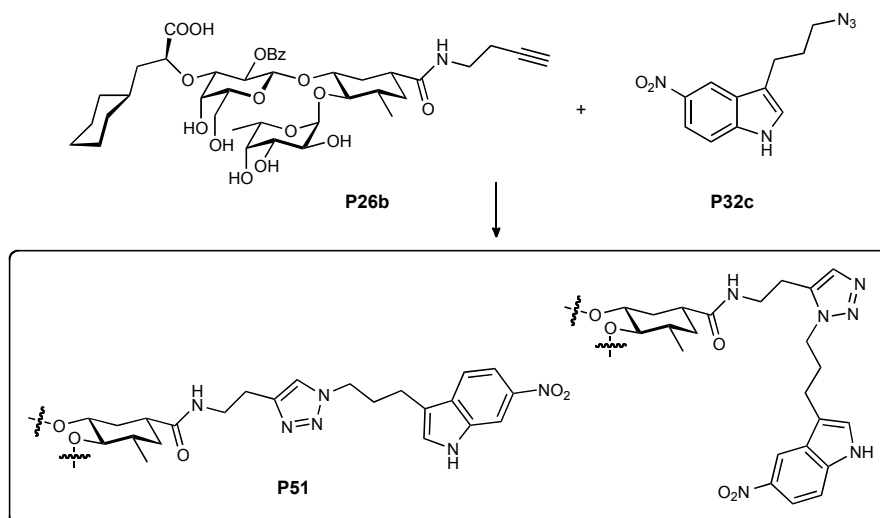
Scheme 3-25. ISCtest8: **P26b**: 500 mM; **P32c**: 600 mM; 5% DMSO; 37 °C.

Rationale:

ISCtest8 was performed to investigate the separation behaviour of the 2s/a3C isomers and as a reference for the ISC experiments.

Discussion and conclusions:

The 2s/a3C isomers were not separable using the standard chromatographic method for the ISC experiments. Their retention times were shorter than the ones of the 2s/a3N isomers (as

exemplified by the chromatogram of **P42**), which may be explained by the hydrogen-bond donor ability of the free indole NH group.
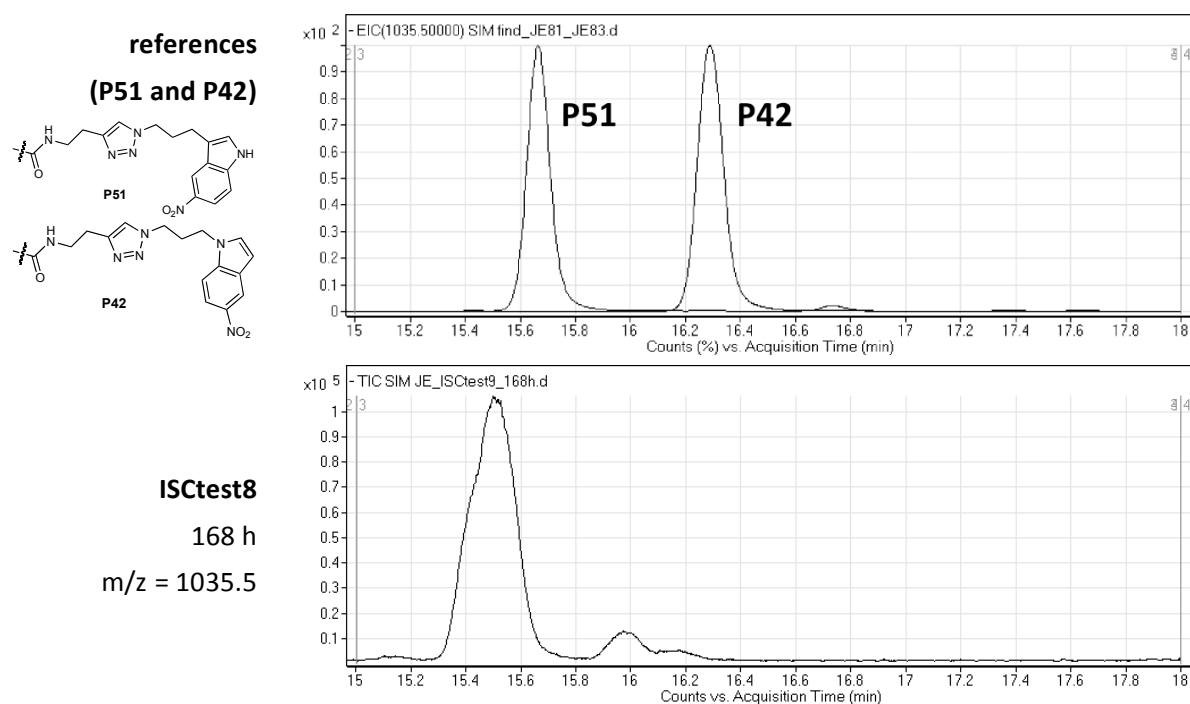
Figure 3-54. Representative chromatograms of ISCtest8. The deviating retention times of reference **P51** and **ISCtest8** were caused by a worn out pre-column.
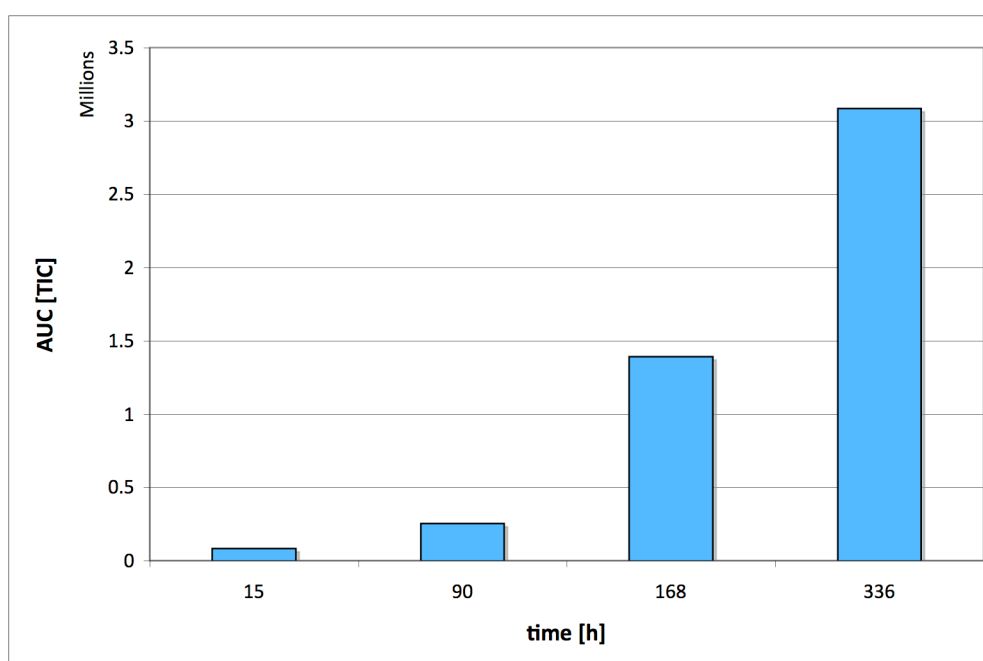
Figure 3-55. Peak intensities (AUC) of ISCtest8.

189

3.6.5.8. Protein denaturation – necessity or not?

This experiment was performed to assess the influence of sample preparation for MS analysis. Specifically, the question should be answered whether diluting the protein with an organic solvent instead of water and formic acid would influence signal intensity, *e.g.* by better liberating potentially protein-bound ligand from the protein. Thus, MeOH or MeCN instead of H_2O + 0.1% HCOOH were used to dilute the samples of an ISC experiment (not shown; the experimental conditions were identical to ISC6), which led to precipitation of the protein. Before injection into the HPLC-MS, the sample was centrifuged, the supernatant was removed and the concentration of first-site ligands was analyzed. At ligand and protein concentrations of 50 and 80 µM, respectively, 97% percent of the first-site ligand **P26c** (K_D used for calculation = 1 µM) is bound to protein. Thus, this setup is expected to be suitable for detecting differences in measured ligand concentrations that may result from differential ligand liberation.

It was found that denaturing the protein with an organic solvent is not advantageous over the previously used procedure with H_2O and formic acid for the following reasons: 1) With MeOH or MeCN, the baseline was elevated, as illustrated in Figure 3-56. This may be caused by the high elution strength of MeOH and MeCN. 2) The measured TIC signal of the first-site ligands in the E-selectin sample was actually *lower* than in the BSA and buffer samples (Figure 3-57). Furthermore, the dilution with MeOH led to a generally lower signal, which may be a result of the elevated baseline or the additional centrifugation step.

When water was used for the dilution, the signal was highest in the BSA sample and approximately equal in the E-selectin and buffer sample. This further indicates that sample preparation using water and formic acid does *not* lead to an underestimation of ligand concentrations in the E-selectin sample. Also in other ISC experiments, a depletion effect caused by E-selectin was not observed, as exemplified in Figure 3-58.
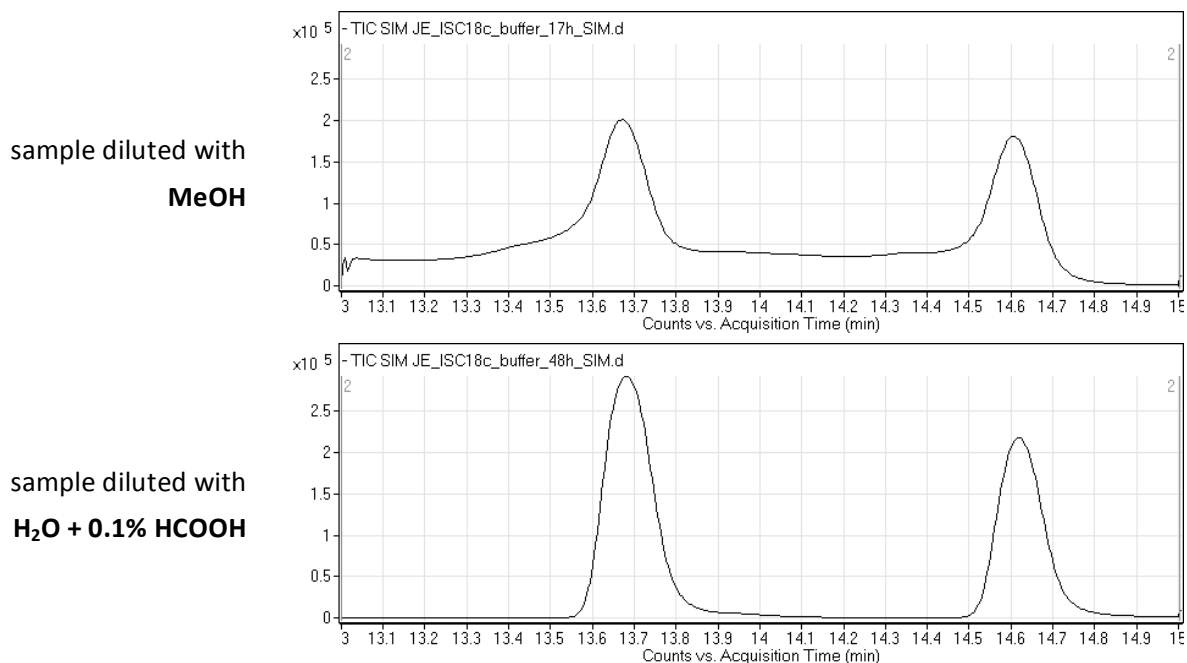
Figure 3-56. Dependence of peak and baseline shapes from the sample preparation.
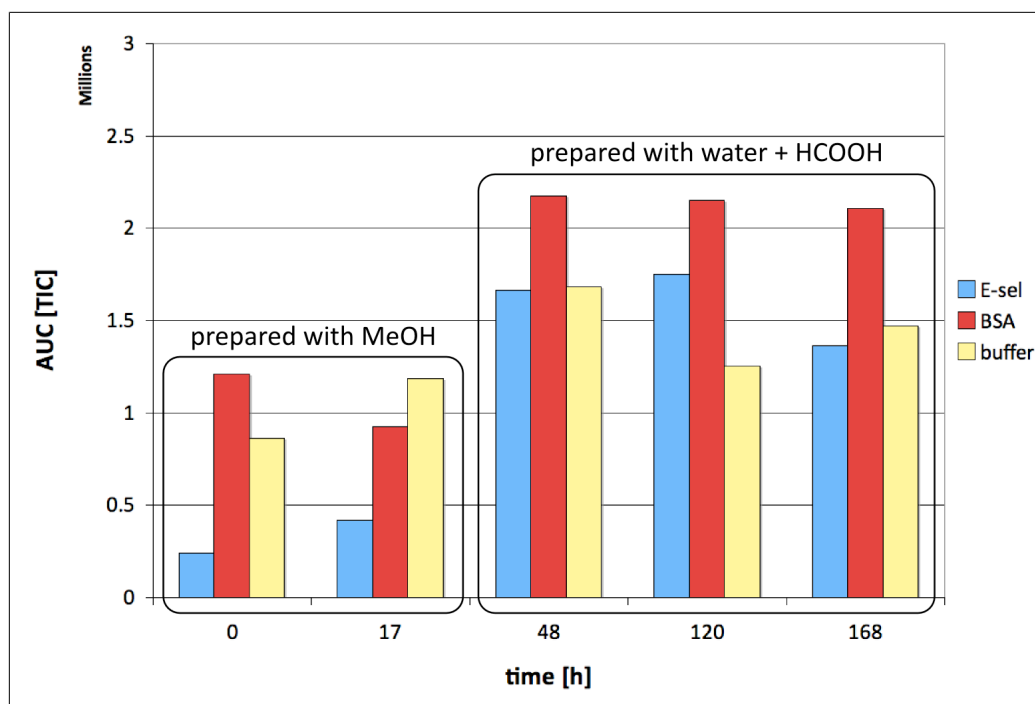
Figure 3-57. Depencence of signal intensities of the first-site ligand **P26c** from the way of sample preparation.
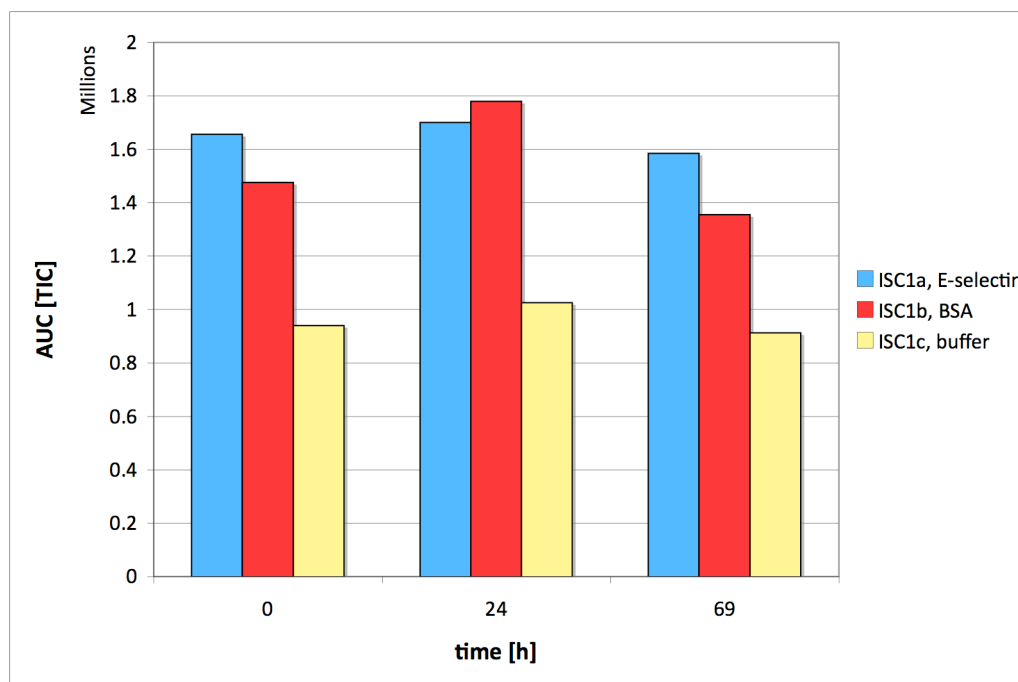
Figure 3-58. Signal intensities of the first-site ligand **P26b** as measured in ISC1.

3.6.6. Nitroindole concentrations in ISC experiments

In most ISC experiments, spontaneous triazole formation appeared to be faster in the BSA sample than in the E-selectin and the buffer samples, an observation that was also made by Fokin and coworkers in their *in situ* click experiment for the identification of inhibitors of HIV protease 1 (184). A series of experiments and tests was performed to elucidate the cause of this phenomenon.

3.6.6.1. Course of nitroindole concentrations during an ISC experiment

Figure 3-59 shows the relative concentrations of second-site ligands in ISC experiment 10 determined from the UV chromatographic trace, which was recorded along with the MS trace. After 24 h, the concentration of **P28c** in the buffer sample was reduced by a factor of 5.2 compared to the BSA sample and remained constant for the residual duration of the experiment. The decrease was slower in the E-selectin sample, but after 188 h, the nitroindole concentration had neverless dropped to about 50% of the original value. Qualitatively, this effect was observed in most other ISC experiments as well. Thus, the apparently faster reaction rates in the BSA samples may result from a higher ligand concentration. This observation can be explained by the pronounced ligand-binding properties of serum albumins, which were, for example, investigated at the Instiute of Molecular Pharmacy (220).
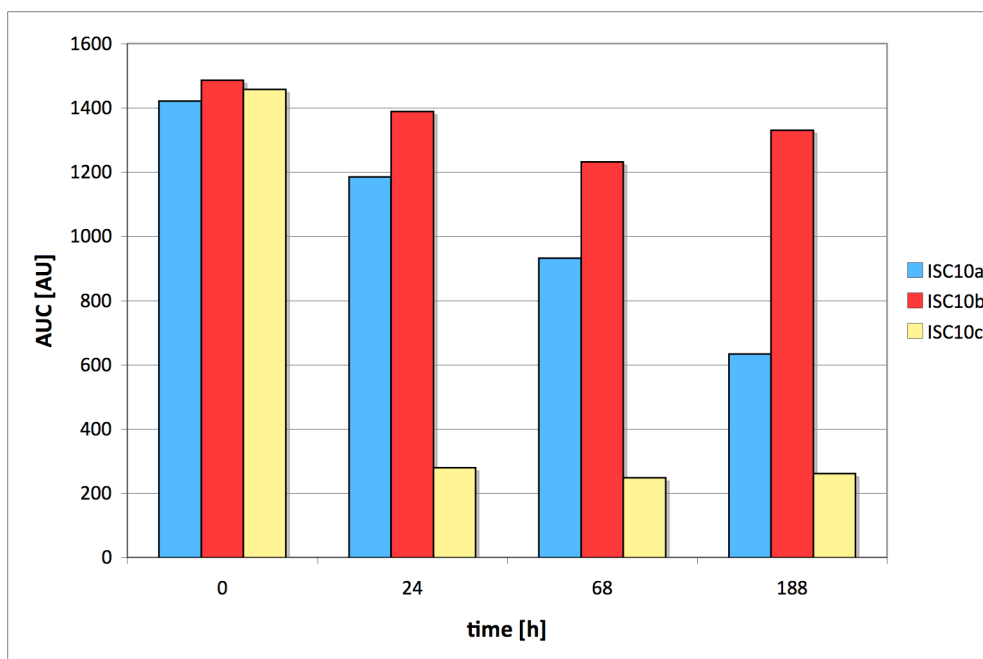
Figure 3-59. Relative concentrations (represented by the AUC of the UV absorption signal at a wavelength of 350 nm) of the second-site ligand **P28c** in ISC10.

3.6.6.2. The influence of DMSO concentrations on nitroindole concentration

As the binding behavior of E-selectin was found to remain constant for DMSO concentrations up to 10% (221), it was tested whether, at a DMSO concentration of 10%, the putative precipitation of the nitroindoles could be prevented (Figure 3-60). However, the decrease of nitroindole concentration was just slightly lower in the vial with 10% DMSO: after 24 h, it had dropped by 75% compared to the vial with BSA. With 5% DMSO, the concentration decrased by 83%.
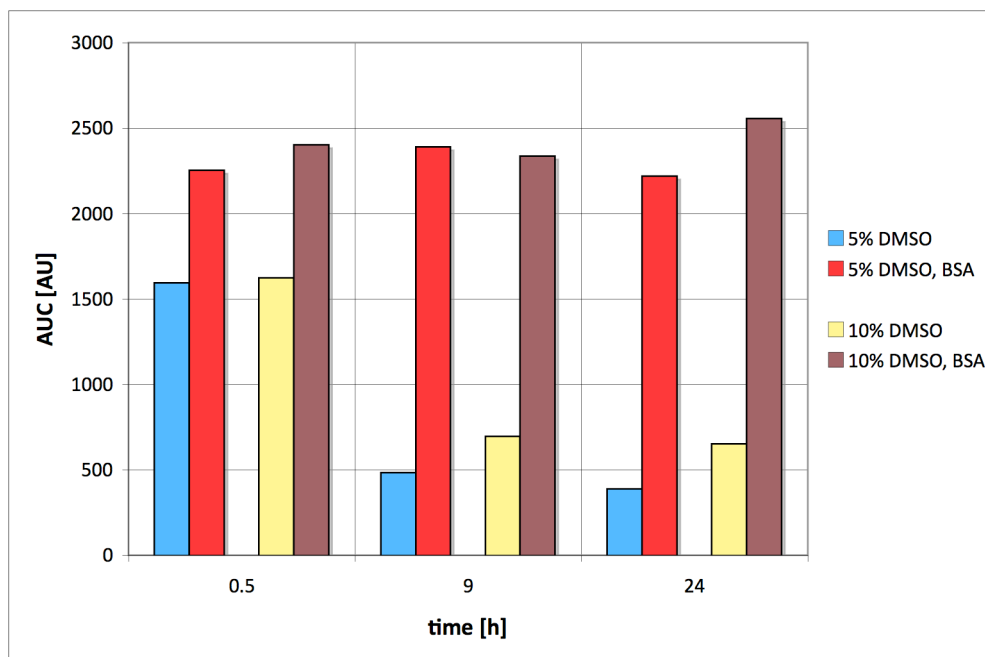
Figure 3-60. Concentrations of nitroindole **P28c** (represented by the AUC of the UV absorption signal at a wavelength of 350 nm). Initial concentration of **P28c**: 500 µM; BSA concentration: 80 µM.

3.6.6.3. Vialtest

To assess whether adsorption of the nitroindole to the tube surface might influence the nitroindole concentration, an experiment with tubes made of glass, standard polypropylene (PP) tubes and "Protein LoBind" was performed (Figure 3-61). Again, only BSA was able to prevent the concentration drop, while there was little to no variation between the different tube materials.
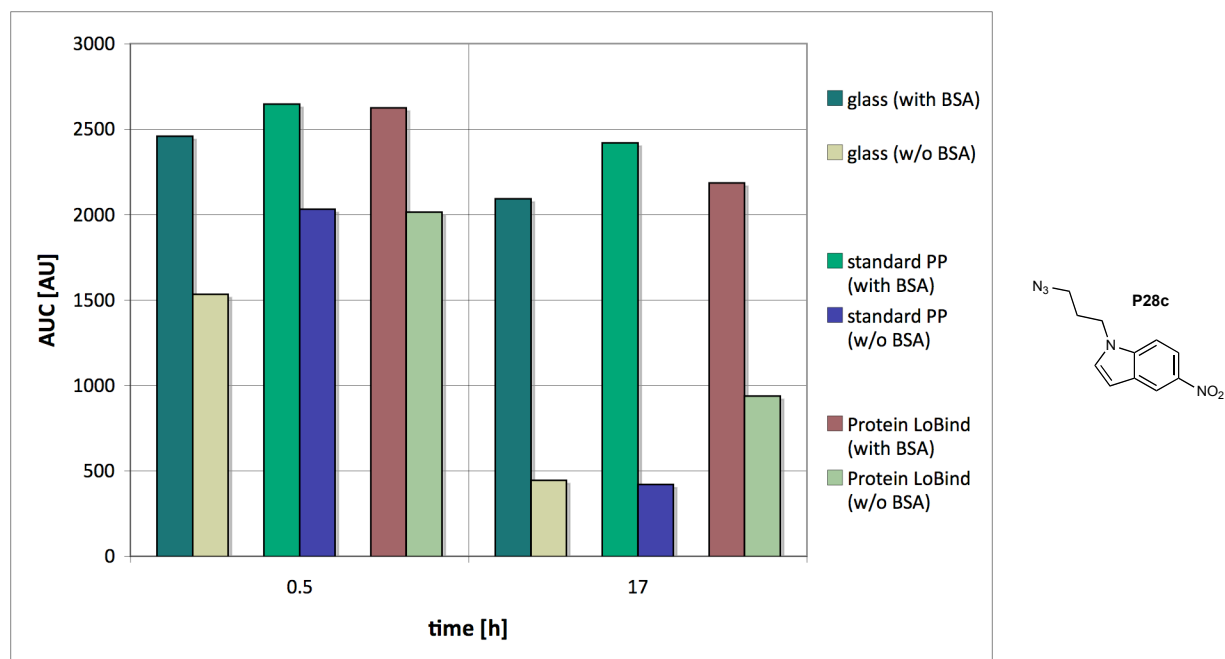
Figure 3-61. Influence of vial material on nitroindole concentrations; PP: polypropylene.

3.6.7. Discussion and conclusions

Despite a careful experimental design and the variety of experimental conditions used, in none of the ISC exepriments a catalytic effect of E-selectin was found. Based on this observation it is concluded that E-selectin does not act as a supramolecular catalyst for the 1,3-dipolar cycloaddition of alkyne and azide first- and second-site ligands as available in the present setup.

The apparent inability of E-selectin to accelerate the alkyne–azide cycloaddition may well be explained by virtue of Menger's "spatiotemparal postulate" mentioned in Section 3.5.5. Due to the shallow nature of the binding site (*cf.* Figure 3-17) and the short half-life time of the ligand–receptor complexes (Section 2), E-selectin is probably not suited to fulfill either the spacial and/or the temporal requirements for supramolecular catalysis.

Several test experiments were performed to validate the observations of the *in situ* click experiments. None of these experiments suggested shortcomings in the experimental setup that might have caused false-negative results. The test experiments further revealed differences in retention times and in rates of *syn* and *anti* triazole formation that depended on the length of the involved linkers. This finding indicates, along with observations in ^{1}H NMR spectra (*cf.* Section 3.4), that the solution conformations of triazole–nitroindole antagonists with different linker patterns differ significantly.

4. Conclusions and Outlook

4.1. Conclusions

The important contributions of E-selectin to chronic inflammatory diseases and cancer make it an attractive drug target. However, small-molecule antagonists of E-selectin have been suffering from comparably low micromolar affinities, which is a result of the shallow and highly solvent-accessible binding site of E-selectin.

This work aimed at the affinity improvement of carbohydrate-based E-selectin antagonists *via* a fragment-based approach that does not rely on structural information and has successfully been applied to another lectin (MAG) previously (160).

4.1.1. New antagonists

Second-site ligands were identified using an NMR-based screening (performed by Céline Weckerle). The attachment of a TEMPO spin label to a given first-site ligand allowed to identify 5-nitroindole as a second-site ligand that binds simultaneously with and in the vicinity of the first-site ligand.

After the identification of the second-site ligand, a library of first-and second-site antagonists bearing azido- or alkynyl-functionalized linker moieties of different length was synthesized. *In situ* click experiments, as first described by Sharpless and coworkers (177), were performed for the identification of a suitable linker pattern. Because these experiments failed (see below), a library of triazole–nitroindole antagonists was synthesized and screened in a specifically designed Biacore assay (Céline Weckerle). The five most potent antagonists identified in the screening were characterized in detail using Biacore, which revealed antagonists with K_Ds between 30 and 90 nM and ligand–protein half-life times in the range of 4 to 5 minutes instead of seconds.

The synthesis of indoleamine and indole acetamide derivatives revealed important contributions of the nitro group to binding, as its replacement was accompanied by a loss of affinity. The same effect was observed for the substitution of the triazole moiety by piperazine.

Owing to their amphiphilic properties, all antagonists exhibited some surface activity and were found to form micelles at concentrations around 1 to 10 mM. The surface activity was reduced by the replacement of the nitro group by the more hydrophilic amine and acetamide,

but not by the introduction of the piperazine moiety.

Based on their pharmacokinetic and physicochemical properties (measurements performed by Matthias Wittwer and Simon Kleeb), none of the tested angatonists is expected to be passively absorbed from the gastrointestinal tract.

4.1.2. *In situ* click experiments

To ensure suitable experimental conditions, the reation kinetics associated with an *in situ* click experiment were analyzed on a theoretical basis. The insights gained were applied to a number of *in situ* click experiments. However, in none of these, a catalytic effect of E-selectin was observed, and it was concluded that E-selectin does not act as a supramolecular catalyst in the present setup. This finding was validated in several control experiments, which did not reveal any shortcomings in the experimental setup. Based on other examples of alkyne–azide cycloadditions accelerated by supramolecular catalysts, the shallow nature of the binding site and the short half-life time of the ligand–receptor complexes were identified as possible causes for the absence of a catalytic effect of E-selectin.

4.2. Outlook

The triazole–nitroindole antagonists described herein are characterized by higher affinity and by markedly altered binding kinetics compared to the tetrasaccharide mimics. To further exploit the potential revealed by the discovery of these antagonists, detailed structural information from a co-crystal structure of E-selectin is necessary. This is further accentuated by observations made in other work (131, 133). For example, STD NMR experiments suggesting a direct interaction of subsitutents at the 2'-position of galactose can currently not be reconciled with the expected and computationally predicted binding mode of E-selectin ligands. In additon, more precise structural knowledge may help explain the failure of the *in situ* click experiment.

Apart from crystal structure data, ITC and STD NMR studies could provide additional insights into the binding of triazole–nitroindole antagonists. However, first experiments were hampered by solubility and aggregation problems (*cf.* Section 3.2.1).

The structure of the second-site ligand and of the linker were at least partly determined by the requirements of the screening process and not by the yet unknown structural needs of the protein. The new ligands are thus expected to have a considerable potential for further improvement of binding affinity.

As outlined in Section 2, the linker may be optimized with respect to flexibility and to additional polar or hydrophobic interactions: The linker of the currently best antagonist (**P43**) contains 8 rotatable bonds, the freezing of which may cause entropy costs upon binding. Consequently, the introduction of rigidity at appropriate locations, *e.g.* by double/triple bonds or heterocycles other than triazole, may be beneficial in terms of ligand preorganization. The studies on piperazine derivative **33** demonstrated that the introduction of positive charges into the linker moiety is rather not favorable with respect to physicochemical and pharmakokinetic properties. For the reduction of the amphiphilic character, polar but uncharged groups, such as ethers, may be more suitable. It must be considered, though, that the introduction of additional hydrogen bond acceptors may not be desirable with respect to oral bioavailability.

The nitroindole modifications described in Section 2 have given a first hint of the structural requirements of the second binding site. Due to the potentially toxic metabolites of nitro groups, future research could be directed towards the investigation of isosteric replacements.

Owing to limited time, in the present work the screening was limited to *anti* triazoles. These have proven high activity and are readily accessible *via* the CuAAC. However, based on currently available data, high affinities of *syn* triazoles cannot be excluded. Given the flexible linkers of the high-affinity antagonists, bent linker conformations in the bound state appear plausible. Such conformations might be achieved by *syn* triazoles equally well or even better, and thus *syn* triazoles may be of interest in the future. Again, structural informations from a crystal structure would be highly beneficial here, as the cost-benefit ratio of another *syn* triazole screening is probably not justifiable.

Similar considerations apply to future *in situ* screening experiments with E-selectin. A screening may rather be indicated for the in-house P-selectin program, where a second-site screening is of interest, too. Based on the failure of the *in situ* click approach, alternative methods should be evaluated for future attempts, however. These may include alternative (irreversible) reactions or be based on a dynamic combinatorial approach.

5. Experimental Section

5.1. General Methods

5.1.1. Chemistry

See Section 2.

5.1.2. *In situ* click experiments

Composition of the HEPES buffer. 4-(2-Hydroxyethyl)-1-piperazineethanesulfonic acid (HEPES) 10 mM (pH 7.4), NaCl 150 mM, CaCl$_2$ 1 mM, surfactant P20 0.005%.

QQQ MS. Separation was performed on a Agilent 1100 Series HPLC instrument with a 1200 series Autosampler, connected to a Agilent 6400 Series Triple Quadrupole mass spectrometer for quantification (Agilent Technologies, Santa Clara CA, USA). Bidestilled water with 0.1% formic acid and acetonitrile with 0.1% formic acid were used as solvents. A gradient of acetonitrile in water (each containing 0.1% HCOOH) was was applied (acetonitrile: 5% → 55% within 18 min) at a flow rate of 0.6 mL/min. For the separation a Waters Atlantis T3 column (2.1 x 50 mm) with a bead size of 3 μm was used (Waters, Milford MA, USA). The column was heated to 60 °C and the flow was set to 0.6 mL/min. 50 μL of analyte were injected per run. The data were performed with the MassHunter software (Agilent Technologies, Version B.01.04).

5.2. Experiments (Chemistry)

2,5-Dioxopyrrolidin-1-yl 2-[2-(2-{[(9*H*-fluoren-9-ylmethoxy)carbonyl]amino}ethoxy)ethoxy]acetate (P36)

2-[2-(2-{[(9*H*-fluoren-9-ylmethoxy)carbonyl]amino}ethoxy)ethoxy]acetic acid (185 mg, 0.480 mmol) and *N*-hydroxysuccinimide (110 mg, 0.956 mmol) were dissolved in anhydrous THF (1.5 mL). DIC was added dropwise to the solution at r.t., leading to the precipitation of a white solid. After 2 h, the reaction mixture was filtrated through a PTFE membrane filter (0.2 μM), and the solvent was removed. The crude product was redissolved in Et$_2$O. The organic phase was washed with aq. NaHCO$_3$ and 0.5 M aq. HCl. The organic layer was dried over Na$_2$SO$_4$, and the solvent was removed. The crude product was dissolved in CH$_2$Cl$_2$, and the solution was filtrated. After removal of the solvent, the crude product **P36** (210 mg) was used in the synthesis of **P35** without further purification.

9*H*-Fluoren-9-ylmethyl-*N*-{2-[2-({[1-(3-azidopropyl)-1*H*-indol-5-yl]carbamoyl}methoxy)ethoxy]ethyl}carbamate (P35)

Amine **P34** (50 mg, 0.232 mmol) and succinimide ester **P36** (120 mg, 0.249 mmol) were dissolved in anhydrous DMF (1 mL) and stirred at r.t. for 15 h. The solvent was removed *in vacuo*, and the residue was purified using silica gel chromatography (EtOAc in CH_2Cl_2, gradient 0 to 80%). 70 mg (52%) of **P35** was obtained as a mixture of inseparable products (green-yellow oil).

^{1}H-NMR (500 MHz, CDCl$_3$): δ 1.88-1.96 (m, 2H, H-2'), 3.10 (t, J = 6.3 Hz, 2H, H-3'), 3.32-3.38 (m, 2H, H-6''), 3.56 (t, J = 5.0 Hz, 2H, H-5''), 3.64 (d, J = 4.2 Hz, 2H, H-4''), 3.73 (d, J = 4.4 Hz, 2H, H-3"), 4.02-4.11 (m, 5H, H-9", H-2". H-1'), 4.25 (d, J = 7.0 Hz, 2H, H-8"), 6.36-6.40 (m, 1H, Ind H-3), 6.96-6.99 (m, 1H, Ind H-2), 7.15-7.25 (m, 4H, Ind H-6. Ind H-7, B), 7.27-7.34 (m, 2H, C), 7.42-7.48 (m, 2H, A), 7.64-7.71 (m, 2H, D), 7.81 (d, J = 1.4 Hz, 1H, Ind H-4), 8.56 (s, 1H, CON*H*); ^{13}C-NMR (125 MHz, CDCl$_3$): δ 29.43 (C-2'), 40.82 (C-6''), 43.23 (C-1'), 47.31 (C-9''), 48.40 (C-3'), 66.83 (C-8''), 70.23 , 70.43, 70.90, 71.28, 101.91 (C-3), 109.60 (C-7), 113.11 (C-4), 115.99 (C-6), 120.11 (Fmoc-C), 125.22 (Fmoc-C), 127.19 (Fmoc-C), 127.83 (Fmoc-C), 128.91 (Fmoc-C), 128.93 (Fmoc-C), 129.62 (C-8), 133.63 (C-5), 141.41 (Fmoc-C), 144.06 (Fmoc-C), 156.60 (O*C*ONH), 167.97 (CH$_2$*C*ONH); MS: m/z calcd for $C_{32}H_{34}N_6O_5$ [M+Na]$^+$: 605.25; found: 605.22.

(1*R*,3*R*,4*R*,5*S*)-*N*-(3-{1-[3-(5-{2-[2-(2-Aminoethoxy)ethoxy]acetamido}-1*H*-indol-1-yl)propyl]-1*H*-1,2,3-triazol-4-yl}propyl)-3-[2-*O*-benzoyl-3-*O*-((1*S*)-1-carboxy-2-cyclohexyl-ethyl)-(β-D-galactopyranosyl)oxy]-4-[(α-L-fucopyranosyl)oxy]-5-methylcyclohexanecarboxamide (P38)

Following general procedure **III** (Section 2), alkyne **P26c** (12.0 mg, 14.9 µmol), azide **P35** (13 mg, 22.3 µmol), Na-L-ascorbate (75 µL, 7.50 µmol) and CuSO$_4$·5H$_2$O (38 µL, 3.80 µmol) were stirred in ^{t}BuOH/H$_2$O/THF 1:1:1 (1 mL; no prior degassing) for 2 h, followed by the addition of piperidine (4.4 µL). After another hour, further 10 µL of piperidine was added, and stirring was continued for 2 h. Following removal of the solvent *in vacuo*, the residue was dissolved in MeOH, filtrated through a PTFE membrane filter, and the solution was centrifuged. The supernatant was subjected to preparative HPLC-MS to afford **P38** as a colorless solid (11.4 mg, 66%).

^{1}H-NMR (500 MHz, MeOD): δ 0.39-0.69 (m, 4H, Cy), 0.79-0.93 (m, 1H, Cy), 1.09 (d, J = 6.4 Hz, 3H, Me), 1.12-1.41 (m, 11H, H-2$_a$, H-6$_a$, 4Cy, Fuc H-6, Lac H-3$_a$), 1.41-1.51 (m, 1H,

Lac H-3$_b$), 1.51-1.61 (m, 2H, H-6$_b$, Cy), 1.61-1.73 (m, 1H, H-5), 1.73-1.84 (m, 2H, H-2'), 2.10-2.15 (m, 1H, H-2$_b$), 2.21-2.29 (m, 1H, H-1), 2.44 (p, J = 6.6 Hz, 2H, H-2"), 2.62-2.69 (m, 2H, H-3'), 3.05-3.20 (m, 5H, H-1', H-4, H-6*), 3.49 (d, J = 9.2 Hz, 1H, Gal H-3), 3.52-3.57 (m, 1H, Gal H-5), 3.65-3.83 (m, 12H, H-3, Fuc H-2, Fuc H-4, Gal H-6, H-3*, H-4*, H-5*, Lac H-2), 3.86 (dd, J = 3.2, 10.3 Hz, 1H, Fuc H-3), 3.89-3.94 (m, 1H, Gal H-4, 4.18-4.25 (m, 4H, H-2*, H-3"), 4.34 (t, J = 6.7 Hz, 2H, H-1"), 4.64 (d, J = 8.1 Hz, 1H, Gal H-1), 4.94-5.00 (m, 3H, Fuc H-1, Fuc H-5), 5.39 (t, J = 8.8 Hz, 1H, Gal H-2), 6.44 (d, J = 3.0 Hz, 1H, Ind H-3), 7.26 (d, J = 3.0 Hz, 1H, Ind H-2), 7.28 (s, 2H, Ind H-6, Ind H-7), 7.31-7.36 (m, 2H, C$_6$H$_5$), 7.43-7.49 (m, 1H, C$_6$H$_5$), 7.61 (s, 1H, H-5'), 7.83 (s, 1H, Ind H-4), 7.95-8.01 (m, 2H, C$_6$H$_5$); ^{13}C-NMR (125 MHz, MeOD): δ 16.79 (Fuc C-6), 19.29 (Me), 23.54 (C-3'), 26.52, 26.77, 27.36 (3C, Cy), 30.19 (C-2'), 31.60 (C-2"), 33.03, 34.37, 35.33 (3C, Cy), 35.53 (C-2), 37.40 (C-6), 39.25, 39.42 (2C, C-5, C-1'), 40.57 (C-6*), 43.23 (C-1), 43.43 (Lac C-3), 44.20 (C-3"), 48.69 (C-1")‡, 63.06 (Gal C-6), 67.59, 67.74 (2C, Gal C-4, Fuc C-5), 68.00 (C-5*), 70.27 (Fuc C-2) 70.33, 71.36 (2C, Fuc C-3, C-2*), 71.48 (2C, C-3*, C-4*), 73.00 (Gal C-2), 73.94 (Fuc C-4), 76.06 (Gal C-5), 79.75 (C-3), 83.02 (C-4), 83.69 (Gal C-3), 100.39 (Fuc C-1), 100.62 (Gal C-1), 102.57 (Ind C-3), 110.52 (Ind C-7), 114.43 (Ind C-), 117.31 (Ind C-6), 123.66 (C-5'), 129.62 (C$_6$H$_5$), 130.13, 130.18 (2C, Ind C-2, Ind C-9), 130.82 (C$_6$H$_5$), 130.96, 131.66 (2C, Ind C-5, C$_6$H$_5$), 134.16 (C$_6$H$_5$), 135.01 (Ind C-8), 148.82 (C-4'), 166.78 (O(C=O)Ph), 170.59 (C-1*), 177.03 (CONH); HPLC (λ = 350 nm): purity = 95%, t$_R$ = 12.483 min; [a]$_D^{20}$ = -44.4 (c = 0.67, MeOH); IR (KBr): ν = 3430 (vs, OH), 3137 (m, NH$_2$), 2925 (vs), 2855 (m), 1724 (m), 1720 (m), 1654 (s), 1649 (s), 1586 (s), 1542 (m), 1489 (m), 1450 (m), 1401 (w), 1385 (w), 1340 (w), 1293 (w), 1272 (s), 1219 (vw), 1163 (w), 1117 (vs), 1098 (vs), 1079 (vs), 1032 (s), 997 (w), 967 (vw), 802 (vw), 763 (vw), 714 (w) cm^{-1}.

3-{4-[3-(5-Nitro-1H-indol-1-yl)propyl]piperazin-1-yl}propan-1-ol (34)

Bromide **P27c** (176 mg, 0.622 mmol), 3-(piperazin-1-yl)propan-1-ol (278 mg, 1.93 mmol), and Et$_3$N (259 μL, 1.87 mmol) were dissolved in anhydrous DMF and stirred at r.t. for 2 h. After removal of the solvent *in vacuo*, the crude product was subjected to silica gel chromatography (MeOH in CH$_2$Cl$_2$, gradient 0 to 20 to 80%) to afford **34** (215 mg, quant.) as yellow crystals.

^{1}H-NMR (500 MHz, CDCl$_3$): δ 1.70-1.76 (m, 2H, H-2"), 1.99 (p, J = 6.7 Hz, 2H, H-2'), 2.04-3.07 (bs, 8H, Pip-H), 2.23 (t, J = 6.7 Hz, 2H, H-3'), 2.61-2.66 (m, 2H, H-1"), 3.77-3.81 (m, 2H, H-3"), 4.25 (t, J = 6.6 Hz, 2H, H-1'), 6.66 (d, J = 2.9 Hz, 1H, H-3), 7.27 (d, J = 3.2 Hz, 1H, H-2), 7.41 (d, J = 9.1 Hz, 1H, H-7), 8.08 (d, J = 9.1 Hz, 1H, H-6), 8.56 (d, J = 2.2 Hz,

1H, H-4); ^{13}C-NMR (125 MHz, CDCl$_3$): δ 27.06 (C-2"), 27.12 (C-2'), 44.10 (C-1'), 52.92 (2C, C-a, C-a'), 53.28 (2C, C-b, C-b'), 54.24 (C-3'), 58.61 (C-1"), 64.38 (C-3"), 103.99 (C-3), 109.44 (C-7), 117.01 (C-6), 118.18 (C-4), 127.58 (C-9), 131.23 (C-2), 138.98 (C-8), 141.39 (C-5); elemental analysis calcd (%) for C$_{18}$H$_{26}$N$_4$O$_3$ (346.42): C 62.41, H 7.56, N 16.17; found: C 62.21/62.02, H 7.67/7.64, N 15.96/16.01; IR (KBr): ν = 3435 (s, OH), 2947 (m), 2922 (m), 2826 (m), 1634 (vw), 1610 (w), 1578 (vw), 1513 (s), 1479 (m), 1464 (m), 1404 (w), 1369 (w), 1328 (vs, NO$_2$), 1306 (s), 1274 (m), 1186 (w), 1157 (m), 1130 (m), 1067 (s), 1006 (m) 899 (vw), 779 (w), 751 (m), 718 (w) cm^{-1}.

1-{3-[4-(3-Azidopropyl)piperazin-1-yl]propyl}-5-nitro-1*H*-indole (35)

Alcohol **34** (181 mg, 0.522 mmol) and diphenyl phosphoryl azide (DPPA; 134 μL, 0.626 mmol) were dissolved in anhydrous THF (2 mL). The solution was cooled to -15 °C in a salt-ice bath, and diazobicyclo undecene (DBU; 93.6 μL, 0.626 mmol) was added dropwise, and the solution was allowed to warm to r.t.. After 2 h, NaN$_3$ (71 mg, 1.09 mmol) was added to the reaction mixture as there was no reaction progress according to TLC (CH$_2$Cl$_2$, MeOH 10:1). After 12 h of stirring, additional 0.5 eq. of DPPA (56 μL, 0.261 mmol) and DBU (39 μL, 0.261 mmol) were added, and stirring was continued for 2 h. The solvent was removed under reduced pressure, the crude mixture was dissolved in EtOAc (30 mL), washed with satd. aq. NaHCO$_3$ (20 mL) and brine (20 mL). The aqueous layers were extracted with EtOAc (2 x 30 mL), and the organic phase was dried over Na$_2$SO$_4$. After removal of the solvent *in vacuo*, the mixture was purified using silica gel chromatography (MeOH in CH$_2$Cl$_2$, gradient 0 to 15 to 70%) to afford a mixture of azide **35** and its diphenyl phosphoryl ester (note: in TLC, azide and ester were not separable using CH$_2$Cl$_2$, MeOH 10:1). The mixture of azide and ester was dissolved in anhydrous DMF, and NaN$_3$ (171 mg, 2.63 mmol) was added. The mixture was stirred at 60 °C for 25 h until TLC (TLC plates were deactivated using petroleum ether + Et$_3$N) and MS indicated full conversion of the phosphoryl ester. H$_2$O (20 mL) was added, and the aqueous phase was extracted with EtOAc (3 x 50 mL). The organic layers were washed with NaHCO$_3$ (20 mL) and brine (20 mL) and subsequently dried over Na$_2$SO$_4$. After removing the solvent *in vacuo*, the crude product was purified using silica gel chromatography (MeOH in CH$_2$Cl$_2$, gradient 0 to 10 to 70%) to give azide **35** (154 mg, 79%) as a viscous yellow oil.

^{1}H-NMR (500 MHz, CDCl$_3$): δ 1.74-1.81 (p, *J* = *J* = 6.7 Hz, 2H, H-2"), 2.00 (p, *J* = 6.7 Hz, 2H, H-2'), 2.23 (t, *J* = 6.7 Hz, 2H, H-1'), 2.28-2.70 (m, 11H, Pip-H, H-1"), 3.34 (t, *J* = 6.7 Hz, 2H, H-3"), 4.26 (t, *J* = 6.6 Hz, 2H, H-1'), 6.67 (d, *J* = 3.2 Hz, 1H, H-3), 7.27 (d, *J* = 3.2 Hz,

1H, H-2), 7.43 (d, J = 9.1 Hz, 1H, H-7),), 8.09 (dd, J = 2.2, 9.1 Hz, 1H, H-6), 8.57 (d, J = 2.2 Hz, 1H, H-4); ^{13}C-NMR (125 MHz, CDCl$_3$): δ 26.35 (C-2″), 27.27 (C-2′), 44.21 (C-1′), 49.65 (C-3″), 53.07, 53.28 (4C, a/a′, b/b′), 54.40 (C-1′), 55.34 (C-1″), 104.05 (C-3), 109.53 (C-7), 117.13 (C-6), 118.28 (C-4), 127.66 (C-9), 131.30 (C-2), 139.08 (C-8), 141.52 (C5); elemental analysis calcd (%) for C$_{18}$H$_{25}$N$_7$O$_2$ (371.44): C 58.20, H 6.78, N 26.40; found: C 58.04/58.14, H 6.86/6.87, N 25.21/25.41; IR (KBr): ν = 2944 (w), 2813 (w), 2777 (vw), 2096 (s, N$_3$), 1611 (vw), 1514 (m), 1480 (w), 1463 (w), 1452 (w), 1403 (vw), 1333 (vs, NO$_2$), 1274 (w) 1159 (w), 1142 (vw), 1069 (w), 745 (m) cm^{-1}.

3-{4-[3-(5-Nitro-1*H*-indol-1-yl)propyl]piperazin-1-yl}propan-1-amine (36)

Azide **35** (149 mg, 0.401 mmol) and triphenyl phosphine (129 mg, 0.492 mmol) were dissolved in THF (4 mL) and H$_2$O (1 mL). The solution was stirred at 60 °C for 3 h, and the solvent was removed under reduced pressure. The mixture was redissolved in MeOH and subjected to preparative HPLC-MS (H$_2$O/MeCN + 0.2% HCOOH) to afford amine **36** (108 mg, 78%) as a viscous yellow oil.

^{1}H-NMR (500 MHz, MeOD): δ 1.89 (p, J = 7.0 Hz, 2H, H-2″), 2.14-2.21 (m, 2H, H-2′), 2.65-2.72 (m, 4H, H-1″, H-3′), 2.83 (d, J = 50.9 Hz, 8H, Pip H-b/b′, Pip H-a-/a′), 3.01 (t, J = 7.2 Hz, 2H, H-3″), 4.36 (t, J = 6.8 Hz, 2H, H-1′), 6.72-6.74 (m, 1H, H-3), 7.49 (d, J = 3.2 Hz, 1H, H-2), 7.60 (d, J = 9.1 Hz, 1H, H-7), 8.08 (dd, J = 2.2, 9.1 Hz, 1H, H-6), 8.54 (d, J = 2.2 Hz, 1H, H-4); ^{13}C-NMR (125 MHz, MeOD): δ 24.46 (C-2″), 27.05 (C-2′), 39.21 (C-3′), 44.84 (C-1′, 52.20 (C-b/b′), 52.70 (C-a/a′), 55.28 (C-3′), 55.67 (C-1″), 105.10 (C-3), 110.80 (C-7), 117.81 (C-6), 118.79 (C-4), 129.29 (C-9), 132.83 (C-2), 140.36 (C-8), 142.76 (C-5); IR (KBr): ν = 2952 (m), 2835 (w), 1632 (s), 1610 (s), 1514 (s, NO$_2$), 1479 (m), 1450 (m), 1400 (s), 1385 (s), 1334 (vs, NO$_2$), 1267 (vw), 1195 (w), 1145 (vw), 1101 (w), 1069 (w), 764 (w), 745 (s) cm^{-1}.

(1*R*,3*R*,4*R*,5*S*)-3-[2-*O*-Benzoyl-3-*O*-((1*S*)-1-carboxy-2-cyclohexyl-ethyl)-(β-D-galactopyranosyl)oxy]-4-[(α-L-fucopyranosyl)oxy]-5-methyl-*N*-(3-{1-[3-(5-nitro-1*H*-indol-1-yl)propyl]piperazin-1-yl}propyl)cyclohexanecarboxamide (33)

Diacid **P24** (30 mg, 40.5 μmol) and HOBt (17.0 mg, 126 μmol) were dissolved in anhydrous DMF under argon. At r.t., HBTU (18.4 mg, 48.5 μmol) was added. After 5 min of stirring, the solution was transferred via a syringe to a flask containing amine **36** (89 mg, 258 μmol) and DIPEA (0.3 mL). The solvent was removed *in vacuo* after another 2.5 h of stirring, and

the crude product was purified using preparative HPLC-MS (H_2O/MeCN + 0.2% HCOOH). **33** (14.6 mg, 34%) was obtained as a yellow solid.

^{1}H-NMR (500 MHz, MeOD): δ 0.41-0.72 (m, 4H, Cy), 0.80-0.94 (m, 1H, Cy), 1.10 (d, J = 6.3 Hz, 3H, Me), 1.14-1.42 (m, 11H, H-6$_a$, H-2$_a$, 5Cy, Fuc H-6, Lac H-3$_a$), 1.45-1.53 (m, 1H, Lac H-3$_b$), 1.55-1.72 (m, 5H, Cy, H-6, H-2', H-5), 2.00-2.09 (m, 2H, H-2''), 2.11-2.20 (m, 1H, H-2), 2.20-2.70 (m, 12H, H-1, H-1'', H-3', Pip-H), 3.13 (t, J = 6.7 Hz, 2H, H-1'), 3.17 (t, J = 9.6 Hz, 1H, H-4), 3.51-3.61 (m, 2H, Gal H-3, Gal H-5), 3.67-3.83 (m, 6H, H-3, Lac H-2, Gal H-6, Fuc H-4, Fuc H-2), 3.89 (dd, J = 3.1, 10.2 Hz, 1H, Fuc H-3), 3.91-3.96 (m, 1H, Gal H-4), 4.33 (t, J = 6.6 Hz, 2H, H-3''), 4.69 (d, J = 8.1 Hz, 1H, Gal H-1), 4.94-5.04 (m, 2H, Fuc H-1, Fuc H-5), 5.42 (t, J = 8.9 Hz, 1H, Gal H-2), 6.72 (d, J = 3.0 Hz, 1H, Ind H-3), 7.43-7.54 (m, 3H, C$_6$H$_5$, Ind H-2), 7.55-7.66 (m, 2H, C$_6$H$_5$, Ind H-7), 8.00-8.13 (m, 3H, C$_6$H$_5$, Ind H-6), 8.56 (d, J = 1.9 Hz, 1H, Ind H-4); ^{13}C-NMR (125 MHz, MeOD): δ 16.77 (Fuc C-6), 19.31 (Me), 26.55, 26.80, 26.92 (4C, Cy, C-2'), 27.39 (C-1''), 28.17 (C-2''), 33.03, 34.42, 35.38 (3C, Cy), 35.48 (C-2), 37.67 (C-6), 39.06, 39.31 (2C, C-5, C-1'), 43.45 (C-1), 43.54 (Lac C-3), 45.30 (C-3''), 53.83, 53.92 (4C, Pip-C), 56.06 (C-1''), 57.37 (C-3'), 63.15 (Gal C-6), 67.63, 67.75 (2C, Gal C-4, Fuc C-5), 70.28 (Fuc C-2), 71.34 (Fuc C-3), 73.03 (Gal C-2), 73.93 (Fuc C-4), 76.04 (Gal C-5), 79.69 (C-3), 80.65 (Lac C-2), 82.94 C-4), 83.79 (Gal C-3), 100.36 (Fuc C-1), 100.64 (Gal C-1), 104.83 (Ind C-3), 110.94 (Ind C-7), 117.64 (Ind C-6), 118.74 (Ind C-4), 129.20 (Ind C-9), 129.68 (C$_6$H$_5$), 130.89 (C$_6$H$_5$), 131.81 (C$_6$H$_5$), 132.97 (Ind C-2), 134.21 (C$_6$H$_5$), 140.47 (Ind C-8), 142.63 (Ind C-5), 166.81 (O(C=O)Ph), 176.97 (CONH), 183.25 (COOH).

(1R,3R,4R,5S)-N-{2-[2-(2-Aminoethoxy)ethoxy]ethyl}-3-[2-O-benzoyl-3-O-((1S)-1-carboxy-2-cyclohexyl-ethyl)-(β-D-galactopyranosyl)oxy]-4-[(α-L-fucopyranosyl)oxy]-5-methyl-cyclohexanecarboxamide (37)

Ester **P3** (15 mg, 0.0199 mmol) was dissolved in 2-[2-(2-aminoethoxy)ethoxy]ethan-1-amine (0.6 mL) and MeOH (0.2 mL) and stirred at 65 to 70 °C for 2 d. The solvent was partially removed under high vacuum at up to 60 °C, and the residual solution was purified by HPLC-MS (H_2O/MeCN + 0.2% HCOOH). **37** was obtained as a colorless solid (6 mg, 35%). 6 mg (40%) of the starting material was recovered.

^{1}H-NMR (500 MHz, MeOD): δ 0.49-0.73 (m, 4H, Cy), 0.84-0.96 (m, 1H, Cy), 1.11 (d, J = 6.4 Hz, 3H, Me), 1.14-1.45 (m, 11H, H-2$_a$, H-6$_a$, 5Cy, Fuc H-6, Lac H-3$_a$), 1.44-1.55 (m, 1H, Lac H-3$_b$), 1.54-1.63 (m, 2H, H-6$_b$, Cy), 1.63-1.72 (m, 1H, H-5), 2.09-2.18 (m, 1H, H-2),

2.22-2.32 (m, 1H, H-1), 3.08-3.19 (m, 3H, H-6', H-4), 3.22-3.38 (m, 2H, H-1'), 3.46-3.53 (m, 2H, H-2'), 3.53-3.82 (m, 12H, Gal H-3, Gal H-5, H-5', H-3', H-4', Gal H-6, Fuc H-2, Fuc H-4), 3.82-3.92 (m, 2H, Fuc H-3, Lac H-2), 3.95 (s, 1H, Gal H-4), 4.68 (d, J = 8.0 Hz, 1H, Gal H-1), 4.93-5.01 (m, 2H, Fuc H-1, Fuc H-5), 5.43 (t, J = 8.8 Hz, 1H, Gal H-2), 7.46-7.52 (m, 2H, C_6H_5), 7.58-7.64 (m, 1H, C_6H_5), 8.04-8.09 (m, 2H, C_6H_5) 7.46-7.52 (m, 2H, C_6H_5), 7.58-7.64 (m, 1H, C_6H_5), 8.04-8.09 (m, 2H, C_6H_5); ^{13}C-NMR (125 MHz, MeOD): δ 16.74 (Fuc C-6), 19.31 (Me), 26.56, 26.77, 27.34 (3C, Cy), 33.15, 34.37, 35.22 (3C, Cy), 35.34 (C-2), 37.56 (C-6), 39.28 (C-5), 40.06 (C-1'), 40.66 (C-6'), 43.15 (C-1), 62.95 (Gal C-6), 67.76, 67.92 (2C, Gal C-4, Fuc C-5), 70.31 (Fuc C-2), 70.63 (C-2'), 71.28 (Fuc C-3), 71.38 (2C, C-3', C-4'), 73.12 (Gal C-2), 73.94 (Fuc C-4), 76.11 (Gal C-5), 79.70 (C-3), 83.05 (C-4), 83.67 (Gal C-3), 100.41 (Fuc C-1), 100.61 (Gal C-1), 129.70 (C_6H_5), 130.90 (C_6H_5), 131.72 (C_6H_5), 134.28 (C_6H_5), 166.79 (O(C=O)Ph), 177.26 (CONH); HR-MS: m/z calcd for $C_{42}H_{66}N_2O_{17}$ [M+H]$^+$: 871.4434; found: 871.4464; [a]$_D^{20}$ = -66.3 (c = 0.22, MeOH); IR (KBr): ν = 3430 (vs, OH), 1726 (m, C=O), 1644 (m, C=O), 1077 (s, NH$_2$) cm^{-1};

6. References

1.   Wikipedia (2010).

2.   Coussens LM & Werb Z (2002) Inflammation and cancer. *Nature* 420(6917):860-867.

3.   Levi M, van der Poll T, & Buller HR (2004) Bidirectional relation between inflammation and coagulation. *Circulation* 109(22):2698-2704.

4.   Lis H & Sharon N (1998) Lectins: Carbohydrate-specific proteins that mediate cellular recognition. *Chem. Rev.* 98(2):637-674.

5.   Erbe DV*, et al.* (1992) Identification of an E-selectin region critical for carbohydrate recognition and cell adhesion. *J. Cell Biol.* 119(1):215-227.

6.   Vestweber D & Blanks JE (1999) Mechanisms that regulate the function of the selectins and their ligands. *Physiol. Rev.* 79(1):181-213.

7.   Drickamer K (1988) 2 Distinct classes of carbohydrate-recognition domains in animal lectins. *J. Biol. Chem.* 263(20):9557-9560.

8.   Somers WS, Tang J, Shaw GD, & Camphausen RT (2000) Insights into the molecular basis of leukocyte tethering and rolling revealed by structures of P- and E-selectin bound to sLe[x] and PSGL-1. *Cell* 103(3):467-479.

9.   Springer TA (2009) Structural basis for selectin mechanochemistry. *Proc. Natl. Acad. Sci. USA* 106(1):91-96.

10.   Kansas GS*, et al.* (1994) A role for the epidermal growth factor-like domain of P-selectin in ligand recognition and cell adhesion. *J. Cell Biol.* 124(4):609-618.

11.   Pigott R, Needham LA, Edwards RM, Walker C, & Power C (1991) Structural and functional studies of the endothelial activation antigen endothelial leucocyte adhesion molecule-1 using a panel of monoclonal antibodies. *J. Immunol.* 147(1):130-135.

12.   Patel KD, Nollert MU, & McEver RP (1995) P-selectin must extend a sufficient length from the plasma membrane to mediate rolling of neutrophils. *J. Cell Biol.* 131(6):1893-1902.

13.   Lorenzon P*, et al.* (1998) Endothelial cell E- and P-selectin and vascular cell adhesion molecule-1 function as signaling receptors. *J. Cell Biol.* 142(5):1381-1391.

14.   Phillips ML*, et al.* (1990) ELAM-1 mediates cell-adhesion by recognition of a carbohydrate ligand, sialyl-Le[x]. *Science* 250(4984):1130-1132.

15.   Berg EL, Robinson MK, Mansson O, Butcher EC, & Magnani JL (1991) A carbohydrate domain common to both sialyl Le(a) and sialyl Le(X) is recognized by the endothelial cell leukocyte adhesion molecule ELAM-1. *J. Biol. Chem.* 266(23):14869-14872.

16.   Berg EL, Magnani J, Warnock RA, Robinson MK, & Butcher EC (1992) Comparison of L-selectin and E-selectin ligand specificities: The L-selectin can bind the E-selectin ligands Sialyl Le[x] and Sialyl Le[a]. *Biochem. Biophys. Res. Commun.* 184(2):1048-1055.

17. Walz G, Aruffo A, Kolanus W, Bevilacqua M, & Seed B (1990) Recognition by ELAM-1 of the sialyl Le^x determinant on myeloid and tumor cells. *Science* 250(4984):1132-1135.

18. Imai Y, Singer MS, Fennie C, Lasky LA, & Rosen SD (1991) Lectin-like cell adhesion molecule 1 mediates leukocyte rolling in mesenteric venules in vivo. *J. Cell Biol.* 113(5):1213-1221.

19. Baumhueter S*, et al.* (1993) Binding of L-selectin to the vascular sialomucin CD34. *Science* 262(5132):436-438.

20. Nakache M, Berg EL, Streeter PR, & Butcher EC (1989) The mucosal vascular addressin is a tissue-specific endothelial cell adhesion molecule for circulating lymphocytes. *Nature* 337(6203):179-181.

21. Streeter PR, Berg EL, Rouse BTN, Bargatze RF, & Butcher EC (1988) A tissue-specific endothelial cell molecule involved in lymphocyte homing. *Nature* 331(6151):41-46.

22. Sassetti C, Tangemann K, Singer MS, Kershaw DB, & Rosen SD (1998) Identification of podocalyxin-like protein as a high endothelial venule ligand for L-selectin: Parallels to CD34. *J. Exp. Med.* 187(12):1965-1975.

23. Kanda H*, et al.* (2004) Endomucin, a sialomucin expressed in high endothelial venules, supports L-selectin-mediated rolling. *Int. Immunol.* 16(9):1265-1274.

24. Fieger CB, Sassetti CM, & Rosen SD (2003) Endoglycan, a member of the CD34 family, functions as an L-selectin ligand through modification with tyrosine sulfation and sialyl Lewis x. *J. Biol. Chem.* 278(30):27390-27398.

25. Brustein M, Kraal G, Mebius RE, & Watson SR (1992) Identification of a soluble form of a ligand for the lymphocyte homing receptor. *J. Exp. Med.* 176(5):1415-1419.

26. Kikuta A & Rosen SD (1994) Localization of ligands for L-selectin in mouse peripheral lymph node high endothelial cells by colloidal gold conjugates. *Blood* 84(11):3766-3775.

27. Hemmerich S, Bertozzi CR, Leffler H, & Rosen SD (1994) Identification of the sulfated monosaccharides of GlyCAM-1, an endothelial-derived ligand for L-selectin. *Biochemistry* 33(16):4820-4829.

28. Hemmerich S & Rosen SD (1994) 6'-sulfated sialyl Lewis x is a major capping group of GlyCAM-1. *Biochemistry* 33(16):4830-4835.

29. Imai Y, Lasky LA, & Rosen SD (1993) Sulfation requirement for GLYCAM-1, an endothelial ligand for L-selectin. *Nature* 361(6412):555-557.

30. Moore KL*, et al.* (1992) Identification of a specific glycoprotein ligand for P-selectin (CD62) on myeloid cells. *J. Cell Biol.* 118(2):445-456.

31. Wilkins PP, Moore KL, McEver RP, & Cummings RD (1995) Tyrosine sulfation of P-selectin glycoprotein ligand-1 is required for high-affinity binding to P-selectin. *J. Biol. Chem.* 270(39):22677-22680.

32. Sako D*, et al.* (1995) A sulfated peptide segment at the amino terminus of PSGL-1 is critical for P-selectin binding. *Cell* 83(2):323-331.

33. Pouyani T & Seed B (1995) PSGL-1 recognition of P-selectin is controlled by a tyrosine sulfation consensus at the PSGL-1 amino terminus. *Cell* 83(2):333-343.

34. Li FG*, et al.* (1996) Post-translational modifications of recombinant P-selectin glycoprotein ligand-1 required for binding to P- and E-selectin. *J. Biol. Chem.* 271(6):3255-3264.

35. Goetz DJ*, et al.* (1997) Isolated P-selectin glycoprotein ligand-1 dynamic adhesion to P- and E-selectin. *J. Cell Biol.* 137(2):509-519.

36. Lenter M, Levinovitz A, Isenmann S, & Vestweber D (1994) Monospecific and common glycoprotein ligands for E-selectin and P-selectin on myeloid cells. *J. Cell Biol.* 125(2):471-481.

37. Levinovitz A, Muhlhoff J, Isenmann S, & Vestweber D (1993) Identification of a glycoprotein ligand for E-selectin on mouse myeloid cells. *J. Cell Biol.* 121(2):449-459.

38. Asa D*, et al.* (1995) The P-selectin glycoprotein ligand functions as a common human-leukocyte ligand for P-selectins and E-selectins. *J. Biol. Chem.* 270(19):11662-11670.

39. Picker LJ*, et al.* (1991) The neutrophil selectin LECAM-1 presents carbohydrate ligands to the vascular selectins ELAM-1 and GMP-140. *Cell* 66(5):921-933.

40. Butcher EC (1991) Leukocyte–endothelial cell recognition – 3 (or more) steps to specificity and diversity. *Cell* 67(6):1033-1036.

41. Springer TA (1994) Traffic signals for lymphocyte recirculation and leukocyte emigration – the multistep paradigm. *Cell* 76(2):301-314.

42. Vögtli A (2006)).

43. Kansas GS (1996) Selectins and their ligands: Current concepts and controversies. *Blood* 88(9):3259-3287.

44. Bevilacqua MP, Pober JS, Mendrick DL, Cotran RS, & Gimbrone MA (1987) Identification of an inducible endothelial leukocyte adhesion molecule. *Proc. Natl. Acad. Sci. USA* 84(24):9238-9242.

45. Pober JS*, et al.* (1987) Activation of cultured human-endothelial cells by recombinant lymphotoxin – comparison with tumor-necrosis-factor and interleukin-1 species. *J. Immunol.* 138(10):3319-3324.

46. Bevilacqua MP, Stengelin S, Gimbrone MA, & Seed B (1989) Endothelial leukocyte adhesion molecule-1 – an inducible receptor for neutrophils related to complement regulatory proteins and lectins. *Science* 243(4895):1160-1165.

47. Keelan ETM, Licence ST, Peters AM, Binns RM, & Haskard DO (1994) Characterization of E-selectin expression in vivo with use of a radiolabeled monoclonal antibody. *Am. J. Physiol.* 266(1):H279-H290.

48. Schweitzer KM*, et al.* (1996) Constitutive expression of E-selectin and vascular cell adhesion molecule-1 on endothelial cells of hematopoietic tissues. *Am. J. Pathol.* 148(1):165-175.

49. Geng JG*, et al.* (1990) Rapid neutrophil adhesion to activated endothelium mediated by GMP-140. *Nature* 343(6260):757-760.

50. Hattori R, Hamilton KK, Fugate RD, McEver RP, & Sims PJ (1989) Stimulated secretion of endothelial von Willebrand-factor is accompanied by rapid redistribution to the cell-surface of the intracellular granule membrane-protein GMP-140. *J. Cell. Biol.* 264(14):7768-7771.

51. McEver RP, Beckstead JH, Moore KL, Marshallcarlson L, & Bainton DF (1989) GMP-140, a platelet alpha-granule membrane-protein, is also synthesized by vascular endothelial-cells and is localized in Weibel-palade bodies. *J. Clin. Invest.* 84(1):92-99.

52. Bischoff J & Brasel C (1995) Regulation of P-selectin by tumor necrosis factor α. *Biochem. Biophys. Res. Commun.* 210(1):174-180.

53. Sanders WE, Wilson RW, Ballantyne CM, & Beaudet AL (1992) Molecular cloning and analysis of *in vivo* expression of murine P-selectin. *Blood* 80(3):795-800.

54. Gotsch U, Jager U, Dominis M, & Vestweber D (1994) Expression of P-selectin on endothelial-cells is up-regulated by LPS and TNF-α *in vivo. Cell Adhes. Commun.* 2(1):7-14.

55. Walcheck B, Moore KL, McEver RP, & Kishimoto TK (1996) Neutrophil-neutrophil interactions under hydrodynamic shear stress involve L-selectin and PSGL-1 - A mechanism that amplifies initial leukocyte accumulation on P-selectin in vitro. *J. Clin. Invest.* 98(5):1081-1087.

56. Bargatze RF, Kurk S, Butcher EC, & Jutila MA (1994) Neutrophils roll on adherent neutrophils bound to cytokine-induced endothelial cells via L-selectin on the rolling cells. *J. Exp. Med.* 180(5):1785-1792.

57. Von Andrian UH*, et al.* (1991) 2-Step model of leukocyte endothelial-cell interaction in inflammation – distinct roles for LECAM-1 and the leukocyte β-2 integrins *in vivo. Proc. Natl. Acad. Sci. USA* 88(17):7538-7542.

58. Lawrence MB & Springer TA (1991) Leukocytes roll on a selectin at physiological flow-rates – distinction from and prerequisite for adhesion through integrins. *Cell* 65(5):859-873.

59. Ernst B, Kolb HC, & Schwardt O (2006) Carbohydrate Mimetics in Drug Discovery. *The Organic Chemistry of Sugars*, eds Levy DE & Fügedi P (CRC Press/Taylor & Francis, Boca Raton), pp 803-845.

60. Tedder TF, Steeber DA, & Pizcueta P (1995) L-selectin-deficient mice have impaired leukocyte recruitment into inflammatory sites. *J. Exp. Med.* 181(6):2259-2264.

61. Albelda SM, Smith CW, & Ward PA (1994) Adhesion molecules and inflammatory injury. *FASEB* 8(8):504-512.

62. Bevilacqua MP, Nelson RM, Mannori G, & Cecconi O (1994) Endothelial-leukocyte adhesion molecules in human disease. *Annu. Rev. Med.* 45:361-378.

63. Lependu J, Cartron JP, Lemieux RU, & Oriol R (1985) The presence of at least two different H-blood-group-related β-D-Gal α-2-L-fucosyltransferases in human serum and the genetics of blood group H substances. *Am. J. Hum. Genet.* 37(4):749-760.

64. Becker DJ & Lowe JB (1999) Leukocyte adhesion deficiency type II. *Biochim. Biophys. Acta Gen. Subj.* 1455(2-3):193-204.

65. Lefer AM, Weyrich AS, & Buerke M (1994) Role of selectins, a new family of adhesion molecules, in ischemia–reperfusion injury. *Cardiovasc. Res.* 28(3):289-294.

66. Lefer DJ, Flynn DM, Phillips ML, Ratcliffe M, & Buda AJ (1994) A novel sialyl Lewis[x] analog attenuates neutrophil accumulation and myocardial necrosis after ischemia and reperfusion. *Circulation* 90(5):2390-2401.

67. Wegner CD*, et al.* (1990) Intercellular adhesion molecule 1 (ICAM-1) in the pathogenesis of asthma. *Science* 247(4941):456-459.

68. Wein M & Bochner BS (1993) Adhesion molecule antagonists – future therapies for allergic diseases. *Eur. Resp. J.* 6(9):1239-1242.

69. Romano SJ & Slee DH (2001) Targeting selectins for the treatment of respiratory diseases. *Curr Opin Investig Drugs* 2(7):907-913.

70. Georas SN*, et al.* (1992) Altered adhesion molecule expression and endothelial-cell activation accompany the recruitment of human granulocytes to the lung after segmental antigen challenge. *Am. J. Respir. Cell Mol. Biol.* 7(3):261-269.

71. Voskuyl AE*, et al.* (2003) Diagnostic strategy for the assessment of rheumatoid vasculitis. *Ann. Rheum. Dis.* 62(5):407-413.

72. Ates A, Kinikli G, Turgay M, & Duman M (2004) Serum-soluble selectin levels in patients with rheumatoid arthritis and systemic sclerosis. *Scand. J. Immunol.* 59(3):315-320.

73. Bloom BJ, Nelson SM, Alario AJ, Miller LC, & Schaller JG (2002) Synovial fluid levels of E-selectin and intercellular adhesion molecule-1: relationship to joint inflammation in children with chronic arthritis. *Rheumatol. Int.* 22(5):175-177.

74. Egerer K*, et al.* (2003) sE-selectin for stratifying outcome in rheumatoid arthritis. *Arthritis Rheum.* 49(4):546-548.

75. Ferran C*, et al.* (1993) Implications of de novo ELAM-1 and VCAM-1 expression in human cardiac allograft rejection. *Transplantation* 55(3):605-609.

76. Briscoe DM*, et al.* (1991) Induced expression of endothelial leukocyte adhesion molecules in human cardiac allografts. Transplantation. *Transplantation* 51(2):537-539.

77. Onai Y*, et al.* (2003) Blockade of cell adhesion by a small molecule selectin antagonist attenuates myocardial ischemia/reperfusion injury. *Eur. J. Pharmacol.* 481(2-3):217-225.

78. Zoldhelyi P*, et al.* (2000) Inhibition of coronary thrombosis and local inflammation by a noncarbohydrate selectin inhibitor. *Am. J. Physiol. Heart Circ. Physiol.* 279(6):H3065-H3075.

79. Gundel RH*, et al.* (1991) Endothelial leukocyte adhesion molecule 1 mediates antigen-induced acute airway inflammation and late-phase airwayobstruction in monkeys. *J. Clin. Invest.* 88(4):1407-1411.

80. Abraham WM*, et al.* (1999) Selectin blockade prevents antigen-induced late bronchial responses and airway hyperresponsiveness in allergic sheep. *Am. J. Respir. Crit. Care Med.* 159(4):1205-1214.

81. Issekutz AC, Mu JY, Liu G, Melrose J, & Berg EL (2001) E-selectin, but not P-selectin, is required for development of adjuvant-induced arthritis in the rat. *Arthritis Rheum.* 44(6):1428-1437.

82. Kaila N*, et al.* (2007) 2-(4-chlorobenzyl)-3-hydroxy-7,8,9,10-tetrahydrobenzo H quinoline-4-carb oxylic acid (PSI-697): Identification of a clinical candidate from the quinoline salicylic acid series of P-selectin antagonists. *J. Med. Chem.* 50:40-64.

83. Witz IP (2008) The selectin–selectin ligand axis in tumor progression. *Cancer Metastasis Rev.* 27(1):19-30.

84. Matsumoto S*, et al.* (2002) Cimetidine increases survival of colorectal cancer patients with high levels of sialyl Lewis-X and sialyl Lewis-A epitope expression on tumour cells. *Brit. J. Cancer* 86(2):161-167.

85. Bock D, Philipp S, & Wolff G (2006) Therapeutic potential of selectin antagonists in psoriasis. *Expert Opin. Investig. Drugs* 15(8):963-979.

86. Barthel SR, Gavino JD, Descheny L, & Dimitroff CJ (2007) Targeting selectins and selectin ligands in inflammation and cancer. *Expert Opin. Ther. Targets* 11(11):1473-1491.

87. Ernst B & Magnani JL (2009) From carbohydrate leads to glycomimetic drugs. *Nat. Rev. Drug Discovery* 8(8):661-677.

88. Laubli H & Borsig L (2010) Selectins promote tumor metastasis. *Sem. Cancer Biol.* 20(3):169-177.

89. Hackert T, Buchler MW, & Werner J (2010) Targeting P-selectin in acute pancreatitis. *Expert Opin. Ther. Targets* 14(9):899-910.

90. Kolb HC & Ernst B (1997) Development of tools for the design of selectin antagonists. *Chem. Eur. J.* 3(10):1571-1578.

91. Simanek EE, McGarvey GJ, Jablonowski JA, & Wong CH (1998) Selectin–carbohydrate interactions: From natural ligands to designed mimics. *Chem. Rev.* 98(2):833-862.

92. Bertozzi CR (1995) Cracking the carbohydrate code for selectin recognition. *Chem. Biol.* 2(11):703-708.

93. Giannis A (1994) The sialyl Lewis[x] group and its analogues as ligands for selectins: Chemoenzymatic syntheses and biological functions. *Angew. Chem. Int. Ed.* 33(2):178-180.

94. Brandley BK*, et al.* (1993) Structure–function studies on selectin carbohydrate ligands – modifications to fucose, sialic acid and sulfate as a sialic acid replacement. *Glycobiology* 3(6):633-641.

95. Ramphal JY*, et al.* (1994) Structure-activity relationships of sialyl Lewis[x]-containing oligosaccharides. 1. Effect of modifications of the fucose moiety. *J. Med. Chem.* 37(21):3459-3463.

96. Bänteli R & Ernst B (2001) Synthesis of sialyl Lewis[x] mimics. Modifications of the 6-position of galactose. *Bioorg. Med. Chem. Lett.* 11(4):459-462.

97. Stahl W, Sprengard U, Kretzschmar G, & Kunz H (1994) Synthesis of deoxy sialyl Lewis^x analogs, potential selectin antagonists. *Angew. Chem. Int. Ed.* 33(20):2096-2098.

98. Ohmoto H*, et al.* (1996) Studies on selectin blocker. 1. Structure-activity relationships of sialyl Lewis X analogs. *J. Med. Chem.* 39(6):1339-1343.

99. Tyrrell D*, et al.* (1991) Structural requirements for the carbohydrate ligand of E-selectin. *Proc. Natl. Acad. Sci. USA* 88(22):10372-10376.

100. Weis WI, Drickamer K, & Hendrickson WA (1992) Structure of a C-type mannoside-binding protein complexed with an oligosaccharide. *Nature* 360(6400):127-134.

101. Finger EB*, et al.* (1996) Adhesion through L-selectin requires a threshold hydrodynamic shear. *Nature* 379(6562):266-269.

102. Lawrence MB, Kansas GS, Kunkel EJ, & Ley K (1997) Threshold levels of fluid shear promote leukocyte adhesion through selectins (CD62L,P,E). *J. Cell Biol.* 136(3):717-727.

103. Marshall BT*, et al.* (2003) Direct observation of catch bonds involving cell-adhesion molecules. *Nature* 423(6936):190-193.

104. Evans E, Leung A, Heinrich V, & Zhu C (2004) Mechanical switching and coupling between two dissociation pathways in a P-selectin adhesion bond. *Proc. Natl. Acad. Sci. USA* 101(31):11281-11286.

105. Thomas W (2008) Catch bonds in adhesion. *Annu. Rev. Biomed. Eng.* 10:39-57.

106. Dembo M, Torney DC, Saxman K, & Hammer D (1988) The reaction-limited kinetics of membrane-to-surface adhesion and detachment. *Proc. R. Soc. Lond. B* 234(1274):55-83.

107. Zhu C, Yago T, Lou JZ, Zarnitsyna VI, & McEver RP (2008) Mechanisms for flow-enhanced cell adhesion. *Ann. Biomed. Eng.* 36(4):604-621.

108. Phan UT, T Waldron T, & Springer TA (2006) Remodeling of the lectin-EGF-like domain interface in P- and L-selectin increases adhesiveness and shear resistance under hydrodynamic force. *Nat. Immunol.* 7(8):883-889.

109. Lou JZ*, et al.* (2006) Flow-enhanced adhesion regulated by a selectin interdomain hinge. *J. Cell Biol.* 174(7):1107-1117.

110. Graves BJ*, et al.* (1994) Insight into E-selectin ligand interaction from the crystal structure and mutagenesis of the Lec-EGF domains. *Nature* 367(6463):532-538.

111. Thomas W (2006) For catch bonds, it all hinges on the interdomain region. *J. Cell Biol.* 174(7):911-913.

112. Lou JZ & Zhu C (2007) A structure-based sliding-rebinding mechanism for catch bonds. *Biophys. J.* 92(5):1471-1485.

113. Waldron TT & Springer TA (2009) Transmission of allostery through the lectin domain in selectin-mediated cell adhesion. *Proc. Natl. Acad. Sci. USA* 106(1):85-90.

114. DeLorbe JE, *et al.* (2009) Thermodynamic and Structural Effects of Conformational Constraints in Protein-Ligand Interactions. Entropic Paradoxy Associated with Ligand Preorganization. *J. Am. Chem. Soc.* 131(46):16758-16770.

115. Kolb HC & Ernst B (1997) Recent progress in the glycodrug area. *Pure Appl. Chem.* 69(9):1879-1884.

116. Scheffler K, *et al.* (1995) Determination of the bioactive conformation of the carbohydrate ligand in the E-selectin sialyl Lewis[x] complex. *Angew. Chem. Int. Ed.* 34(17):1841-1844.

117. Scheffler K, *et al.* (1997) Application of homonuclear 3D NMR experiments and 1D analogs to study the conformation of sialyl Lewis(x) bound to E-selectin. *J. Biomol. NMR* 9(4):423-436.

118. Hiramatsu Y, Tsukida T, Nakai Y, Inoue Y, & Kondo H (2000) Study on selectin blocker. 8. Lead discovery of a non-sugar antagonist using a 3D-pharmacophore model. *J. Med. Chem.* 43(8):1476-1483.

119. Kretzschmar G, Toepfer A, Hills C, & Krause M (1997) Pitfalls in the synthesis and biological evaluation of Sialyl-Lewis(X) mimetics as potential selectin antagonists. *Tetrahedron* 53(7):2485-2494.

120. Mehta P, Cummings RD, & McEver RP (1998) Affinity and kinetic analysis of P-selectin binding to P-selectin glycoprotein ligand-1. *J. Biol. Chem.* 273(49):32506-32513.

121. Wild MK, Huang MC, Schulze-Horsel U, van der Merwe PA, & Vestweber D (2001) Affinity, kinetics, and thermodynamics of E-selectin binding to E-selectin ligand-1. *J. Biol. Chem.* 276(34):31602-31612.

122. Nicholson MW, Barclay AN, Singer MS, Rosen SD, & van der Merwe PA (1998) Affinity and kinetic analysis of L-selectin (CD62L) binding to glycosylation-dependent cell-adhesion molecule-1. *J. Biol. Chem.* 273(2):763-770.

123. Copeland RA, Pompliano DL, & Meek TD (2006) Drug-target residence time and its implications for lead optimization. *Nat. Rev. Drug Discovery* 5(9):730-739.

124. Copeland RA (2010) The dynamics of drug-target interactions: drug-target residence time and its impact on efficacy and safety. *Expert Opin. Drug Discovery* 5(4):305-310.

125. Titz A & Ernst B (2007) Mimetics of sialyl Lewis[x]: The pre-organization of the carboxylic acid is essential for binding to selectins. *Chimia* 61(4):194-197.

126. Kaila N & Thomas BE (2003) Selectin inhibitors. *Expert Opin. Ther. Patents* 13(000181482000002):305-317.

127. Bedard PW & Kaila N (2010) Selectin inhibitors: a patent review. *Expert Opin. Ther. Patents* 20(20408735):781-793.

128. Töpfer A, Kretzschmar G, & Bartnik E (1995) Synthesis of novel mimetics of the sialyl Lewis X determinant. *Tetrahedron Lett.* 36(50):9161-9164.

129. Titz A, *et al.* (2008) Is adamantane a suitable substituent to pre-organize the acid orientation in E-selectin antagonists? *Bioorg. Med. Chem.* 16(2):1046-1056.

130. Thoma G, Magnani JL, Patton JT, Ernst B, & Jahnke W (2001) Preorganization of the bioactive conformation of sialyl Lewis^x analogues correlates with their affinity to E-selectin. *Angew. Chem. Int. Ed.* 40(10):1941-1945.

131. Schwizer D (2007) Lead Optimization Studies on E-Selectin Antagonists. (University of Basel).

132. Ernst B, Schwizer D, Sarkar AK, & Magnani JL (2008) Glycomimetic replacements for hexoses and N-acetyl hexosamines. *freepatentsonline.com*.

133. Weckerle C (2010) E-selectin antagonists: Fragment-based drug discovery and lead optimization by NMR and BIAcore. (University of Basel, Basel).

134. Drews J (2000) Drug discovery: a historical perspective. *Science* 287(5460):1960-1964.

135. Brown D & Superti-Furga G (2003) Rediscovering the sweet spot in drug discovery. *Drug Discovery Today* 8(23):1067-1077.

136. Cherry M & Mitchell T (2008) Introduction to Fragment-based Drug Discovery. *Fragment-Based Drug Discovery*, eds Zartler ER & Shapiro MJ (John Wiley & Sons, Ltd., Chichester), pp 1-13.

137. Chessari G & Woodhead AJ (2009) From fragment to clinical candidate-a historical perspective. *Drug Discovery Today* 14(13-14):668-675.

138. Murray C & Rees D (2009) The rise of fragment-based drug discovery. *Nature Chemistry* 1(3):187-192.

139. Kubinyi H (2003) Drug research: myths, hype and reality. *Nat. Rev. Drug Discovery* 2(8):665-668.

140. Jencks W (1981) On the attribution and additivity of binding energies. *Proc. Nat. Acad. Sci. U.S.A.* 78(7):4046-4050.

141. Shuker SB, Hajduk PJ, Meadows RP, & Fesik SW (1996) Discovering high-affinity ligands for proteins: SAR by NMR. *Science* 274(5292):1531-1534.

142. Congreve M, Chessari G, Tisi D, & Woodhead AJ (2008) Recent developments in fragment-based drug discovery. *J. Med. Chem.* 51(13):3661-3680.

143. Carr R, Congreve M, Murray C, & Rees D (2005) Fragment-based lead discovery: leads by design. *Drug Discovery Today* 10(14):987-992.

144. Zartler ER & Shapiro MJ (2005) Fragonomics: fragment-based drug discovery. *Curr. Opin. Chem. Biol.* 9(4):366-370.

145. Hajduk PJ & Greer J (2007) A decade of fragment-based drug design: Strategic advances and lessons learned. *Nat. Rev. Drug Discovery* 6(3):211-219.

146. de Kloe GE, Bailey D, Leurs R, & de Esch IJP (2009) Transforming fragments into candidates: small becomes big in medicinal chemistry. *Drug Discovery Today* 14(13-14):630-646.

147. Orita M, Warizaya M, Amano Y, Ohno K, & Niimi T (2009) Advances in fragment-based drug discovery platforms. *Expert Opin. Drug Discovery* 4(11):1125-1144.

148. Coyne AG, Scott DE, & Abell C (2010) Drugging challenging targets using fragment-based approaches. *Curr. Opin. Chem. Biol.* 14(3):299-307.

149. Zartler ER & Shapiro MJ (2008) *Fragment-Based Drug Discovery* (John Wiley & Sons, Ltd., Chichester).

150. Congreve M, Carr R, Murray C, & Jhoti H (2003) A 'rule of three' for fragment-based lead discovery? *Drug Discovery Today* 8(19):876-877.

151. Lipinski C, Lombardo F, Dominy B, & Feeney P (2001) Experimental and computational approaches to estimate solubility and permeability in drug discovery and development settings. *Adv. Drug Del. Rev.* 46(1-3):3-26.

152. Page MI & Jencks WP (1971) Entropic contributions to rate accelerations in enzymic and intramolecular reactions and the chelate effect. *Proc. Nat. Acad. Sci. USA* 68(8):1678-1683.

153. Page MI (1973) Energetics of neighboring group participation. *Chem. Soc. Rev.* 2(3):295-323.

154. Murray CW & Verdonk ML (2002) The consequences of translational and rotational entropy lost by small molecules on binding to proteins. *J. Comput.-Aided Mol. Des.* 16(10):741-753.

155. Bembenek SD, Tounge BA, & Reynolds CH (2009) Ligand efficiency and fragment-based drug discovery. *Drug Discovery Today* 14(5-6):278-283.

156. Erlanson DA, McDowell RS, & O'Brien T (2004) Fragment-based drug discovery. *Journal of Medicinal Chemistry* 47(14):3463-3482.

157. Dalvit C (2009) NMR methods in fragment screening: theory and a comparison with other biophysical techniques. *Drug Discovery Today* 14(21-22):1051-1057.

158. Pellecchia M, Sem DS, & Wüthrich K (2002) NMR in drug discovery. *Nat. Rev. Drug Discovery* 1(3):211-219.

159. Jahnke W*, et al.* (2000) Second-site NMR screening with a spin-labeled first ligand. *J. Am. Chem. Soc.* 122(30):7394-7395.

160. Shelke S*, et al.* (2010) A fragment-based in situ combinatorial approach to identify high-affinity ligands for unknown binding sites. *Angew. Chem. Int. Ed.* 49(33):5721-5725.

161. Bertini I, Fragai M, Lee YM, Luchinat C, & Terni B (2004) Paramagnetic metal ions in ligand screening: The Co-II matrix metalloproteinase 12. *Angew. Chem. Int. Ed.* 43(17):2254-2256.

162. Hartshorn MJ*, et al.* (2005) Fragment-based lead discovery using X-ray crystallography. *J. Med. Chem.* 48(2):403-413.

163. Navratilova I & Hopkins AL (2010) Fragment Screening by Surface Plasmon Resonance. *ACS Med. Chem. Lett.* 1(1):44-48.

164. Taylor JD, Gilbert PJ, Williams MA, Pitt WR, & Ladbury JE (2007) Identification of novel fragment compounds targeted against the pY pocket of v-Src SH2 by computational and NMR screening and thermodynamic evaluation. *Proteins Struct. Funct. Bioinf.* 67(4):981-990.

165. Ladbury JE, Klebe G, & Freire E (2010) Adding calorimetric data to decision making in lead discovery: a hot tip. *Nat. Rev. Drug Discovery* 9(1):23-27.

166. Zehender H & Mayr LM (2007) Application of mass spectrometry technologies for the discovery of low-molecular weight modulators of enzymes and protein–protein interactions. *Curr. Opin. Chem. Biol.* 11(5):511-517.

167. Seth PP*, et al.* (2005) SAR by MS: Discovery of a new class of RNA-binding small molecules for the hepatitis C virus: Internal ribosome entry site IIA subdomain. *J. Med. Chem.* 48(23):7099-7102.

168. Cooper MA (2002) Optical biosensors in drug discovery. *Nat. Rev. Drug Discovery* 1(7):515-528.

169. Navratilova I*, et al.* (2007) Thermodynamic benchmark study using Biacore technology. *Anal. Biochem.* 364(1):67-77.

170. Poulsen S-A & Kruppa GH (2008) *In situ* Fragment-based Medicinal Chemistry: Screening by Mass Spectrometry. *Fragment-Based Drug Discovery*, eds Zartler ER & Shapiro MJ (John Wiley & Sons, Ltd, Chichester), pp 159-198.

171. Huc I & Lehn JM (1997) Virtual combinatorial libraries: Dynamic generation of molecular and supramolecular diversity by self-assembly. *Proc. Nat. Acad. Sci. U.S.A.* 94(6):2106-2110.

172. Corbett PT*, et al.* (2006) Dynamic combinatorial chemistry. *Chem. Rev.* 106(9):3652-3711.

173. Ladame S (2008) Dynamic combinatorial chemistry: on the road to fulfilling the promise. *Org. Biomol. Chem.* 6(2):219-226.

174. Prins LJ & Scrimin P (2009) Covalent capture: Merging covalent and noncovalent synthesis. *Angew. Chem. Int. Ed.* 48(13):2288-2306.

175. Hu XD & Manetsch R (2010) Kinetic target-guided synthesis. *Chem. Soc. Rev.* 39(4):1316-1324.

176. Nguyen R & Huc I (2001) Using an enzyme's active site to template inhibitors. *Angew. Chem. Int. Ed.* 40(9):1774-1776.

177. Lewis WG*, et al.* (2002) Click chemistry in situ: acetylcholinesterase as a reaction vessel for the selective assembly of a femtomolar inhibitor from an array of building blocks. *Angew. Chem. Int. Ed.* 41(6):1053-1057.

178. Huisgen R, Szeimies G, & Mobius L (1967) 1,3-Dipolare Cycloadditionen. 32. Kinetik der Additionen organischer Azide an CC-Mehrfachbindungen. *Chem. Ber.* 100(8):2494-2507.

179. Manetsch R*, et al.* (2004) In situ click chemistry: enzyme inhibitors made to their own specifications. *J. Am. Chem. Soc.* 126(40):12809-12818.

180. Krasiński A*, et al.* (2005) In situ selection of lead compounds by click chemistry: target-guided optimization of acetylcholinesterase inhibitors. *J. Am. Chem. Soc.* 127(18):6686-6692.

181. Mocharla VP*, et al.* (2005) In situ click chemistry: enzyme-generated inhibitors of carbonic anhydrase II. *Angew. Chem. Int. Ed.* 44(1):116-120.

182. Wang JY*, et al.* (2006) Integrated microfluidics for parallel screening of an in situ click chemistry library. *Angew. Chem. Int. Ed.* 45(32):5276-5281.

183. Agnew HD, *et al.* (2009) Iterative in situ click chemistry creates antibody-like protein-capture agents. *Angew. Chem. Int. Ed.* 48(27):4944-4948.

184. Whiting M, *et al.* (2006) Inhibitors of HIV-1 protease by using in situ click chemistry. *Angew. Chem. Int. Ed.* 45(9):1435-1439.

185. Poulin-Kerstien AT & Dervan PB (2003) DNA-templated dimerization of hairpin polyamides. *J. Am. Chem. Soc.* 125(51):15811-15821.

186. Hirose T, *et al.* (2009) Chitinase inhibitors: Extraction of the active framework from natural argifin and use of in situ click chemistry. *J. Antibiot.* 62(5):277-282.

187. Mamidyala SK & Finn MG (2010) In situ click chemistry: probing the binding landscapes of biological molecules. *Chem. Soc. Rev.* 39(4):1252-1261.

188. Mock W, Irra T, Wepsiec J, & Manimaran T (1983) Cycloaddition induced by cucurbituril. A case of Pauling principle catalysis. *J. Org. Chem.* 48(20):3619-3620.

189. Mock W, Irra T, Wepsiec J, & Adhya M (1989) Catalysis by cucurbituril. The significance of bound-substrate destabilization for induced triazole formation. *J. Org. Chem.* 54(22):5302-5308.

190. Mock WL & Shih NY (1983) Host–guest binding capacity of cucurbituril. *J. Org. Chem.* 48(20):3618-3619.

191. Cacciapaglia R, Di Stefano S, & Mandolini L (2004) Effective molarities in supramolecular catalysis of two-substrate reactions. *Acc. Chem. Res.* 37(2):113-122.

192. Glish GL & Vachet RW (2003) The basics of mass spectrometry in the twenty-first century. *Nat. Rev. Drug Discovery* 2(2):140-150.

193. de Hoffmann E & Stroobant V (2007) *Mass Spectrometry – Principles and Applications* (John Wiley & Sons Ltd., Chichester) 3 Ed.

194. Hogberg T, Strom P, Ebner M, & Ramsby S (1987) Cyanide as an efficient and mild catalyst in the aminolysis of esters. *J. Org. Chem.* 52(10):2033-2036.

195. Zipse H, Wang LH, & Houk KN (1996) Polyether catalysis of ester aminolysis - a computational and experimental study. *Liebigs Ann.* (10):1511-1522.

196. Basha A, Lipton M, & Weinreb SM (1977) Mild, general method for conversion of esters to amides. *Tetrahedron Lett.* (48):4171-4174.

197. Novak A, Humphreys LD, Walker MD, & Woodward S (2006) Amide bond formation using an air-stable source of AlMe$_3$. *Tetrahedron Lett.* 47(32):5767-5769.

198. Schreier S, Malheiros SVP, & de Paula E (2000) Surface active drugs: self-association and interaction with membranes and surfactants. Physicochemical and biological aspects. *Biochim. Biophys. Acta, Biomembr.* 1508(1-2):210-234.

199. Seddon AM, *et al.* (2009) Drug interactions with lipid membranes. *Chem. Soc. Rev.* 38(9):2509-2519.

200. Suomalainen P, Johans C, Söderlund T, & Kinnunen PK (2004) Surface activity profiling of drugs applied to the prediction of blood-brain barrier permeability. *J. Med. Chem.* 47(15027870):1783-1788.

201. Fischer H, Gottschlich R, & Seelig A (1998) Blood-brain barrier permeation: Molecular parameters governing passive diffusion. *J. Membr. Biol.* 165(3):201-211.

202. Seelig A & Landwojtowicz E (2000) Structure-activity relationship of P-glycoprotein substrates and modifiers. *Eur. J. Pharm. Sci.* 12(1):31-40.

203. scifinder (2010) SciFinder, web version; Chemical Abstracts Service: Columbus, OH (accessed Jul 17, 2010); calculated using ACD/Labs software, version 9.04; ACD/Labs 1994-2010.].

204. Kelly TR, Zhao C, & Bridger GJ (1989) A bisubstrate reaction template. *J. Am. Chem. Soc.* 111(10):3744-3745.

205. Kelly T, Bridger G, & Zhao C (1990) Bisubstrate reaction templates. Examination of the consequences of identical versus different binding sites. *J. Am. Chem. Soc.* 112(22):8024-8034.

206. Wittwer M (2010) (University of Basel).

207. Kansy M, Senner F, & Gubernator K (1998) Physicochemical high throughput screening: Parallel artificial membrane permeation assay in the description of passive absorption processes. *J. Med. Chem.* 41(7):1007-1010.

208. Avdeef A, *et al.* (2007) PAMPA - Critical factors for better predictions of absorption. *J. Pharm. Sci.* 96(11):2893-2909.

209. Wittwer M & Kleeb S (2010) personal communication.

210. Wunderli-Allenspach H (2004) Grundlagen der Pharmakokinetik. *Biopharmazie*, (Wiley-VCH Verlag GmbH & Co. KGaA, Weinheim).

211. Kerns EH & Di L (2008) *Drug-like properties: concepts, structure design and methods: from ADME to toxicity optimization* (Academic Press, Elsevier, San Diego).

212. Mazzenga GC & Berner B (1991) The transdermal delivery of zwitterionic drugs I: the solubility of zwitterion salts. *J. Controlled Release* 16(1-2):77-88.

213. Halliwell WH (1997) Cationic amphiphilic drug-induced phospholipidosis. *Toxicol. Pathol.* 25(1):53-60.

214. Reasor MJ, Hastings KL, & Ulrich RG (2006) Drug-induced phospholipidosis: issues and future directions. *Expert Opin. Drug Saf.* 5(4):567-583.

215. Recanatini M, Poluzzi E, Masetti M, Cavalli A, & De Ponti F (2005) QT prolongation through hERG K+ channel blockade: current knowledge and strategies for the early prediction during drug development. *Med. Res. Rev.* 25(2):133-166.

216. Aronov MM (2005) Predictive in silico modeling for hERG channel blockers. *Drug Discovery Today* 10(2):149-155.

217. Lepre CA, Moore JM, & Peng JW (2004) Theory and applications of NMR-based screening in pharmaceutical research. *Chem. Rev.* 104(8):3641-3675.

218. Chen J & Rebek J (2002) Selectivity in an encapsulated cycloaddition reaction. *Org. Lett.* 4(3):327-329.

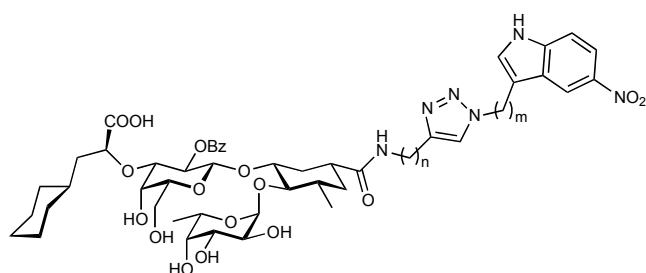219. Menger FM (1985) On the source of intramolecular and enzymatic reactivity. *Acc. Chem. Res.* 18(5):128-134.

220. Ricklin D (2005) Surface Plasmon Resonance Applications in Drug Discovery. (University of Basel).

221. MeschA S, *et al.* (2010) Kinetic and thermodynamic properties of MAG antagonists. *Carbohydr. Res.* 345(10):1348-1359.
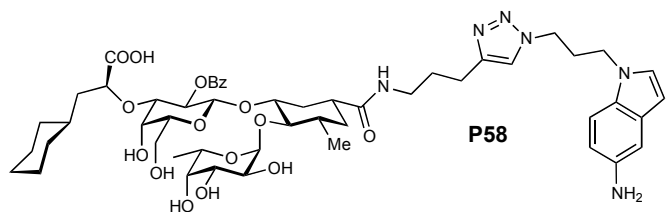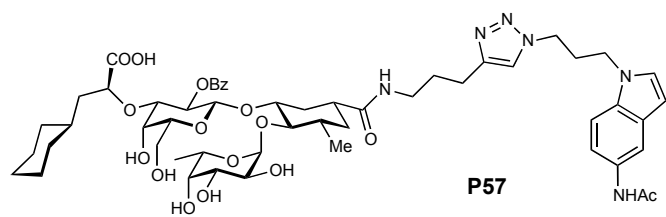
7. Compound Index

7.1. Chapter 2

P18•

P18*

P26a, n = 1
P26b, n = 2
P26c, n = 3
P26d, n = 4

P32a, m = 1
P32b, m = 2
P32c, m = 3
P32d, m = 4
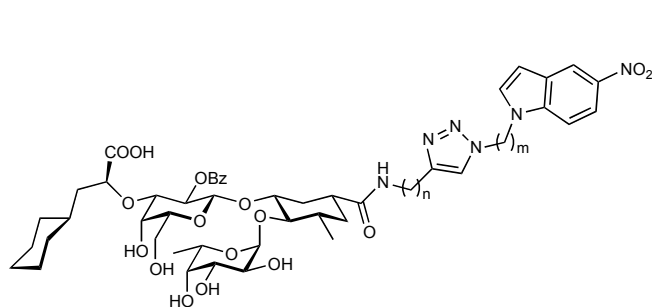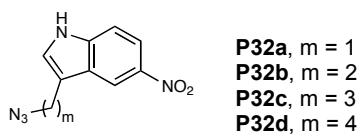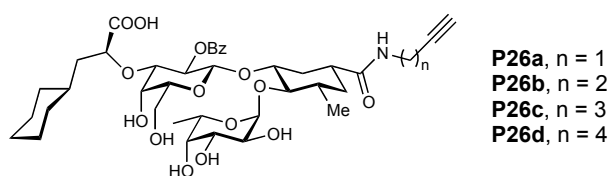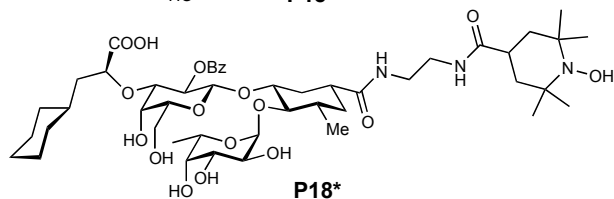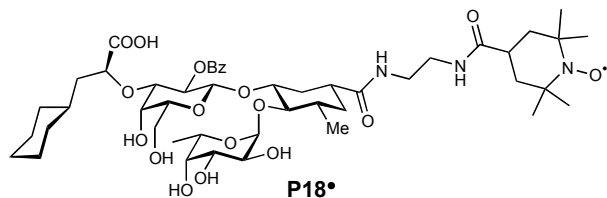
n / m	1	2	3	4
1	P33	P34	P35	P36
2	P37	P38	P39	P40
3	P41	P42	P43	-
4	P44	P45	P46	

n / m	1	2	3
2	P47	P48	P49
3	P50	P51	P52

P57

P58

7.2. Chapter 3.1.3

32

7.3. Chapter 3.2.2.3

P33

7.4. Chapter 3.3

37

39